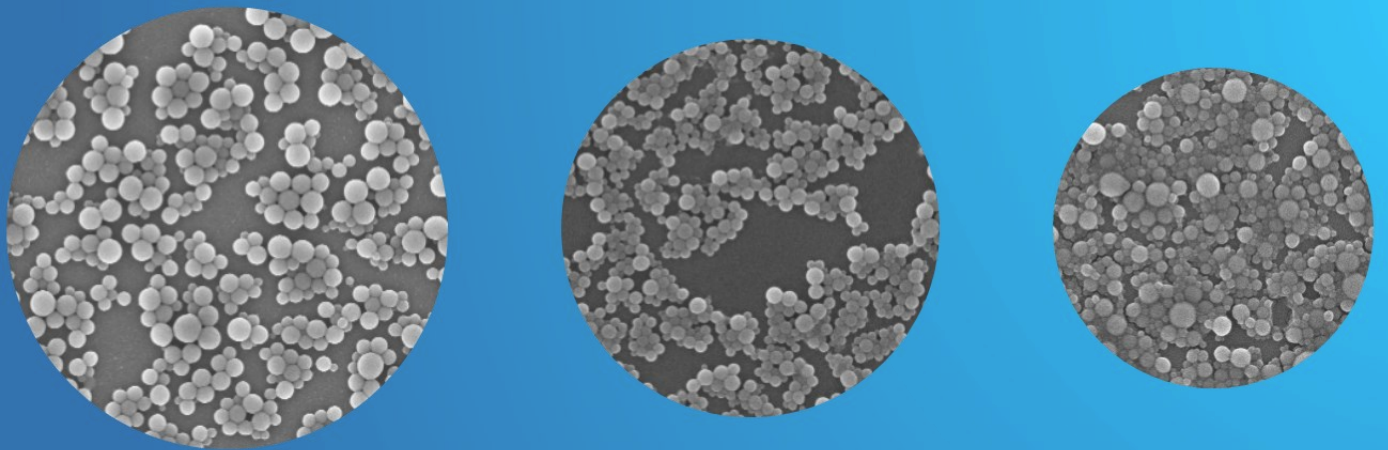


# **Dissertation:**

Synthesis of bio- and synthetic-based functional nanoparticles via inverse miniemulsion for the adsorption and detection of pharmaceuticals in aqueous media

**Benjamin R. Riegger**

Universität Stuttgart, 2021





# Synthesis of bio- and synthetic-based functional nanoparticles via inverse miniemulsion for the adsorption and detection of pharmaceuticals in aqueous media

Von der Fakultät Energie-, Verfahrens-und Biotechnik  
der Universität Stuttgart  
zur Erlangung der Würde eines Doktors der  
Naturwissenschaften (Dr. rer. nat.) genehmigte kumulative Abhandlung

Vorgelegt von  
**Benjamin R. Riegger**  
aus Stuttgart

Hauptberichter: Prof. Dr. Günter E. M. Tovar  
Mitberichterin: Prof. Dr. Ingrid Weiss

Tag der mündlichen Prüfung:  
24.09.2020

Institut für Grenzflächenverfahrenstechnik und Plasmatechnologie  
der Universität Stuttgart 2021





***Für Silke und meine Eltern***



# **I. Declaration of Authorship/Erklärung über die Eigenständigkeit der Dissertation**

## **Declaration of Authorship**

I hereby certify that the dissertation entitled

*Synthesis of bio- and synthetic-based functional nanoparticles via inverse miniemulsion for the adsorption and detection of pharmaceuticals in aqueous media*

is entirely my own work except where otherwise indicated. Passages and ideas from other sources have been clearly indicated. This thesis has never been submitted in the same or substantially similar version to any other examination office.

---

## **Erklärung über die Eigenständigkeit der Dissertation**

Ich versichere, dass ich die vorliegende Arbeit mit dem Titel

*Synthese biobasierter und synthetischer funktioneller Nanopartikel mittels inverser Miniemulsion für die Adsorption und Detektion von Pharmazeutika in wässrigem Medium*

selbständig verfasst und keine anderen als die angegebenen Quellen und Hilfsmittel benutzt habe; aus fremden Quellen entnommene Passagen und Gedanken sind als solche kenntlich gemacht. Diese Dissertation wurde zu keiner Zeit in derselben oder substantiell ähnlichen Version bei einem anderen Prüfungsamt eingereicht.

Benjamin Riegger

---

## II. Acknowledgments

My sincere thanks to...

- ... my PhD supervisor and *Doktorvater* **Prof. Dr. Günter E.M. Tovar** for his support during my time as a PhD student at the institute. He encouraged me to pursue my scientific ideas freely and provided guidance whenever I needed support.
- ... **Dr. Monika Bach** my scientific advisor and group leader for her outstanding readiness to support me with discussions and guidance at all times. Working with her on different projects taught me the skills I needed to cope with the challenges of doing the PhD thesis.
- ... **Prof. Dr. Ingrid Weiss** for her scientific input which allowed me to further improve my thesis as well as her willingness to give a second opinion on this thesis.
- ... **Klaus Niedergall** for his continuous support and discussions about (inverse) miniemulsion and related topics like particle formation, monomers and particle characterization. Your input significantly contributed to my work and allowed me the successful preparation of several emulsions and nanoparticles.
- ... **Dr. Thomas Schiestel** for granting me access to his laboratories and **Christopher Hänel** for his help with membrane preparation and membrane characterization.
- ... my PhD colleague from the university of Tübingen **Patricia Weber** and her supervisor **Prof. Dr. Günter Gauglitz** with whom I very successfully collaborated in the joint project „BioMIP - biomimetischer Sensor zur in-line Prozessanalytik“.
- ... my colleague and friend from day one of being a PhD-student **Dr. Alexander Southan** for his constant help and support with questions concerning research, lab techniques and daily routines.
- ... my office mates, colleagues and friends **Tobias Götz, Michael Walz** and **Vanessa Albernaz** for an outstanding working atmosphere, continuous scientific discussions and help with analytical challenges.
- ... the students **Bernd Bäurer, Regina Kowalski, Luise Hilfert, Aziza Mirzayeva, Vanessa Fronk** and **Petra Maier** for their support in the laboratory and their willingness to learn and improve their scientific skills at our institute.
- ... my colleague **Melanie Dettling** for supporting me with analytical questions and organizing the daily lab routines.
- ... the groups **Chemisch-physikalische Grenzflächen (CPG), Partikuläre Systeme und Formulierungen (PSF), Grenzflächentechnologie und Materialwissenschaft (GTM)** for their help, support and for providing such an enjoyably working atmosphere.
- ... the **Ministry of Science, Research and the Arts** of Baden-Württemberg, Germany for funding the project „BioMIP - biomimetischer Sensor zur in-line Prozessanalytik“ (Az: 7533-7-11.6, program “Ideenwettbewerb Biotechnologie und Medizintechnik Baden-Württemberg”).

# III. Contents

<b>I. Declaration of Authorship/Erklärung über die Eigenständigkeit der Dissertation</b>	<b>I</b>
<b>II. Acknowledgments</b>	<b>II</b>
<b>III. Contents</b>	<b>III</b>
<b>1. Abstract/Kurzzusammenfassung</b>	<b>1</b>
<b>2. Introduction</b>	<b>7</b>
<b>3. Structure of Thesis: Working Hypotheses</b>	<b>9</b>
<b>4. Theoretical Background</b>	<b>13</b>
4.1. Emulsions	13
4.1.1. Definition and Denotations	13
4.1.2. Emulsifiers	14
4.1.3. Colloidal Stability: EDL and (X)DLVO-Theory	19
4.1.4. Means of Emulsification: Rotor-Stator, Probe Sonication and High-Pressure Homogenization (HPH)	24
4.1.5. Emulsion Stability: Droplet Loss Mechanism	27
4.1.6. Different Types of Emulsion-based Polymerization Techniques: Suspension-, Macro-, Micro- and Miniemulsion Polymerization	29
4.1.7. Particle Preparation via Miniemulsion Technique	35
4.2. Chitin and Chitosan	37
4.3. Molecular Imprinting	39
<b>5. Preparation of Chitosan Nanoparticles via Emulsion Crosslinking</b>	<b>42</b>
5.1. Hypothesis I.I.	44
5.2. A Systematic Approach of Chitosan Nanoparticle Preparation via Emulsion Crosslinking as Potential Adsorbent in Wastewater Treatment	45
5.3. Abstract	46
5.4. Introduction	46
5.5. Experimental	48

5.5.1. Materials .....	48
5.5.2. Methods.....	49
5.5.3. Characterization of Chi-NPs .....	51
5.6. Results and Discussion.....	53
5.6.1. Preparation of Chi-NPs.....	53
5.6.2. Variation of crosslinker concentration .....	56
5.6.3. Variation of MWs .....	58
5.6.4. Adsorption behavior .....	63
5.7. Conclusions.....	65
5.8. Acknowledgements .....	66
<b>6. Chitosan Nanoparticles as Adsorber in Mixed-Matrix Membranes .....</b>	<b>67</b>
6.1. Hypotheses I.II and I.III.....	69
6.2. Chitosan Nanoparticles via High-Pressure Homogenization-Assisted Miniemulsion Crosslinking for Mixed-Matrix Membrane Adsorbers.....	70
6.3. Abstract.....	71
6.4. Introduction.....	71
6.5. Experimental.....	74
6.5.1. Materials .....	74
6.5.2. Methods.....	75
6.5.3. Characterization of Chi-NPs and Membranes.....	78
6.6. Results and Discussion.....	80
6.6.1. Preparation of Chi-NPs via HPH .....	80
6.6.2. Static Adsorption .....	85
6.6.3. Dynamic Adsorption.....	89
6.7. Conclusions.....	93
6.8. Acknowledgements .....	94
<b>7. Synthetic Nanoparticles for Sensing.....</b>	<b>95</b>
7.1. Hypotheses II.I and II.II.....	97
7.2. Polymer Nanoparticles via Inverse Miniemulsion Polymerization: Preliminary Results.....	97
7.3. Nano-MIP Based Sensor for Penicillin G: Sensitive Layer and Analytical Validation 105	
7.4. Abstract.....	106
7.5. Introduction.....	106
7.6. Experimental.....	109
7.6.1. Materials .....	109

7.6.2. Methods .....	110
7.6.3. RIFs setup .....	112
7.7. Results and Discussion .....	113
7.7.1. Preparation and Characterization of the Sensitive Layer .....	113
7.7.2. Sensor Stability .....	117
7.7.3. RIFs Measurements – Sensor Calibration .....	118
7.7.4. Cross Sensitivities with Phenylacetic Acid and 6-APA .....	120
7.7.5. Conclusions .....	122
7.7.6. Acknowledgements.....	123
7.8. Supplementary data.....	123
7.8.1. Si-1: Preparation of MIPs/NIPs .....	123
7.8.2. Si-2: Modification of MIPs/NIPs.....	124
7.8.3. Si-3: Characterization of MIPs/NIPs: DLS, FT-IR and SEM.....	124
7.8.4. Si-4: Preparation of the sensor surface: Particle immobilization protocol .....	126
7.8.5. Si-5: Spectral RIFs setup .....	127
7.8.6. Si-6: Evaluation of sensor stability.....	128
7.9. Further Characterization of the MIPs and NIPs: Surface Area via Nitrogen Sorption and Selectivity via ITC .....	128
<b>8. Novel Ionic Liquid-based miniemulsion .....</b>	<b>131</b>
8.1. Hypothesis III .....	132
8.2. Preliminary Results.....	133
8.2.1. Dissolving Chitosan in Ionic Liquids (ILs).....	133
8.2.2. IL Emulsions .....	137
8.3. Miniemulsification of the ionic liquid <i>EMIM Ac</i> in cyclohexane for the preparation of glutaraldehyde-crosslinked chitosan nanoparticles .....	140
<b>9. Discussion.....</b>	<b>145</b>
9.1. Hypothesis I .....	146
9.1.1. Hypothesis I.I.....	146
9.1.2. Hypothesis I.II .....	148
9.1.3. Hypothesis I.III.....	151
9.2. Hypothesis II.....	153
9.2.1. Hypothesis II.I .....	154
9.2.2. Hypothesis II.II.....	155
9.3. Hypothesis III .....	157
<b>10. Conclusion &amp; Outlook .....</b>	<b>161</b>

<b>11. Publications.....</b>	<b>164</b>
<b>12. Appendix.....</b>	<b>165</b>
12.1. Preparation of AMPS Nanoparticles.....	165
12.2. Preparation of SPM Nanoparticles.....	166
12.3. Preparation of MAPTAC Nanoparticles.....	168
12.4. Preparation of NAEMA Nanoparticles.....	169
12.5. ITC control experiments.....	171
<b>13. Image Index.....</b>	<b>172</b>
<b>14. References.....</b>	<b>178</b>



# 1. Abstract/Kurzzusammenfassung

Thesis title:

**Synthesis of bio- and synthetic-based functional nanoparticles via inverse miniemulsion for the adsorption and detection of pharmaceuticals in aqueous media**

In this thesis, bio-based and synthetic nanomaterials in the form of crosslinked nanoparticles for the use in **adsorption-based processes** were prepared via *inverse miniemulsion technique*. The synthesized nanomaterials were used for adsorption applications in water purification or as sensing material.

For the use of nanoparticles as adsorbent in water purification, glutaraldehyde-crosslinked **bio-based nanoparticles** were synthesized. This was achieved by processing an already existing biopolymer – namely chitosan – via inverse miniemulsion crosslinking into chitosan nanoparticles (Chi-NPs). For the use of the nanoparticles in adsorption processes, the chitosan nanoparticles were incorporated into porous mixed-matrix membranes.

The chitosan was characterized via size exclusion chromatography (SEC), nuclear magnetic resonance spectroscopy ( $^1\text{H-NMR}$ ) and rheology, the resulting particles via scanning electron microscope (SEM) as well as dynamic light scattering (DLS). Capillary flow measurement, flux measurements and SEM were applied for the characterization of the prepared membranes.

For the emulsification of chitosan solutions, i.e. the preparation of chitosan nanoparticles, probe sonication as well as high-pressure homogenization (HPH) were used. Both processes were optimized in terms of molecular weight (MW) of the used chitosans as well as emulsification efficiency. For the sonication-based emulsification, the use of six chitosans of different MW was examined ranging from a MW of  $12.7 \text{ kg mol}^{-1}$  up to  $121.4 \text{ kg mol}^{-1}$ . For the HPH process, three different chitosans were used with a MW of  $24.0 \text{ kg mol}^{-1}$  up to  $121.4 \text{ kg mol}^{-1}$ .

The diameter ( $d_p$ ) of the chitosan nanoparticles (Chi-NPs) prepared via sonication-based emulsification ranged from  $100 \text{ nm} \leq d_p \leq 200 \text{ nm}$  and decreased with decreasing MW of chitosan. A similar behavior was observed for particles prepared via high-pressure

## 1 Abstract/Kurzzusammenfassung

homogenization (HPH), although these particles were slightly larger with a span of size ranging from  $d_p$  180 nm for lowest MW Chi-NPs up to  $d_p$  260 nm for the highest MW Chi-NPs.

The adsorption behavior of the particles was determined via high-performance liquid chromatography (HPLC) in static (nanoparticle dispersion) and dynamic (membrane-based) adsorption experiments for diclofenac and carbamazepine. The adsorption capacity of carbamazepine was low ( $\approx 2 \text{ mg g}^{-1}$ ) on the Chi-NPs as well as on the untreated, macroscopic chitosan powder. However, with a maximum of  $\approx 350 \text{ mg g}^{-1}$  the adsorption capacity of diclofenac on Chi-NPs was about ten times higher compared to untreated chitosan powder. Overall, the smallest nanoparticles exhibited the highest adsorption capacity.

The Chi-NPs served as adsorbent material in a mixed-matrix membrane-based water purification processes. The membranes loaded with low MW Chi-NPs showed an adsorption capacity (diclofenac) of  $3.6 \text{ mg m}^{-2}$  which was twice as high compared to a reference membrane containing no nanoparticles.

For the potential use of a layer of immobilized nanoparticles as the sensitive layer in an optical sensor application, **synthetic nanoparticles** were prepared by the polymerization of four different hydrophilic monomers (3-(methacryloylamino)propyl] trimethylammonium chlorid (MAPTAC), 3-sulfopropyl methacrylate potassium salt (SPM), 2-acrylamido-2-methyl-1-propanesulfonic acid sodium salt (AMPS), N-(2-aminoethyl) methacrylamide hydrochloride (NAEMA) in inverse miniemulsion polymerization. With all monomers it was possible to prepare crosslinked nanoparticles with spherical shape and narrow sizes distribution in the size of about 200 nm.

Molecularly imprinted NAEMA-nanoparticles, were successfully prepared using penicillin G (PenG) as template. By the process of molecularly imprinting, an imprint (three dimensional cavity) of the template molecule is created in a crosslinked polymer matrix. The imprint could be imagined as a “negative” of the template. It matches the template in size and shape and can therefore be used for the selective binding/recognition of the template.

After preparation, the particles were chemically modified with azide moieties to allow for a covalent immobilization on the transducer surface via copper (I)-catalyzed azide-alkyne click reaction. The particles were characterized via SEM, DLS, nitrogen adsorption

(Brunauer–Emmett–Teller, BET) as well as isothermal titration calorimetry (ITC). Both, the molecularly imprinted particles (MIPs) and non-imprinted particles (NIPs) were narrowly distributed, spherical shaped particles of comparable size. While the particles kept their spherical shape and low polydispersity ( $PDI < 0.05$ ) after the modification, they had a size of about 400 nm which was twice as large in comparison to the unmodified particles. The binding enthalpy of the MIPs was about three times as high when compared to the NIPs, indicating a successful imprinting of PenG. The particles were immobilized covalently and successfully served as sensitive layer in a *reflectometric interference spectroscopy* (RIfS)-based sensor in cooperation with the University of Tübingen. It was possible to calibrate the sensor and analyze PenG concentrations in aqueous media in range of 0.0015–0.0195 mol L<sup>-1</sup>. The sensitivity of the MIP towards PenG is about twice as high when compared to the NIP. To verify the sensors selectivity, structural building blocks of PenG were tested. The sensor experiments showed a high selective adsorption of PenG on the MIPs compared to the low analytical signal given by the adsorption of the structural building blocks.

In an exploratory approach, the emulsification of ionic liquids (ILs) for the preparation of chitosan nanoparticles in **novel IL-in-oil (inverse) miniemulsion** was investigated. Four different imidazolium-based ILs were tested on their ability to dissolve chitosan. Among these, 1-ethyl-3-methylimidazolium-acetate [Emim] [Ac] showed the best results in order to dissolve chitosan. An empirical approach was successfully applied using several different nonionic surfactants in order to find a suitable formulation for the emulsification of [Emim] [Ac]/chitosan solutions in cyclohexane. With this formulation, it was possible to prepare glutaraldehyde-crosslinked chitosan nanoparticles.

Titel:

**Synthese biobasierter und synthetischer funktioneller Nanopartikel mittels inverser Miniemulsion für die Adsorption und Detektion von Pharmazeutika in wässrigen Medien**

In Rahmen dieser Arbeit wurden biobasierte und synthetische Nanomaterialien in Form von vernetzten Nanopartikeln für den Einsatz in **adsorptionsbasierten Prozessen** mittels inverser Miniemulsionstechnik hergestellt. Die synthetisierten Nanomaterialien wurden für Adsorptionsanwendungen in der Wasseraufbereitung und als Sensormaterial eingesetzt.

Für den Einsatz der Nanopartikel als Adsorber in der Wasseraufbereitung wurden Glutaraldehyd-vernetzte, **biobasierte Nanopartikel** synthetisiert. Dies wurde erreicht, indem ein bereits vorhandenes Biopolymer - namentlich Chitosan - über *inverse Miniemulsionsvernetzung* zu Chitosan-Nanopartikeln (Chi-NPs) verarbeitet wurde. Um die Nanopartikel anschließend in einem Adsorptionsprozess einzusetzen, wurden die Chitosan-Nanopartikel in poröse *Mixed-Matrix* Membranen eingebracht.

Das Chitosan wurde mittels Gelpermeationschromatographie (GPC), Kernspinresonanzspektroskopie ( $^1\text{H-NMR}$ ) und Rheologie charakterisiert, die erhaltenen Nanopartikel mittels Rasterelektronenmikroskop (REM) sowie Dynamische Lichtstreuung (DLS). Zur Charakterisierung der hergestellten Membranen wurden Kapillarfluss-Porometrie, Flussmessungen und REM angewandt.

Für die Herstellung der Emulsionen, sprich zur Herstellung der Partikel, wurde Ultraschallsonotoden- sowie Hochdruckhomogenisierung (HDH) verwendet. Beide Verfahren wurden hinsichtlich des Molekulargewichts (MW) der verwendeten Chitosane sowie der Emulgierungseffizienz optimiert. Für die auf Ultraschallbehandlung basierende Emulgierung wurden sechs Chitosane mit unterschiedlichem Molekulargewicht getestet, die von einem MW von  $12.7 \text{ kg mol}^{-1}$  bis zu  $121.4 \text{ kg mol}^{-1}$  reichen. Für das HDH-Verfahren wurden drei verschiedene Chitosane mit einem Molekulargewicht von  $24.0 \text{ kg mol}^{-1}$  bis  $121.4 \text{ kg mol}^{-1}$  verwendet.

Der Durchmesser ( $d_p$ ) der Chitosan-Nanopartikel (Chi-NPs) hergestellt mittels Ultraschallbehandlung reichte von  $100 \text{ nm} \leq d_p \leq 200 \text{ nm}$  und nahm mit abnehmendem MW des Chitosans ab. Ein ähnliches Verhalten wurde für die über HDH hergestellte Partikel beobachtet. Allerdings waren diese Partikel mit einem Größenbereich von  $d_p 180 \text{ nm}$  (niedrigstes MW-Chi-NPs) bis  $d_p 260 \text{ nm}$  (höchstes MW-Chi-NPs) etwas größer.

Das Adsorptionsverhalten der Partikel wurde mittels Hochleistungsflüssigkeitschromatographie (HPLC) in statischen (Nanopartikeldispersion) und dynamischen (Membran-basierten) Adsorptions-experimenten für Diclofenac und Carbamazepin bestimmt. Die Adsorptionskapazität von Carbamazepin war sowohl auf den Chitosan-Nanopartikeln als auch auf dem unbehandelten makroskopischen Chitosan-Pulver niedrig ( $\approx 2 \text{ mg g}^{-1}$ ).

Mit einem Maximum von  $\approx 350 \text{ mg g}^{-1}$  war die Adsorptionskapazität von Diclofenac an Chi-NPs jedoch etwa zehnmal höher als bei unbehandeltem Chitosanpulver. Insgesamt zeigten die kleinsten Nanopartikel die höchste Adsorptionskapazität. Die Chitosan-Nanopartikel dienten als Adsorbensmaterial in Wasserreinigungsprozessen auf Basis von *Mixed-Matrix*-Membranen. Die Membranen, welche mit den Chitosan-Nanopartikeln (bestehend aus dem nieder MW-Chitosan) beladen wurden, zeigten mit  $3,6 \text{ mg m}^{-2}$  eine doppelt so hohe Adsorptionskapazität (Diclofenac) im Vergleich zu einer Referenzmembran, die keine Nanopartikel enthielt.

Für die mögliche Verwendung einer immobilisierten Schicht aus Nanopartikeln als sensitive Schicht in einer optischen Sensoranwendung wurden **synthetische Nanopartikel** durch Polymerisation vier verschiedener hydrophiler Monomere (3-(methacryloylamino)propyl] trimethylammonium chlorid (MAPTAC), 3-sulfopropyl methacrylate Kalium-Salz (SPM), 2-acrylamido-2-methyl-1-propanesulfonsäure Natrium-Salz (AMPS) und N-(2-aminoethyl) methacrylamid hydrochlorid (NAEMA) in inverser Miniemulsionspolymerisation hergestellt. Mit allen Monomeren konnten vernetzte Nanopartikel mit sphärischer Form und enger Größenverteilung ( $\text{PDI} > 0,16$ ) in der Größe von ca. 200 nm hergestellt werden.

Molekular-geprägte NAEMA-Nanopartikel (N-(2-Aminoethyl) methacrylamid-Hydrochlorid) wurden erfolgreich mit Penicillin G als Templat hergestellt. Durch den Vorgang des molekularen Prägens wird ein Abdruck (dreidimensionaler Hohlraum) des Templatmoleküls in einer vernetzten Polymermatrix erzeugt. Der „Prägung“ kann als "Negativ" der Vorlage angesehen werden. Es stimmt in Größe und Form mit dem Templat überein und kann daher zum selektiven Binden / Erkennen der Vorlage verwendet werden.

Anschließend wurden die Partikel mit Azid-Funktionen chemisch modifiziert. Dies ermöglichte eine kovalente Immobilisierung auf der *Transducer*-Oberfläche über eine Kupfer (I)-katalysierte Azid-Alkin-Clickreaktion. Die Partikel wurden mithilfe von REM,

## 1 Abstract/Kurzzusammenfassung

DLS, Stickstoffadsorption (Brunauer–Emmett–Teller, BET) sowie Isotherme Titrationskalorimetrie (ITC) charakterisiert. Sowohl die geprägten Nanopartikel (MIPs) als auch die ungeprägten Nanopartikel (NIPs) waren eng verteilte, sphärisch geformte Partikel vergleichbarer Größe. Während die Nanopartikel nach der Modifikation ihre Kugelform und niedrige Polydispersität ( $PDI < 0,05$ ) beibehielten, wiesen sie eine Größe von etwa 400 nm auf, die im Vergleich zu den unmodifizierten Partikeln doppelt so groß war.

Die Bindungsenthalpie der MIPs (molekular-geprägte Partikel) war im Vergleich zu den NIPs (nicht-geprägte Partikel etwa dreimal so hoch, was auf eine erfolgreiche Prägung von PenG hindeutet. In Zusammenarbeit mit der Universität Tübingen wurden die Partikel kovalent immobilisiert und dienten als sensitive Schicht in einem auf Reflektometrische Interferenzspektroskopie (RifS)-basierenden Sensor. Es war möglich, den Sensor zu kalibrieren und die PenG-Konzentration von  $0,0015 \text{ mol L}^{-1}$  bis  $0,0195 \text{ mol L}^{-1}$  in wässrigen Medien zu analysieren. Um die Selektivität der Sensoren zu überprüfen, wurden strukturelle Bausteine von Pen G getestet. Die Sensorexperimente zeigten eine hohe selektive Adsorption von Pen G an den MIPs im Vergleich zu dem niedrigen Messsignal, das durch die Adsorption der Strukturbausteine erhalten wurde.

In einem dritten Forschungsprojekt wurde die Emulgierung ionischer Flüssigkeiten (ILs; engl. *Ionic Liquids*) zur Herstellung von Chitosan-Nanopartikeln in **neuartigen (inversen) IL-in-Öl-Miniemulsionen** untersucht. Es wurden vier Imidazolium-basierte ILs auf Ihre Fähigkeit getestet, Chitosan zu lösen. Unter diesen zeigte das 1-Ethyl-3-methylimidazoliumacetat [Emim] [Ac] die besten Ergebnisse beim Lösen von Chitosan. Ein empirischer Ansatz wurde erfolgreich angewandt, um eine geeignete Tensidmischung für die Emulgierung von [Emim] [Ac] / Chitosan-Lösungen in Cyclohexan zu finden. Mit dieser Formulierung war es möglich, Glutaraldehyd-vernetzte Chitosannanopartikel herzustellen.

## 2. Introduction

Providing clean water will be one of the major challenges of the next decades to come (Jury and Vaux 2005). Hence, improved techniques and materials for the removal of pollutants as well as the monitoring of the water quality are of great interest. Next to oxidation processes, the process of adsorption is an important tool for water remediation (Westerhoff, Yoon, et al. 2005). The controlled removal of pollutants from aqueous media via adsorption is a critical step. Common pollutants in drinking water (surface and groundwater) are active pharmaceutical ingredients (APIs). Next to several other drugs like hormones and antibiotics, two of these APIs – namely diclofenac (DCL) and carbamazepine (CBZ) – are the most frequently detected ones (Zhang, Geissen, et al. 2008). The adsorption of small organic molecules from aqueous media via adsorption is a critical step not only for water remediation but also for the sensing i.e. detection of substances in aqueous media. Next to the detection of small molecules in drinking water and/or wastewater samples, such a sensing technique is also of great interest for biotechnological applications. The vast majority of the biotechnological production processes are run in aqueous media. For process control (conversion, byproducts, stability), an adsorption-based in-line sensing would be a valuable tool.

As adsorption is a process that occurs at the interface between the adsorbent and its surrounding media, the provided surface area is highly relevant. In comparison to other material classes, nanomaterials and especially nanoparticles possess properties, which are favorable for adsorption applications (Santhosh, Velmurugan, et al. 2016). Besides their defined architecture, particularly the high surface to volume ratio, i.e. the high specific surface area, is beneficial (Hristovski, Baumgardner, et al. 2007).

Among these nanomaterials, polymer nanoparticles are of great interest for adsorption applications. Due to the broad variety of existing polymeric materials, the particle properties can be controlled by choosing a certain polymer or polymer compositions. For the remediation of water, a raw material from a renewable, biobased source is desirable. Chitosan, a derivative of the second most abundant polysaccharide chitin shows promising adsorption capabilities for a variety of substances. Chitin is mainly found in crustacean shells such as shrimp, crab, lobster, which are available as waste from the seafood processing industry (Kurita 2006). For the selective adsorption of small molecules, which is needed for an application in a sensing platform, the polymerization of synthetic

## 2 Introduction

monomers via a molecular imprinting technique is a promising approach. During polymerization, the target molecule gets “imprinted” in the polymer matrix, leading to an increased affinity of the polymeric material towards the imprinted molecule in an adsorption process.

For the preparation of biobased (chitosan) nanoparticles as well as for the synthesis of molecularly imprinted nanoparticles a suitable preparation technique needs to be applied. Nanoparticle preparation based on miniemulsions is the best choice. In comparison to other emulsion-based systems, this technique allows the use of polymeric substances such as chitosan, as no considerable diffusion is required. Additionally, in miniemulsion the droplets keep their droplet identity during the process, which is preferred for molecularly imprinting.



### 3. Structure of Thesis: Working Hypotheses

In this thesis, three main topics were investigated. All three topics are based on the use of inverse miniemulsion technique for the preparation of polymer nanoparticles (Fig. 1).

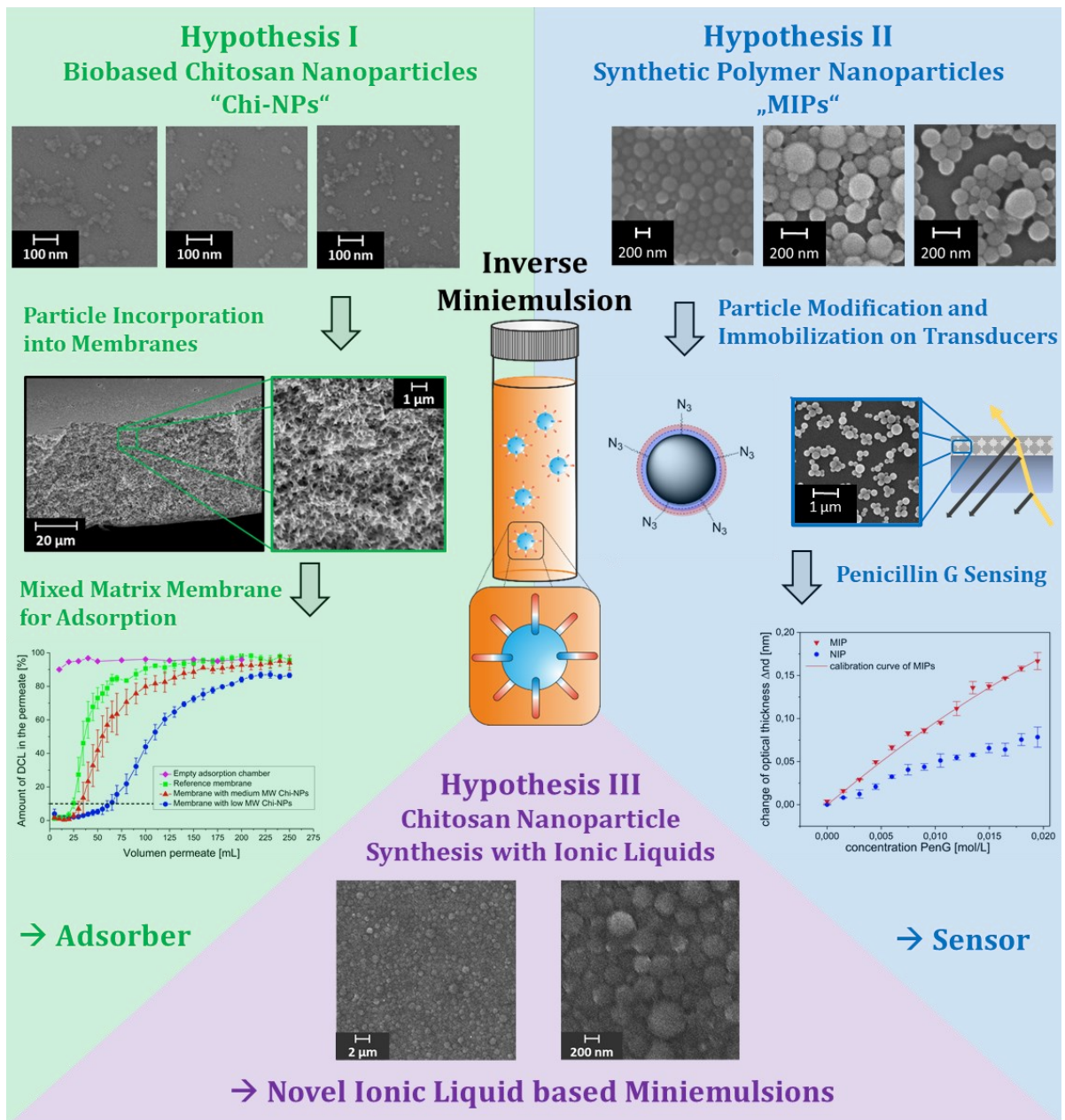


Fig. 1 Structure of this thesis and schematic representation of the three main topics a) "Biobased Chitosan Nanoparticles", b) "Synthetic Nanoparticles" and c) "Chitosan Nanoparticles - Synthesis with Ionic Liquids" which were investigated. All three topics are based on the use of inverse miniemulsion technique for nanoparticle preparation.

### 3 Structure of Thesis: Working Hypotheses

The preparation of biobased chitosan nanoparticles for water remediation (Hypothesis I), the preparation of molecularly imprinted synthetic nanoparticles for the application as sensitive layer in a sensor application (Hypothesis II) and the preparation of novel ionic-liquid (IL) based *IL-in-oil (inverse) miniemulsion* for the preparation of chitosan nanoparticles (Hypothesis III).

For each topic hypotheses were developed. Each hypothesis was clustered in sub hypotheses. The scopes of these hypotheses are introduced and discussed on the following pages.

The results on which the discussion of the hypotheses is based are presented in chapter 5, 6, 7, and 8 followed by the discussion of the hypotheses in chapter 9. The conclusions and an outlook is given in chapter 10.

#### First hypothesis block – Chapter 5 & 6

The first hypothesis block Fig. 1 (a) consist of hypothesis I.I, I.II and I.III, which addresses the development of different synthesis strategies for chitosan nanoparticles (Chi-NPs) and their use as adsorbent for pharmaceuticals. Subsequently, the Chi-NPs were incorporated into flat sheet polymer membranes in order to prepare mixed-matrix membrane absorbers for the adsorption of pharmaceutical compounds from aqueous media. The results of the experiments for the discussion of hypothesis I.I can be found in chapter 5 “Preparation of Chitosan Nanoparticles via Emulsion Crosslinking”. The experimental results for the discussion of hypothesis I.II and I.III are presented in chapter 6 “Chitosan Nanoparticles as Adsorber in Mixed-Matrix Membranes”. The discussion of the hypotheses can be found in chapter 9.1. The hypothesis for this part reads as follows:

#### Hypothesis I.I: Chapter 5

*It is possible to prepare crosslinked chitosan nanoparticles (Chi-NPs) reproducibly via inverse miniemulsion crosslinking technique using highly deacetylated chitosans with different molecular weight.*

- *The molecular weight (MW) has an impact on particle size.*
- *Compared to pristine chitosan, the crosslinked Chi-NPs show a superior adsorption behavior for a relevant active pharmaceutical ingredient (API).*

### **Hypothesis I.II: Chapter 6**

*It is possible to transfer an emulsion formulation, which was optimized for a discontinuous ultrasonication emulsification to a continuous high-pressure homogenization (HPH)-based process.*

- *Similar to the ultrasonication emulsification it is possible to process chitosan of different MW via high-pressure homogenization to reproducibly prepare Chi-NPs.*

### **Hypothesis I.III: Chapter 6**

*It is possible to disperse the Chi-NPs from 1.2 in a membrane polymer solution in order to prepare Chi-NP loaded mixed-matrix membranes.*

- *The Chi-NP mixed-matrix membranes can be applied for the adsorption of pharmaceutical compounds in aqueous media.*

## **Second hypothesis block – Chapter 7**

The second hypothesis block Fig. 1 (b) consist out of hypothesis II.I and II.II, which addresses the development of synthesis strategies for synthetic polymer nanoparticles which are potentially usable for molecular imprinting of penicillin G. Subsequently, these particles were chemically functionalized in order to immobilize them on a sensor transducer surface for the preparation of an optical penicillin G sensor. The sensor technology and the measurements were conducted in cooperation with the University of Tübingen. The results of the experiments for the discussion of hypothesis II.I and II.II can be found in chapter 7 “Synthetic Nanoparticles for Sensing”. The discussion of the hypotheses can be found in chapter 9.2. The hypothesis for this part reads as follows:

### **Hypothesis II.I:**

*By using appropriate functional monomers, it is possible to prepare imprinted polymer nanoparticles via miniemulsion polymerization, which exhibit a selective adsorption behavior towards penicillin G.*

#### **Hypothesis II.II:**

*Through suitable functionalization of the nanoparticles they can be covalently immobilized on the sensor surface.*

- *This covalently immobilized sensitive layer is impervious against overflow in the measuring chamber and despite the functionalization still bears its ability to selectively bind penicillin G in aqueous solution.*
- *The covalent immobilization benefits the sensors lifespan.*

#### **The third hypothesis – Chapter 8**

The third hypothesis Fig. 1 (c) addresses the development of synthesis strategies for the preparation of chitosan nanoparticles in novel ionic liquid emulsions. The goal was to prepare both, *ionic liquid in oil* and *ionic liquid in water* miniemulsions. In order to emulsify chitosan dissolved in ionic liquids, appropriate ionic liquids had to be identified first. Subsequently, surfactants (mixtures) had to be identified to enable the production of stable miniemulsions. The results of these experiments for the discussion of hypothesis III can be found in chapter 8 “Novel Ionic Liquid-based miniemulsion”. The discussion of the hypotheses can be found in chapter 9.3. The hypothesis for this part reads as follows:

#### **Hypothesis III:**

*Chitosan dissolved in an ionic liquid (IL) can act as disperse phase in a miniemulsion formulation in order to prepare crosslinked Chi-NPs.*

- *It is possible to dissolve chitosan in an oil miscible (water immiscible) ionic liquid. This solution can be emulsified in water resulting in an IL-in-water emulsion.*
- *It is possible to dissolve chitosan in a water miscible (oil immiscible) ionic liquid. This solution can be emulsified in oil resulting in an IL-in-oil emulsion.*

## 4. Theoretical Background

The focus of this work was the preparation of nanoparticles via miniemulsion-based synthesis techniques. Hence, the theoretical background relevant for this work with an emphasis on emulsion formulation and colloid chemistry is presented in the following sub chapters.

In the first part of this chapter the basic principles of emulsions and emulsion stability (surfactants, EDL, DLVO theory, droplet loss mechanisms) are presented. In the second part of the chapter, different emulsion-based particle synthesis strategies with an emphasis on the (inverse) miniemulsion are explained. Further, the properties of chitosan, the basic principles of molecular imprinting and the fundamentals of adsorption processes are discussed.

### 4.1. Emulsions

In this chapter, the basic principles of emulsions, their stabilization, formation and different emulsion types are reviewed. Considering the core of this work, the explanations in this chapter are focused on inverse emulsions and inverse emulsion polymerization techniques.

#### 4.1.1. Definition and Denotations

An **emulsion** is a fine dispersed mixture of one or more liquids in another immiscible liquid. The definition in the *Compendium of Chemical Terminology* (IUPAC) is as follows:

*“A fluid colloidal system in which liquid droplets and/or liquid crystals are dispersed in a liquid. The droplets often exceed the usual limits for colloids in size. An emulsion is denoted by the symbol O/W if the continuous phase is an aqueous solution and by W/O if the continuous phase is an organic liquid (an 'oil'). More complicated emulsions such as O/W/O (i.e. oil droplets contained within aqueous droplets dispersed in a continuous oil phase) are also possible.[...]”*(Quotation: Sawai & Orgel, 2009)

## 4 Theoretical Background

O/W (Oil-in-Water) emulsions are also denoted as *direct* emulsions, while W/O (water in oil) emulsions are called *inverse* emulsions. In the case of an O/W emulsion, the oil is *dispersed* (oil droplets) in an aqueous *continuum*. Hence, the oil acts as *disperse phase* whereas the water phase acts as *continuous phase*. Consequently, for a W/O (inverse) emulsion these terms are used conversely i.e. the water is the *disperse phase* while the oil is the *continuous phase*.

The general accepted definition of **nanomaterials** is a material which has one or more dimensions < 100 nm. Several of these definitions, from the European Union, US-government initiatives, and many more were summarized by Kreyling et al. (2010).

The definition of **nanoparticles** on the other hand is still a matter of debate. The current edition of the IUPAC *Compendium of Chemical Terminology*, the so-called “Gold Book”, contains no definition of nanoparticles as of yet (Sawai and Orgel 2009). However, there is an IUPAC recommendation from 2012, which states that nanoparticles are “particles in any shape with a dimension in the range of 1 nm to 100 nm”. Additionally, the definition allows to extend the use of the prefix “*nano*” for particles up to 500 nm, if their properties, for example dispersion stability, are attributed to their size in the nanometer range (Vert, Doi, et al. 2012). Further, a *nanosphere* is also a *nanoparticle*, but its shape is defined as spherical, meaning the term *nanosphere* is included in the term *nanoparticle*.

To be precise in accordance to the IUPAC-definitions, all *nanomaterials* prepared in this work are *nanospheres*. However, the use of the term *nanoparticle* for spherical nanoparticles is generally accepted in the colloid community. Hence, throughout this work the term *nanoparticle* instead of *nanosphere* is used.

### 4.1.2. Emulsifiers

When two immiscible liquids (oil and water) are mixed by means of stirring, agitation or high shear forces a dispersion of droplets i.e., an emulsion will form. Such a colloidal suspension is highly unstable and will rapidly demix mostly in the order of seconds to minutes, resulting in the pristine macroscopic oil- and water-phase (Fig. 2 A). In order to create stable emulsions, it is necessary to suppress the demixing of the disperse phase (droplets). This is usually done by the addition of an *emulsifier* (Fig. 2 B). There are different types of *emulsifiers* but the most important and widely used class is *surface active compounds* (i.e. *surfactants*).

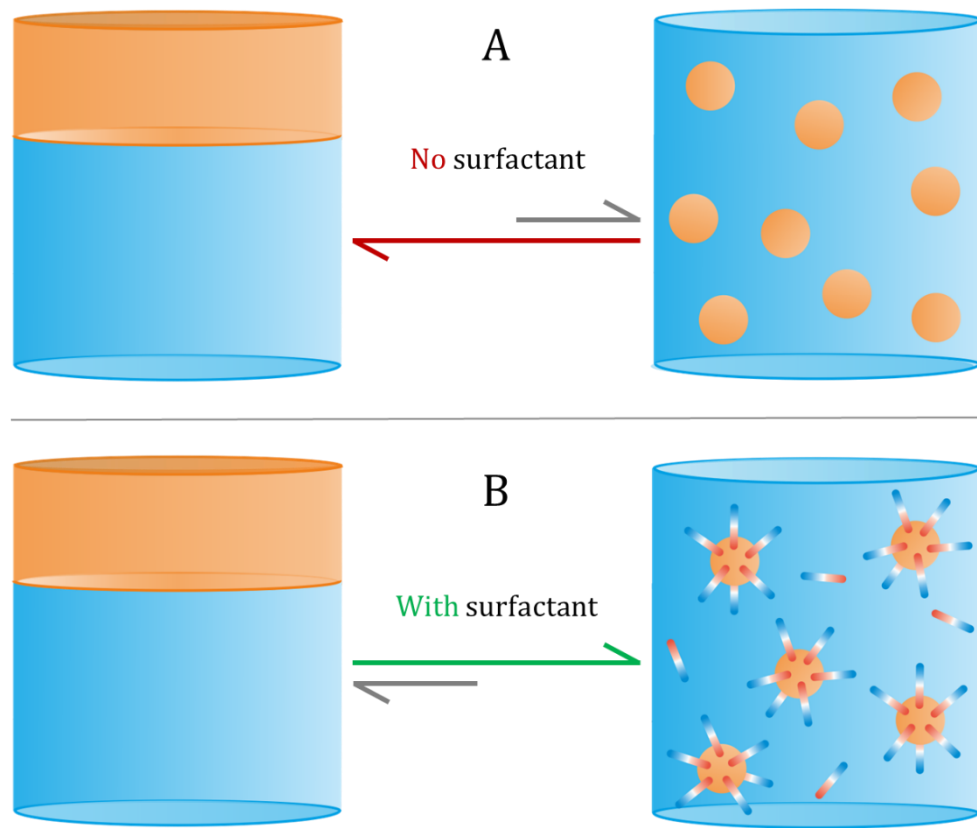


**Fig. 2** Schematic representation of demixing (A) and stabilization (B) process with and without surfactant in an oil in water (O/W) emulsion.

A main characteristic of surfactants is their amphiphilic behavior meaning they have a polar and nonpolar part. Surfactants have a water-soluble (hydrophilic) “head group” and a water insoluble i.e. oil soluble (hydrophobic) “tail” (Fig. 3).

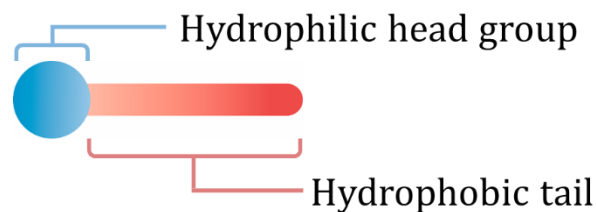


**Fig. 3** Schematical representation of a surfactant.

Although all surfactants are amphiphilic, it should be noted that this does not apply vice versa. For example, ethanol is by definition amphiphilic, but it is not considered to be a surfactant (Davis 1994). A surfactant has to be surface active, i.e. it has to be able to form a layer of surfactant molecules along the interface between the dispersed and the

## 4 Theoretical Background

continuous phase. The accumulation of surfactants at that interface leads to a decrease in surface tension, which ultimately leads to the stabilization of the droplets.

Surfactants are subdivided in two main classes regarding their chemical composition: nonionic surfactants (also sometimes referred to as polymeric surfactants) and ionic surfactants. The group of ionic surfactants can be further clustered into anionic and cationic. Special subtypes, for example gemini surfactants or zwitterionic surfactants will not be discussed in this work. Table 1 shows several examples of above-mentioned surfactants. Structure, type name and HLB-value (hydrophilic lipophilic balance) are shown.

Besides the decrease in surface tension, secondary stabilizing mechanisms can take effect. The manner of these effects depends on the type of surfactant (Holmberg, Jönsson, et al. 2002).

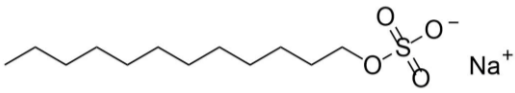
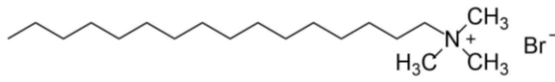
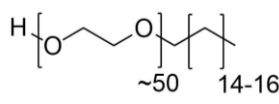
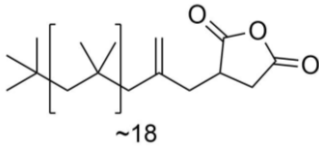
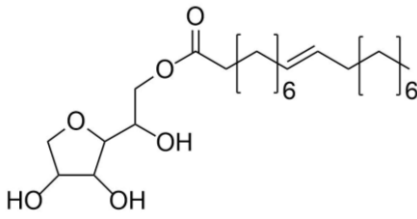
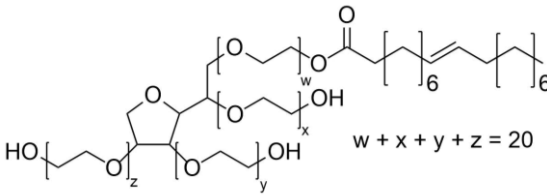
Ionic surfactants (in particular anionic ones) lead to electrostatic stabilization of the emulsion droplets. When the surfaces of charged droplets come in close proximity to each other, the diffuse double layers start to overlap resulting in repulsive interaction.

In contrast to electrostatic stabilization, nonionic (polymeric) surfactants can promote a steric stabilization. The long polymer chains located at the droplet interface prevent droplets from coming in too close proximity.

SDS and CTAB are members of the class of anionic and cationic surfactants respectively. Due to their charged headgroups, anionic surfactants are susceptible to the presence of electrolytes and/or change in pH in the emulsion system. Both factors decrease the effectiveness of ionic surfactants and can ultimately lead to a destabilization of an emulsion. By comparison, nonionic surfactants are considerably less vulnerable to the factors mentioned above. The stabilization and destabilization mechanisms of emulsions will be discussed in more detail in the next chapter *4.1.3 Colloidal Stability: EDL and (X)DLVO*. Lutensol is an example of the class of widely used fatty alcohol ethoxylates. PIBSA is an example for polyisobutylene-based surfactants, which are used as lubricants in engine oils or as additives in the preparation of explosives (Giesecking, Jäck, et al. 2012).



Table 1 Structure, type, name and HLB-value of different anionic, cationic and nonionic surfactants.

Structure	Type/Name	HLB
 <p><math>M = 288.4 \text{ g mol}^{-1}</math></p>	<b>Anionic</b> surfactant Sodium dodecyl sulfate <b>(SDS)</b>	<b>40</b> (Y. Kong et al. 2015)
 <p><math>M = 364.5 \text{ g mol}^{-1}</math></p>	<b>Cationic</b> surfactant Cetyltrimethylammonium bromide <b>(CTAB)</b>	<b>10</b> (Doolaanea et al. 2015)
 <p><math>M \approx 2500 \text{ g mol}^{-1}</math></p>	<b>Nonionic</b> surfactant Fatty alcohol ethoxylate <b>(Lutensol® AT 50)</b>	<b>18</b> (Ash and Ash 2004)
 <p><math>M \approx 1000 \text{ g mol}^{-1}</math></p>	<b>Nonionic</b> surfactant polyisobutylene succinic anhydride (PIBSA) <b>(Addconate H®)</b>	$\approx 4 - 5$ (Mamedov 2015; SEPPIC 2016)
 <p><math>M = 428.6 \text{ g mol}^{-1}</math></p>	<b>Nonionic</b> surfactant Sorbitan monooleate <b>(Span 80®)</b>	<b>4.3</b> (Debnath et al. 2015)
 <p><math>M = 1227.5 \text{ g mol}^{-1}</math></p>	<b>Nonionic</b> surfactant Polyoxyethylene (20) sorbitan monooleate <b>(Tween 80®)</b>	<b>15</b> (Debnath, Saha, et al. 2015)

## 4 Theoretical Background

Tween 80 and Span 80 are both sorbitan based surfactants. While both are esters of sorbitan and oleic acid, Tween 80 additionally is polyethoxylated. The introduction of polyethoxylate groups increases the water solubility and as a result, Tween 80 is a good surfactant for O/W emulsion. In contrast, the more hydrophobic Span 80 is predestined for W/O systems.

A general rule describing which surfactant is suitable for which type of emulsion (W/O or O/W) is straight forward. The so called “Bancroft’s rule” states, that *“a surfactant which preferentially partitions into water, favors the formation of oil-in-water (O/W) emulsions, and that a surfactant, which preferentially partitions into oil favors the formation of water in oil (W/O) emulsions”* (Quotation: Davis, 1994).

An important question in emulsion techniques is “which surfactant to use for which emulsion?”

To further subdivide surfactants in regard of their application, a more complex concept, the hydrophilic-lipophilic-balance (HLB) can be applied (Myers 2005). The HLB system allows calculating the HLB value of a nonionic surfactant via the following formula:

$$HLB = 20 * \frac{M_h}{M}$$

$M_h$  = molecular weight of surfactants’ hydrophilic part

$M$  = molecular weight of the whole surfactant

The resulting HLB values can theoretically range between 0 and 20. However, a molecule with a HLB of 0 (or 20) would only consist of hydrophobic (or hydrophilic) groups and would therefore possess no amphiphilic character i.e. would not be a surfactant. HLB values of amphiphilic substances usually are in the range between 1 and 19 while 4 is a very hydrophobic and 18 a very hydrophilic surfactant. Table 2 shows the application of surface-active substances depending on their HLB value.

It should be pointed out that nonionic surfactants can cover the whole HLB range. Especially due to adjustable degrees of ethoxylation (hydrophilic groups), it is possible to produce different surfactants. A W/O emulsion can be stabilized by using low HLB nonionic surfactants like Span 80 or Addconate H. A styrene-in-water (O/W) emulsion can be stabilized using a high HLB nonionic surfactant, for example Lutensol AT 50.

**Table 2** The range of HLB values and the use/application of the corresponding surface-active substances.

HLB Range	Use
1-3	Anti-foaming agents
4-6	W/O emulsifiers
7-9	Wetting agents
8-18	O/W emulsifiers
13-15	Detergents
10-18	Solubilizers

The HLB system is of empirical nature and does not allow for a sounder theoretical characterization of surfactants (Myers 2005). Nevertheless, it is a very useful guideline, when choosing surfactants and is therefore widely used in all fields working with emulsions. The HLB concept was introduced by Griffin in 1949 (Davis 1994). In 1957, Davies introduced a modified version of the HLB concept, which worked via assigning number values for each chemical group. This method better accounts for hydrophilic groups.

One drawback of the HLB concept is its unsuitability for the calculation of reliable HLB values for ethoxylated hydrocarbons, as they can undergo phase inversion at a certain temperature. This phase inversion temperature (PIT) depends on the lower critical solution temperature (LCST) of the surfactant. An “LCST” behavior is common, especially amongst ethoxylated surfactants. As the PIT concept accounts for these special properties, Shinoda and co-workers proposed that the HLB should be replaced by the PIT concept especially for ethoxylated surfactants (Davis 1994).

There are other, less commonly used concepts, for example the “Hydrophilic-Lipophilic Difference” (HLD), which will not be further discussed in this work.

#### **4.1.3. Colloidal Stability: EDL and (X)DLVO-Theory**

Independent of which system or concept (HLB, PIB, HLD...) a surfactant was chosen, the mechanisms of stability/instability in colloidal systems (i.e. emulsions) can be described by the DLVO theory. It was named after Derjaguin, Landau, Verwey and Overbeek and was developed in the first half of the 20<sup>th</sup> century (Matthews and Rhodes

#### 4 Theoretical Background

1970). In general, the DLVO theory describes the potential interaction energy between two surfaces of colloids, such as emulsion droplets, nanoparticles and similar systems. For the discussion of the DLVO theory, it is necessary to introduce various surface phenomena. One of the main stabilizing forces, which prevent colloids from aggregating, is the electrical double layer (EDL) (Fig. 4). The EDL plays a vital role in the DLVO theory as it represents a major repulsive force, which prevents two colloids from aggregating.

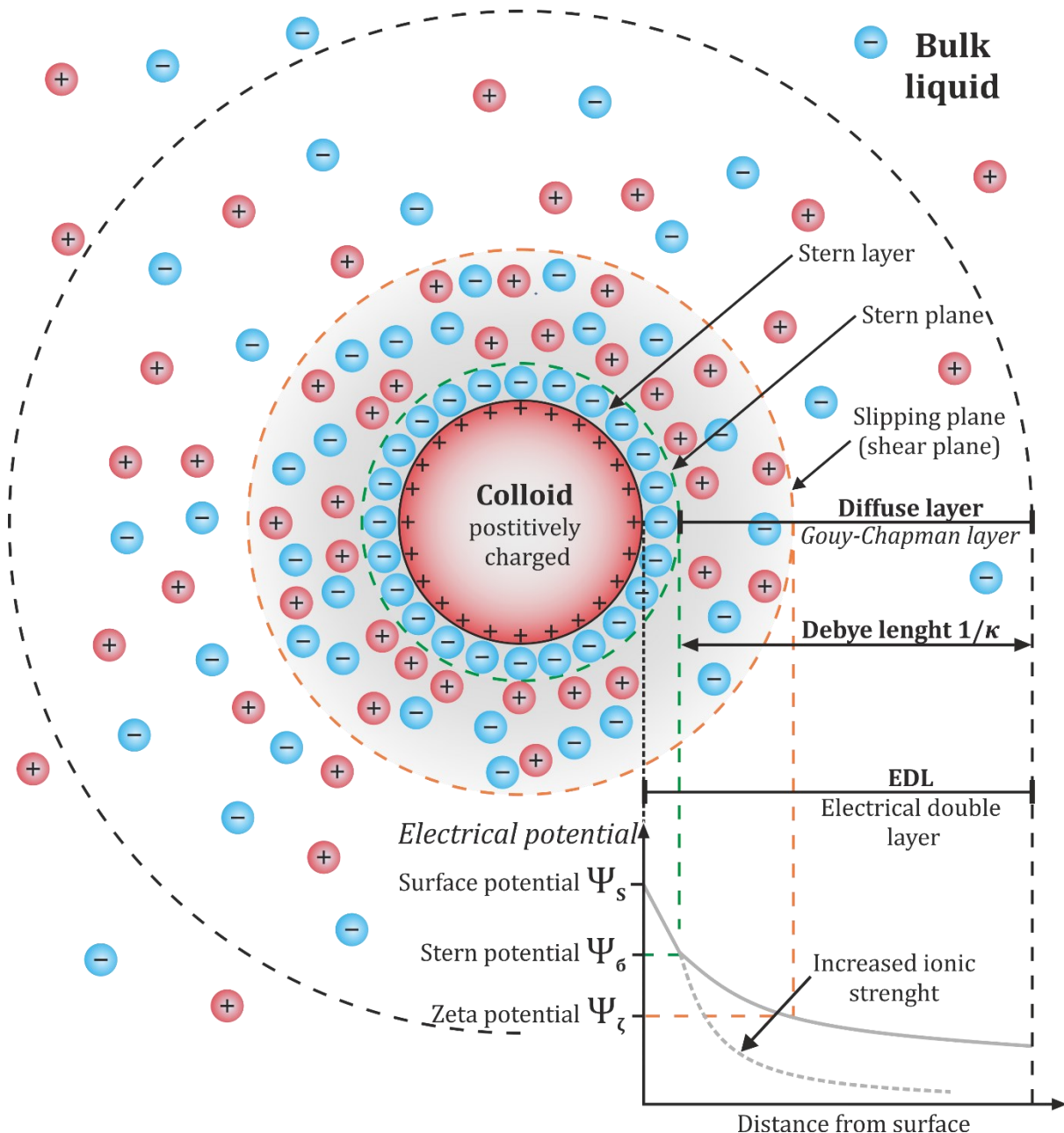


**Fig. 4** Schematical representation of the electrical double layer (EDL). Own representation based on (M. A. Alsharif, Taha, et al. 2017)

In Fig. 4, the different electric layers and the electric potential as a function of the distance from the surface is shown on the example of a positively charged colloid.

In the middle of the 19<sup>th</sup> century, Helmholtz was the first, who suggested the model of a layer of oppositely charged ions on a charged surface. In the beginning of the 20<sup>th</sup> century, Gouy and Chapman developed the “Gouy-Chapman model” which accounted for the ion concentration and the decrease of electric potential as a function of distance from the surface in form of a diffuse layer. Otto Stern combined both, the Helmholtz and Gouy-Chapman model in 1924. The EDL can be divided into two main layers. The first layer, the so-called “Stern layer” describes the adhered ions on the surface and can be further subdivided into an inner and outer Helmholtz plane (not shown in the representation). The electrical potential decreases in a linear manner while moving outwards through this layer (Hiemenz 1977; Israelachvili 2011).

The second layer, the diffuse part of the EDL (Gouy-Chapman layer) begins at the end of the Stern plane (i.e. outer Helmholtz plane). The length of this layer is called Debye length. This length indicates the distance into the solution up to which the ions *feel* the effect of the surface. Further out the ions are in the bulk liquid and are not affected by the EDL. The Debye length is highly influenced by the concentration of ions in the solution (Oldham 2008). Due to the shielding of charge at the solid solution interface, the extent of the double layer decreases with increase in ion concentration. Ions of higher valence are more effective in screening the charge.

The shear plane (or slipping plane) is located inside the double layer, somewhat farther out than the Stern layer. The shear plane is the distance at which relative motion sets in between the immobilized layer (Stern layer) and the diffuse layer, when liquid moves past the colloids surface. The potential of this surface is known as *zeta potential* ( $\zeta$ ). Based on the zeta potential the type (positive, negative, neutral) and the magnitude of surface charge can be determined. Usually experimental techniques such as electrophoresis or electroosmosis are applied in order to determine the zeta potential i.e. the charge of a colloid.

The EDL represents one of the major repulsive forces in the DLVO theory. The DLVO theory describes the potential interaction energy between two colloidal surfaces (Fig. 5.). In the case of emulsion droplets, the surface characteristics are mainly governed by the surfactant type and surfactant composition. The DLVO theory sums the repulsive ( $V_R$ ) and attractive ( $V_A$ ) forces and combining them to the superposition net potential energy ( $V_T$ ) as in  $V_T = V_A + V_T$  (Polte 2015). The course of this graph allows discussing the forces which are involved in stabilizing and destabilizing a colloidal system.

#### 4 Theoretical Background

These forces are shown in detail in Fig. 5. The main attractive force  $V_{A(V)}$  in the DLVO theory are the Van der Waals forces. The main repulsive force  $V_{R(EDL)}$  originates from the electrical double layer. The weaker repulsive Born-forces  $V_{R(B)}$  become important in close proximity to the surface.

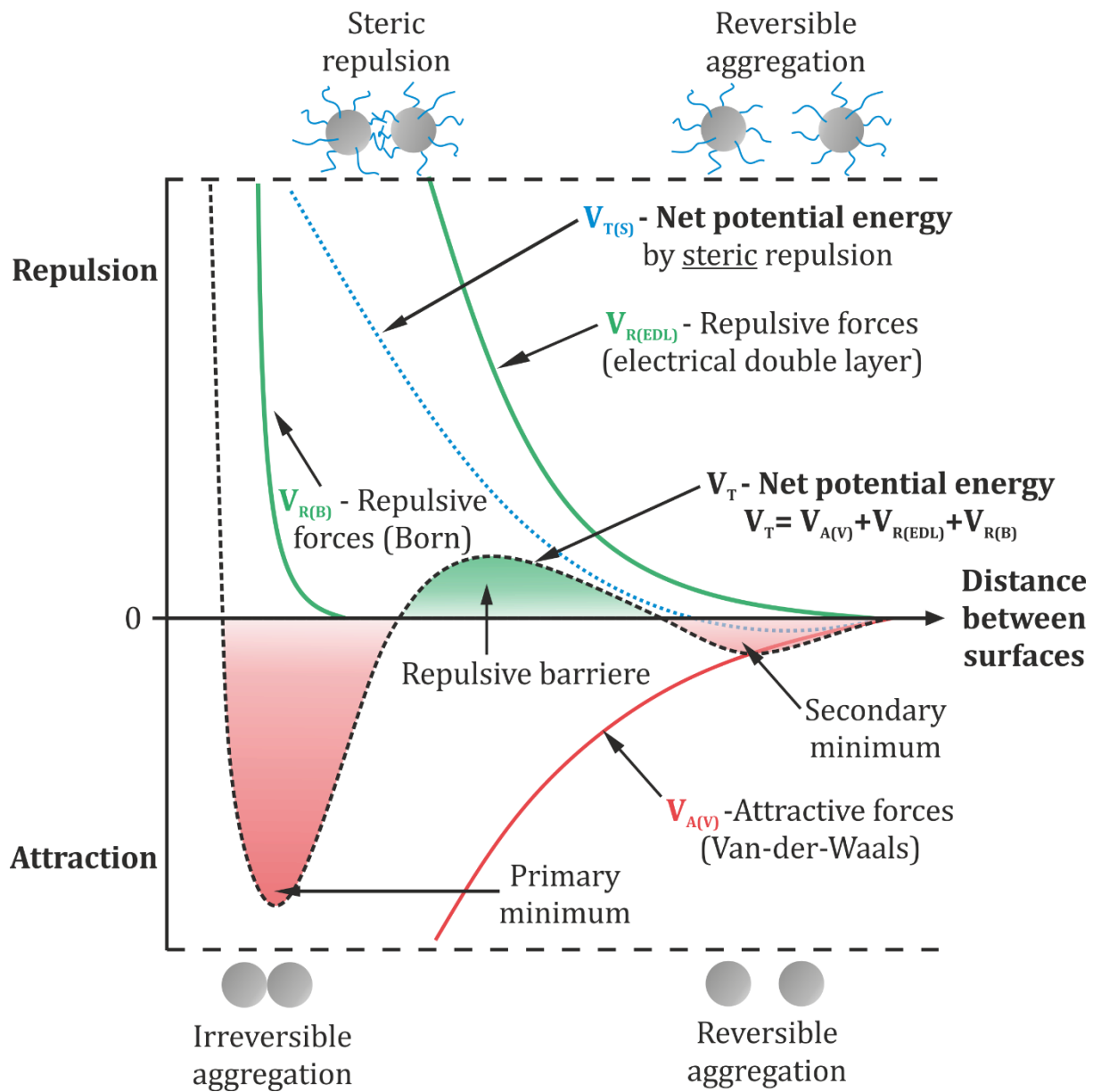


**Fig. 5** Schematical representation of DLVO and XDLVO.

Building the sum of attractive and repulsive forces results in a superposition called the net potential energy  $V_T$ . In the case of  $V_R \gg V_A$  the colloidal system is indefinitely stable in terms of agglomeration (not accounting for other destabilization mechanism like Ostwald

ripening in the case of emulsions). In the opposite case ( $V_R \ll V_A$ ) the colloids will agglomerate instantly. If  $V_A \approx V_R$  (as indicated by the black, dashed line in the graph) a *primary minimum* and *secondary minimum* as well as a *repulsive barrier* is present (Matthews and Rhodes 1970). The attractive *van der Waals forces* are largely insensitive to variations in electrolyte concentration and pH. Hence, the height of the *repulsive barrier* and the position of the *secondary minimum* mainly depend on the electrolyte concentration, as electrolytes greatly affect the characteristics of the *electrical double layer*. In general, for highly charged colloids, a low electrolyte concentration results in a high *repulsive barrier* and an increased *Debye length* (Israelachvili 2011).

In a more concentrated electrolyte solution, the range of the *electrical double layer* decreases (due to shielding) and a significant *secondary minimum* will be formed in closer proximity to the *repulsive barrier*. The *primary minimum* exists at close proximity to the surface and is caused by the *Born forces*, which are increasingly strong at close range.

In order for the colloids to reach the primary minimum, the *repulsive barrier* must be surmounted. If the height of the barrier greatly exceeds the thermal energy of the colloids, they will not overcome the barrier. A value of about 50 mV (zeta potential) is considered sufficient to prevent colloids from reaching the *primary minimum*. If the *secondary minimum* isn't deep, it has no effect on the colloids and they will simply remain totally dispersed. In this case, the colloids are *kinetically stable* as opposed to being *thermodynamically stable*. In the case of thermodynamic stability, agglomerates would lead to an increase in free energy and, therefore, are thermodynamically unfavorable. However, if the *secondary minimum* is distinct enough, colloids will form loose aggregates, which are reversible and can readily be broken by agitation or dilution (means: "moving" the colloids out of the minimum).

Lastly, if the *repulsive barrier* is lowered sufficiently due to increased electrolyte concentration (or it is not existing at all), the colloids will come into close proximity (*primary minimum*), ultimately resulting in irreversible agglomeration.

The DLVO-theory mainly describes colloid stability induced by the *electrical double layer*. This is the case for particles with a charged surface, or in the case of emulsions, droplets covered by ionic surfactants. Particles with a low charge i.e. no significant zeta potential can be stabilized with the help of nonionic (polymeric) surfactants. For emulsions this means that they can be stabilized without the use of a charged surfactant. As the DLVO-theory does not account for these effects, the extended DLVO-theory (XDLVO) was developed. When using nonionic surfactants, colloidal stabilization is mainly induced by

## 4 Theoretical Background

*steric stabilization* also called *steric repulsion*. In order to promote *steric repulsion*, the polymer or nonionic surfactant needs to be adsorbed onto the colloid's surface/interface. In addition to *steric repulsion* forces the XDLVO-theory is able to account for short range forces, such as osmotic-, bridging- and elastic-forces (Hotze, Phenrat, et al. 2010) which will not be discussed further in this work. The superposition ( $V_{T(S)} = V_{A(V)} + V_{R(B, EDL)} + V_{R(S)}$ ), shown as a function of separation distance between the colloids, is shown in Fig. 5 (blue dotted line). Similar to the classic DLVO this function may also exhibit a *secondary minimum*, which can lead to reversible aggregation. However, there is no primary minimum in the case of *steric repulsion*. As the inter-colloid distance becomes smaller, an increase in entropy, thus an increase of Gibbs free energy will occur, which is thermodynamically unfavorable. As a consequence, colloids coated with polymers (nonionic surfactants) are considerably less prone to irreversible aggregation. This is of practical relevance when it comes to breaking colloidal systems. Unlike for electrostatic forces, the *steric repulsion* forces can usually not be weakened by change in electrolyte concentration or pH.

### 4.1.4. Means of Emulsification: Rotor-Stator, Probe Sonication and High-Pressure Homogenization (HPH)

The three most common high shear devices - also the ones used in this work - *rotor-stator*, *probe sonication* and *high-pressure homogenization* are shown in Fig. 6. In this figure, emulsification on the examples of direct emulsions (oil in water) is shown. However, emulsification works similar for inverse (water in oil) emulsions.

The rotor-stator homogenizer breaks droplets mainly due to inertia forces and via shearing by turbulent flow (Fig. 6 A). The *rotor*, which is built inside in close proximity to the *stator*, turns at a speed ranging from 10 to 50 m s<sup>-1</sup>. The shear intensity can be controlled by varying the speed, the rotor stator geometry and its shear gap. Typical dimensions of the shear gap are 0.1 – 3 mm (Schuchmann and Schuchmann 2005). They can be used in dis-continuous or quasi-continuous mode up to flow rates of about 3500 L min<sup>-1</sup>, which is relevant, if an industrial application is desired (Paul, Atiemo-obeng, et al. 2003). In contrast to the other techniques, rotor-stator systems are suitable especially for the production of emulsions with higher viscosities (20 – 5000 mPa s). The



drawback of this technique is, that it has the lowest energy input of all three techniques, only resulting in a mean droplet diameter of about 2  $\mu\text{m}$  (Schultz, Wagner, et al. 2004).

Fig. 6 B schematically shows the representation of emulsification via *probe sonication*. In this process, emulsification is mainly the result of cavitation, which is induced by the ultrasound waves passing through the liquid. The piezoelectric transducer converts high voltage electrical energy into mechanical vibration. As a result, the tip of the probe/horn expands and contracts longitudinally. If this movement is above a frequency of 20 kHz, it results in the creation of ultrasound waves (T. Y. Wu, Guo, et al. 2013). As the range of these waves is short, the choice of a sufficient probe and the depth of probe immersion are critical. Additionally, the choice of a suitable vessel is important. Further, external stirring or pumping of the mixture during sonication may be necessary, especially when emulsifying larger volumes. The compression and expansion of the molecular distance in the liquid medium, resulting from the ultrasonic waves, creates small cavities (e.g. vacuum bubbles or cavitation bubbles). Under constant sonication, these bubbles will eventually reach a critical size, at which they violently collapse (Santos, Lodeiro, et al. 2008). The process of bubble formation, bubble growth and eventually its collapse (implosion) happens in the range of hundreds of microseconds. This implosion causes a variety of extreme local effects in from of a pressure of  $\sim 1000$  bar, a rise in temperature of  $\sim 5000$  K and liquid microjets with a velocity of  $\sim 250$   $\text{m s}^{-1}$  (Bang and Suslick 2010). These microjets produce asymmetrical shockwaves, which lead to droplet breaking (T. Y. Wu, Guo, et al. 2013). This cavitation process can lead to formation of small droplet sizes below 0.4  $\mu\text{m}$  (Schultz, Wagner, et al. 2004). Interestingly, these extreme conditions created during acoustic cavitation can result in light emission (Bang and Suslick 2010). Compared to the rotor-stator system, probe sonication has a sufficient power input. However, the drawback of sonication is its difficult scalability. Therefore, it is mostly used in laboratories for the preparation of small emulsion batches, usually in the range of hundreds of milliliters.

## 4 Theoretical Background

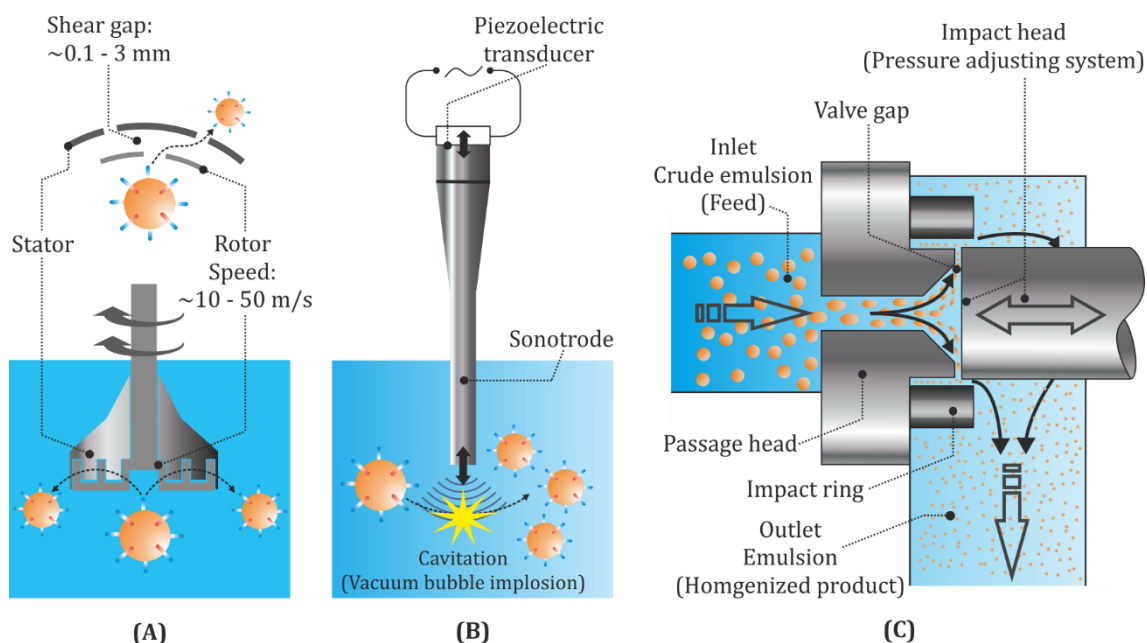


**Fig. 6** The three homogenization devices used in this work. (A) rotor-stator, (B) probe sonication and (C) high-pressure homogenizer (HPH). Schematical representation of the preparation of oil-in-water emulsions. Schematic representation of the high-pressure homogenizer (C) is an own representation based on [https://commons.wikimedia.org/wiki/File:Homogenizing\\_valve.svg](https://commons.wikimedia.org/wiki/File:Homogenizing_valve.svg) (accessed in September 2020)

The third homogenization device used in this work is the *high-pressure homogenizer* (HPH) as shown in Fig. 6 C. Next to forces of inertia and turbulent shearing, cavitation also contributes to droplet disruption. The mixture is pumped through the passage head under high pressure (up to 2500 bar). As the cross-section of the valve decreases, the stream is elongated and accelerated, which results in shear stress. Inside the valve the stream is deflected by 90° and directed towards the impact ring, where it hits the impact ring. This leads to further droplet breakup due to turbulent disturbance (Kulisiewicz, Wierschem, et al. 2012). There are several different valve/nozzle geometries, which lead to different predominant droplet breakup mechanisms like cavitation (Kulisiewicz, Wierschem, et al. 2012). In general HDH is better suited for lower viscosity mixtures ranging from 1 - 200 mPa s (Schultz, Wagner, et al. 2004). The advantage of HPH systems is their high power input, resulting in droplet sizes below 0.5  $\mu\text{m}$  and their continuous mode of operation. This allows for the processing of up to several hundred or thousand liters at a time. For satisfactory emulsification results, usually more than one homogenization cycle needs to be run. This is considered a drawback of this technique, especially when trying to emulsify reactive mixtures, for example in *miniemulsion polymerization*. In these monomer mixtures, polymerization can be induced by HPH prior to the existence of a stable

mini-emulsion. Worst case scenario would be the polymerization of non-emulsified bulk monomer phases inside the HDH device.

#### **4.1.5. Emulsion Stability: Droplet Loss Mechanism**

The stability of an emulsion depends on the ability of the surfactant (surfactant composition) to suppress destabilization mechanisms, as described above. This happens primarily by electrostatic, steric or a combination of both interactions (Myers 2005) (see chapter 4.1.3). If a surfactant fails to provide the necessary stabilization, the emulsion will break due to agglomeration, followed by coalescence and eventually complete macrophase separation. Even if an appropriate surfactant is used, the resulting emulsion is not stable indefinitely – but instead of breaking in the course of seconds or minutes to hours, such an emulsion can be stable for month to years. An exception to this statement would be a thermodynamically stable microemulsion, which indeed is considered to be stable indefinitely.

Generally, there are four processes which are responsible for the breaking of an emulsion. These are Flocculation (Brownian- and sedimentation flocculation), creaming, coalescence and Ostwald ripening (disproportionation). The latter one is of special significance to mini-emulsion. A schematical overview of these processes is shown in Fig. 7 on the example of an oil in water emulsion.

All four processes may occur in any order and simultaneously (Becher 1957, 1983). Creaming is the general process of emulsion separation, but not emulsion breaking - it is considered to be the precursor event to coalescence. As a result of the creaming processes, basically two emulsions are formed. One emulsion (the cream) with a higher disperse phase content and an emulsion with reduced disperse phase content. One of the main driving forces is the difference in density between disperse and continuous phase. It can be inhibited by a small droplet radius, a highly viscous continuous phase and a low difference in density between disperse and continuous phase. The term creaming (rising of droplets to the surface) is used when the density of the disperse phase is lower compared to the continuous phase. Typical examples are most oil in water emulsions. In the opposite case (water in oil) emulsions, the water usually is more dense than the oil, hence the droplets will settle. The process therefore is referred to as settling.

## 4 Theoretical Background

Coalescence is the process of droplet fusion into one large droplet and therefore results in irreversible breaking of the emulsion. This usually happens in the creamed part of the emulsion, where the emulsion droplets are already in close proximity.

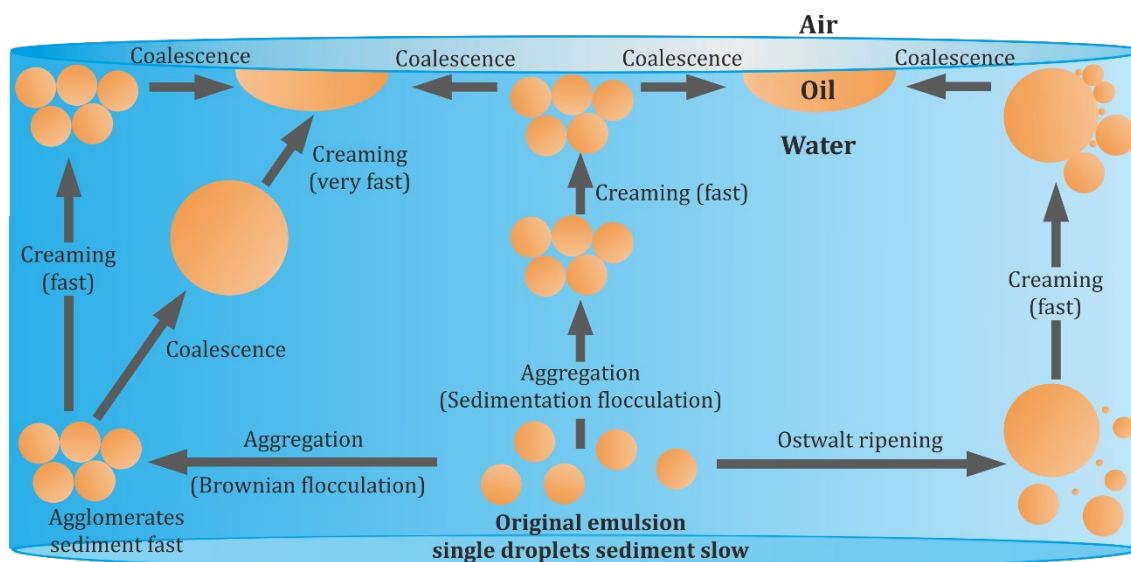


**Fig. 7. Schematical representation of the four main droplet loss mechanisms on the example of an oil in water emulsion.**

An illustrative example of creaming (and the assumed origin of the term) is the separation of milk into *cream* and *skimmed milk* (Particle Sciences 2011).

Flocculation describes the process of single droplets aggregating - while retaining their droplet form - resulting in three-dimensional droplet clusters. Flocculation is the result of insufficient (electrostatic and/or steric) stabilization resulting in attraction between droplets as described above by the DLVO theory. This process can be subdivided into sedimentation flocculation and Brownian flocculation (Reddy and Fogler 1981). In sedimentation flocculation the path of droplet movement is assumed to be in a strictly vertical linear manner. Larger droplets move, i.e. cream faster than smaller droplets. Due to their accelerated ascent (or descent - depending on density) they have an increased chance of colliding and thus trap smaller droplets resulting in small aggregates, which in turn, further increases their velocity. As the name indicates, Brownian flocculation induced by random Brownian (thermal) motion resulting in the aggregation of droplets. In contrast to sedimentation flocculation, this process can happen in any spatial direction. Usually, both flocculation processes occur simultaneously. Nevertheless, for smaller droplets ( $> 1 \mu\text{m}$ ) Brownian flocculation, for larger droplets ( $< 2 \mu\text{m}$ ) sedimentation flocculation is more significant.

The fourth mechanism involved in emulsification degradation is Ostwald-ripening (disproportionation). Ostwald ripening describes the diffusion of disperse phase molecules (monomer) from smaller to larger droplets through the continuous phase. As this mechanism is of special interest when working with miniemulsions, it will be discussed in more detail in the chapter 4.1.6.

#### **4.1.6. Different Types of Emulsion-based Polymerization Techniques: Suspension-, Macro-, Micro- and Miniemulsion Polymerization**

Emulsions have been used for decades in a number of different industries. Examples for the use of emulsions are found in the food industry as mayonnaise or salad dressings, the pharmaceutical field to administer water insoluble anesthetics, in cosmetic applications and in agriculture or automotive sector (Debnath, Saha, et al. 2015; Chappat 1994). Another important use of emulsions and the focus of this work, is the preparation of polymer nanoparticles and the polymerization of monomers in emulsions. Hence, different emulsion types, with an emphasis on miniemulsion, will be discussed in the light of their use as polymerization technique and as particle preparation tool.

The term *emulsion* (as used in different polymerization techniques), can be further subdivided in the following polymerization techniques: *suspension polymerization*, *(macro)emulsion polymerization*, *miniemulsion polymerization* (also called *nanoemulsion polymerization*) and *microemulsion polymerization* (Slomkowski, Alemán, et al. 2011).

While the term *suspension polymerization* describes the emulsion with the largest resulting particle sizes (50 - 2000  $\mu\text{m}$ ), it is more difficult to link the particle size to the term in the case of *mini-* (i.e. *nano-*) and *microemulsion polymerization*. In contrast to their names, the *miniemulsion (nanoemulsion)* polymerization exhibits droplets i.e. particles in the range of 50-500 nm, while the *microemulsion* actually produces the smallest droplet sizes ranging from 10-100 nm (Fonseca, McKenna, et al. 2010; Lovell and Wiley 1997; Asua 2007). As the term nanoemulsion can be misleading, instead the term miniemulsion is used throughout this work. The herein called *(macro)emulsion polymerization* (also denoted just as *emulsion polymerization*) covers a broader range in terms of droplet i.e. particle size. Depending on the recipe and polymerization conditions, the size can vary between 20 nm and several microns but more commonly 50 to 1000 nm (Vanderhoff, El-Aasser, et al. 1984; Asua 2007; Schork, Luo, et al. 2005). There are more subtypes of emulsion polymerizations for example *microsuspension polymerization* or *seeded emulsion*

## 4 Theoretical Background

*polymerization* - these will not be discussed in this work. Further, all polymerization techniques discussed in this chapter relate to free-radical polymerization techniques.

Due to historical reasons, these denotations follow a logic, which is hardly recognizable at best. Nonetheless, a distinct terminology for these polymerization techniques is indispensable, as the content of this chapter will show.

Next to droplet size, the four types of emulsions-based polymerization techniques mentioned above, show inherent differences in their composition, preparation technique, stability, thermodynamics, polymerization kinetics and applications.

In order to demonstrate the special properties of the miniemulsion polymerization technique - the focus of this work - it is compared with other emulsion types (Fig. 8). This allows to demonstrate the special characteristics of the *miniemulsion polymerization technique*. As previously described, *emulsion* refers to an unpolymerized monomeric emulsion. In addition, the term *latex* will be defined as a polymerized monomeric emulsion (Schork, Luo, et al. 2005).

As pointed out above, these polymerization techniques differ in resulting particle sizes. However, the range of sizes in which particles can be prepared via these different polymerization techniques is broad. Indeed, these techniques are not defined by droplet or particle size but rather by mode of operation.

In the **suspension polymerization** (Fig. 8 A) usually water insoluble monomer(s) are dispersed in water via agitation i.e. stirring in the presence of an oil-soluble initiator. At the start of the procedure an emulsion is formed, which eventually will result in a suspension – hence the name *suspension polymerization*. To promote suspension stability, small amounts of surfactant may be used (Schork, Luo, et al. 2005). In contrast to other emulsion types, the surfactants used here are mainly inorganic, colloidal particles (also called Pickering dispersants, for example tricalcium phosphate, barium sulfate, calcium carbonate) or water-soluble polymers like poly(vinyl alcohol) and cellulose ethers.

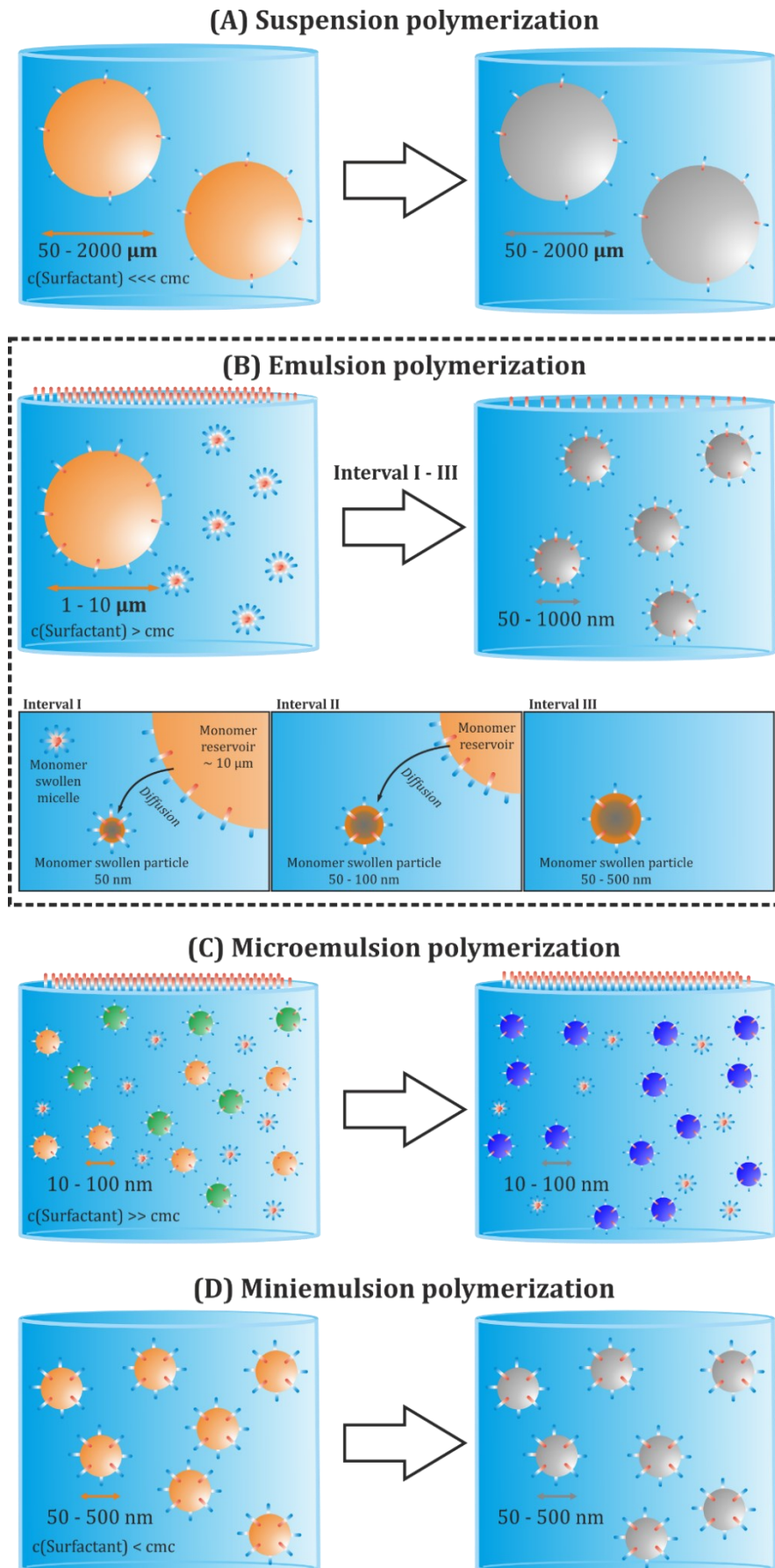


Fig. 8 Schematical representation of suspension-, emulsion-, microemulsion- and miniemulsion polymerization.

## 4 Theoretical Background

The relevant parameters in the control of the *suspension polymerization* i.e. control of resulting particle size are type and concentration of surfactant, physical properties (densities, viscosities, interfacial tension) of the continuous and disperse phases and most importantly the quality of agitation (reactor geometry, impeller type, stirring speed)(Asua 2007). As the formed suspension (emulsion) is unstable, continuous stirring is necessary to keep the droplets in a suspended state i.e. keep them in the equilibrium between droplet coalescence and droplet breakage. During the breakage and diffusion, monomer is exchanged between droplets. The existence of this equilibrium is the reason why the droplets do not retain their identity during the polymerization. Polymerization is initiated inside the droplets (called droplet nucleation) by means of the oil-(disperse phase)-soluble initiator. Eventually, when high conversions are reached the droplets/particles will keep their identity.

In the case of (conventional) **emulsion polymerization** (Fig. 8 B) the mechanisms involved are quite different. Initially, a coarse emulsion consisting of monomer, water, water-soluble initiator and surfactant is prepared via agitation. The surfactant-types used are mostly ionic or polymeric (see Table 1). Due to the large droplet sizes (1 – 10  $\mu\text{m}$ ) the total surface area of the dispersion is small. This leads to a surfactant concentration, which exceeds the critical micelle concentration (cmc) resulting in the formation of micelles in the disperse phase. The prepared coarse emulsion is not stable. Similar to the *suspension polymerization*, this emulsion needs to be stabilized by continuous stirring to counteract the agglomeration/coalescence processes. If the stirring is insufficient (or completely stopped) macrophase separation will occur rather quickly. In contrast to the *suspension polymerization*, the loci (location) of polymerization is not in the larger monomer droplets (droplet nucleation) but inside the micelles (micellar nucleation). This means that radicals are trapped inside the micelles (interval I). The necessary monomer, originating from the monomer droplets (hence also called monomer reservoirs), reaches the micelles via diffusion through the continuous phase (interval I-II). As the polymerization reaction and therefore the monomer-to-polymer conversion advances, the monomer reservoirs will finally deplete (interval III). Due to this particle formation mechanism and the resulting size increase of the micelles, the total surface area of the dispersion will increase. The resulting nanoparticles are usually rather monodisperse. The described mechanism of emulsion polymerization (diffusion through the continuous phase) does not enable the preparation of particles with a fixed identity. For the *emulsion polymerization* the quality of agitation – especially the stirring speed i.e. power input – is important. As described



above, a low power input will result in phase separation. However, an excessive power input leads to increased disruption of the monomer droplets, leading to an increased number of droplets. In this case, the likelihood of droplet nucleation is strongly increased. Such a polymerization would resemble a *suspension polymerization* and the product would be rather heterogeneous in size and size distribution compared to the normal product of an *emulsion polymerization* (Lechner, Gehrke, et al. 2014).

In **microemulsion polymerization** (Fig. 8 C), excessive amounts of surfactant have to be used in order to form thermodynamically stable, isotropic mixtures. For their fabrication almost no agitation or shear force is necessary. Usually, gentle shaking of the mixture is sufficient for the formation of the microemulsion. Due to the large amounts of surfactant, these emulsions possess special properties in terms of thermodynamics, which will not be discussed in further detail. In fact, the amount of surfactant is so large, that all monomer droplets (size 10 – 100 nm) are completely covered with surfactant and, in addition, a larger number of empty micelles are formed. In this type of polymerization solely droplet nucleation occurs. Nonetheless, the droplets do not hold their identity. As the interfacial tension in such a system is close to zero, a bicontinuous network may be formed, resulting in a constant exchange of monomer between the droplets.

The focus of this work is the **miniemulsion polymerization** technique (Fig. 8 D). In terms of location of nucleation, there are similarities to the microemulsion – in both types mainly droplet nucleation occurs. Due to the special thermodynamics, which apply for microemulsions, the concept of *miniemulsion polymerization* actually shows many similarities to *conventional emulsion polymerization* (Schork, Luo, et al. 2005). The recipe i.e. the composition of the mixture used in *emulsion polymerization* may be identical to a *miniemulsion polymerization*. Solely, the procedure (high shear or continuous stirring) for preparing an emulsion, differs (Fontenot and Schork 1993).

In contrast to other types of emulsions, it is necessary to apply high shear forces for the preparation of miniemulsions. The power input of conventional stirring or agitating is not sufficient to produce droplets in the range of 50 – 500 nm. The three most common high shear devices - also the ones used in this work - *rotor-stator*, *probe sonication* and *high-pressure homogenization* are discussed in Chapter 4.1.4. Other techniques for example membrane emulsification are not discussed in this work.

When the droplet size falls below the critical size of about 0.5  $\mu\text{m}$ , they can be effectively stabilized against coalescing with a surfactant (See chapter: 4.1.3 Colloidal Stability: EDL and (X)DLVO-Theory). Contrary to other emulsion polymerization techniques, there is no

## 4 Theoretical Background

continuous and precisely controlled agitation necessary to keep the emulsion stable, i.e. prevent the droplets from coalescing.

The main degradation mechanism in miniemulsion is Ostwald ripening (schematically shown in Fig. 7). It occurs when the monomer is even only slightly soluble in the continuous phase. Most monomers are slightly soluble - as evidenced by the fact that interval II takes place in *emulsion polymerization* (Fig. 8 B). If the miniemulsion is not protected from Ostwald ripening, creaming will occur in the matter of seconds to minutes. The main driving force is the difference in Laplace pressure in the droplets. As any 'real' emulsion is polydisperse, i.e. not all droplets are the same size, there is a difference in Laplace pressure between these droplets. Smaller droplets possess a higher pressure compared to larger ones. The rate of diffusion depends on the solubility of the disperse phase molecules in the continuous phase. To suppress Ostwald ripening an osmotic agent (also called costabilizer, or in earlier works called cosurfactant) is added to the disperse phase. Osmotic agents usually are small molecules with a very poor continuous phase solubility. Polymers mostly are insufficient to server as osmotic agents (Schork, Luo, et al. 2005). The presence of an osmotic agent in the disperse phase creates an osmotic pressure in the droplets, which counteracts the Laplace pressure (Capek 2010; Schork, Luo, et al. 2005). This can improve emulsion stability on a timescale of months, which is more than sufficient in miniemulsion polymerization, since the timescale for most polymerizations is in the range of hours. Miniemulsion droplets, which are stabilized by the means of a surfactant and a cosurfactant, barley succumb to any diffusion or destabilization mechanisms. Thus, these *nano reactors* hold their identity. This easily allows for the incorporation of severely hydrophobic components as well as solids into nanoparticles (Landfester 2001). In terms of polydispersity, the nanoparticles produced via *miniemulsion polymerization* can be equal to those prepared via *emulsion polymerization*. Although it was shown that both, a disperse- and a continuous phase-soluble initiator works in *miniemulsion polymerization*, the polymerization reaction takes place solely inside the droplets (droplet nucleation) (Choi, El-Aasser, et al. 1985).

In this chapter, all polymerization tools were discussed in the light of their use for the preparation of direct (O/W) emulsions. All techniques presented can also be used in inverse (W/O) emulsions. Since the inverse miniemulsion technique is the focus of this work, this technique will be explained in further detail in the next chapter.

### 4.1.7. Particle Preparation via Miniemulsion Technique

In the following chapter, further insight on inverse miniemulsion technique is given. Two main methods of particle preparation via inverse (*water in oil*) miniemulsion will be discussed. The first is the *inverse miniemulsion polymerization* of (radical) polymerizable monomers as a tool for nanoparticle synthesis (discussed in the previous chapter 4.1.6). The second approach is the preparation of miniemulsion, which contain already existing polymer inside the droplets. After emulsification, a crosslinker is added to produce covalently crosslinked polymer nanoparticles. This technique is called *miniemulsion crosslinking* (MiniEX).

Below, a schematical example for the preparation of an inverse miniemulsion containing monomer and the subsequent polymerization is shown (Fig. 9.)

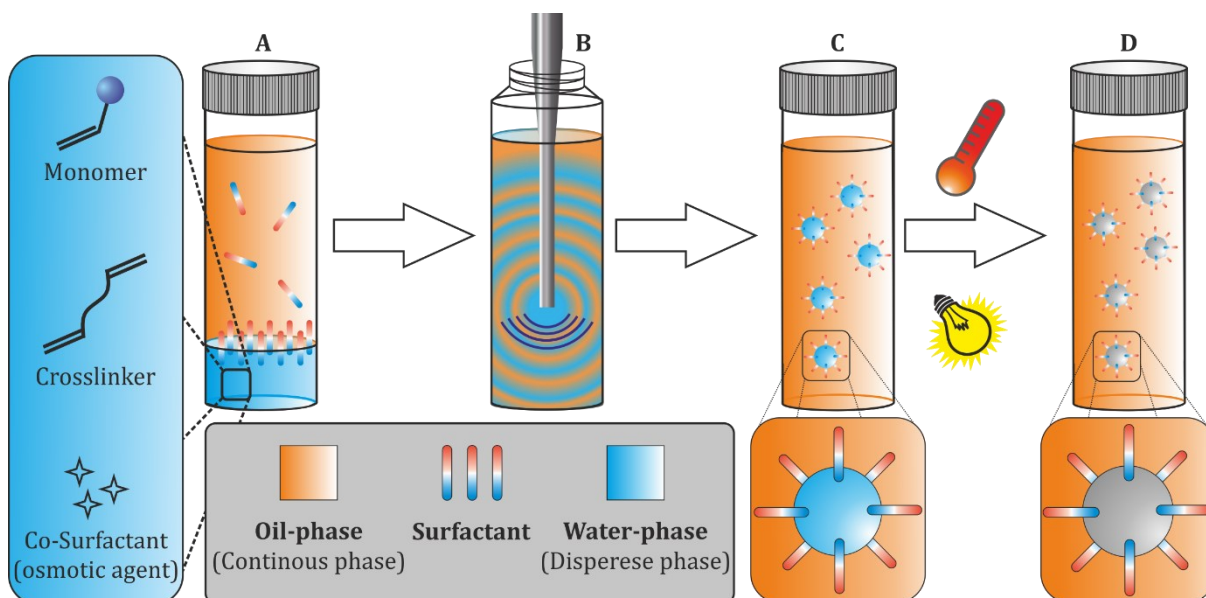


**Fig. 9** Schematical representation for the preparation of a miniemulsion containing monomer and the subsequent process of conducting a miniemulsion polymerization.

In a first step the monomer and, if desired, a crosslinker are dissolved in water acting as disperse phase (Fig. 9. A). Further, an osmotic agent, for example sodium chloride, needs to be added (osmotic use and function of osmotic agents are discussed in chapter 4.1.5). As an alternative, the components can be dissolved in an aqueous buffer medium with sufficient ionic strength – the buffer media ions act as osmotic agent. Note: in direct (oil in water) miniemulsion an osmotic agent would be a very hydrophobic i.e. water insoluble

## 4 Theoretical Background

substance like hexadecane. The aqueous phase is added to an oil phase (continuous phase) which consists of a hydrophobic oil (immiscible with water) and a suitable surfactant. The radical initiator necessary for initiating the polymerization reaction is usually added to the oil phase (but it is also possible to add it to the disperse phase). Subsequently, the mixture is usually emulsified via probe sonication (Fig. 9. B) or by other means of homogenization (see Chapter 4.1.4). If high-pressure homogenization is chosen, caution is required. Due to the high shear stress, some monomers tend to start polymerizing prematurely before a stable emulsion is formed. This is exceptionally unfavorable when the polymerization happens inside the homogenization device.

The resulting miniemulsion is milky white most of the times. However, there are situations when a stable miniemulsion is almost transparent. This usually happens when the refractive index of the continuous and disperse phase match (this depends mainly on the monomer mixture used) (Abbott 2015).

After emulsification, the miniemulsion is exposed to heat or UV-light to induce initiator decomposition i.e. radical formation, which will start the polymerization inside the droplets. After the polymerization is finished, the final polymer latex (dispersed polymer nanoparticles) can be recovered via centrifugation. To improve centrifugation efficiency, the emulsion (now actually a suspension) should be broken by adding a phase mediating component. Usually ethanol is a good choice as it is soluble in water as well as in most organic oils.

Miniemulsion crosslinking (MiniEX) in its basic principles is similar to miniemulsion polymerization (Fig. 10).

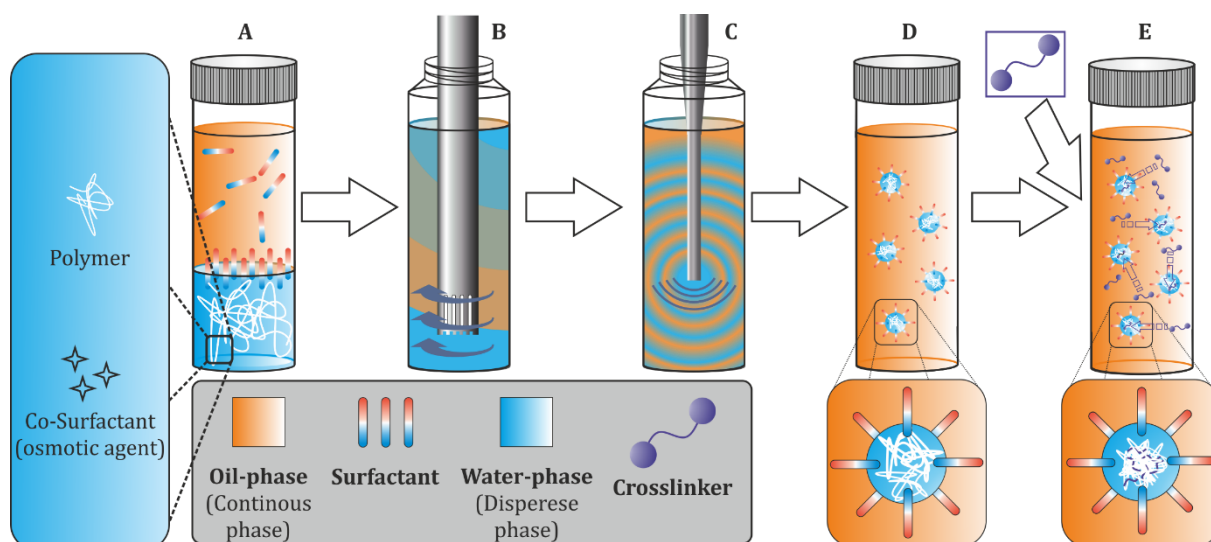


**Fig. 10** Schematical representation for the preparation of a miniemulsion containing polymer and the subsequent process of crosslinking.

In a first step, the polymer is dissolved in a suitable aqueous medium (Fig. 10 A). An osmotic agent needs to be added as well. The presence of the polymer leads to an increased disperse phase viscosity. Hence, a pre-emulsification via rotor-stator mixing may be helpful. Due to the increased viscosity, the emulsification technique may have to be further adjusted. Subsequent emulsification via probe sonication or high-pressure homogenization results in the desired miniemulsion. Unlike in miniemulsion polymerization, in MiniEX no initiation of a polymerization reaction is necessary, as the polymer already exists. In order to keep the particle shape, the polymer needs to be crosslinked inside the droplets. This is achieved by adding a crosslinker to the emulsion under stirring. After sufficient time the crosslinker diffuses inside the droplets and reacts (covalently) with the polymer. The recovery is usually also done by means of centrifugation.

## 4.2. Chitin and Chitosan

While the polysaccharide cellulose is the most abundant biopolymer on earth, chitin, also a polysaccharide, is the second most abundant biopolymer. Cellulose is mainly derived from plant sources such as reeds, stalks, wood and grass. Chitin is mainly found in crustacean shells such as shrimp, crab, lobster, which are available as waste from the seafood processing industry and are therefore used for commercial production of chitin (Kurita 2006). Chitin is made up from  $\beta$ -(1 $\rightarrow$ 4) linkages of *N*-acetyl-*D*-glucosamine and

## 4 Theoretical Background

*D*-glucosamine. The existence of nitrogen in chitin was verified by Lassaigne in 1843 (Olivera, Muralidhara, et al. 2016). If the degree of deacetylation (DD) of chitin is > 50 %, the polymer is referred to as chitosan as shown in Fig. 11 (Rinaudo 2006).

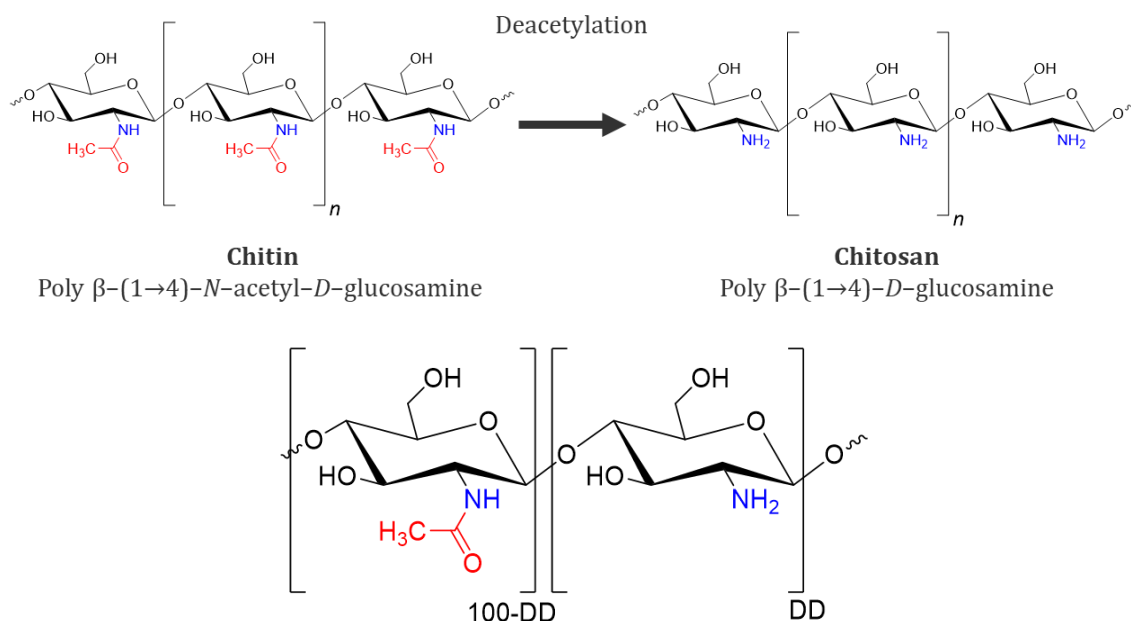


**Fig. 11** Schematical representation of fully acetylated chitin (top left) and completely deacetylated chitosan (top right). If the degree of deacetylation of chitin is > 50 % it is called chitosan. Usually chitosan is not deacetylated completely. Thus, the degree of deacetylation (DD) describes the percentage of free primary amines while the 100-DD (also called degree of *acetylation* - DA) describes the remaining acetylated amines (bottom). The deacetylation does usually not appear locally as implied by the bottom figure - chitosan is no block-copolymer. Deacetylation is randomly distributed all over the polymer.

Chitosan was synthesized for the first time in 1859 by C. Rouget (Rouget 1859). In contrast to chitin, chitosan bears a sufficient number of primary amines, which allows dissolution in diluted acidic media via protonation of the primary amines ( $pK_a \approx 6.5$ ) (Panzarasa, Osypova, et al. 2018). This solubility enables the processing of the cationic biopolymer by various techniques. For the preparation of chitosan solutions, mostly acetic acid is used. However, lactic acid, formic acid or oxalic acid are can also be used. Mineral acids such as hydrochloric or nitric acid also result in chitosan solutions, while phosphoric and sulfuric acids may not be suitable (Kurita 2006).

There are several steps necessary for the production of chitin out of shells and hulls and the subsequent conversion to chitosan on an industrial scale as described by Mathur & Narang (1990). First, the shells and hulls are ground and dried. In order to demineralize this chitin powder, it is treated with a 10 % stoichiometric excess (regarding the ash content) of 0.5 M HCl. 60-85 % of residue consist out of chitin, the rest (15-40 %) are mainly proteins and pigments. In order to dissolve and remove (deproteination) those components, the powder is treated with 1 % (w/w) NaOH for 24 h at 65° C. The resulting

product is commercial chitin powder, which can be further purified and used. To obtain chitosan, the chitin needs to be deacetylated. Crude chitin is treated with 50 % (w/w) NaOH at 100 °C for 2-5 h under nitrogen atmosphere. Organic solvents can be added to enhance the deacetylation process. The residue is thoroughly washed to remove the alkaline components and dried at 110 °C for 24 °h. Depending on reaction parameters and feedstock, the resulting chitosan powder usually exhibits a degree of deacetylation in the range of 70-90 %. A more descriptive representation of the necessary components is listing the amounts needed for the production of 1 kg of chitosan. 10 kg of shrimp shell are converted into 1 kg of chitosan with the use of 6.3 kg HCl, 1.8 kg NaOH, 0.5 tons process water and 0.9 tons of cooling water (Ravi Kumar 2000).

Due to its distinct biological and physiochemical characteristics, chitosan attracted a great deal of attention in the last two decades. Next to its non-toxicity, biocompatibility and biodegradability it is known to promote wound healing (Kurita 2006). Further, it exhibits mucoadhesive behavior which was first shown by Lehr et. al, (1992). In addition to its biological relevance, chitosan possesses properties, which makes it an attractive material for adsorption applications. Especially, the primary amines and other moieties like hydroxyl groups and acetamido groups facilitate this adsorption behavior towards a wide variety of substances (Olivera, Muralidhara, et al. 2016). Chitosan has been used as adsorbent for metal ions and organic compounds in the form of flakes, beads, hollow fiber membranes, flat sheet membranes and nanoparticles (Gerente, Lee, et al. 2007; Gupta and Suhas 2009; Olivera, Muralidhara, et al. 2016). Especially, the use of chitosan nanoparticles gained increasing attention in many different research fields. In a review by Divya et al. (2018) the main applications are listed. Next to biomedical topics such as *tissue engineering*, *cancer therapy* and *drug delivery* applications, other fields like *agriculture* and *water treatment* are discussed.

### 4.3. Molecular Imprinting

In this chapter, the technique of molecular imprinting with an emphasis on molecular imprinted polymer nanoparticles will be discussed.

Molecularly imprinted polymers (MIPs) are tailor-made crosslinked polymer materials, which possess binding sites with a high affinity and selectivity towards a specified template molecule. One of the first reports on imprinting of organic polymers was

## 4 Theoretical Background

reported by Wulff research group in 1972 (G Wulff and Sarhan 1972; Günter Wulff 1995; Saylan, Yilmaz, et al. 2017).

The basic principle of the formation of molecular imprints is based on the formation of noncovalent interaction between the target molecule and one or more functional monomers. The functional monomers interact with the template molecule in solution, resulting in a template-monomer-complex. The spatial arrangement of this complex is *frozen* via polymerization of the mixture in the presence of suitable amount of a crosslinker. After polymerization and subsequent extraction of the template, the crosslinked three-dimensional and preferably rigid polymer network is left with the desired binding sites. The selectivity/affinity arises from “imprinted” binding sites, which match the template molecule in shape, size and complementary spatial (steric) configuration of functional groups. Figuratively spoken – a chemical and stereochemical ‘negative image’ of the template molecule is “stamped” into the polymer matrix (S. Li, Cao, et al. 2014). Template coordination in those nanocavities depends on the corresponding monomer(s) and crosslinker(s) and thus, is based on non-covalent forces such as ionic, electrostatic, hydrophobic/hydrophilic, Van der Waals, hydrogen bond or  $\pi$ - $\pi$  interactions (Vaihinger, Landfester, et al. 2002; Gryshchenko and Bottaro 2014; Alexander, Andersson, et al. 2006).

Due to the straightforward synthesis and the use of easily accessible precursors, MIPs qualify as a good and cost effective candidate as recognition elements even in single use or disposable sensors (Poma et al. 2013). Especially due to their polymeric matrix, MIPs exhibit a high thermal, chemical and temporal stability (Pichon, 2007). In contrast to a bio-based recognition layer (i.e. antibodies, peptides), MIPs can be sterilized by autoclaving (Ramström, Ye, et al. 1996; Molinelli, Janotta, et al. 2008).

A common way to prepare MIPs is through the bulk copolymerization of functional monomer and suitable crosslinker in presence of a non-polymerizable template molecule (Haupt and Mosbach 2000). Subsequently, grinding and sieving of the MIP monolith yields micron sized MIP fragments. One drawback of this technique is the heterogeneity in size and shape of micron-MIPs, resulting in slow mass transfer, which is impractical particularly when the MIPs are intended to be used for sensing applications (Zimmerman and Lemcoff 2004).

Hence, a good control and reproducibility in size and shape is desired when the purpose of MIPs is to serve as recognition layer, for example, in optical sensor systems. These requirements can be fulfilled by using spherical nanoparticle MIPs (nano-MIPs). Due to



their size, nano-MIPs provide a high specific surface, i.e. high imprinted surface with a large number of easily accessible binding sites, resulting in short diffusion times. The technique of inverse (water in oil) miniemulsion polymerization (miniEP) can be applied to reproducibly prepare nanoscaled, spherically shaped, hydrophilic nano-MIPs.

In contrast to other techniques, the inverse MiniEP allows the use of hydrophilic monomers in the aqueous phase and the easily imprinting of water-soluble substances, for example penicillin G sodium salt. For the preparation of nano-MIPs the template, a suitable monomer and crosslinker are dissolved in water, acting as aqueous (disperse) phase. This solution is emulsified in a mixture of oil, initiator and surfactant, resulting in water in oil emulsion. If the parameters (phase ratio, means of emulsification and amount of surfactant) were chosen right, the prepared emulsion qualifies as miniemulsion. This is crucial for the preparation of nano-MIPs as in miniemulsions each droplet acts as a *nano-reactor* (Fig. 12 left). Compared with other emulsion techniques, in miniemulsions inter-droplet-diffusion of monomer is reduced to a minimum, which is favorable for the imprinting process. Polymerization is then induced via thermal or UV-initiation resulting in crosslinked polymer nanoparticles (Fig. 12 mid).

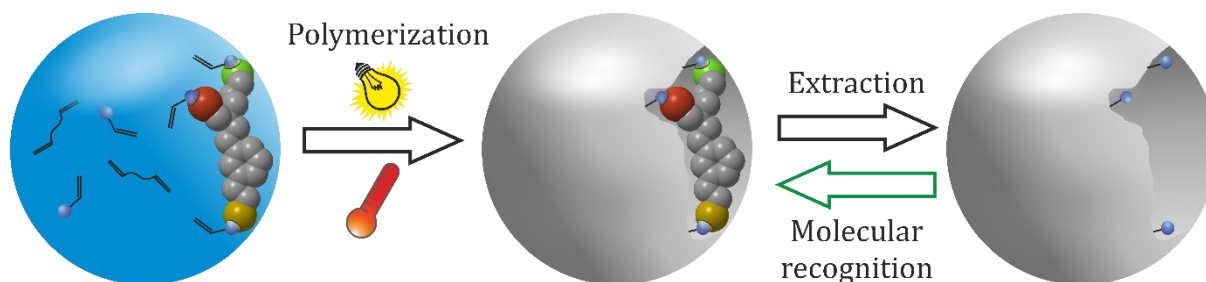


**Fig. 12 Schematical representation of nano-MIP preparation via inverse miniemulsion technique.**

Subsequently, the non-covalently bound template molecule is extracted, leaving the MIP with a free recognition site (Fig. 12 right). As this process is reversible, this binding site can now be used for molecular recognition of the template for example in a sensor element or as filling material in HPLC columns.

## 5. Preparation of Chitosan Nanoparticles via Emulsion Crosslinking

In this chapter, the results for the discussion of hypotheses I.I (5.1) are presented. Chapter 5.2 to 5.8 represents a manuscript with the title “*Systematic approach for preparation of chitosan nanoparticles via emulsion crosslinking as potential adsorbent in wastewater treatment*”, which was published as a research paper in the peer-reviewed journal *Carbohydrate Polymers* (Riegger, Bäurer, et al. 2018). The discussion of hypothesis I.I can be found in the discussion section in chapter 9.1.1.

Please note: Minor modifications were made to the original manuscript concerning layout and orthography in order to fit the style of this thesis. No content-related changes were performed.

### Declaration about my own contribution

*I conceived the study and elaborated the detailed experimental design.*

*This specifically included:*

- *Conceptualization and formulation of the overarching research goals within the study.*
- *Design of the experimental approach for particle synthesis via ultrasonication-assisted miniemulsion crosslinking.*
- *Investigation and implementation of protocols for the handling and preparation of chitosan solutions such as: duration of dissolution, filtration and storage properties.*
- *Investigation and selection of suitable chitosans, crosslinkers and emulsifiers used for the synthesis in this study.*
- *Investigation and implementation of the use of an osmotic agent for emulsion stabilization.*
- *Determining the range of concentrations and stoichiometric calculation of synthesis educts and components, especially the amount of chitosan, crosslinker, stabilizers and emulsion phase ratios.*

## 5 Preparation of Chitosan Nanoparticles via Emulsion Crosslinking

- *Elaboration and implementation of emulsion/particle preparation protocols in terms of selecting ultrasonication parameters, durations and particle separation/purification.*
- *Elaboration and implementation of sample preparation protocols and the necessary procedures for analytical methods such as scanning electron microscopy (SEM), dynamic light scattering (DLS), size exclusion chromatography (SEC), rheology, high performance liquid chromatography (HPLC) as well as protocols for data evaluation and analysis.*
- *Selection and investigation of relevant active pharmaceutical ingredients (APIs) which were used in the adsorption experiments to evaluate the adsorption behavior of the prepared chitosan nanoparticles.*
- *Conceptualization and implementation of the particle synthesis experiments and particle characterization experiments. The data on synthesis and characterization of particles shown in this study, was partly collected by Bernd Baurer in the course his master thesis under my supervision and by applying my methodology.*
- *Conceptualization and implementation of the experiments to study the characterization of the adsorption behavior of chitosan nanoparticles via HPLC. The data on adsorption characterization shown in this study, was collected by Aziza Mirzayeva in the course her master thesis under my supervision and by applying my methodology.*
- *Conduction of studies to validate the reproducibility of nanoparticle synthesis with chitosans of different molecular weights.*
- *Evaluation and discussion of all data in an overall context of this study.*
- *Visualization of the acquired data (graphs) and schematic representation.*
- *Writing of the entire original draft of the publication and taking the leading role in incorporating changes proposed by co-authors and reviewers.*

## 5.1. Hypothesis I.I

*It is possible to prepare crosslinked chitosan nanoparticles (Chi-NPs) reproducibly via inverse miniemulsion crosslinking technique using highly deacetylated chitosans with different molecular weight.*

- *The molecular weight (MW) has an impact on particle size.*
- *Compared to pristine chitosan, the crosslinked Chi-NPs show a superior adsorption behavior for a relevant active pharmaceutical ingredient (API).*

Riegger, Benjamin R, Bernd Bäurer, Aziza Mirzayeva, Günter E.M. Tovar, and Monika Bach. (2018). "A Systematic Approach of Chitosan Nanoparticle Preparation via Emulsion Crosslinking as Potential Adsorbent in Wastewater Treatment." Carbohydrate Polymers 180 (January): 46–54. <https://doi.org/10.1016/j.carbpol.2017.10.002>.

## **5.2. A Systematic Approach of Chitosan Nanoparticle Preparation via Emulsion Crosslinking as Potential Adsorbent in Wastewater Treatment**

Benjamin R. Riegger <sup>a</sup>, Bernd Bäurer <sup>a</sup>, Aziza Mirzayeva <sup>a</sup>, Günter E.M. Tovar <sup>a,b,\*</sup>, Monika Bach <sup>b,\*</sup>

<sup>a</sup>Institute of Interfacial Process Engineering and Plasma Technology IGVP, University of Stuttgart, Nobelstr. 12, 70569 Stuttgart, Germany. Tel: +49 711 68568162;

<sup>b</sup>Fraunhofer Institute for Interfacial Engineering and Biotechnology IGB, Nobelstr. 12, 70569 Stuttgart, Germany. Tel: +49 711 9704109;

\*Corresponding authors.

E-mail addresses: guenter.tovar@igvp.uni-stuttgart.de (G.E.M. Tovar), monika.bach@igb.fraunhofer.de (M. Bach).

**Published in the peer-reviewed journal Carbohydrate Polymer**

Publisher: Elsevier

DOI: 10.1016/j.carbpol.2017.10.002

Volume: 180; Pages: 46-56

Received 3 February 2017; Received in revised form 25 September 2017; Accepted 1 October 2017; Available online 03 October 2017

### 5.3. Abstract

This study investigates the impact of glutaraldehyde (glut) concentration and molecular weight (MW) of six commercially available, highly deacetylated chitosans (Chi) on nanoparticle (Chi-NP) formation by emulsion crosslinking technique and their use as potential adsorber for diclofenac (DCL) and carbamazepine (CBZ). With a glut:primary amine ratio of 1:1 and NaCl as a hydrophile, it was possible to reproducibly synthesize narrowly distributed, spherical Chi-NPs over a broad range of chitosan MW with a high yield. Increasing Chi MW resulted in larger particle sizes ranging from 109.9 nm, for lowest MW, up to 200.3 nm for the highest MW, measured by DLS. To evaluate the static adsorption behavior of the Chi-NPs, CBZ and DCL were used in single point adsorption experiments. An adsorption capacity of up to 351.8 mg g<sup>-1</sup> DCL for low MW Chi-NPs was observed and all Chi-NPs showed superior adsorptions when compared to untreated Chi.

Keywords: chitosan nanoparticles; emulsion crosslinking; adsorption; active pharmaceutical ingredients (API); wastewater treatment

### 5.4. Introduction

Providing clean water will be one of the major challenges of the next decades to come. Beside oxidation processes, one of the main ways for water remediation is adsorption of the pollutants by activated carbon (Westerhoff, Yoon, et al. 2005). Since the beginning of the 21<sup>st</sup> century, the appearance of active pharmaceutical ingredients (APIs) in the aquatic environment, particularly in drinking water, has been a major concern. Several priority lists for APIs have been established using different prioritizing parameters (Singer, Wössner, et al. 2016). Two of these substances – namely diclofenac (DCL) and carbamazepine (CBZ) – are the most frequently detected ones (Yongjun Zhang, Geissen, et al. 2008). The development of a recyclable adsorber system with a high adsorption capacity could be a viable alternative for the remediation of aquatic pollution caused by pharmaceuticals. The material used in the development of such a system should ideally come from a sustainable origin.

Since the end of the last century, the second most abundant biopolymer chitin, and especially its derivative chitosan, gathered increasingly scientific attention. Chitin is widely available in crustacean shells, such as prawns, shrimps, and crabs, and it is a linear polymer of (1,4)-linked 2-acetamido-2-deoxy- $\beta$ -D-glucan (N-acetylglucosamine) units.

## 5 Preparation of Chitosan Nanoparticles via Emulsion Crosslinking

The treatment of chitin with strong alkaline media leads to the deacetylation of this polymer. Chitosan was first reported by Rouget in 1859, who boiled chitin in a concentrated potassium hydroxide solution and collected the acid fraction (Rouget 1859). It is generally accepted that, if the degree of deacetylation (DD) of chitin is > 50 %, the polymer is referred to as chitosan (Rinaudo 2006). Chitosan is the only known pseudo-natural cationic polymer and it offers a variety of highly interesting properties. Bearing free primary amines, chitosan is soluble in diluted acidic media. The solubility enables the easy processing of chitosan and its derivatives. Besides its antimicrobial character (M. Kong, Chen, et al. 2010) and its uses for improving mucoadhesivity (Lehr, Bouwstra, et al. 1992), chitosan is considered as a promising material for adsorption of pollutants like metal ions (Varma, Deshpande, et al. 2004; Wan Ngah, Teong, et al. 2011; L. Zhang, Zeng, et al. 2016), organic compounds such as dyes (Crini and Badot 2008; Vakili, Rafatullah, et al. 2014), phthalates (Julinová and Slavík 2012) and pharmaceutical compounds (Oladoja, Adelagun, et al. 2014; Kyzas, Fu, et al. 2015). To serve as adsorber, chitosan or chitosan composites have been prepared in the form of flakes (Suc and Ly 2013; Iqbal, Wattoo, et al. 2011), flat sheet membranes (Beppu, Arruda, et al. 2004; Ghaee, Shariaty-Niassar, et al. 2010) hollow fiber membranes (C. Liu and Bai 2006), beads (Azlan, Wan Saime, et al. 2009; Chiou and Li 2003), electrospun fibers (Chauhan, Dwivedi, et al. 2014), microparticles (Chen and Chen 2009; L. Wu and Zhang 2013) and nanoparticles (Hu, Zhang, et al. 2006; Olivera, Muralidhara, et al. 2016). Chitosan nanoparticles (Chi-NPs) as a material have been widely investigated primarily in the field of biomedicine. However compared to other forms of chitosan, Chi-NPs were less frequently investigated as an adsorber material. Covalently crosslinked Chi-NPs have been created the first time by Ohya et al. in 1994 for drug delivery purposes of an anticancer agent (Ohya, Shiratani, et al. 1994). Since then, a large number of research groups investigate the preparation and use of Chi-NPs mainly for drug delivery applications (Z. Liu, Jiao, et al. 2008; Alves and Mano 2008). A large variety of preparation methods for Chi-NPs was described in detail in a review article by Agnihotri, Mallikarjuna, & Aminabhavi (2004). Among others, they discuss several particle preparation methods: coacervation or precipitation, ionic gelation, and oil-in-water emulsion-based technique (i.e. emulsion-droplet coalescence, reverse micellar method and emulsion crosslinking). Among said techniques, the emulsion crosslinking facilitates the preparation of narrowly distributed, covalent crosslinked and nanoscaled chitosan particles. Next to epichlorhydrin (Chiou and Li 2003) and ethylene glycol diglycidyl ether (Azlan, Wan Saime, et al. 2009), glutaraldehyde (glut) can be used

## 5 Preparation of Chitosan Nanoparticles via Emulsion Crosslinking

for the crosslinking of chitosan (Monteiro and Airoidi 1999). Due to none or not covalent crosslinking, Chi-NPs prepared via ionic gelation show an insufficient long-term stability, especially towards changes in pH or ion concentration (Huang, Cai, et al. 2015). Therefore, covalent crosslinking is desired, in particular if a material is used for adsorption applications, which include regeneration processes (adsorption/desorption) with strong pH shifts. If glut reacts with primary amines, the resulting products show a high chemical and thermal stability (Migneault, Dartiguenave, Bertrand, & Waldron, 2004). Since the described material is not designed for *in vivo* or biomedical applications, a potential cytotoxicity of remaining glut or its reaction byproducts is negligible.

The aim of this study was to investigate the impact of crosslinker concentration and the chitosan molecular weight (MW) on chitosan nanoparticle preparation and to assess the possibility to utilize chitosan nanoparticles in water remediation. In particular, we want to present a synthesis strategy which leads to reproducible, narrowly distributed Chi-NPs. Due to the chitosan's potential in remediation, we tested the effects of the developed nanostructured bio-based particles in the treatment of drug-contaminated drinking water. Hence, we evaluated the adsorption behavior for DCL and CBZ which represent two highly relevant APIs.

## 5.5. Experimental

### 5.5.1. Materials

Chitosans of different molecular weights (MWs) (see Fig. 17) were purchased from Heppe Medical Chitosan GmbH (HMC), Halle (Saale), Germany. The MW was also quantified via size exclusion chromatography (SEC) measurements. Degree of deacetylation was verified by <sup>1</sup>H-NMR-spectroscopy. Acetic acid solution for HPLC (assay 49-51 %), glutaraldehyde solution (25 % in H<sub>2</sub>O, d=1.06 g mL<sup>-1</sup>), trifluoroacetic acid (TFA) (99 %) and sorbitan monooleate (Span 80, viscosity 1000-2000 mPa s) were purchased from Sigma-Aldrich (Germany). Cyclohexane (Applichem, > 99.5 %) was obtained from Häberle LABORTECHNIK GmbH, Germany. D<sub>2</sub>O and CD<sub>3</sub>COOD (acetic acid-D<sub>4</sub>) were purchased from DEUTERO GmbH, Kastellaun, Germany.

All chemicals were used as received. ASTM Type I water (TKA GenPure) was used throughout this study (herein referred to as water). Rotor-stator homogenizer, Heidolph Silentcrusher M (homogenizer tool 12F). Ultrasonicator Branson 450-D equipped with a



## 5 Preparation of Chitosan Nanoparticles via Emulsion Crosslinking

5 mm Tip (G. Heinemann Labortechnik). The centrifuge used was a Beckmann & Coulter Avanti J-26 XPI with JA-25.50 Rotor.

### 5.5.2. Methods

#### Calculation of primary amine content

The amount of primary amines was calculated using the degree of deacetylation (DD) provided by the manufacturer. In these calculations the molecular weight of glucosamine was used as the *structural repeating unit* (SRU).

$$n(\text{primary amine}) = \left( \frac{m_{Chi}}{M_{Chi(SRU)}} \right) \cdot \frac{DD}{100}$$

To confirm the DDs provided by the manufacturer, <sup>1</sup>H-NMR spectroscopy (Bruker BioSpin Avance 500) was performed. Chitosan samples ( $\approx 10 \text{ mg mL}^{-1}$ ) were prepared in deuterated 1 % acetic acid in D<sub>2</sub>O solution. For DD determination, the integral of H<sub>N-COCH<sub>3</sub></sub> at 1.90 - 2.10 ppm and the integrals of H<sub>2</sub>-H<sub>6</sub> ranging from 3.0 - 4.25 ppm were used. The DDs were calculated using the following equation described elsewhere (Hirai, Odani, et al. 1991).

$$DD = \left( 1 - \frac{I_{CH_3}/3}{I_{H_2-H_6}/6} \right) \cdot 100$$

#### Size exclusion chromatography (SEC)

SEC measurements were performed at 40 °C in water (0.1 % trifluoroacetic acid (TFA) (v/v), 0.1 M NaCl ) on a 1260 Infinity GPC-SEC Analysis System (Agilent Technologies) equipped with a refractive index (RI) detector and a PSS NOVEMA Max linear XL 5 000 – 3 000 000 Da (Polymer Standards Service GmbH) column with a Poly-2-vinylpyridine (PVP) calibration. For sample preparation chitosan (2 mg mL<sup>-1</sup>) was dissolved in eluent.

## 5 Preparation of Chitosan Nanoparticles via Emulsion Crosslinking

### Preparation of chitosan solutions

3000 mg of chitosan were dissolved in 100 mL of 1 % acetic acid. The mixture was stirred until a clear solution was obtained (several hours for the low MW chitosans, overnight for high MW chitosans). To remove insoluble components, the resulting solution was filtered through a filter crucible (porosity 2), under reduced pressure. If not mentioned otherwise, a hydrophile – namely sodium chloride (NaCl, 0.584 g) – was added to this solution, resulting in a NaCl concentration of 0.1 M.

### Rheology

All rheological measurements were performed on a *Physica MCR 301* (Anton Paar) rheometer using a coaxial cylinder geometry. The chitosan solutions were prepared as described above (3000 mg chitosan in 100 mL of 1 % acetic acid). Flow curves were obtained with a logarithmic shear rate ramp with shear rates between  $0.01 \text{ s}^{-1}$  and  $2000 \text{ s}^{-1}$  divided in 34 single data points (data recording time of 5 seconds per data point, temperature =  $20 \text{ }^{\circ}\text{C}$ ). Viscosity was also measured at constant shear rate of  $100 \text{ s}^{-1}$  over 2 minutes.

### Preparation of chitosan nanoparticles

Below, a general experimental procedure for the preparation of Chi-NPs is described. Particle preparation with different chitosans and chitosan concentrations always followed this procedure. Different amounts of glut have been used due to different degrees of deacetylation. The amount of glut was adjusted regarding the amount of primary amines. The amount of primary amines was calculated using the DDs provided by the manufacturer (see Table 3)

Chi-NPs were synthesized using emulsion crosslinking technique. As disperse phase (aqueous phase) 6 mL of the previously mentioned chitosan solution was used (chitosan content 180 mg). The continuous phase (oil phase) consisted of 800 mg Span 80 dissolved in 20 mL cyclohexane. A pre-emulsion was formed by adding the aqueous phase to the oil phase under rotor-stator mixing (24 k rpm, ice cooling) with the help of a syringe (hypodermic needle measures: 2.10 mm x 80 mm). The large needle diameter allowed an easy and exact handling of the viscous chitosan solutions. The rotor-stator mixing was performed for 10 minutes. Subsequently, the desired emulsion was formed by ultrasonication (10 minutes: 10 sec “on” / 5 sec “off”, at 60 % intensity, ice cooling). To

## 5 Preparation of Chitosan Nanoparticles via Emulsion Crosslinking

prevent freezing of the emulsion (cyclohexane  $T_m = \approx 7\text{ }^\circ\text{C}$ ) the ice cooling was removed immediately after completion of the sonication. Glut solution (25 % in  $\text{H}_2\text{O}$ ) was added. Unless noted, the concentration of glut was chosen to be equal to the amount of primary amines (1 mol glut per mol primary amine). The emulsion was stirred for 18 h at room temperature in a sealed vial to allow for full crosslinking of chitosan with glutaraldehyde following the time regime chosen by (Banerjee, Mitra, et al. 2002).

### Purification of Chi-NPs

Chi-NPs were purified via centrifugation. The emulsion was transferred into polycarbonate centrifugation tubes. The emulsion was broken by adding 10 mL acetone and centrifugation at 12.096 g (10 k rpm) for 10 minutes. The supernatant was discarded, the resulting pellet was redispersed in ethanol, sonicated for 2 minutes (sonication bath), shaken for 15 minutes (2000 rpm Heidolph Schüttler) and centrifuged. This procedure was repeated three times with ethanol and three times with water. DLS samples were prepared using the aqueous pellet. For adsorption experiments, a known solid content was mandatory. Thus, the pellet was dried under vacuum at room temperature for at least 48 h until constant weight. In preparation for further adsorption experiments, the resulting solid was powdered using mortar and pestle.

### **5.5.3. Characterization of Chi-NPs**

#### Dynamic Light Scattering (DLS)

Measurements of size and polydispersity index (PDI) of Chi-NPs were performed via dynamic light scattering (DLS) equipped with a 4 mW He-Ne Laser  $\lambda = 632.8\text{ nm}$  (Zetasizer ZEN 3600 - NanoZS, Malvern Instruments). Scattering photons were collected in backscattering mode at an angle of  $173^\circ$ . For sample preparation a sufficient amount of Chi-NPs was redispersed in 3 % acetic acid by applying ultrasonication treatment (5 sec "on" / 5 sec "off") for 120 seconds. To remove larger sized agglomerates, a  $1.2\text{ }\mu\text{m}$ -syringe filter was used. The refractive index of 3 % acetic acid was calculated and applied within the Malvern Zetasizer software. Measurements were performed in single use polystyrene cuvettes at  $20\text{ }^\circ\text{C}$ . The reported sizes are the intensity-based z-average diameters of three measurements (> 10 runs each).

## 5 Preparation of Chitosan Nanoparticles via Emulsion Crosslinking

### Scanning Electron Microscopy (SEM)

To determine the morphology and size of the particles, scanning electron microscopy (SEM) was performed using a Zeiss Leo 1530 VP (Jena, Germany). Diluted dispersions of Chi-NPs were placed on silicon wafers and dried at ambient conditions. To minimize electrostatic charging, the samples were sputter-coated with platinum.

### Helium Pycnometer

Densities of Chi-NPs with different amounts of crosslinker were investigated by helium pycnometry. The device used was a Quantachrome Ultrapycnometer 1200eT (Quantachrome GmbH, Germany). About 1 g of vacuum dried nanoparticles was used for each sample.

### Adsorption Behavior

Adsorption behavior for carbamazepine (CBZ) and diclofenac (DCL) was tested in batch experiments for all six chitosan powders and the six resulting types of Chi-NPs respectively. Either 10 mg of untreated chitosan powder or the corresponding Chi-NPs were redispersed in 1 mL phosphate buffer (0.01 M, pH = 7) with ultrasonication treatment. To the resulting dispersion a fixed amount of drug solution was added and placed on a shaker. After 2 h the suspension was centrifuged. The remaining drug concentration in the supernatant was analyzed by High Performance Liquid Chromatography (HPLC) (Device: Shimadzu prominence). A volume of 100  $\mu$ L was injected on a reversed phase column (Ascentis C18 HPLC Column 5  $\mu$ m particle size, L  $\times$  I. D. 25 cm  $\times$  4.6 mm). A flowrate of 1 mL min<sup>-1</sup> was used. Mobile phase composition for diclofenac was *water (+0.1 % TFA) : AcN (40:60, v/v)* and for carbamazepine *water (+0.1 % TFA) : AcN (60:40, v/v)*. Signal detection was conducted via UV/Vis detector set to a wavelength of 280 nm. Experiments were run in triplicate measurements.

## 5.6. Results and Discussion

### 5.6.1. Preparation of Chi-NPs

For the preparation of chitosan nanoparticles (Chi-NPs), microemulsion and emulsion techniques have been used so far. Banerjee et al. (2002) prepared Chi-NPs applying a microemulsion technique where a large excess in continuous phase and surfactant concentrations well above the critical micelle concentration (CMC) are used to provide thermodynamically stable microemulsions. In their study, they emulsified 400  $\mu\text{L}$  of aqueous chitosan solution in 40 mL of hexane/AOT hence the phase ratio of the dispersed phase to the continuous phase was only 1:100. Brunel et al. (2009) used an emulsion technique applying a water-to-oil ratio of 1:3 (V/V) using Span 80 as surfactant in a concentration of  $\approx 1$  w.t % in relation to the oil phase. As their study was concerned with non-covalent crosslinked chitosan nanoparticles for pharmaceutical aspects, Miglyol 812N was used as oil phase, since it is generally regarded as a pharmaceutically safe product. The emulsion formulation used here was derived from Brunel et al. (2009) but using cyclohexane instead of Miglyol 812N and Span 80 with a concentration of 4 w.t %. As pharmaceutical aspects are not relevant in this study, we chose cyclohexane as oil phase for its potential recyclability. Due to its boiling point of around 80  $^{\circ}\text{C}$ , cyclohexane could be easily removed from the emulsion formulation via evaporation after particle synthesis. This is desirable especially, if larger quantities of nanoparticles have to be synthesized.

In contrast to the microemulsions of Banerjee et al. (2002), in this study inverse miniemulsions are prepared, where surfactant concentrations are below the CMC and the miniemulsion is stabilized by an osmotic agent (herein called hydrophile) to prevent nanodroplets from *Ostwald* ripening (Landfester, Willert, et al. 2000). Molecular diffusion (also called *Ostwald* ripening) describes the diffusion of molecules from smaller droplets towards larger droplets and, therefore, it describes a process of emulsion destabilization. This process is driven by different *Laplace* pressures inside the droplets, which are determined by the droplet size. A substance qualifies as a hydrophile if it exhibits an extremely low solubility in the continuous phase. For inverse miniemulsions, adding a hydrophile to the dispersed phase leads to an increase in osmotic pressure inside the droplet. This pressure counteracts the Laplace pressure resulting in a decreasing or even complete inhibiting of the *Ostwald* ripening (Capek 2010).

## 5 Preparation of Chitosan Nanoparticles via Emulsion Crosslinking

In order to increase emulsion stability, we evaluated the impact of the hydrophile sodium chloride (NaCl) on our miniemulsion formulations. In the course of these experiments, emulsions with low MW chitosan (95/5) were prepared with no NaCl, 0.01 M NaCl, and 0.1 M NaCl being present in the formulation. In Fig. 13A, emulsions of 95/5 without adding glut after 18 hours containing different amounts of NaCl are shown. For the emulsions without NaCl and with 0.01 M NaCl, macrophase separation could be optically detected within several minutes to hours.

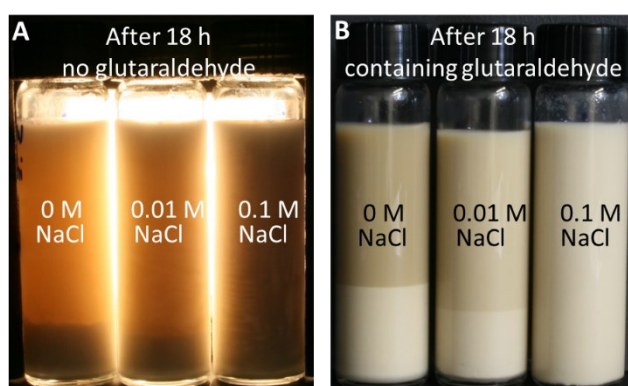


**Fig. 13: Photographs of chitosan emulsions after 18 h stirring without glut (Fig. 13 A) with backlight (left) and with glut (Fig. 13 B) at ambient light (right). No phase separation was observed with 0.1 M NaCl in contrast to phase separation with no NaCl or 0.01 M NaCl with or without glutaraldehyde present.**

Emulsion formulations containing NaCl at a concentration of 0.1 M showed high stability, with no detectable phase separation over the course of 18 hours. We further increased the NaCl concentrations to 0.2 M and 0.3 M with no visible effects. At a concentration of 0.4 M NaCl precipitation of chitosan was observed. Based on these results, we chose to prepare the water phase with a NaCl content of 0.1 M. With this optimized emulsion formulation, we conducted similar experiments to prepare Chi-NPs. Glut (1:1 ratio) was added right after emulsification and the resulting emulsions are shown in Fig. 13B. After 18 hours, solely the crosslinked emulsion with 0.1 M NaCl was optically stable and showed no phase separation.

Crosslinking of the Chi-NPs was achieved using glutaraldehyde (18 h) following a time regime of crosslinking time applied by Banerjee et al. (2002). Ohya et al. (1994) used shorter crosslinking times of 8 hours but as the miniemulsions applied here were stable for 18 h we used the full 18 h to ensure maximal crosslinking of the Chi-NPs.

In summary, we prepared water/oil (w/o) emulsions, stabilized with Span 80/NaCl and containing highly deacetylated chitosans of different MWs. Chitosan was dissolved in 1 %

## 5 Preparation of Chitosan Nanoparticles via Emulsion Crosslinking

aqueous acetic acid and was then used as water phase. Span 80 was dissolved in cyclohexane ( $40 \text{ mg mL}^{-1}$ ) and this solution was then used as oil phase. We optimized the water/oil ratio in our formulation regarding a preferably low volume fraction of cyclohexane. It was possible to create stable emulsions with a chitosan in water/oil ratio of 1:3.3 (V/V). To ensure a sufficient emulsification, a two-step emulsion preparation was chosen (schematically displayed in Fig. 14). In a first step, the continuous phase was premixed with the disperse phase by rotor-stator treatment (a) followed by ultrasonication (b). To the resulting white and optically opaque emulsion (c) the crosslinker glut was added (d). To complete the crosslinking reaction, the emulsion was stirred for 18 h. After several washing steps by centrifugation, drying and powdering, Chi-NPs were isolated in form of a brown powder.

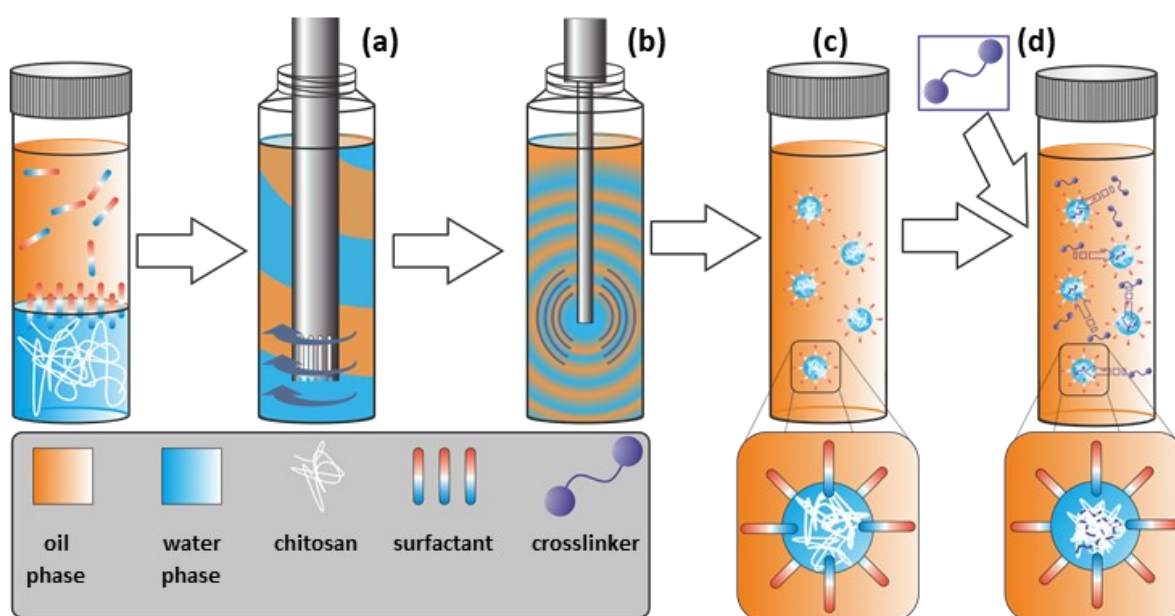


**Fig. 14: Schematic representation of emulsion crosslinking technique.**

The particles were purified via centrifugation, as described in the experimental section. Particle yield of crosslinked particle samples with no NaCl, 0.01 M NaCl and 0.1 M NaCl (Fig. 2 B) were estimated gravimetrically before and after drying. The experiment was performed in triplicate. The respective mean yields for these three NaCl concentrations were  $35 \pm 4 \%$ ,  $44 \pm 4 \%$  and  $88 \pm 1 \%$ . Thus, increasing NaCl to a concentration of 0.1 M leads to a high emulsion stability ultimately resulting in a yield of 88%. In the course of the experiments, we observed that emulsions prepared with no NaCl and 0.01 M NaCl are difficult to separate via centrifugation. Even at 25 krpm for 30 min the supernatant was of transparent red/brown color, while particles synthesized with 0.1 M NaCl were easily centrifuged at 10 krpm and exhibited a clear supernatant. We conclude that the emulsion

## 5 Preparation of Chitosan Nanoparticles via Emulsion Crosslinking

instability caused by low amounts or absence of NaCl leads to the formation of undefined structures, which could not be centrifuged. This assumption is supported by the increasing Chi-NP yield with higher NaCl concentrations up to 0.1M. All further emulsions were prepared with chitosan solutions containing 0.1 M NaCl.

### 5.6.2. Variation of crosslinker concentration

Chitosan crosslinking with the homobifunctional aldehyde-glut is described by a simplified imine formation with primary amines originating from chitosan (Fig. 15). Considering this mechanism, the theoretical stoichiometric ratio for a complete conversion would be 0.5 mol glut per 1.0 mol primary amine.

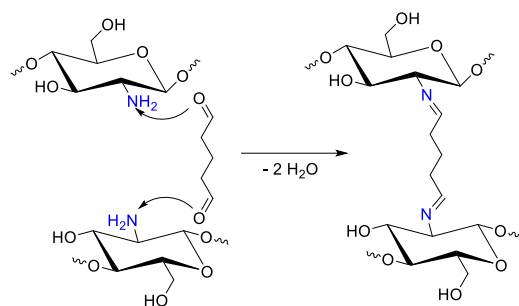


**Fig. 15: Simplified chitosan/glut crosslinking mechanism.**

In fact, a broad variety of reactions products are formed. The results of several studies show that it is likely for glut not only to react exclusively with the primary amines originated from chitosan, but also with itself. The characteristic orange/red/brown color of glut-crosslinked chitosans is attributed to the complex processes during the reaction of glut with primary amines, leading to oligomerization of glut, rearrangements, and/or cyclization of glut, results in irregular products, i.e. aromatic/heterocyclic structures (Migneault, Dartiguenave, et al. 2004; Kildeeva, Perminov, et al. 2009; Wang, Yuan, et al. 2014). The findings of Kildeeva et al. (2009) show that the primary amine of chitosan catalyzes the oligo-merization/polymerization of glut. Thus, the influence of the glut concentration on Chi-NPs formation via emulsion crosslinking technique was investigated. For those experiments, the aforementioned emulsion formulation (containing low MW chitosan and 0.1 M NaCl) was applied using different concentrations of glut: 0, 0.125 mol, 0.25 mol, 0.5 mol, 1.0 mol, 1.5 mol and 2.5 mol glut per mol of primary amine. As expected, the SEM micrographs of a formulation containing no glut, show only undefined, film like structures. Although, particles were probably formed during the emulsion process, the



## 5 Preparation of Chitosan Nanoparticles via Emulsion Crosslinking

absence of crosslinker leads to destruction of the particle structure during the centrifugation process. SEM micrographs of three different glut/amine ratios are displayed (Fig. 16). For a concentration of glut as low as 0.25 mol, strongly agglomerated but spherical-shaped particles were obtained (Fig. 16a). Particles synthesized with 1 mol glut per amine are shown in Fig. 16b. Ratios of 1 mol glut and higher (2.5 mol, Fig. 16c) lead to nanoscaled, dispersed and spherical particles.

For concentrations up to 1 mol of glut, the density of the chitosan/glut composite materials strongly decreases. A further increase of the glut concentration, from 1.0 mol to 2.5 mol, leads to a markedly lower decrease in density. The density of the resulting materials was analyzed by helium pycnometry. The pycnometry data (Fig. 16d) indicates a dependency of the material density on the glut concentration. The density measurements support the assumption that glut acts as a spacer molecule between the polymer chains, leading to inter- and intramolecular hydrogen bond breakage in chitosan. Similar results and corresponding explanations have been reported by Uragami et al. (1994).

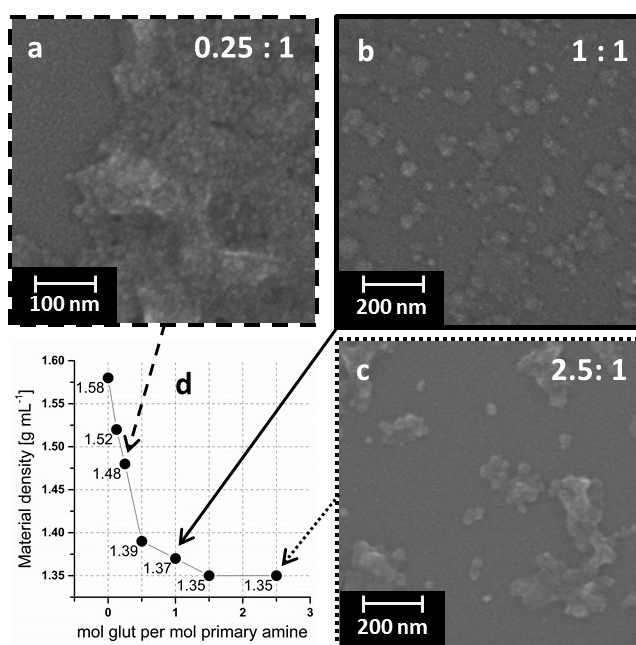


**Fig. 16:** SEM-micrographs (a-c) and pycnometry (d) of Chi-NPs synthesized with different glut concentrations (the line is drawn to guide the eye).

They analyzed the density of glutaraldehyde-crosslinked chitosan membranes at different crosslinker concentrations and also found a decrease in density with increasing glut concentration. As shown in Fig. 16d, the theoretical stoichiometric ratio of 1:1 glut : amine leads to a decrease in density by about 13 % compared to pure chitosan. Further increase of glut leads to a negligible decrease in density. Based on these results, a ratio of 1:1 provided a satisfactory compromise between redispersibility, a preferably low glut

concentration and particle stability. Hence, all further particle syntheses were performed with this 1:1 ratio, meaning 1 mole glut per mole primary amine in chitosan.

### 5.6.3. Variation of MWs

To determine the influence of chitosan MWs on particle properties and the reliability of the emulsion system, in terms of process robustness, emulsion preparation of Chi-NPs was conducted using different chitosan MWs. Six different chitosans were characterized by  $^1\text{H-NMR}$  spectroscopy, viscosity (solutions 3 % chitosan in 1 % acetic acid) shown in Table 3 and SEC (Fig. 17) using the protocols described in the experimental section. All chitosans share a high degree of deacetylation of about 95 %. The DD results provided by the manufacturers' titration method were confirmed by NMR spectroscopy (for calculation of DD, see materials and methods). The dynamic viscosity of chitosan solutions was determined for samples with 0.1 M NaCl in the aqueous phase. Viscosity of the chitosan solutions ranged from 19.3 mPa s up to 2149.5 mPa s.

The MWs were quantified via SEC with a relative calibration to a PVP standard. SEC results (Fig. 17) show MW ranging from  $M_w$  62 kg mol $^{-1}$  for the lowest molecular weight chitosan up to 270 kg mol $^{-1}$  for the chitosan with highest molecular weight. As expected for biopolymers, the chitosan samples exhibit a broad distribution in MW which is confirmed by the  $\text{PDI}_{\text{sec}}$  ranging from 2.52 to 4.9. The shown data for  $M_w$ ,  $M_n$  and PDI are in accordance with the data provided by the manufacturer.

## 5 Preparation of Chitosan Nanoparticles via Emulsion Crosslinking

**Table 3: Chitosan description and respective characterization data regarding viscosity and degree of deacetylation (DD).**

Chitosan type	DD <sup>a</sup> %	DD <sup>1</sup> H-NMR%	Dynamic viscosity <sup>b</sup> [mPa s]	Viscosity ratio <sup>c</sup> $\lambda$
95/5	93.8	98.7	19.3	21.4
95/10	95.2	99.5	74.3	82.6
95/20	93.6	97.2	182.6	202.9
95/50	94.3	97.8	429.5	477.2
95/100	92.8	97.2	1019.6	1132.9
95/200	94.5	97.9	2149.5	2388.3

<sup>a</sup> provided by manufacturer (titration method)

<sup>b</sup> 3 % chitosan solutions in 1 % acetic acid, containing 0.1 M NaCl

<sup>c</sup> Cyclohexane viscosity: 0.9 mPa s

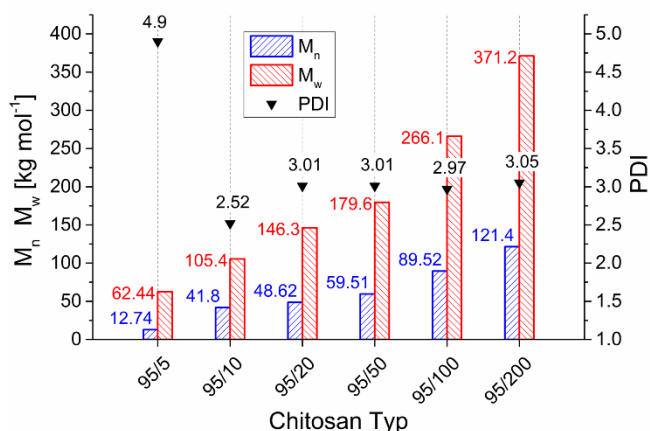


**Fig. 17: SEC measurements of the six used chitosans showing M<sub>n</sub>, M<sub>w</sub> and PDI.**

To determine the impact of chitosan MW on particle formation and on adsorption properties, six chitosans were used for Chi-NP preparation. For particle preparation, the optimized emulsion formulation described above was applied. The resulting nanoparticles were characterized by DLS and SEM.

The SEM micrographs (Fig. 18A) show spherical shaped, narrowly distributed particles for all six samples thus, confirming that monodisperse Chi-NPs could be synthesized with all tested formulations using different chitosans.

## 5 Preparation of Chitosan Nanoparticles via Emulsion Crosslinking

A

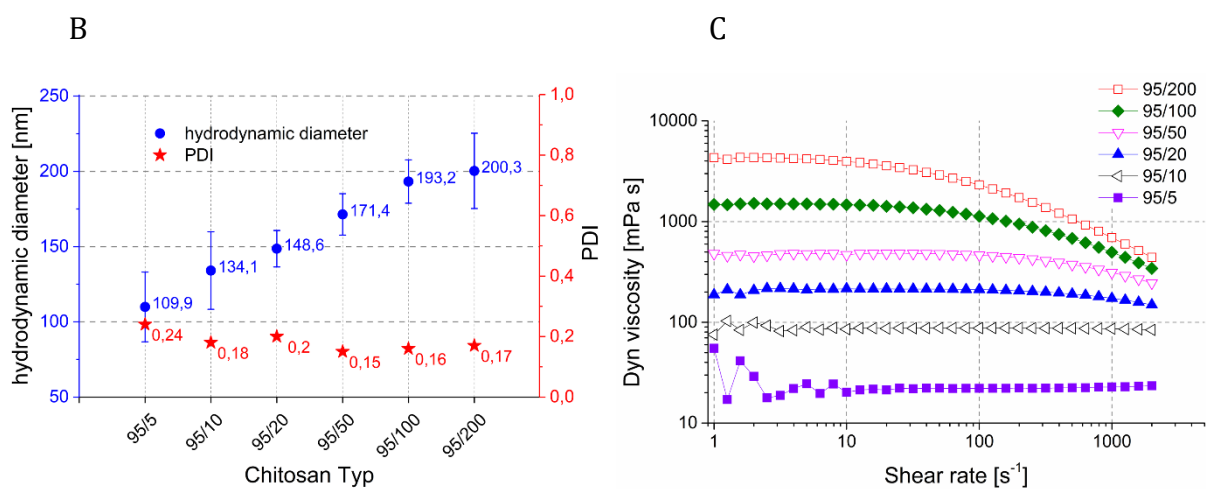
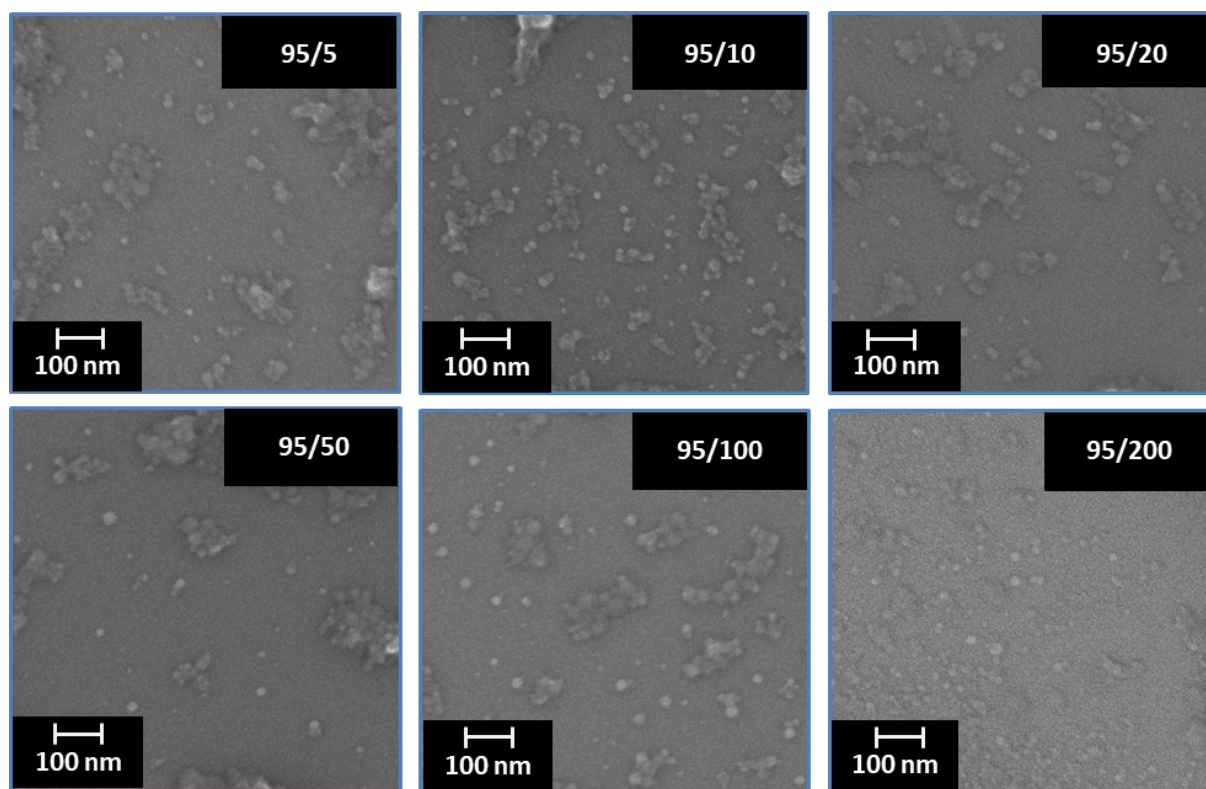


**Fig. 18: A: SEM-micrographs of synthesized Chi-NPs with six different chitosan types.**

**B: DLS measurements of six Chi-NPs. Particles were prepared in triplicates. The data points shown are the mean value of these three independent samples. Error bars indicate standard deviation of the three different particle samples.**

**C: Flow curves of different MW chitosan solutions (3 % chitosan in 1 % acetic acid).**

## 5 Preparation of Chitosan Nanoparticles via Emulsion Crosslinking

Due to the drying process in SEM sample preparation, the particles showed a smaller diameter compared to the particles used for the DLS measurements (Fig. 18B). Aside from that, a 3 % acetic acid was used for DLS sample preparation with a pH of 2.8. At this pH, crosslinked Chi-NPs tend to appear larger in DLS due to swelling. Each particle formulation was performed in triplicate and measured individually through DLS. The samples were always kept in a small volume of water. Each of these samples was characterized by DLS as described in the experimental section. Except for the lowest MW sample 95/50 ( $PDI_{DLS}=0.24$ ) the  $PDI_{DLS}$  for all samples is  $\geq 0.2$ . [Note: In order to resolve a logical inconsistency, this sentence was altered. Hence, the phrasing of this sentence now differs from the original publication]. Hence, all six samples can be described as narrowly distributed. We assume that the described emulsion system allowed the synthesis of narrow distributed Chi-NPs over a broad range of molecular weights of highly deacetylated chitosan.

Another finding was the correlation between particle size and chitosan MW. An increase in MW leads to larger particles. Chitosan particles with the lowest MW chitosan could be obtained with a hydrodynamic diameter of 109.9 nm up to a diameter of 200.3 nm for the highest MW. The same correlation was reported by Goycoolea et al. (2016) with non-crosslinked chitosan particles. They propose that a better control over particle size and distribution is attributed by a lower disperse phase viscosity during processing (Brunel, Véron, et al. 2009). This explanation is supported by Nazarzadeh & Sajjadi (2010) who stated that for the preparation of stable emulsions the viscosity of the disperse ( $\eta_d$ ) and the continuous ( $\eta_c$ ) phase can be crucial. They found that emulsion stability and droplet size correlate directly with the resulting particle size and their distribution. The ratio of  $\eta_d/\eta_c$  is called viscosity ratio ( $\lambda$ ). Nazarzadeh & Sajjadi (2010) investigated the impact of  $\lambda$  on the colloidal formation and stability of emulsions (o/w) prepared by ultrasonication treatment by varying  $\eta_d$  by using ten different silicon oils ranging from 0.5 mPa s to 100 mPa s. They showed that emulsification via sonication worked efficient till  $\lambda$  reached a value of 100. Exceeding a viscosity ratio of 390 drop rupturing did not occur at all. As shown in Table 3, particularly our high MW chitosan emulsion formulations exceeded the value of  $\lambda = 100$  by far with values of  $\lambda$  up to 2388.

There are two explanations for the formation of narrow distributed and spherical Chi-NP, regardless of the high viscosity of high MW. The first is that sonication of the chitosan solutions will induce chain scission of the chitosan molecules. Wu et al. (2008) showed that sonication of dissolved chitosan in acetic acid for 10 minutes can decrease the MW

## 5 Preparation of Chitosan Nanoparticles via Emulsion Crosslinking

particular of high chitosans of about 50 %. The lowering of the MW of chitosan would result in a reduction of  $\eta_d$  and, consequently, a lower value for  $\lambda$  will be obtained, which allows a better emulsification.

We assume that a second possibility is the composition of the dispersed phase itself being responsible for the successful particle preparation, despite the high viscosities. In this case, the aqueous phase consists of chitosan dissolved in 1 % acetic acid solution. Thus, the viscosity  $\eta_d$  of the aqueous phase arises from a two component mixture. As shown in Fig. 18C, notably the high MW chitosan solutions showed a shear-thinning behavior. For example, for samples with the highest MW (95/200 and 95/100), the viscosity at a shear rate of  $2000 \text{ s}^{-1}$  is about 80 % lower compared to a shear rate of  $100 \text{ s}^{-1}$ . The shear stress applied to the samples shown in Fig. 18 C was moderate when compared to the shear stress induced by the sonication probe. Hence, we estimate a trend of further shear-thinning behavior at higher shear rates, which can be seen not only for the high viscosity chitosan solutions, but also for the low MW ones.

Based on these results, we assume that the aqueous emulsion droplets (chitosan/acetic acid) undergo a shear thinning processes during sonication. Due to the high shear force applied by the probe sonotrode, we suppose that these low viscous droplets will burst instead of stretching or rupturing, which results in small narrowly distributed droplets. Nevertheless, Newtonian liquids do not exhibit a shear thinning behavior, such as the low viscosity silicon oils used by Nazarzadeh & Sajjadi (2010). In their work they showed that sonication of the disperse phases with a high viscosity lead to the rupture of the droplets via stretching, which resulted in larger droplets that, in turn, leads to emulsion instability. Emulsified high MW chitosan solutions, despite the shear-thinning effect, will still lead to larger droplets when compared to droplets from low viscous chitosan solutions. Increasing chitosan MW results in higher viscosity, which leads to larger droplets, ultimately resulting in larger particles. We propose that this is one of the main reasons for an increase in particle size with increasing chitosan WM.

All things considered, as long as the viscosity of the disperse phase is low enough (i.e. small  $\lambda$ ) *during* the emulsification process - by shear-thinning or chain scission - it is possible to formulate stable emulsions with high viscous disperse phases. In the future, these effects will be further investigated by rheology measurements of the disperse phase before and after emulsification. Determination of MW of the chitosans by SEC measurements and the comparison of MWs before and also after emulsification will further clarify the contributing of chain scission in this context.

#### 5.6.4. Adsorption behavior

In order to show that Chi-NPs can be used as a potential adsorption material, we compared the adsorption behavior of our Chi-NPs with the adsorption behavior of untreated chitosan powder in single-point sorption tests using two drugs which are highly relevant in wastewater treatment.

The adsorption behavior for carbamazepine (CBZ) and diclofenac (DCL) was tested in batch experiments. The particles were redispersed in 0.01 M phosphate buffer as media. This ensured drug and pH stability of the system over the adsorption time. A fixed amount of dissolved drug was added to a known amount of Chi-NPs. After 2 h, the suspensions were centrifuged and the remaining drug concentration in the supernatant was quantified by HPLC. The adsorption experiment for each sample was done in triplicate and the obtained data is shown in Fig. 19. We found that the adsorption of CBZ for untreated chitosan and Chi-NPs was below 20 % (Fig. 19A), although most of the Chi-NPs still showed an increased adsorption behavior compared to untreated chitosan and a maximum of 2.7 mg g<sup>-1</sup> CBZ was adsorbed. The overall low adsorption could be attributed to the lack of charge in the CBZ, which results in a low affinity towards the untreated chitosan and Chi-NPs.

As a second model drug, we used the negatively charged DCL (sodium salt). Preliminary adsorption experiments with Chi-NPs at lower DCL concentration (1 µg mL<sup>-1</sup> and 10 µg mL<sup>-1</sup>) showed an adsorption of almost 100 %. Thus, we further increased the concentration of DCL. The remediation for DCL at a concentration of 100 µg mL<sup>-1</sup> (1.5 mL sample volume) was in the range of 60 % for the low MW Chi-NPs and decreased to 25 % for Chi-NPs derived from chitosan with the highest MW (Fig. 19 B). These single point adsorption values corresponded to an amount of adsorbed DCL of 9.54 mg g<sup>-1</sup> for the lowest MW Chi-NPs and 3.83 mg g<sup>-1</sup> for the highest MW Chi-NPs.

In contrast, the untreated chitosans exhibited a low adsorption capacity towards the DCL at a maximum of 1 %. Regardless of the chitosan MW, the adsorption for all samples was below 10 %.

## 5 Preparation of Chitosan Nanoparticles via Emulsion Crosslinking

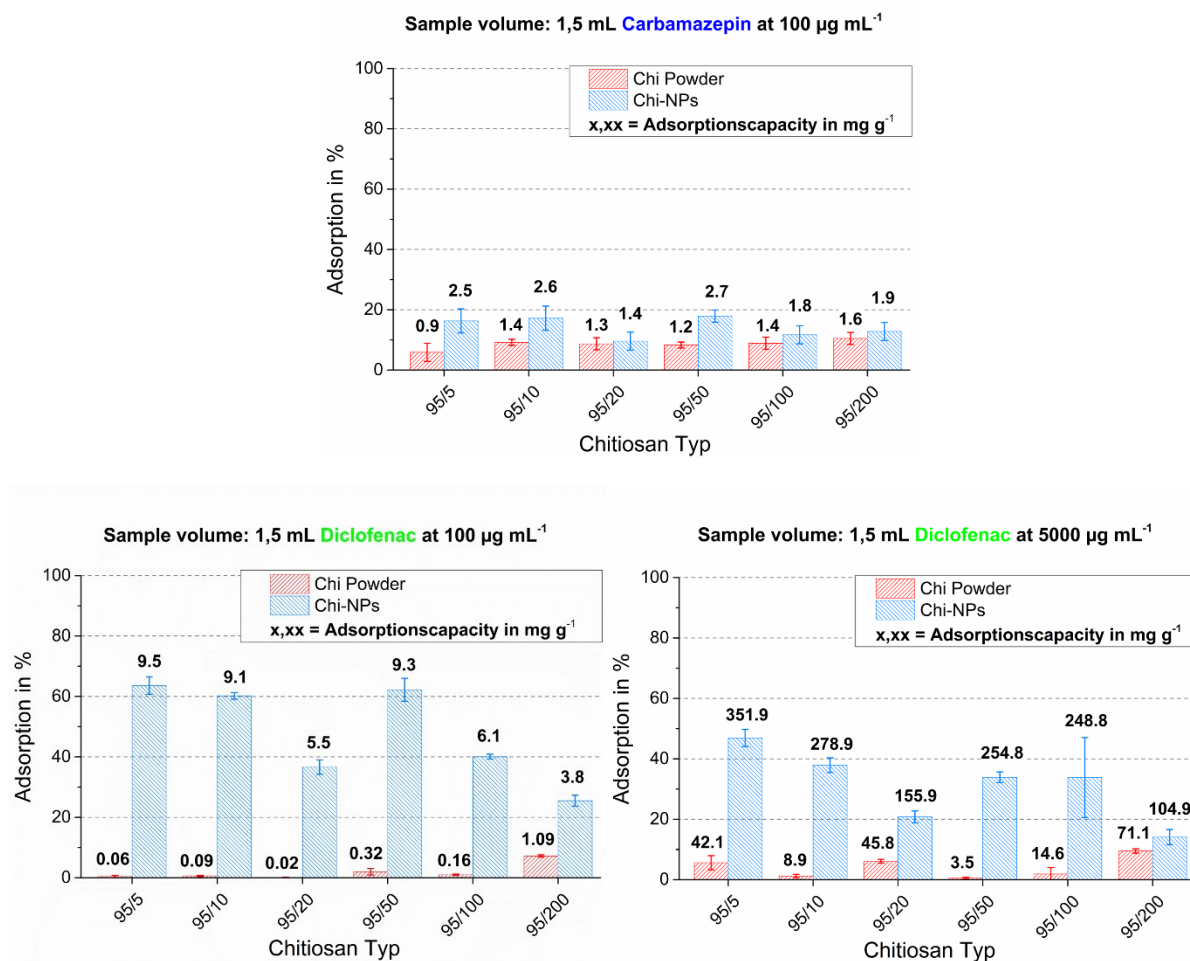


**Fig. 19: Adsorption behavior of Chi-NPs for A) Carbamazepin at a concentration of 100  $\mu\text{g mL}^{-1}$ , B) Diclofenac at 100  $\mu\text{g mL}^{-1}$  and C) Diclofenac at 5000  $\mu\text{g mL}^{-1}$ . All measurements were done in triplicates and the error bars indicate the standard deviation among them. The numbers above the bars indicate the adsorption capacity ( $\text{mg drug adsorbed per g adsorbent at a certain drug concentration}$ ).**

As shown above, particles synthesized with lower molecular weight chitosans result in smaller particles and therefore, in a better *surface - to - volume* ratio. Considering the adsorption results for DCL, we assume that in general smaller Chi-NPs are more suitable for adsorption.

In order to determine the adsorption of Chi-NPs at higher concentration we increased the DCL dosage to 5000  $\mu\text{g mL}^{-1}$  with a 1.5 mL sample volume (Fig. 19 C). Low MW Chi-NPs showed the best adsorption behavior by adsorbing 351.8  $\text{mg g}^{-1}$  respectively with a remediation of about 47 %, whereas the Chi-NPs prepared with high MW chitosan showed an adsorption with only 14 % remediation and 104.97  $\text{mg g}^{-1}$ . The adsorption values for 5000  $\mu\text{g mL}^{-1}$  between lowest and highest MW showed a behavior comparable to data obtained with 100  $\mu\text{g mL}^{-1}$ . A general tendency of a decrease in adsorption capacity with an increase in MW could be observed for the 5000  $\mu\text{g mL}^{-1}$  samples. The high adsorption of DCL on Chi-NPs is presumably attributed to the negative charge of the compound. Due



to its amine content, chitosan can act as a weak ion exchanger and, therefore, DCL could exhibit an increased affinity towards the Chi-NPs.

The difference between Chi-NPs and untreated chitosan is evident. The untreated chitosan powder itself is a dense, nonporous material with a low surface/volume ratio. Therefore, low adsorption values for chitosan powder were expected when compared to nano-structured Chi-NPs. Moreover, the high adsorption values of Chi-NPs are not solely attributed to the size and surface/volume ratio, but also to the presence of glut in the composite material. As described above, crosslinking with glut leads to a decrease in chitosan density, which results in a more swellable composite material. (Poon, Wilson, et al. 2014) prepared bulk chitosan/glut composite powders with a macroparticle size, in the range of mm, by varying the glut content. They evaluated the adsorption behavior of these materials towards p-nitrophenol and their results indicated an improvement in adsorption behavior with increasing glut content.

### 5.7. Conclusions

In this work, we present a miniemulsion formulation containing cyclohexane as oil phase, Span 80 as surfactant, and a chitosan solution in 1 % acetic acid as disperse phase for the synthesis of covalently crosslinked Chi-NPs. Emulsions with the preferable low water/oil ratio of 1 : 3.3 (v/v) have been prepared. To further optimize the long term emulsion stability, NaCl was added to the formulation as hydrophile. The utilization of 0.1 M NaCl in the disperse phase lead to an increased emulsion stability (> 18 h) and further increased the particle yield up to 80 %.

Regarding the primary amine content of chitosan, different crosslinker concentrations of glut have been tested. The results indicated that a primary amine : glut ratio of 1 : 1 is sufficient to produce spherical and narrowly distributed crosslinked particles.

With these optimized parameters, Chi-NPs were synthesized using six highly deacetylated chitosans of different MWs. Particularly high MW chitosan solutions exhibited a shear-thinning behavior even at low sheer forces. Accordingly, the disperse phase viscosity was strongly decreased due to the high sheer forces applied by sonication. This allowed for the successful emulsification even of the high MW chitosan solutions. Consequently, it was possible to synthesize Chi-NPs with all six chitosans. The results of DLS measurements indicated an increasing particle size with increasing chitosan MW ranging from 109.9 d.nm for lowest chitosan MW up to 200.3 d.nm for the highest chitosan

## 5 Preparation of Chitosan Nanoparticles via Emulsion Crosslinking

MW. We suggest this effect is attributed to the disperse phase viscosity. Higher viscosity leads to larger droplets, which ultimately results in larger particles.

The adsorption behavior towards the two chosen drugs - CBZ and DCL - was tested for all six untreated chitosan powders and the corresponding formulated Chi-NPs. The remediation of CBZ ( $100 \mu\text{g mL}^{-1}$ , 1.5 mL) was below 20 % for Chi-NPs and below 10 % for untreated chitosan. The remediation of DCL at  $100 \mu\text{g mL}^{-1}$  was found to be in the range of 60 % for low MW Chi-NPs and 25 % to Chi-NPs synthesized with the highest MW chitosan. At an increased DCL concentration ( $5000 \mu\text{g mL}^{-1}$ , 1.5 mL) a similar tendency was observed. Low MW Chi-NPs showed the best adsorption properties against  $5000 \mu\text{g mL}^{-1}$  DCL, with a capacity of  $351.8 \text{ mg g}^{-1}$  and a remediation of about 47 %. Again, a general tendency of increasing adsorption capacity of Chi-NPs proceeding from low chitosan MW was observed. We propose that this effect is attributed to the nanostructure of the particles and its consequent high surface to volume ratio, besides from the glut presence, which increases the swellability of the Chi-NPs, thus contributing to an increase in its adsorption capacity. Future experiments should focus on the determination of dynamic adsorption capacities, adsorption equilibrium and desorption behavior.

### 5.8. Acknowledgements

We gratefully acknowledge the help of Alec Nienhauser with particle synthesis and DLS measurements and Monika Riedl (Fraunhofer IGB) for conducting SEM.

## 6. Chitosan Nanoparticles as Adsorber in Mixed-Matrix Membranes

In this chapter, the results for the discussion of hypotheses I.II and I.III (6.1) are presented. Chapter 6.2 to 6.8 represents a manuscript with the title “*Chitosan nanoparticles via high-pressure homogenization-assisted miniemulsion crosslinking for mixed-matrix membrane adsorber*”, which was published as a research paper in the peer-reviewed journal *Carbohydrate Polymers* (Riegger, Kowalski, et al. 2018). As basis for this work, the results from chapter 5 were used. The discussion of hypothesis I.II and I.III can be found in the discussion section in chapter 9.1.2 and 9.1.3.

Please note: Minor modifications were made to the original manuscript concerning layout and orthography in order to fit the style of this thesis. No content-related changes were performed.

### **Declaration about my own contribution**

*I conceived the study and elaborated the detailed experimental design.*

*This specifically included:*

- *Conceptualization and formulation of the overarching research goals within the study.*
- *Design of the experimental approach for particle synthesis via high-pressure homogenization-assisted miniemulsion crosslinking.*
- *Investigation and implementation of protocols for the handling and preparation of chitosan solutions and emulsions such as: duration of dissolution, filtration and premixing.*
- *Investigation and selection of suitable chitosans, crosslinkers and emulsifiers used for the synthesis in this study.*
- *Determining the range of concentrations and stoichiometric calculation of synthesis educts and components, especially the amount of chitosan, primary amine content, crosslinker, stabilizers and emulsion phase ratios.*

## 6 Chitosan Nanoparticles as Adsorber in Mixed-Matrix Membranes

- *Elaboration and implementation of emulsion/particle preparation protocols in terms of selecting high-pressure homogenization parameters, durations and particle separation/purification.*
- *Elaboration and implementation of membrane preparation protocols in terms of selecting the approach for redispersing particles in membrane polymer solutions and calculating/validating particle content in the resulting membranes.*
- *Elaboration and implementation of sample preparation protocols and the necessary procedures for analytical methods such as scanning electron microscopy (SEM), dynamic light scattering (DLS), size exclusion chromatography (SEC), rheology, high performance liquid chromatography (HPLC) as well as protocols for data evaluation and analysis.*
- *Selection and investigation of relevant active pharmaceutical ingredients (APIs) which were used in the adsorption experiments to evaluate the adsorption behavior of the prepared chitosan nanoparticles.*
- *Conceptualization and implementation of the particle synthesis experiments and membrane preparation as well as particle- and membrane characterization. The data on particle- and membrane preparation and characterization shown in this study, were collected by Regina Kowalski in the course her master thesis under my supervision and by applying my methodology.*
- *Research and implementation of computational applications for the modeling of adsorption isotherms.*
- *Conceptualization and implementation of the experiments for the characterization of the static adsorption behavior on chitosan nanoparticles (kinetics and modeling adsorption isotherms) as well as the dynamic adsorption of nanoparticle-loaded mixed-matrix membranes via HPLC. The data on adsorption characterization shown in this study, was collected by Luise Hilfert in the course her master thesis under my supervision and by applying my methodology.*
- *Evaluation and discussion of all data in an overall context of this study.*
- *Visualization of the acquired data (graphs) and schematic representation.*
- *Writing of the entire original draft of the publication and taking the leading role in incorporating changes proposed by co-authors and reviewers.*

## 6.1. Hypotheses I.II and I.III

### Hypothesis I.II:

*It is possible to transfer an emulsion formulation, which was optimized for a discontinuous ultrasonication emulsification to a continuous high-pressure homogenization (HPH)-based process.*

- *Similar to the ultrasonication emulsification it is possible to process chitosan of different MW via high-pressure homogenization to reproducibly prepare Chi-NPs.*

### Hypothesis I.III:

*It is possible to disperse the Chi-NPs from 1.2 in a membrane polymer solution in order to prepare Chi-NP loaded mixed-matrix membranes.*

- *The Chi-NP mixed-matrix membranes can be applied for the adsorption of pharmaceutical compounds in aqueous media.*

Riegger, Benjamin R., Regina Kowalski, Luise Hilfert, Günter E.M. Tovar, and Monika Bach. (2018). "Chitosan Nanoparticles via High-Pressure Homogenization-Assisted Miniemulsion Crosslinking for Mixed-Matrix Membrane Adsorbers." *Carbohydrate Polymers* 201 (December): 172–81. <https://doi.org/10.1016/j.carbpol.2018.07.059>.

## **6.2. Chitosan Nanoparticles via High-Pressure Homogenization-Assisted Miniemulsion Crosslinking for Mixed-Matrix Membrane Adsorbers**

Benjamin R. Riegger<sup>a</sup>, Regina Kowalski<sup>a</sup>, Luise Hilfert<sup>a</sup>, Günter E.M. Tovar<sup>\*a,b</sup>, Monika Bach<sup>\*a,‡</sup>

<sup>a</sup>Institute for Interfacial Process Engineering and Plasma Technology IGVP, University of Stuttgart, Nobelstr. 12, 70569 Stuttgart, Germany. Tel: +49 711 685 68162;

<sup>b</sup>Fraunhofer Institute for Interfacial Engineering and Biotechnology IGB, Nobelstr. 12, 70569 Stuttgart, Germany.

<sup>‡</sup>Present address: Core Facility, University of Hohenheim, Emil-Wolff-Straße 12, 70599 Stuttgart, Germany. Tel: +49 711 45922735

\*Corresponding Authors: E-mail: [monika.bach@uni-hohenheim.de](mailto:monika.bach@uni-hohenheim.de) and [guenter.tovar@igvp.uni-stuttgart.de](mailto:guenter.tovar@igvp.uni-stuttgart.de)

**Published in the peer-reviewed journal Carbohydrate Polymer**

Publisher: Elsevier

DOI: 10.1016/j.carbpol.2018.07.059

Volume: 201; Pages: 172-181

Received 27 March 2018; Received in revised form 20 June 2018; Accepted 17 July 2018;

Available online 21 July 2018

### 6.3. Abstract

Glutaraldehyde-crosslinked chitosan nanoparticles (Chi-NPs) were prepared reproducibly via miniemulsion crosslinking for effective adsorption of the active pharmaceutical ingredient (API) diclofenac (DCL). Three different molecular weights (MWs) of highly deacetylated (> 90%) chitosans (low, medium and high MW) were used to vary the disperse phase viscosity. Particle formation was evaluated ranging from one to seven homogenization cycles at 40 MPa. Particles were prepared successfully with the low and medium MW chitosan in the range of 125 nm - 250 nm (z-average). In HPLC assisted, static adsorption experiments, all particles showed a rapid sorption rate (< 2 min) with an adsorption capacity of up to 256.2 mg g<sup>-1</sup> DCL. Modelling of adsorption isotherms resulted in a  $q_{\max}$  358.3 mg g<sup>-1</sup> for Langmuir and 502.5 mg g<sup>-1</sup> for Sips, respectively. Membrane adsorbers were prepared by processing Chi-NPs into porous polyether sulfone microfiltration membranes via a casting and phase inversion process, resulting in an adsorption capacity of up to 3.6 mg m<sup>-2</sup> DCL in dynamic adsorption experiments.

Keywords: chitosan nanoparticles; adsorption; active pharmaceutical ingredients (API); water purification; membrane adsorbers

### 6.4. Introduction

An increasing contamination of the aquatic environment with substances from industrial sources is expected to become one of the major challenges for the next decades. Especially, the appearance of active pharmaceutical ingredients (APIs), particularly in drinking water (surface and groundwater), is a major concern. Next to several other drugs like hormones and antibiotics, the widely used painkiller diclofenac (DCL) has been added to the watch list of substances for European Union-wide monitoring (Decision 2015/495/EU of 20 March 2015; Barbosa, Moreira, Ribeiro, Pereira, & Silva, 2016).

The development of high capacity adsorbers could be a viable method for the remediation of aquatic pollution caused by APIs and therefore is the main subject of many current research projects. Ideally, such adsorption systems would originate from renewable sources such as cellulose or chitin.

After cellulose, the second most abundant biopolymer is chitin, which is widely available in exoskeletons of crustaceans. Chitin is insoluble in conventional solvents. When treated with strong alkaline media, the deacetylated derivative named chitosan is formed, a method, which was first reported by Rouget in 1859. Chitosan bears primary amines, which allow dissolution in diluted acidic media, enabling a processing of the cationic biopolymer. Chitosan and its composite materials have been reported to be a promising material for adsorption of various substances like organic dyes (Vakili, Rafatullah, et al. 2014) and metal ions (L. Zhang, Zeng, et al. 2016; Wan Ngah, Teong, et al. 2011). The adsorption of pharmaceutical compounds like pramipexole (Kyzas, Kostoglou, et al. 2013), tetracycline (Oladoja, Adelagun, et al. 2014; Ma, Zhuang, et al. 2015), dorzolamide (Kyzas, Bikiaris, et al. 2014) and diclofenac (Yalei Zhang, Shen, et al. 2014) have also been reported. The primary amines and other moieties like hydroxyl groups and acetamido groups facilitate this adsorption behavior towards a wide variety of substances (Olivera, Muralidhara, et al. 2016).

Compared to other material classes, nanomaterials and in particular nanoparticles, possess properties, which are favorable for adsorption applications (Santhosh, Velmurugan, et al. 2016). Next to their defined architecture, especially the high surface to volume ratio i.e. the high specific area is beneficial (Hristovski, Baumgardner, et al. 2007). There are several different techniques for the preparation of covalently and non-covalently crosslinked chitosan nanoparticles (Chi-NPs) (Agnihotri, Mallikarjuna, et al. 2004). Covalently crosslinked materials are desired, specifically if they are used in adsorption processes, which can include regeneration processes (adsorption/desorption) with pH or solvent shifts. With the use of a suitable crosslinker like glutaraldehyde, covalently crosslinked and narrowly distributed Chi-NPs can be prepared via oil-in-water-based miniemulsion technique (Ohya, Shiratani, et al. 1994; Zhi, Wang, et al. 2005; Riegger, Bäurer, et al. 2018). Usually such miniemulsions (also called nanoemulsions) are prepared via high shear stress-induced by probe sonication or rotor-stator. However, these sonication techniques are limited in terms of volume (sonication) or emulsification efficiency (rotor-stator). For the application of such adsorber materials, larger amounts of particles are required. In industry, high-pressure homogenization (HPH) is often used for the preparation of emulsions (Schultz, Wagner, et al. 2004). Compared to the aforementioned techniques, the advantage of HPH is the high volume throughput and its emulsification efficiency, which is necessary for the preparation of larger amounts of emulsion i.e. particles (Shi, Li, et al. 2011). HPH process parameters, which influence the



resulting emulsion, are mainly the orifice/nozzle geometry, the applied pressure and the number of homogenization cycles, i.e. homogenization time (Schuchmann, Karbstein, et al. 2012). The HPH technique has already successfully been used for the preparation of starch nanoparticles via miniemulsion crosslinking (Shi, Li, et al. 2011).

Evidently, such nanoparticles should not be introduced to the aquatic environment without having the means to remove them after the adsorption process. There are two main techniques to use nanoparticles in adsorption processes without introducing them irretrievably to the aqueous system. One approach is the use of magnetic nanoparticles. For the adsorption of a contaminated media, the NPs are dispersed and then separated by using a permanent magnet. Several magnetic chitosan nanoparticles for the removal of chromium (Thin, Hanh, et al. 2013), copper (Yuwei and Jianlong 2011), palladium/platinum (L. Zhou, Xu, et al. 2010) or DCL (Yalei Zhang, Shen, Dai, & Zhou, 2014) have been reported.

An alternative approach, which allows the processing of regular, non-magnetic nanoparticles, is the preparation of mixed-matrix membranes, also called membrane adsorbers. Nanoparticles are dispersed in a suitable polymer solution and processed to flat sheet membranes. The particles are entrapped in the highly porous polymer membrane resulting in an increased adsorption capacity compared to a membrane containing no nanoparticles. This concept has been shown to work with different synthetic polymer nanoparticles entrapped in high flux microfiltration polyethersulfone (PES) membranes for the adsorption of bisphenol A (Niedergall, Bach, et al. 2013), penicillin G / bisphenol A (Niedergall, Bach, et al. 2014) and various metal ions like copper, silver and lead (Niedergall, Kopp, et al. 2016). PES mixed-matrix nanofiltration membranes containing O-carboxymethyl chitosan coated  $\text{Fe}_3\text{O}_4$  nanoparticles for dye removal in wastewater were reported by (Zinadini, Zinatizadeh, et al. 2014).

The aim of this study was the development of a high-pressure homogenization-assisted processing method of chitosan solutions containing chitosans of different molecular weights for the preparation of Chi-NPs via miniemulsion crosslinking technique. The goal was to present a straightforward synthesis strategy, which reproducibly leads to suitable amounts of narrowly distributed Chi-NPs. The different Chi-NPs were tested extensively for their static adsorption behavior towards the example of a highly relevant API, namely Diclofenac (DCL). For this purpose, the adsorption kinetics and isotherms of the Chi-NPs in HPLC-assisted batch adsorption experiments were determined. As a proof of concept, the Chi-NPs were used subsequently for the preparation of mixed-matrix membrane

adsorbers. In order to characterize those Chi-NP-filled membranes, their dynamic adsorption behavior and adsorption capacity for DCL was investigated.

### 6.5. Experimental

#### 6.5.1. Materials

Commercially available chitosans of different molecular weights (MWs) were purchased: low MW chitosan (90/10/A1) from Kraeber & Co GmbH, Germany; medium MW chitosan (90/60/A1) was a kind gift of Textilchemie Dr. Petry GmbH, Germany; and high MW chitosan (95/200) was purchased from Heppe Medical Chitosan GmbH (HMC), Germany. The MW was quantified via size exclusion chromatography (SEC) measurements and the degree of deacetylation was verified by  $^1\text{H-NMR}$ -spectroscopy (see Table 4). Acetic acid solution for HPLC (assay 49-51 %), glutaraldehyde solution (25 % in  $\text{H}_2\text{O}$ ,  $d=1.06\text{ g mL}^{-1}$ ), trifluoroacetic acid (TFA) (99 %), acetonitrile HPLC-grade, diclofenac-sodium, Dulbecco's phosphate buffered saline and sorbitan monooleate (Span 80, viscosity 1000-2000 mPa s) were purchased from Sigma-Aldrich, Germany. Cyclohexane (Applichem, > 99.5 %) and polyethylenglycol 600 (PEG600) were obtained from Häberle Labortechnik GmbH, Germany.  $\text{D}_2\text{O}$  and  $\text{CD}_3\text{COOD}$  (acetic acid-D4) were purchased from Deutero GmbH, Germany. N-Ethyl-2-pyrrolidon (NEP) was purchased from Carl Roth, Germany. Polyethersulfone (PES) Veradel 3000P was obtained from Solvay.

All chemicals were used as received. ASTM Type I water (TKA GenPure) was used throughout this study (herein referred to as water). The used rotor-stator homogenizer was obtained from Heidolph Silentcrusher M (homogenizer tool 12F). High-pressure homogenizer (HPH) EmulsiFlex-C3 (throughput 3 L/h) was purchased from Avestin, Germany. The ultrasonicator Branson 450-D equipped with a 5 mm Tip used in this study was obtained from G. Heinemann Labortechnik, Germany. The centrifuge used was a Beckmann & Coulter Avanti J-26 XPI with JA-25.50 Rotor and JLA 10.500.

## 6.5.2. Methods

### Calculation of Primary Amine Content

<sup>1</sup>H-NMR spectroscopy (Bruker BioSpin Avance 500) was performed to confirm the degrees of deacetylation (DDs) provided by the manufacturer (see Table 4). The procedure for sample preparation was described elsewhere (Riegger, Bäurer, et al. 2018). For DD determination, the integral of H<sub>N-COCH<sub>3</sub></sub> at 1.90 - 2.10 ppm and the integrals of H<sub>2</sub>-H<sub>6</sub> ranging from 3.0 - 4.25 ppm were used. The DDs were calculated using the following equation (1) described by Hirai, Odani, & Nakajima (1991).

$$DD = \left( 1 - \frac{I_{CH_3/3}}{I_{H_2-H_6/6}} \right) \cdot 100 \quad (1)$$

As shown in Table 4, the DDs determined by <sup>1</sup>H-NMR spectroscopy confirmed the DDs provided by the manufacturer. The primary amine content was calculated individually for each chitosan. For the calculation of the primary amine content of chitosan, equations (2) and (3) were applied using the DDs provided by the manufacturer. In a first step (2), the average molecular mass of the structural repeating unit (SRU) of chitosan was calculated. For the calculation of the SRU this equation takes both, the degree of deacetylation (DD) and the degree of polymerization (DP) of chitosan into account. The DD has a significant influence on the SRU while the influence of the DP on the SRU decreases with an increase of the DP. The value for the DP was calculated from the SEC data.

$$M_{Chi(SRU)} = M_{GlcNAc} - M_{H_2O} + \frac{M_{H_2O}}{DP} - DD (M_{GlcNAc} - M_{GlcN}) \quad (2)$$

The amount of primary amines was then calculated applying equation (3) using the calculated SRU from above.

$$n_{(primary\ amine)} = \frac{m_{Chi}}{M_{Chi(SRU)}} \cdot \frac{DD}{100} \quad (3)$$

### Size Exclusion Chromatography (SEC)

SEC measurements were performed at 40 °C in water (0.1 % trifluoroacetic acid (TFA) (v/v), 0.1 M NaCl, flow rate 0.5 mL min<sup>-1</sup>) on a 1260 Infinity GPC-SEC Analysis System (Agilent Technologies) equipped with a refractive index (RI) detector and a PSS NOVEMA Max linear XL 5 000 – 3 000 000 Da (Polymer Standards Service GmbH) column with a Poly-2-vinylpyridine (PVP) calibration. For sample preparation, chitosan (2 mg mL<sup>-1</sup>) was dissolved in eluent.

### Rheology

All rheological measurements were performed on a *Physica MCR 301* (Anton Paar) rheometer using a coaxial cylinder geometry. Flow curves were obtained with a logarithmic shear rate ramp with shear rates between 1 s<sup>-1</sup> and 2000 s<sup>-1</sup>. Chitosan sample composition and NaCl content were as described above.

### Preparation of Chitosan Nanoparticles

The emulsion formulation used was described in a previous work (Riegger, Bäurer, et al. 2018). A general schematical representation of the particle preparation process is given in the previous work. Particle preparation with chitosans of different MWs always followed the following procedure. Chitosan (1620 mg) was dissolved in 54 mL of 1 % (v/v) acetic acid containing 0.315 g (0.1 M) NaCl. The sodium chloride was used as hydrophile to prevent nanodroplets from *Ostwald* ripening as discussed previously (Riegger, Bäurer, et al. 2018). The mixture was stirred until a clear solution was obtained. To remove insoluble components, the resulting solution was filtered through a filter crucible under reduced pressure. The continuous phase (oil phase) consisted of 7.2 g Span 80 dissolved in 180 mL cyclohexane. Aqueous phase and oil phase were combined and premixed through brief rotor-stator mixing. This emulsion was filled into the high-pressure homogenizer (HPH) feed vessel, run for seven cycles at 40 MPa, and subsequently transferred to a sealed vial. To this solution, a calculated amount of glutaraldehyde (glut) was added under magnetic stirring to enable the crosslinking process. An amount of one mole glut per mole primary amine was chosen. Due to different DDs, the amount of glut was adjusted according to the calculated amount of primary amines. The amount of primary amines was calculated using the DDs provided by the manufacturer and the equations as described above. The emulsion containing the crosslinker was agitated

overnight. Afterwards, the emulsion was transferred into a 500 mL-polycarbonate centrifugation tube to purify Chi-NPs via centrifugation. The emulsion was broken by filling the tube with ethanol and centrifugation at 18.592 G (10k rpm, rotor: JLA 10.500) for 10 minutes. The supernatant was discarded, the resulting gel-like pellet was redispersed in ethanol, sonicated for 20 seconds via sonotrode (60 % amplitude 5 seconds on; 5 seconds off) and shaken for 10 minutes. This procedure was repeated four times with ethanol and twice with water.

Subsequently, particles were treated depending on their further use. DLS samples were prepared using a part of the aqueous pellet. Chi-NP samples for the characterization of static adsorption behavior were produced by freeze-drying the aqueous particles suspensions. For the embedding of particles in membranes, a solvent exchange with N-Ethyl-2-pyrrolidon (NEP) was conducted after the last centrifugation in water. In order to remove the water, the aqueous particle pellet was redispersed in NEP by ultrasonication, shaken for one hour and subsequently centrifuged. The resulting pellet was ready for further use in the formulation of particle containing membrane polymer solutions.

### Preparation of Mixed-Matrix Membranes

A general method for the preparation of mixed-matrix membranes was described by Niedergall et al. (2014). The NEP-swollen Chi-NP pellets (see preparation section) were redispersed via probe sonication in 144.7 mL NEP. Subsequently, PEG 600 (273.8 g) as performing agent and the membrane polymer PES (79.65 g) were added and mixed on a tube roller until complete dissolution of the PES. The resulting casting solution (membrane polymer solution) had a particle content of 0.9 % for low MW particles and 1.18 % for medium MW Chi-NPs. The particle mass content related to the membrane polymer, i.e. in the resulting membrane, was 6.4 % and 7.42 % for low MW particles and medium MW Chi-NPs respectively. Casting solutions for the preparation of reference membranes contained no particles.

Mixed-matrix membranes were prepared via casting and phase inversion process using water as non-solvent. The solution was casted over a clean glass plate (approx. 20 cm x 35 cm) with the help of a doctor blade (200  $\mu\text{m}$ ). Immediately after casting, the glass plate was transferred into a climate chamber at 25 °C and 80 % rel. humidity for 5 minutes. Subsequently, the glass plate was submerged in a water bath containing water at room temperature. After several minutes, the thin polymeric film

peeled off from the glass plate. The membrane was washed intensely with water and stored in water until further use.

### **6.5.3. Characterization of Chi-NPs and Membranes**

#### Dynamic Light Scattering (DLS)

Measurements of size (z-average, intensity-based) and polydispersity index (PDI) of Chi-NPs were performed via DLS. The device was equipped with a 4 mW He-Ne Laser  $\lambda = 632.8$  nm (Zetasizer ZEN 3600 - NanoZS, Malvern Instruments). Scattering photons were collected in backscattering mode at an angle of  $173^\circ$ . For sample preparation, a sufficient amount of Chi-NPs was redispersed in 3 % acetic acid by applying probe sonication treatment (5 seconds “on” / 5 seconds “off”) for 120 seconds. A  $1.2 \mu\text{m}$ -syringe filter was used to remove larger sized agglomerates. The refractive index of 3 % acetic acid was calculated and applied within the Malvern Zetasizer software. Measurements were performed in single use polystyrene cuvettes at  $20^\circ\text{C}$ . The reported sizes are the intensity-based z-average diameters of three measurements (> 10 runs each).

#### Scanning Electron Microscopy (SEM)

To determine morphology and size of the particles, scanning electron microscopy (SEM) was performed using a Zeiss Leo 1530 VP (Jena, Germany). Diluted dispersions of Chi-NPs were placed on silicon wafers and dried at ambient conditions. To minimize electrostatic charging, the samples were sputter-coated with platinum.

#### Determination of Static Adsorption Behavior

Adsorption kinetics for diclofenac (DCL) were tested in batch experiments for both types of Chi-NPs at nine different concentrations ranging from  $0.3 \text{ mg L}^{-1}$  to  $2500 \text{ mg L}^{-1}$ . Chi-NPs (10 mg) were redispersed in 4 mL phosphate buffer (0.01 M, pH = 7) with ultrasonication treatment. To the resulting dispersion, 2 mL of a drug stock solution was added and placed on a shaker. For the determination of adsorption kinetics, the adsorption capacity was measured at 15 different contact times (5 seconds up to 60 minutes). Subsequently, the particle suspension was centrifuged for 2 minutes at 12000 rpm resulting in a range of contact time of 125 seconds to 62 minutes. The remaining drug concentration in the supernatant was analyzed by High Performance Liquid

Chromatography (HPLC) (device: Shimadzu prominence) as described elsewhere. (Riegger, Bäurer, et al. 2018) A volume of 10  $\mu\text{L}$  (for  $c = 300 \text{ mg L}^{-1} - 2500 \text{ mg L}^{-1}$ ) and a volume of 100  $\mu\text{L}$  (for  $c = 0,3 \text{ mg L}^{-1} - 30 \text{ mg L}^{-1}$ ) was injected on a reversed phase column. To ensure that the system is at full equilibrium, we chose to use the last four data points from the kinetic experiments for the calculation of a mean  $q_e$ . These mean  $q_e$  were plotted against  $C_e$  and fitted by Langmuir, Freundlich and Sips isotherm (also known as Langmuir-Freundlich isotherm) equation using OriginPro 2017 (OriginLab). The equations and the procedure for modeling the adsorption isotherms was applied as described by Repo et al. (2010).

### Determination of porosity

The membrane porosity was determined via capillary flow porometry (Porolux 1000, Porotec GmbH). The device was pressurized with nitrogen and the diameter of membrane samples was 25 mm. Before measuring the porosity, the samples were repeatedly washed with ethanol. In a final step, the samples were fully wetted with ethanol (surface tension  $22.6 \text{ mN m}^{-1}$ ) and subsequently used for determining the mean pore size. Wet and dry curves were determined. As the capillaries are assumed to be fully wetted, a contact angle of  $0^\circ$  as well as a shape factor of 1 was assumed for the calculation of the mean pore size via Young-Laplace equation.

### Determination of Flux

The flux of the prepared membranes was characterized with the help of a pressurized adsorption chamber (plastic) with a maximum capacity of 400 mL. The diameter of the chamber, and therefore the diameter of the membrane samples, was 7.6 cm. The membrane was put into place and in a first step, the chamber was filled with water. With the help of a needle valve, a nitrogen pressure of 1 bar was applied to the adsorption chamber. The permeate was collected in a vessel which was placed on a digital scale. The scale was connected to a computer which plotted the increase in weight (i.e. amount of water) over time. As the amount of permeate (water), the area of the membrane sample, the permeation time and the applied pressure are known the flux was calculated in  $\text{L m}^{-2} \text{ h}^{-1} \text{ bar}^{-1}$ .

### Determination of Dynamic Adsorption Behavior

The dynamic adsorption behavior of the prepared membranes was characterized with the help of a pressurized adsorption chamber (see Determination of Flux). With the help of a needle valve, a nitrogen pressure was applied to the adsorption chamber resulting in a water flow rate through the membrane of 20 mL min<sup>-1</sup>. Afterwards the water is removed from the chamber. The chamber containing the membrane was then dried using a nitrogen stream. Finally, the chamber was filled with 250 mL of DCL solution with a concentration of 200 µg L<sup>-1</sup>. With the pressure determined in the first step, the experiment was started. The permeate was collected in the following manner: 14 samples of 5 mL, followed by 18 samples of 10 mL. The remaining DCL concentration in each sample was quantified via HPLC as described above in the static adsorption section. Three distinct membranes samples of each membrane type were used for the adsorption experiments. The adsorption capacity of the adsorption chamber was also tested.

## **6.6. Results and Discussion**

### **6.6.1. Preparation of Chi-NPs via HPH**

For the preparation of sufficient amounts of chitosan nanoparticles (Chi-NPs) via miniemulsion crosslinking, high-pressure homogenization (HPH) was applied for the emulsion formation. Emulsions were prepared with three different highly deacetylated chitosans (3 % chitosan solutions in 1 % acetic acid, containing 0.1 M NaCl). While the chitosan solutions acted as the water phase, cyclohexane containing Span 80 as emulsifier served as the oil phase. To determine the influence of homogenization time on the emulsion generation, which in turn controls the particle formation, seven homogenization cycles were run for each emulsion. The emulsion formulation applied in this work was developed, optimized and tested for the use in-probe sonication-based emulsification process as described in a previous work. As described previously, the aqueous phase viscosity affects the emulsion process i.e. the resulting particle size (Riegger, Bäurer, et al. 2018). Therefore, three chitosans (DD > 90) with different molecular weights (MW) herein called low, medium and high-MW chitosan were tested. These chitosans were characterized (Table 4) by size exclusion chromatography (SEC). Viscosities of chitosan solutions were determined at different shear rates (Fig. 20). The DD provided by the manufacturer was verified via <sup>1</sup>H-NMR spectroscopy.



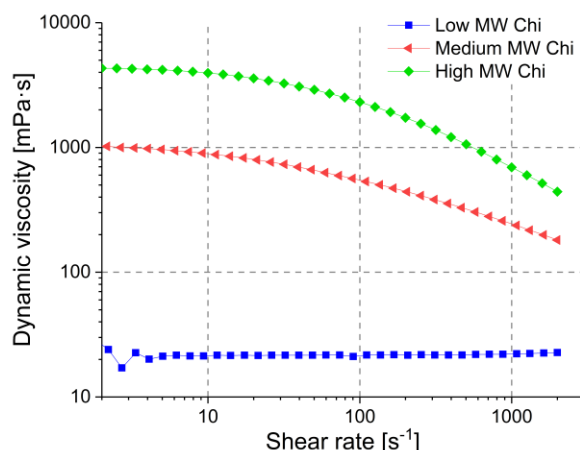


**Fig. 20:** The shear-dependent dynamic viscosity of the low, medium and high MW chitosans solutions (3 % chitosan solutions in 1 % acetic acid, containing 0.1 M NaCl).

For all three samples the SEC data show a broad molar-mass dispersity  $\mathcal{D}_M$  (polydispersity index,  $PDI_{SEC}$ ) (Stepito 2009) which is common for commercially available chitosans (Nguyen, Hisiger, et al. 2009). The measurements of the shear dependent viscosity of 3 % chitosan dissolved in 1 % HAc (0.1 M NaCl) show a shear-thinning behavior for the medium and high MW chitosans at the tested shear rates.

In contrast, the low WM chitosan exhibits a low viscosity over the whole range of shear, showing no shear-thinning behavior. This is in accordance with results reported earlier (Riegger, Bäurer, et al. 2018). The shear-thinning behavior, especially of high MW i.e. high viscous chitosans, is desirable because a lower viscosity facilitates droplet disruption in homogenization processes.

Emulsion preparation via HPH was conducted as described above. The emulsions were prepared in seven homogenization cycles at 40 MPa. After each cycle, a sufficient amount of emulsion was drawn from the HPH. To each emulsion, glutaraldehyde (glut) as crosslinker was added. These experiments were performed in triplicate. The size (z-average, intensity-based) and size distribution (PDI) of each Chi-NPs sample was characterized via DLS (Fig. 21A and B). Error bars indicate the standard deviation in size and PDI for the triplicate particle preparation.

## 6 Chitosan Nanoparticles as Adsorber in Mixed-Matrix Membranes

**Table 4: Chitosan description and characterization of molecular weight ( $M_w$ ,  $M_n$ ) via SEC, degree of deacetylation via  $^1\text{H-NMR}$  and dynamic viscosities.**

Chitosan type	$M_w$	$M_n$	$\bar{D}_M$	DD <sup>a</sup> %	DD % <sup>1</sup> H-NMR	Dynamic viscosity <sup>b</sup> [mPa s]	Viscosity ratio <sup>c</sup> $\lambda$
	SEC [g mol <sup>-1</sup> ]	SEC [g mol <sup>-1</sup> ]					
Low MW	77 750	24 010	3.24	93.5	94.6	21.4	23.7
medium MW	349 000	67 870	5.14	91,5	92.3	542.5	602.7
high MW	371 200	121 400	3.06	94.5	97.9	2149.5	2388.3

<sup>a</sup> provided by manufacturer

<sup>b</sup> 3 % chitosan solutions in 1 % acetic acid, containing 0.1 M NaCl at 100 s<sup>-1</sup>

<sup>c</sup> Cyclohexane viscosity: 0.9 mPa s

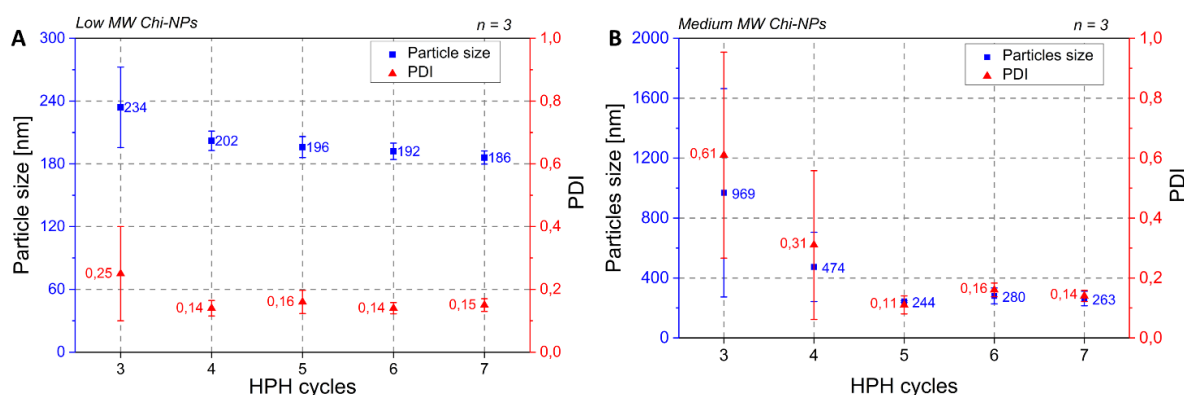


**Fig. 21: DLS measurements of low MW Chi-NPs (A) and medium MW Chi-NPs (B) after varied HPH cycles. Particles were prepared and measured in triplicates.**

For the low MW chitosan, four cycles were necessary to reproducibly yield narrowly distributed nanoparticles (PDI < 0.2) in the range of 200 nm. Further homogenization led to a negligible decrease in size and no observable improvement in dispersity. For the medium MW chitosan, at least five cycles were necessary for the reproducible preparation of narrowly distributed Chi-NPs (PDI < 0.2) in the range of 250 nm. Similar to the low MW chitosan further homogenization did not improve the size/distribution of the particles considerably. The SEM micrographs of the low and medium MW Chi-NPs show spherically shaped, narrowly distributed particles (Fig. 22). The shape and size distribution is similar to Chi-NPs prepared via probe-sonicated emulsion crosslinking technique (Riegger,

Bäurer, et al. 2018). The observed size in the SEM micrographs does not match the size determined by DLS. This is due to the drying process, which is involved in SEM sample preparation. In this dry state, the particles are in a non-swollen, collapsed state. We assume that the observed agglomerates are formed during the sample preparation due to the adhesive behavior of chitosan (Banerjee, Mitra, et al. 2002).

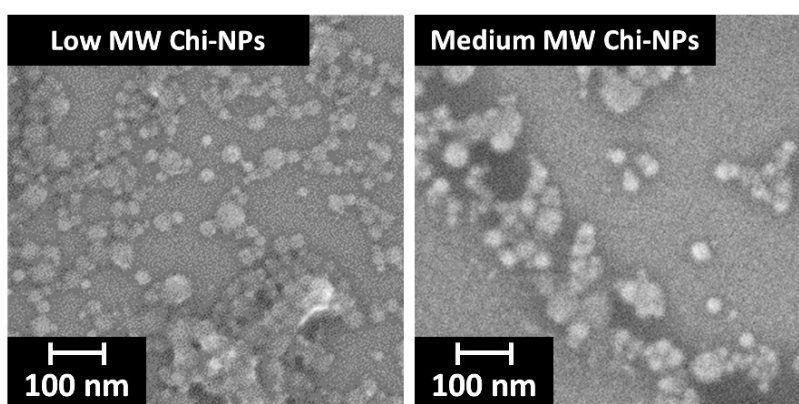


**Fig. 22:** SEM micrographs of the low and medium Mw Chi-NPs show spherically shaped, narrowly distributed particles.

For the high MW chitosan, it was not possible to prepare stable emulsion with the HPH in seven homogenization cycles at 40 MPa (no DLS data shown). The disperse phase viscosity plays an important role in the emulsification processes, via HPH or probe sonication. (Nazarzadeh and Sajjadi 2010; Schultz, Wagner, et al. 2004). If the disperse phase viscosity exceeds a certain level, emulsification does not lead to sufficient droplet disruption. The high MW chitosan exhibits a viscosity (Fig. 20) at which emulsification via HPH at 40 MPa was insufficient, hence only an instable coarse emulsion with large droplet sizes was formed. By increasing the homogenization pressure and/or changing the homogenization nozzle, we assume it would be possible to successfully emulsify the high MW chitosan solution (Stang, Schuchmann, et al. 2001). However, the aim of this work was to compare the three chitosans at the parameter setting of 40 MPa. Hence, no further experiments were performed with the high MW chitosan in this study.

By comparing Fig. 21A and 2B, it can be seen that the smallest Chi-NPs are formed using the low MW chitosan, which exhibits the lowest viscosity. This concurs with the results of Stang et al. (2001) who demonstrated that the droplet size (which correlates with particle size) in HPH emulsification processes increased with increasing disperse phase viscosity. This behavior also agrees with previous findings of Chi-NP preparation via probe

sonication-assisted emulsion. With increasing MW of chitosan, i.e. increasing aqueous phase viscosity, the resulting particle size increases (Goycoolea, Brunel, et al. 2016; Riegger, Baurer, et al. 2018). Shi and co-workers (2011) developed an HPH-assisted miniemulsion crosslinking formulation for the preparation of starch nanoparticles. Along with other parameters, they investigated the effect of starch concentration in the aqueous phase on nanoparticle formation applying one to five homogenization cycles at 30 MPa. They found that the aqueous phase with the lowest starch concentration (i.e. lowest viscosity) results in the smallest starch nanoparticles. Further, their data show that after exceeding a certain starch concentration, it was not possible to produce narrowly distributed nanoparticles ( $PDI < 0.2$ ).

We were able to further optimize the Chi-NP preparation by stirring the crude emulsion in the feed vessel throughout the whole HPH process. This reduces phase separation of the crude emulsion in the first homogenization cycles and therefore improves the homogenization efficiency, which eventually leads to a better dispersion result. After seven cycles the DLS measurement showed that the resulting particles were in the range of 125 nm ( $PDI : 0,19$ ) for low MW and 160 nm ( $PDI : 0,16$ ) for medium MW while the process without continuous stirring led to Chi-NPs in the range of 200 nm for low MW and 250 nm for medium MW as described above.

It has been shown that at sufficiently high process pressures, HPH can be used for the depolymerization of polysaccharides (HARTE and VENEGAS 2010). To investigate the influence of the HPH on the chitosans MW, SEC analyses of the pristine polymer after one and after seven HPH cycles at 40 MPa in the emulsion without crosslinker was performed. After emulsification via HPH the chitosan was regained via centrifugation and analyzed by SEC. Fig. 23A shows the results of these experiments for low MW chitosan and Fig. 23B for the medium MW chitosan. In both cases, the SEC data show no considerable change in MW by the HPH, meaning that the HPH process at 40 MPa does not lead to significant depolymerization. Hence, we assume that the chitosans retain their MWs and MW distributions throughout the emulsification process. We conclude this can be explained by the low pressure we used compared to others (HARTE and VENEGAS 2010; Lyons 2011) but more importantly to the fact that in our case a two-phase system (emulsion) instead of a plain polymer solution/dispersion was homogenized.

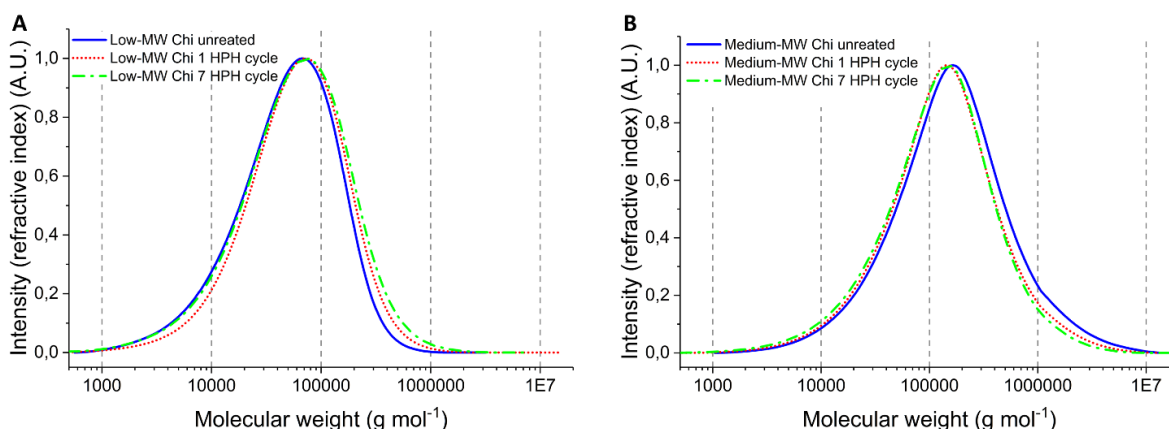
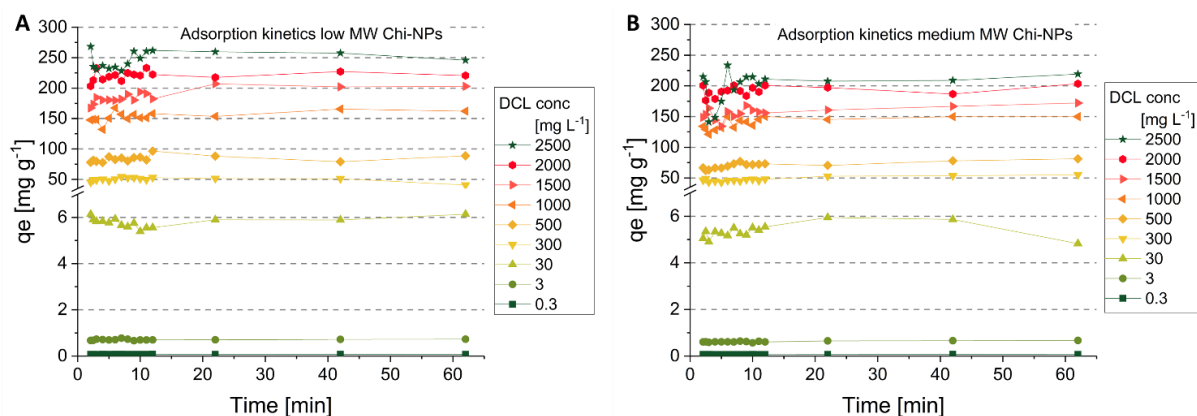


Fig. 23 SEC MW distribution of low (A) and medium (B) MW chitosan after 0, 1 and 7 cycles of HPH.

### 6.6.2. Static Adsorption

In a first step, the adsorption kinetics for DCL were evaluated at different starting concentrations on low and medium MW Chi-NPs prepared with the HPH process. As we showed earlier, macroscopic and untreated chitosan (independent of its MW) is a poor adsorbent for DCL (Riegger, Bäurer, et al. 2018). Nine different concentrations were chosen and the adsorption capacity ( $q_e$  in  $\text{mg g}^{-1}$ ) was quantified at 15 points in time ranging from 125 seconds to 62 minutes (Fig. 24A and B). Due to the necessary centrifugation (2 min) of the particles for the preparation of HPLC samples, the shortest adsorption time that we were able to record in this experimental setup was 125 seconds. Hence, shorter adsorption times could not be detected. The observed adsorption rates for both particle types were independent of the starting concentration and instant. In contrast to common adsorbents like activated carbon, adsorption kinetics for DCL in the range of several minutes (Nam et al. 2014;  $C_0$  100  $\text{ng/L}$ , contact time 30-360 min at 20 °C) to hours (Chang et al. 2015;  $C_0$  10  $\text{mg/L}$ , contact time 0-72 h at 25 °C) especially at high concentrations (Vedenyapina et al. 2016;  $C_0$  500  $\text{mg/L}$ , contact time 1-9 h at 18 °C) could not be detected. Although the adsorption kinetics for DCL on Chi-NPs could not be determined, the rapid adsorption process (< 2 min) is very useful for the application of these particles in membrane-based processes, where the contact time between pollutant and adsorbent is quite short. Zhang and co-workers (2014) found a similar rapid adsorption rate for DCL on glutaraldehyde-crosslinked magnetic chitosan nanoparticles. Even at a sampling point of 0.5 minutes, they found the adsorption to be complete. Since the adsorption was so fast, no kinetic could be determined.

## 6 Chitosan Nanoparticles as Adsorber in Mixed-Matrix Membranes



**Fig. 24: Adsorption kinetics of low MW (A) and medium MW Chi-NPs (B) at different DCL concentrations.**

To ensure that the system is at full equilibrium the last four data points (12, 22, 42 and 62 minutes) were chosen for the calculation of a mean  $q_e$  (Fig. 25A and B, black squares). At the highest starting concentration ( $C_0 = 2500 \text{ mg L}^{-1}$ ) the low MW Chi-NPs show a  $q_e$  for DCL of  $256.2 \pm 7.1 \text{ mg g}^{-1}$  and the medium MW Chi-NPs show a  $q_e$  of  $211.7 \pm 5.2 \text{ mg g}^{-1}$ . At a  $C_0$  of  $500 \text{ mg L}^{-1}$  a capacity of  $88.1 \pm 7.2 \text{ mg g}^{-1}$  for the low MW Chi-NPs and a capacity of  $76.5 \pm 4.8 \text{ mg g}^{-1}$  for the medium MW Chi-NPs was found. These values are in accordance with the results shown by Zhang et al. (2014). They found a maximum  $q_e$  for their magnetic chitosan nanoparticles of  $57.5 \text{ mg g}^{-1}$  at a starting concentration ( $C_0$ ) of  $500 \text{ mg L}^{-1}$ . We assume that the low MW Chi-NPs resemble the more effective adsorber material compared to the medium MW Chi-NPs due to the smaller particle size i.e. the larger surface area of the particles. These results are also in accordance with previous findings (Riegger, Bäurer, et al. 2018) where the impact on different chitosan MWs on the adsorption behavior of the resulting particles was investigated. The results of these single-point sorption tests showed that in general lower MW Chi-NPs lead to a higher adsorption capacity and are therefore preferred when adsorbing DCL.

Possible adsorption mechanisms for DCL on glutaraldehyde crosslinked Chi-NPs are hydrogen-bonding (enals, hydroxyl) or  $\pi$ - $\pi$  interactions (Poon, Younus, et al. 2014). The reaction between glut and chitosan resulting in covalent crosslinking is well documented (Crini 2005; Crini and Badot 2008; Wang, Yuan, et al. 2014; Monteiro and Airoidi 1999). Primary amine moieties of chitosan are consumed during the reaction with glutaraldehyde. Generally, primary amines are considered to be suitable adsorption sites for anionic compounds like DCL. Despite containing many primary amine groups, pristine chitosan is a poor adsorbent for DCL (Riegger, Bäurer, et al. 2018). Thus, it is evident that

the mere presence of primary amines in chitosan is not responsible for a high adsorption of DCL. Results from our previous work, as well as from the work presented here, indicate that the chitosan glutaraldehyde composite material possess a high adsorption capacity for DCL. Poon et al. (2014) conducted experiments with chi/glut composite materials containing different ratios of glut for the adsorption of p-nitrophenol (PNP). While pristine chitosan was a poor adsorbent, the adsorption capacity of chi/glut composites increased with increasing glut-concentration i.e. increasing crosslinking. A possible explanation could be given by the increased swelling of crosslinked chitosan compared to pristine chitosan (Poon, Younus, et al. 2014). In addition, an increased glut content (as in this work one mole glut per mole primary amine) can lead to self-oligomerization or self-polymerization of glutaraldehyde. Among the products of this reaction are pyridinium adducts, enal, hydroxyl and imine moieties (Migneault, Dartiguenave, et al. 2004; Kildeeva, Perminov, et al. 2009). These groups might further enhance the adsorption of substances containing aromatic and hydrophilic moieties such as DCL.

For the modeling of adsorption isotherms the mean  $q_e$  values were plotted against  $C_e$  (Fig. 25A and B) and fitted by Langmuir, Freundlich and Sips isotherm (also known as Langmuir-Freundlich isotherm) equation. The equations and the procedure for modeling the adsorption isotherms were applied as described by Repo et al. (2010).

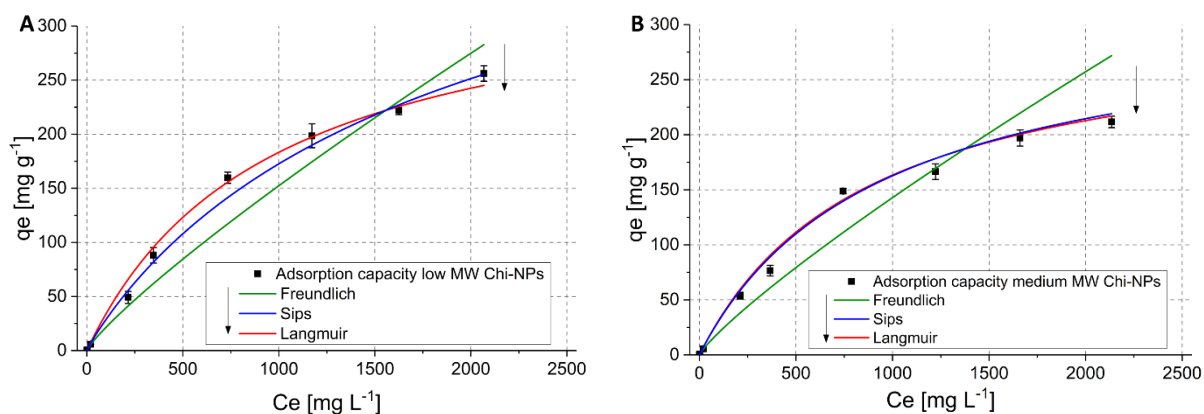


**Fig. 25: Adsorption isotherms for DCL in low MW Chi-NPs and medium Chi-NPs fitted with Freundlich, Sips and Langmuir at ambient conditions.**

The models show similar behavior for both particle types. Isotherm parameters are presented in Table 5. The Freundlich model, which accounts for multilayer adsorption, shows a poor fit for the experimental data. Compared to the Langmuir and Sips model, the Freundlich model has the lowest  $R^2$  for both particles (low MW 0.982, medium MW 0.935) [Note: In order to resolve a logical inconsistency, this sentence was altered. Hence, the

phrasing of this sentence now differs from the original publication]. Therefore, it is not a suitable model to describe the adsorption of DCL on Chi-NPs. The Sips and the Langmuir model show an  $R^2 > 0.99$  for both particle types. The high similarity in correlation and parameters for both fits can be explained by  $n_s$  (Sips heterogeneity factor) being  $\approx 1$  (Table 5). In the case of  $n_s = 1$  the Sips model is reduced to a model with Langmuir behavior (Repo, Warchol, et al. 2010; Poon, Wilson, et al. 2014).

**Table 5: Adsorption isotherms parameter for DCL adsorption on low and medium MW Chi-NPs at ambient conditions including standard deviation.**

<b>Modell</b>	<b>Low MW Chi-NPs</b>	<b>Medium MW Chi-NPs</b>
<b>Freundlich</b>		
$K_F [L \text{ mg}^{-1}]$	$0.42 \pm 0.033$	$0.40 \pm 0.093$
$n_F$	$1.175 \pm 0.018$	$1.178 \pm 0.049$
$R^2$	0.982	0.935
<b>Langmuir</b>		
$q_{\max} [\text{mg g}^{-1}]$	$358.3 \pm 27.95$	$305.3 \pm 22.06$
$K_L [L \text{ mg}^{-1}]$	$10.5 \times 10^{-4} \pm 1.20 \times 10^{-4}$	$11.5 \times 10^{-4} \pm 1,463 \times 10^{-4}$
$R^2$	0.991	0.994
<b>Sips</b>		
$q_{\max} [\text{mg g}^{-1}]$	$502.5 \pm 87.18$	$317.3 \pm 38.6$
$n_s$	$0.936 \pm 0.021$	$0.989 \pm 0,025$
$K_s [L \text{ mg}^{-1}]$	$5.0 \times 10^{-4} \pm 1.63 \times 10^{-4}$	$10.5 \times 10^{-4} \pm 2.63 \times 10^{-4}$
$R^2$	0.997	0.993

A value of  $n_s \approx 1$  also indicates heterogenic sorption sites for both particle types. The maximum adsorption capacity ( $q_{\max}$ ) for the low MW Chi-NPs is  $358.3 \text{ mg g}^{-1}$  for the Langmuir model and  $502.5 \text{ mg g}^{-1}$  for the Sips model. Thus, the Sips model predicts a substantially higher  $q_{\max}$  for DCL on low MW Chi-NPs. The  $q_{\max}$  values which were calculated for the low MW Chi-NPs differ substantially from each other. Compared to these results, the values calculated for the medium MW Chi-NPs are similar for both models.



Here, values of  $305.3 \text{ mg g}^{-1}$  and  $317.3 \text{ mg g}^{-1}$  were calculated for Langmuir and Sips models, respectively. Nevertheless, the isotherm results (Langmuir and Sips model) as well as the experimental data (Fig. 24) show a higher adsorption capacity for the low MW Chi-NPs.

### 6.6.3. Dynamic Adsorption

To evaluate the dynamic adsorption behavior, Chi-NPs were incorporated into polymer membranes via a casting process (Niedergall, Bach, et al. 2014). In addition, membranes containing no particles were prepared as reference. Since water is a non-solvent in the membrane formation process, it needed to be removed from the particles. The particles were dried in vacuum. It was then attempted to redisperse them in N-Ethyl-2-pyrrolidon (NEP) using probe sonication. The resulting dispersion showed macroscopic agglomerates, which could not be broken down even with prolonged sonication treatment. Due to their size, the Chi-NP agglomerates would inevitably lead to macroscopic defects in the resulting membrane structure, which would substantially reduce membrane adsorption performance. Hence, these macroscopic Chi-NP dispersions in NEP were inadequate to serve as membrane polymer solvent. In order to obtain a fine Chi-NP/NEP dispersion a solvent exchange with NEP was performed. After particle preparation, the aqueous Chi-NP pellets were dispersed in an excess of NEP, centrifuged and subsequently redispersed in NEP. The resulting dispersions showed no macroscopic agglomerates, thus were further processed to prepare the casting solutions. Mixed-matrix membranes were then prepared via a casting and phase inversion process using water as non-solvent. Due to the use of NEP-swollen Chi-NPs in the preparation of the casting solutions, the mass content of medium MW and low MW Chi-NPs is not identical. The particle mass content related to the membrane polymer, i.e. particle mass content, in the resulting mixed-matrix membrane was 7.4 % and 6.4 % for medium MW and low MW Chi-NPs, respectively.

In Fig. 26 SEM micrographs (cross sections) of the reference membrane as well as membranes containing low MW and medium MW Chi-NPs are shown together with mean values for membrane thickness. The thickness was determined on each membrane at five different points with the help of a micrometer screw. The membranes containing particles ( $60 \mu\text{m}$  and  $69 \mu\text{m}$ ) are slightly thicker than the reference membrane ( $60 \mu\text{m}$ ). Considering the solid (polymer) content of the membrane polymer solution and the gap width of the doctor blade ( $200 \mu\text{m}$ ) all three mean values for the thickness are in the expected range. The micrographs show that the reference membrane exhibits the desired highly porous

structure across the entire cross section without any macroscopic defects (Fig. 26 A1). The magnification (A2) shows a homogenous pore size distribution. Fig. 26 B1 and C1 show the membranes containing Chi-NPs. A partially macro void formation in these membranes can be observed. We assume that the addition of Chi-NPs and, as a consequence, the change in rheological behavior has a negative effect on the phase inversion process and is therefore responsible for the inhomogeneities in the macroscopic structure of the membranes. However, the porous microstructures observed in the magnifications (A2, B2, C2) are rather similar. There is no distinct difference of the porous microstructure between the reference membrane and the particle-containing membranes.

Due to the small size of the Chi-NPs and the low contrast between particles and the membrane polymer, individual particles or small agglomerates are not visible in the membrane micrographs. As shown in Fig. 22 the particles are in a collapsed state when dried. It is to be expected that larger particle agglomerates would be visible in the SEM, but the micrographs show no indication of the presence of such agglomerates. The flux mainly depends on the pore size of the membranes as shown in Fig. 26D. The membrane prepared with medium MW Chi-NPs exhibits a flux roughly twice as large ( $10063 \text{ L m}^{-2} \text{ h}^{-1} \text{ bar}^{-1}$ ) compared to the reference membrane ( $5355 \text{ L m}^{-2} \text{ h}^{-1} \text{ bar}^{-1}$ ) and the membrane containing low MW Chi-NPs ( $5119 \text{ L m}^{-2} \text{ h}^{-1} \text{ bar}^{-1}$ ). As discussed above, the microstructure of all three membranes is similar. Therefore, we assume that the increased flux for the medium MW Chi-NP-filled membrane is attributable to defects in the membrane. This is in agreement with the values for the pore size, which also are roughly twice the size ( $0.73 \mu\text{m}$ ) as in the reference membrane ( $0.3 \mu\text{m}$ ). The membrane containing low MW Chi-NPs, exhibits a pore size ( $0.43 \mu\text{m}$ ) similar to the reference membrane.

The influence of the added particles on the phase inversion process should be minimal i.e. the particle-filled membrane should be similar to the reference membrane in terms of porosity and flux. Particles in the range of several micrometers would dramatically increase the formation of membrane defects. In the case of low MW Chi-NPs, the data for flux and porosity are similar to the reference membrane. In this case, it was possible to entrap nanoparticles and potential small nanoparticle agglomerates in the membrane without compromising the membrane in its general structure and functional behavior.

## 6 Chitosan Nanoparticles as Adsorber in Mixed-Matrix Membranes

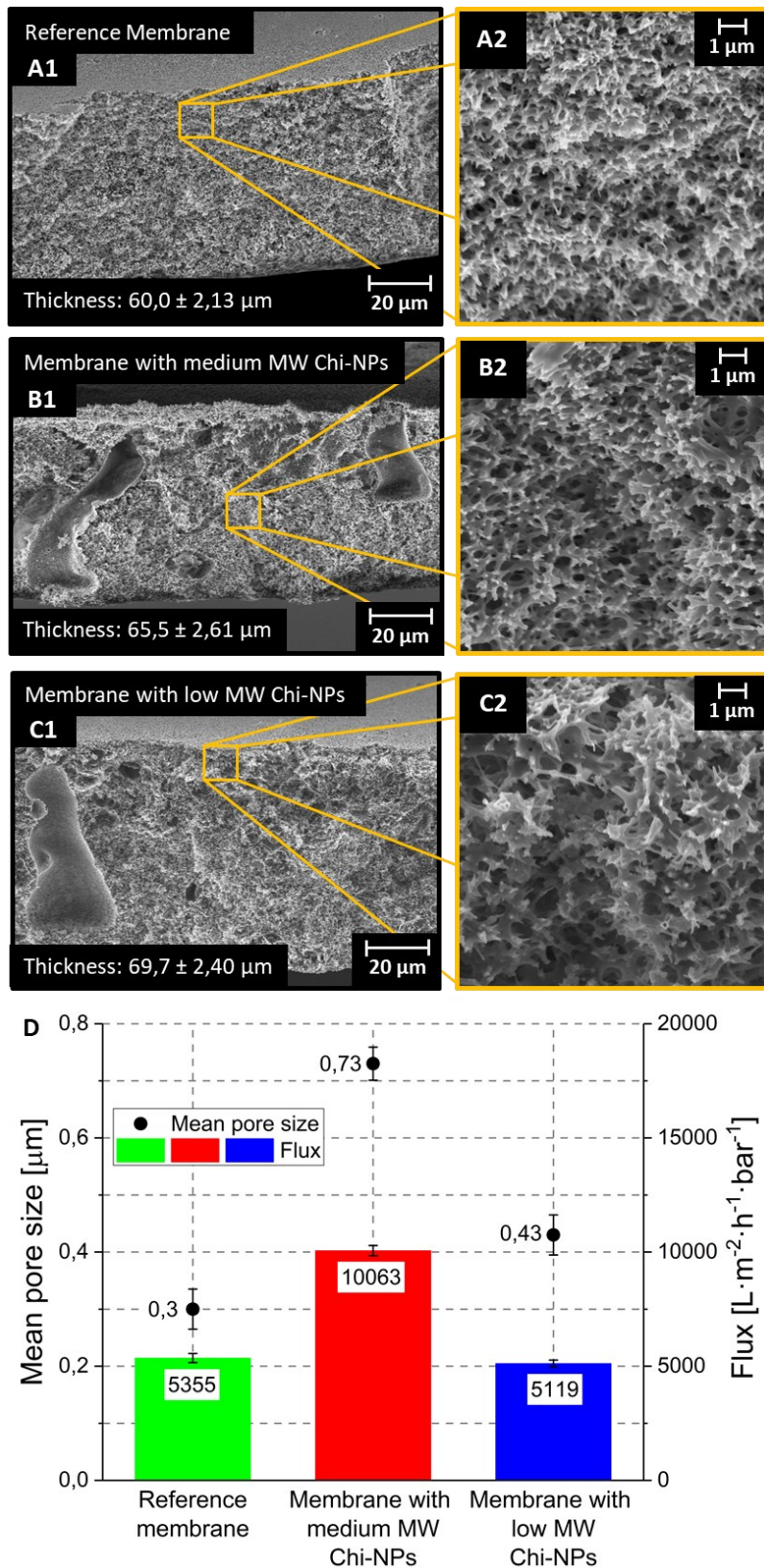


**Fig. 26:** SEM micrographs (cross section) of the reference membrane (A), low MW Chi-NP membrane (B) and medium MW Chi-NP membrane (C) with magnification of the porous membrane structure. (D) Mean pore size (capillary flow porometry) and flux (at 1 bar) for all three membranes. In both cases, the error bars indicate the standard deviation of nine different measurements for each sample type.

## 6 Chitosan Nanoparticles as Adsorber in Mixed-Matrix Membranes

The mixed-matrix membranes were tested for their adsorption capacity. For the adsorption experiments, three distinct membrane samples for each membrane type were used. In Fig. 27A the mean values of these triplicate measurements are shown. The adsorption capacity of the adsorption chamber was tested as blank measurement.

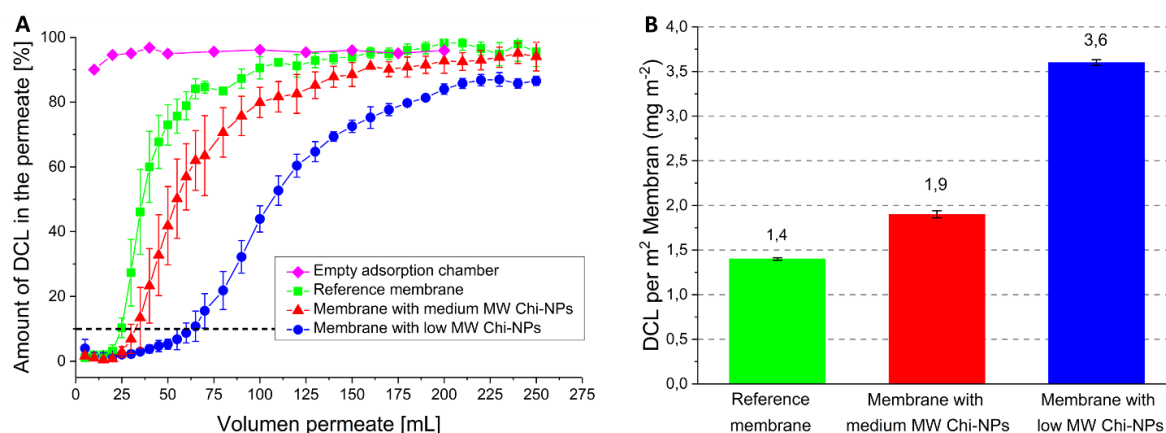


**Fig. 27:** Mean dynamic adsorption plot of DCL for the adsorption chamber, the reference membrane and low and medium MW Chi-NP membrane including standard deviation of triplicate measurements (A). The dashed line in (A) indicates the breakthrough point (10 %) of the membranes. The resulting adsorption capacity of DCL for the respective membranes in  $\text{mg m}^{-2}$  (B) at the breakthrough point. For each membrane type, the adsorption experiment was performed with three different membrane samples.

As expected, the adsorption chamber itself showed no considerable adsorption. In membrane processes, *breakthrough* can be defined as the point where the target molecule concentration in the permeate equals 10 % of the feed concentration (indicated by dashed line)(Suen, Caracotsios, et al. 1993). The reference membrane containing no Chi-NPs showed the lowest DCL capacity ( $1.4 \text{ mg m}^{-2}$ ) and thus, the fastest breakthrough. Nonetheless, these results show that DCL has a certain affinity towards the membrane polymer (PES) itself. Due to the use of NEP-swollen Chi-NPs in the preparation of the membrane polymer solutions, the mass content of low MW and medium MW Chi-NPs is not identical. The particle mass content related to the membrane polymer in the resulting mixed-matrix membrane was 7.4 % and 6.4 % for medium MW and low MW Chi-NPs, respectively. To allow for a comparison with other membranes, the resulting adsorption capacity was calculated per square meter of membrane. The membranes containing medium MW and low MW Chi-NPs showed an adsorption capacity of  $1.9 \text{ mg m}^{-2}$  and  $3.6 \text{ mg m}^{-2}$ , respectively. Although the particle content in the low MW Chi-NPs membrane (6.4 wt %) was  $\approx 15 \%$  lower compared to the medium MW Chi-NP (7.4 wt %), its adsorption capacity with  $3.6 \text{ mg m}^{-2}$  is almost twice as high (Fig. 27B). These results are in

accordance with the static adsorption tests discussed above. In both cases - static and dynamic adsorption - the low MW-Chi-NPs show a superior adsorption behavior. The larger pore size may be an explanation for the lower adsorption capacity of the medium MW Chi-NP filled-membrane (Fig. 26D). Overall, the use of low MW Chi-NPs in membranes leads to the best results in terms of adsorption and membrane structure. The low standard deviation of the triplicate experiments (three different membrane samples) indicates a high reproducibility of membrane formation, a homogenous membrane structure and a homogenous particle distribution throughout the membrane.

The adsorption capacity for DCL is in the range of other membrane adsorbers, which target organic molecules like DCL. Niedergall et al. (2014) presented a membrane adsorber for PenG (penicillin G) and BPA (Bisphenol A). This anti-PenG-anti-BPA membrane adsorbed up to 32.8 mg m<sup>-2</sup> and 1.05 mg m<sup>-2</sup> BPA, respectively. It is notable that their membrane had a substantially higher particle content (30 wt %) compared to the membranes shown in the present work.

### 6.7. Conclusions

In this work, we present a straightforward approach for the preparation of chitosan nanoparticles (Chi-NPs) via high-pressure homogenization-assisted emulsion crosslinking. With the set HPH parameters (40 MPa, 7 cycles), it was possible to prepare nanoparticles with chitosans up to a viscosity of 542.5 mPa s (3 % chitosan solutions in 1 % acetic acid, containing 0.1 M NaCl at 100 s<sup>-1</sup>). The particles prepared with the low and medium MW chitosan were in the range of 125 nm - 250 nm (z-average) with a PDI < 0.2. It was not possible to emulsify the high MW chitosan under the same conditions. It would therefore be interesting in future to find a way of processing any kind of highly deacetylated chitosan into Chi-NPs independent of their MW. An interesting approach could be to optimize the HPH emulsification parameters to depolymerize the chitosan in a first step and emulsify it in a second step. In consequence there should be no limitation in terms of chitosan MW i.e. viscosity which would be desirable for an industrial process.

The Chi-NPs prepared with the low MW chitosan showed the best adsorption performance (256.2±7.1 mg g<sup>-1</sup>), although the adsorption capacity for the medium MW Chi-NPs is also highly satisfactory (211.7±5.2 mg g<sup>-1</sup>). The particles showed a rapid sorption rate (< 2 min). This is beneficial for application in dynamic adsorption processes such as mixed-matrix membranes. Modelling of adsorption isotherms resulted in a q<sub>max</sub> of 358.3

mg g<sup>-1</sup> for Langmuir and 502.5 mg g<sup>-1</sup> for Sips, respectively. Both the experimental adsorption results and the results of the modelled adsorption isotherms indicate that Chi-NPs prepared with low MW chitosan are the most effective adsorbents for DCL, when compared to higher MW Chi-NPs.

Membrane adsorbers were successfully prepared by processing low or medium MW Chi-NPs into porous polyether sulfone microfiltration membranes. Flux and porosity data show that the medium MW Chi-NPs have a considerable impact on the membrane formation (i.e. structure) and its performance when compared to the reference membrane, which contained no particles. The membrane containing medium MW Chi-NPs exhibits a flux and a mean pore size (10063 L m<sup>-2</sup> h<sup>-1</sup> bar<sup>-1</sup>, 0.73 μm) roughly twice as large as the reference membrane (5355 L m<sup>-2</sup> h<sup>-1</sup> bar<sup>-1</sup>, 0.3 μm). On the other hand, the membranes filled with low MW Chi-NPs showed a very similar flux and porosity (5119 L m<sup>-2</sup> h<sup>-1</sup> bar<sup>-1</sup>, 0.43 μm) compared to the reference membrane. The difference in porosity and flux also has an impact on the dynamic adsorption performance. Due to the larger size of the particles, the higher flux and the larger pore sizes, the membrane containing medium MW Chi-NPs exhibits an adsorption capacity of 1.9 mg m<sup>-2</sup>, which is in the range of the reference membrane (1.6 mg m<sup>-2</sup>). The membrane containing low MW Chi-NPs shows a considerably higher adsorption capacity of 3.6 mg m<sup>-2</sup>.

The low MW Chi-NP membrane adsorbers performed well, given the particle content in the membranes. Future experiments will have to focus on the optimization of the membrane polymer solution with the goal to increase their particle content. Another important goal is to verify the regeneration of such membrane adsorbers by flushing the membrane with a different solvent or pH shift. As a part of these experiments, it would be interesting to evaluate adsorption of other organic pollutants e.g. sulfamethoxazole or penicillin G as well as metal ions like platinum, copper or cadmium (and combinations of these) using such membrane adsorbers.

### 6.8. Acknowledgements

The authors thank Klaus Niedergall and Thomas Schiestel for their help with the membrane preparation and characterization, Achim Weber and Carmen Gruber-Traub for their help with the high-pressure homogenizer, Monika Riedl for conducting SEM measurements (all Fraunhofer IGB) and Alec Nienhauser (IGVP) for conducting preliminary experiments employing the high-pressure homogenizer.

## 7. Synthetic Nanoparticles for Sensing

In this chapter, the results for the discussion of hypotheses II.I and II.II (7.1) are presented. Chapter 7.2 to 7.9 contain preliminary results for the preparation of synthetic nanoparticles, the modification and application of these nanoparticles as sensitive layer and further particle characterization which are the basis for the discussion of hypotheses II.I and II.II.

Chapter 7.3 to 7.8 represent a manuscript with the title “*Nano-MIP based sensor for penicillin G: Sensitive layer and analytical validation*” which was published as a research paper in the peer reviewed journal *Sensors and Actuators B: Chemical* (Weber, Riegger, Niedergall, Tovar, Bach, & Gauglitz, 2018). The discussion of hypothesis II.I and II.II can be found in the discussion section in chapter 9.2.

Please note: Minor modifications were made to the original manuscript (chapter 7.3) concerning layout and orthography in order to fit the style of this thesis. No content-related changes were performed.

### **Declaration about my own contribution**

*I conceived the study regarding the preparation/modification of imprinted and non-imprinted nanoparticles and elaborated the detailed experimental design. This specifically included:*

- *Conceptualization and formulation of the overarching research goals for particle preparation/modification within the study.*
- *Design of the experimental approach for particle synthesis via ultrasonication-assisted miniemulsion polymerization.*
- *Investigation and implementation of protocols for the handling and preparation of monomer/crosslinker solutions and emulsions such as: duration of dissolution, shelf stability and premixing.*
- *Investigation and selection of suitable monomers, crosslinkers and emulsifiers used for the synthesis in this study.*
- *Determining the range of concentrations and stoichiometric calculation of synthesis educts and components, especially the amount and ratio of monomer/crosslinker, the amount of template, stabilizers and emulsion phase ratios.*

## 7 Synthetic Nanoparticles for Sensing

- *Elaboration and implementation of emulsion/particle preparation protocols in terms of selecting emulsification parameters, durations and particle separation/purification.*
- *Decisive contribution to the strategy development for particle immobilization on transducer surfaces.*
- *Development and implementation of synthesis strategies for polymer-analogous modifications of imprinted and non-imprinted nanoparticles which allowed covalent immobilization on transducer surfaces.*
- *Decisive contribution to the development of the strategy for redispersing particles in order to facilitate immobilization on transducer surfaces.*
- *Elaboration and implementation of sample preparation protocols and the necessary procedures for analytical methods such as scanning electron microscopy (SEM), dynamic light scattering (DLS), Fourier-transform infrared spectroscopy (FTIR), zeta potential as well as protocols for data evaluation and analysis.*
- *Selection and investigation of the relevant Penicillin G building blocks phenylacetic acid and 6-aminopenicillanic acid which were used in the cross-sensitivity experiments.*
- *Significant contribution to the discussion and experimental design for the characterization of immobilized nanoparticle layer stability as well as the cross-sensitivity experiments.*
- *Evaluation and discussion of all the particle-related data in an overall context of this study.*
- *Visualization of the acquired data (graphs) and schematic representation.*
- *Taking a leading role in writing the original draft of the publication and incorporating changes proposed by co-authors and reviewers in close cooperation with Patricia Weber (shared co-first authorship).*



## 7.1. Hypotheses II.I and II.II

### Hypothesis II.I:

*By using appropriate functional monomers, it is possible to prepare imprinted polymer nanoparticles via miniemulsion polymerization, which exhibit a selective adsorption behavior towards penicillin G.*

### Hypothesis II.II:

*Through suitable functionalization of the nanoparticles they can be covalently immobilized on the sensor surface.*

- *This covalently immobilized sensitive layer is impervious against overflow in the measuring chamber and despite the functionalization still bears its ability to selectively bind penicillin G in aqueous solution.*
- *The covalent immobilization benefits the sensors lifespan.*

## 7.2. Polymer Nanoparticles via Inverse Miniemulsion

### Polymerization: Preliminary Results

In earlier works at the IGVP/IGB, several research projects have already been conducted, using water-soluble monomers for nanoparticle preparation via inverse miniemulsion polymerization (inverse MiniEP) (Niedergall, Bach, et al. 2014; Niedergall, Kopp, et al. 2016). For example, 2-hydroxy-3-methacryloyloxypropyltrimethylammonium chloride (HYMOPTA) or vinylphosphonic acid (also called vinylphosphonate, VPS) as shown in Fig. 28 were used. As crosslinker, usually *N,N'*-Ethylenbisacrylamid (EBA) is used due to its superior solubility compared to the common crosslinker *N,N'*-Methylenbisacrylamid (MBA). Especially for the preparation of MIPs, an increased degree of crosslinking is desired.

Dynamic light scattering (DLS) measurements of the particles prepared with these monomers indicated good dispersion stability, a size in the range of 150-300 nm and low polydispersity index (PDI) of about ~0.1. However, SEM micrographs revealed that the particles seem to be only stable while in dispersion. When dried, for example done so for the preparation of SEM samples, the particles collapsed and barely held the spherical identity Fig. 29.

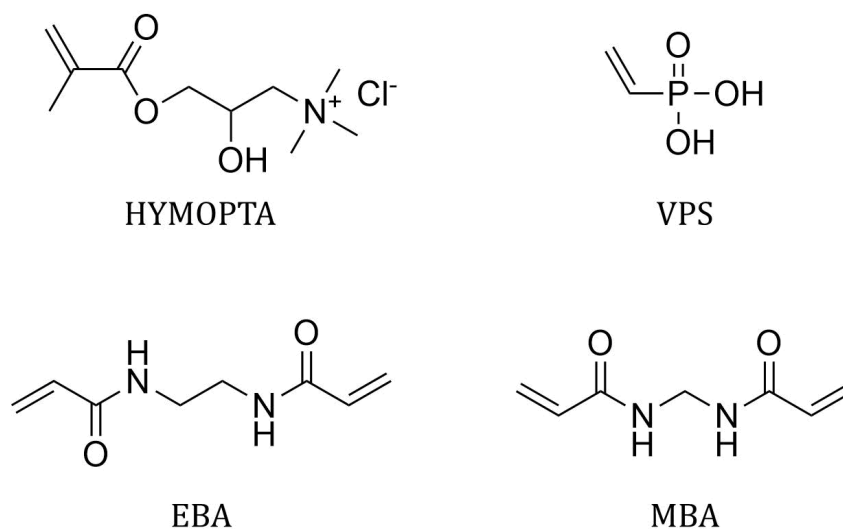


**Fig. 28** Chemical structures of water-soluble radically polymerizable monomers and crosslinkers HYMOPTA (3-methacryloyloxypropyltrimethyl-ammonium chloride), vinylphosphonic acid (also called vinylphosphonate, VPS) *N,N'*-Ethylenbisacrylamid (EBA) and *N,N'*-Methylenbisacrylamid (MBA) used in the beginning of this work for the preparation of nanoparticles via inverse miniemulsion.

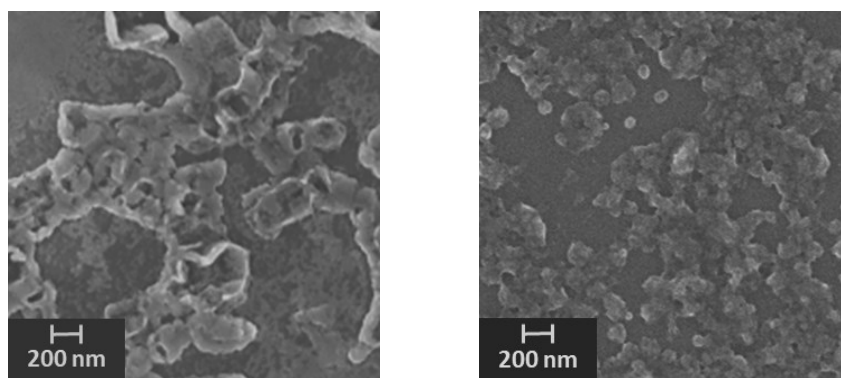


**Fig. 29** SEM-micrographs of HYMOPTA nanoparticles (left) and VPS nanoparticles (right) crosslinked with EBA. Both prepared via inverse MiniEP.

This behavior is undesirable, especially when the goal is to immobilize such particles on a transducer surface to act as sensitive layer in an optical sensing application such as RIFS (see chapter 7.6.3). In RIFS-based sensors, the adsorption processes are read out by analyzing the change in refractive index and thickness of the sensitive layer. Hence, the particles need to present a highly uniform spherical architecture. To provide the necessary reproducibility of the sensitive layer and its long-term stability in a dried state, particles which keep their shape are highly desirable.

For the synthesizes of particles with the required attributes via inverse miniemulsion polymerization, four different water-soluble acrylic/acrylamide-based monomers were

tested. The goal was to prepare narrowly distributed (low PDI) polymer nanoparticles via inverse MiniEP, which keep their shape after purification and drying.

In Fig. 30 four monomers as well as the corresponding SEM micrographs and DLS data of the resulting nanoparticles are shown. NAEMA, AMPS and SPM were commercially available. MAPTAC was generously gifted from the Evonik Industries AG. It was possible to prepare spherical and low disperse nanoparticles with all four monomers shown (synthesis protocols can be found in Chapter 12). Most importantly, all four particle types showed a high structural integrity – even after drying, as shown by the SEM micrographs. A common formulation for inverse miniemulsion polymerization is the use of cyclohexane as oil phase and Span 80 as low HLB surfactant, as was used for MAPTAC and NAEMA nanoparticles. However, in case of the sulfonates APMS and SPM the cyclohexane/Span 80 system did not result in stable miniemulsions. Landfester et al. (2000) investigated the use of Span 80-based inverse emulsion systems for the preparation of acrylic acid nanoparticles. The result of their research was that Span 80 is not appropriate for the emulsification of this acid monomer (Landfester, Willert, et al. 2000). The acidic monomers strongly interact with the surfactant, resulting in the formation of complexes, which lead to destabilization of the emulsion. This is assumed to also be the case for sulfonate monomers.

Wiechers and Schmidt-Naake (2008, 2009) published two research papers in which they reported the polymerization of AMPS in inverse miniemulsion. However, they did not prepare crosslinked nanoparticles. Their goal was to harness the inverse miniemulsion polymerization technique to synthesize linear AMPS copolymers with other hydrophilic monomers, such as vinylimidazole (VIm) or 2-(Dimethylamino)ethyl methacrylate (DAMA). To create stable emulsions containing AMPS (or mixtures of AMPS and other monomers), they used a PIBSA based surfactant – namely Addconate WO (see Table 1). As Addconate WO was no longer commercially available, Addconate H was used in this work, which was generously gifted from Lubrizol. Lubrizol stated that the difference between the two surfactants is only in the concentration of the product. While Addconate WO supposedly was the pure surfactant, Addconate H is a  $\approx 50$  w.t. % solution in mineral oil.

## 7 Synthetic Nanoparticles for Sensing

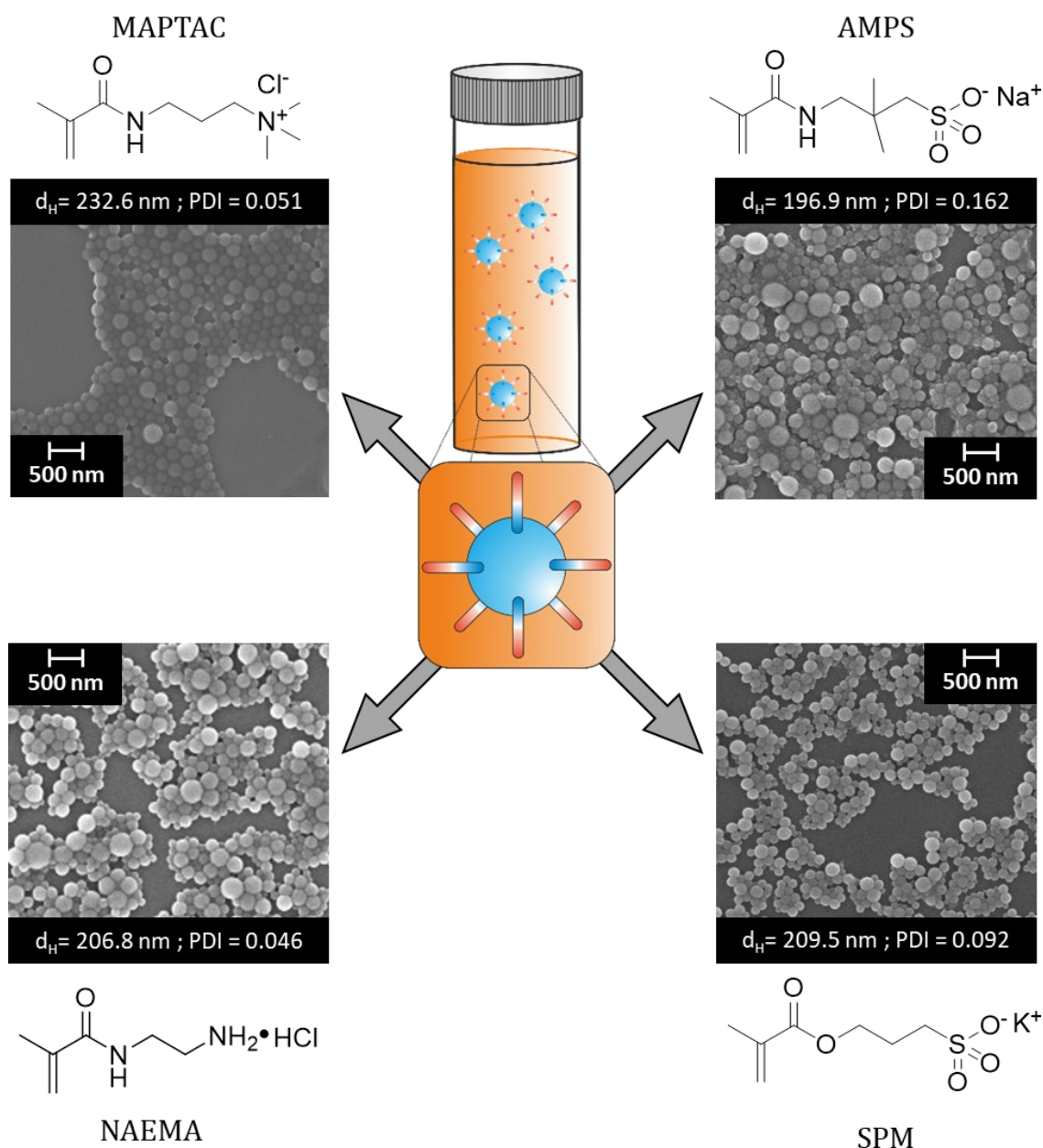


**Fig. 30** Summary of nanoparticles prepared with water-soluble monomers via inverse MiniEP. All particles are crosslinked with EBA (see Fig. 28). SEM micrographs, the hydrodynamic diameter ( $d_H$  via DLS) and Polydispersity index (PDI) are shown.

[3-(Methacryloylamino)propyl]trimethylammonium chloride (MAPTAC, top left)

N-(2-aminoethyl) methacrylamide hydrochloride (NAEMA, bottom left)

2-Acrylamido-2-methyl-1-propanesulfonic acid sodium salt (AMPS, top right)

3-Sulfopropyl methacrylate potassium salt (SPM, bottom left)

Inverse miniemulsions prepared with AMPS or SPM using Addconate H as surfactant were sufficiently stable and resulted in narrow distributed polymer nanoparticles as shown in Fig. 30. It is obvious that Addconate H is superior for the stabilization of sulfonic acid-based monomers when compared to Span 80.

The main goal of this work was the preparation of penicillin G (PenG) imprinted polymer nanoparticles for application as sensitive layer in an optical sensor array. PenG is an anion

and usually exists in the form of a sodium or potassium salt. NAEMA was chosen as monomer for the preparation of PenG imprinted nanoparticles. This decision was based on functionality (moiety) and shape, as well as size and reproducibility of the resulting nanoparticles. The results of particle preparation, modification and characterization as well as sensor results are presented in the next chapter (7.3).

In parallel to the development on PenG imprinted nanoparticles attempts were made to explain why some monomers result in film like particle structures and others in low disperse, spherical particles that keep their shape even after drying. In contrast to direct miniemulsion polymerization, in which most of the used monomers (e.g. styrene or methyl methacrylate) are liquid, the monomers used in the inverse miniemulsion are usually solids (salts). Hence, they need to be applied in aqueous, i.e. to some extent diluted solution in order to be able to emulsify them.

All the monomers shown above (i.e. NAEMA, MAPTAC, APMS and SPM), with which it was possible to prepare nanoparticles in inverse miniemulsion, share a high solubility in aqueous media. Total monomer solutions in the range of 50 w.t. % can easily be prepared. In comparison to that, the water solubility of HYMOPTA is low (~20 %). We assumed that particles prepared with preferably a high amount of dissolved monomer are more *solid* i.e. more likely to be stable against mechanical forces, hence keep their shape after centrifugation and drying. To verify this hypothesis, AMPS-EBA nanoparticles were prepared with different disperse phase monomer content. Five different total monomer/crosslinker contents were chosen (52.9 wt. %, 42.1 wt. %, 31.6 wt. %, 21.1 wt. % and 10.5 wt. %) while the disperse/continuous phase ratios and the total phase volumes stayed the same. The resulting particles were characterized via SEM and DLS as shown in Fig. 31. The SEM micrographs clearly reveal, that a high monomer content is preferable for the preparation of spherical and stable polymer nanoparticles. The intensity-based size distribution, the PDI and the correlation curve for 52.9 wt. % and 41.1 wt. % are adequate. In particular, at 31.6 wt. % the correlation curve and the PDI indicate an unsatisfactory particle sample. This is also demonstrated by the SEM micrographs. At lower monomer contents (21.1 wt. % and 10.5 wt. %) the DLS results are insufficient, particularly the PDI and the correlation curve indicate an inhomogeneous sample.

## 7 Synthetic Nanoparticles for Sensing

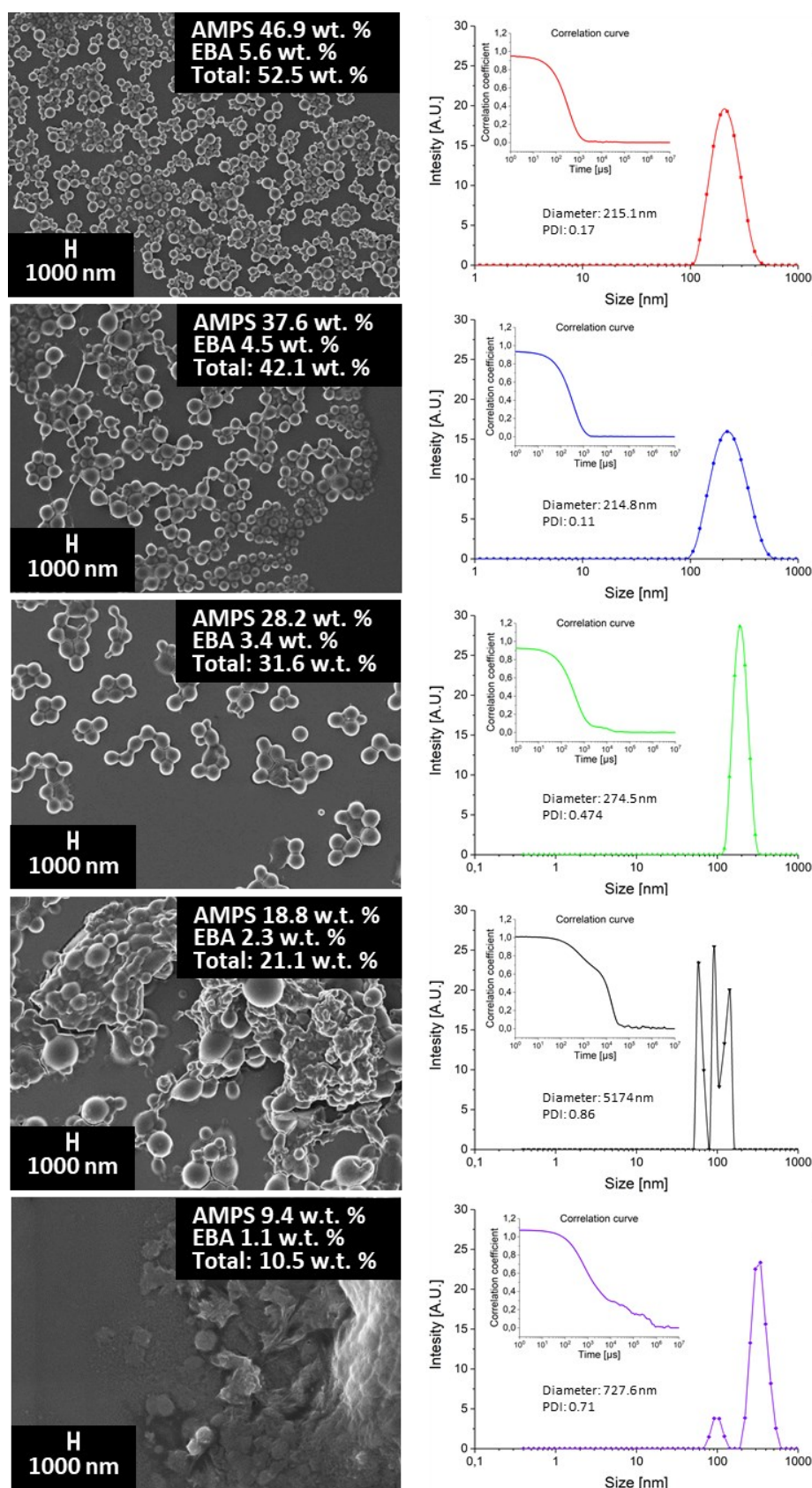


**Fig. 31** AMPS nanoparticles were prepared with different monomer/crosslinker content in the disperse phase (decreasing monomer content from top to bottom). EBA was used as crosslinker. The oil phase used was identical for all five particle syntheses. SEM micrographs and DLS measurements (intensity based particle diameter) including correlation curves are shown. With decreasing monomer content, the ability of the resulting particles to keep their shape decreases.

The materials shown in the SEM micrographs barely resemble particle structures anymore but rather film-like structures. The conclusion drawn from these results is that a high monomer content in the disperse phase is preferable in inverse miniemulsion. As dissolved monomers will occupy the whole droplet, it is assumed, that an increased monomer content results in particles with a denser polymer network. Hence, emulsions with a low monomer contents would lead to particles with a loose and gel-like polymer network resulting in mechanical instability.

It should be noted, that the use of VPS constitutes an exception to these findings. Although emulsions with a disperse phase content of up to  $\sim 40\%$  can be prepared with VPS, the resulting particles present themselves as mechanically instable after centrifugation. It is possible that several factors contribute to whether a nanomaterial is mechanically stable or not. In the case of VPS it is assumed that the chemical/sterical composition of pure poly-VPS and the resulting (electrostatic) repulsive forces may impair the mechanical properties of the resulting material. In the literature the synthesis of PVA-*co*-AA (acrylic acid) gels is described (Dey, Wimpenny, et al. 2018). As this material was tested as a potential bone tissue scaffold, in this work also the mechanical stability was tested. Compared to the pure VPS microgels presented in this thesis, in this work the PVA-*co*-AA showed a sufficient mechanical stability.



Weber, Patricia, Benjamin R. Riegger, Klaus Niedergall, Günter E.M. Tovar, Monika Bach, and Günter Gauglitz. (2018). “**Nano-MIP Based Sensor for Penicillin G: Sensitive Layer and Analytical Validation.**” *Sensors and Actuators B: Chemical* 267 (August): 26–33. <https://doi.org/10.1016/j.snb.2018.03.142>.



### **7.3. Nano-MIP Based Sensor for Penicillin G: Sensitive Layer and Analytical Validation**

Patricia Weber<sup>§,a</sup>, Benjamin R. Riegger<sup>§,b</sup>, Klaus Niedergall<sup>c</sup>, Günter E.M. Tovar<sup>\*,b,c</sup>, Monika Bach<sup>\*,b,‡</sup>, Günter Gauglitz<sup>\*,a</sup>

<sup>§</sup> Equally contributing / joint first authors.

<sup>a</sup>Institute of Physical and Theoretical Chemistry IPTC, Eberhard Karls Universität Tübingen, Auf der Morgenstelle 18, 72076 Tübingen, Germany. Tel: +49 7071 29 76927,

<sup>b</sup>Institute for Interfacial Process Engineering and Plasma Technology IGVP, University of Stuttgart, Nobelstr. 12, 70569 Stuttgart, Germany. Tel: +49 711 685 68162;

<sup>c</sup>Fraunhofer Institute for Interfacial Engineering and Biotechnology IGB, Nobelstr. 12, 70569 Stuttgart, Germany.

<sup>‡</sup>Present address: Modul 3: Analytical Chemistry Unit, University of Hohenheim, Emil-Wolff-Straße 12, 70599 Stuttgart, Germany

\*Corresponding Author: E-mail: [guenter.gauglitz@ipc.uni-tuebingen.de](mailto:guenter.gauglitz@ipc.uni-tuebingen.de); [monika.bach@uni-hohenheim.de](mailto:monika.bach@uni-hohenheim.de) and [guenter.tovar@igvp.uni-stuttgart.de](mailto:guenter.tovar@igvp.uni-stuttgart.de)

**Published in the peer-reviewed journal Sensors and Actuators B: Chemical**

Publisher: Elsevier

DOI: 10.1016/j.snb.2018.03.142

Volume: 267; Pages: 26-33

Received 14 November 2017; Received in revised form 12 March 2018; Accepted 23 March 2018; Available online 31 March 2018

### 7.4. Abstract

We herein report the synthesis of novel penicillin G (PenG)-imprinted polymer nanoparticles (MIPs) via inverse miniemulsion polymerization. Nanoscaled co-polymer particles consisting of N-(2-aminoethyl) methacrylamide hydrochloride as functional monomer and N,N'-Ethylenebisacrylamide as crosslinker have been synthesized in the presence of PenG. These particles have been applied to form a sensitive layer for label-free direct optical sensing of penicillin G. As reference material non-imprinted particles (NIPs) were used. The particles were characterized via scanning electron microscopy (SEM) and dynamic light scattering (DLS). Particles in the size of  $\approx 400$  nm (z-average) and a low polydispersity index ( $PDI < 0.05$ ) were observed. Azide modified MIPs/NIPs were covalently immobilized on alkyne-modified glass transducers by Cu(I) catalyzed 1,3-dipolar cycloaddition. The resulting particle-modified transducers served as sensing layer in an optical sensor setup (Reflectometric Interference Spectroscopy - RIfS). To prove its reliability and stability the transducer was tested in 78 reproducible PenG measurements over the course of 26 h. The response time of the sensor was  $\approx 1$  minute. For sensor calibration 14 randomized triplicate concentration dependency measurements for MIP and NIP transducers were conducted with different PenG concentrations ranging from 0.0015 – 0.0195 mol/L. MIP binding signals were significantly higher compared to the NIP. Determined recovery rates of three different transducers were in the range of 70-120 % which indicates a good chip to chip reproducibility. Sensor cross sensitivities between PenG and its structural building blocks phenylacetic acid and 6-aminopenicillanic acid were evaluated indicating a high selectivity for the presented sensor system.

Keywords: Molecularly imprinted polymer nanoparticles; inverse miniemulsion polymerization; Reflectometric Interference Spectroscopy (RIfS); molecular interactions; recognition elements; penicillin G

### 7.5. Introduction

*Molecularly Imprinted Polymers* (MIPs) are tailor-made crosslinked polymer materials, with a high affinity and selectivity towards a specified template molecule. The selectivity/affinity arises from “imprinted” binding sites, which match the template

molecule in shape, size and complementary spatial (steric) configuration of functional groups (Mosbach and Ramström 1996). Hence, a high specific surface, a precise control and reproducibility in size and shape is desired when MIPs serve as a recognition layer in a sensing application. These requirements can be fulfilled by using spherical nanoparticle MIPs (nano-MIPs). Due to their size, nano-MIPs provide a high specific surface, i.e. high imprinted surface with a large number of easily accessible binding sites, resulting in short diffusion times (Kolarov, Niedergall, et al. 2012; Hussain, Iqbal, et al. 2013). The synthetic MIPs exhibit a high mechanical, thermal, and chemical stability (Svenson and Nicholls 2001). In contrast to a bio-based recognition layer (i.e. antibodies, peptides) MIPs are cost-efficient and can be sterilized by autoclaving (Poma, Guerreiro, et al. 2013). In the past, Nano-MIPs have been synthesized by various methods (Poma, Turner, et al. 2010) and have been reported in several label-free sensing applications for example *Surface Plasmon Resonance* (SPR) (Sener, Uzun, et al. 2011), Quartz crystal microbalance (QCM) (Hoshino, Kodama, et al. 2008) and electrochemical sensors (Mazzotta, Turco, et al. 2016).

The technique of inverse (water in oil) miniemulsion polymerization (miniEP) is suitable to reproducibly prepare nanoscaled, spherical shaped, hydrophilic nano-MIPs (Vaihinger, Landfester, et al. 2002; Landfester and Musyanovych 2010; Capek 2010). In contrast to other techniques, the inverse miniEP allows the use of hydrophilic monomers and the easily imprinting of water-soluble substances, such as the penicillin G (PenG) sodium salt. If nano-MIPs are immobilized in a non-covalent manner (i.e. via electrostatic interactions), there is a high chance of particles to come off when they get in contact with the aqueous reagent flow during the sensing process. An instable sensing layer has a strong impact on the measurement signal and, eventually, renders the sensor useless when a critical number of particles are detached. In order to obtain a stable sensing layer, nano-MIPs can be attached on the sensor surface via covalent immobilization. Kamra and co-workers used either epoxysilanes or carbodiimide coupling chemistry for covalent immobilization of nano-MIPs (Kamra, Chaudhary, et al. 2015, 2016). Herein we propose a covalent immobilization strategy of azide modified PenG-imprinted nano-MIPs on an alkyne-modified transducer surface via 1,3-dipolar cycloaddition which was inspired by the work of Kinge et al (Kinge, Gang, et al. 2011). The advantage of the click chemistry approach is its large thermodynamic driving force, high yield and the generation of small and easily removable byproducts (copper salt and reduction compound). The resulting transducers were used as sensing layer in an optical sensor referred to as Reflectometric Interference Spectroscopy (RIfS).

## 7 Synthetic Nanoparticles for Sensing

RIfS as the wanted direct optical detection method is based on white light interference at thin layers. The interaction of molecules with the sensitive layer is monitored by changes of the optical thickness. Other examples of established label-free sensing techniques are mass sensitive devices (Lucklum and Hauptmann 2006; Martin and Hager 1989; Yang Thompson, M., Duncan-Hewitt, W. C. 1993), different electrochemical measurement techniques (Bard and Faulkner 2001; Janata 2009; Koryta, Dvorak, et al. 1993) and other direct optical methods (Brandenburg, Hinkov, et al. 2008; Colthup, Daly, et al. 1990; Kretschmann and Raether 1968). The most known label-free and time-resolved technique is the *Surface Plasmon Resonance* (SPR). Compared to RIfS, a decisive disadvantage of the SPR technique is the temperature dependence and the unavoidable use of a metal. Because of the temperature flexibility and the optional use of glass or even polymer transducers instead of metal layer, the RIfS instrumental set-up is straightforward, highly flexible and cheaper than the SPR. However, many SPR sensors with antibodies as recognition elements have been developed for the detection of the antibiotic PenG (Pennacchio, Varriale, et al. 2015; Raz, Bremer, et al. 2009; Cacciatore, Petz, et al. 2004).

The first combination of MIPs and RIfS technique is reported by Nopper and co-workers for the detection of O-benzoyl tartaric acid and  $\alpha$ -D-mannopyranoside (Nopper, Lammershop, et al. 2003). Belmont et al. published the first MIP-RIfS sensor with imprinted nanospheres received by miniemulsion polymerization, which was used for the detection of atrazine in toluene (Belmont, Jaeger, et al. 2007). Nevertheless, a complete characterization of the sensor was not possible because of insufficient long-term stability and unsatisfactory reproducibility. In contrast, Kolarov et al. published a successful combination of MIP nanospheres also received by inverse miniemulsion polymerization and RIfS (Kolarov, Niedergall, et al. 2012). With this setup, it was possible to completely calibrate a sensor for the detection of L-Boc-phenylalanine anilide.

In this work, we present a sensing approach using the example of PenG. As proof of principle, we tested the sensors selectivity towards the basic building blocks of the PenG fermentation process. We completely validated the use of a hydrophilic and covalently immobilized PenG-imprinted nano-MIP sensing layer in a direct optical RIfS sensor for the detection of PenG in buffer media. The goal is to develop a sensing platform, which will eventually be able to be used for the in-line monitoring of the PenG concentration during the fermentation.

## 7.6. Experimental

### 7.6.1. Materials

N-(2-aminoethyl) methacrylamide hydrochloride (NAEMA) was purchased from Polysciences Europe GmbH, Germany. N,N'-Ethylenebisacrylamide; 96 % (EBA) was purchased from abcr GmbH, Germany. penicillin G sodium salt (PenG)  $\geq$  98 %, (+)-6-aminopenicillanic acid (6-APA) 96 %, phenyl acetic acid (PAA)  $\geq$ 99 %, 2,2'-Azobis(2-methylpropionitrile) 98 % (AIBN), sorbitan monooleate (Span 80, viscosity 1000-2000 mPa s), 3-Chloro-1-propanethiol 98%, Triethylamine 99,5 % (TEA); sodium azide 99,5 %, acetonitrile HPLC grade; PBS-buffer (Dulbecco's Phosphate Buffered Saline) were purchased from Sigma Aldrich (Germany). Cyclohexane  $>$  99.5 % Applichem and N,N-dimethylformamide (DMF) p.A. was obtained from Häberle LABORTECHNIK GmbH, Germany. Ethanol absolut ACS reagent was purchased from VWR. 3- Glycidoxypropyltrimethoxysilane (GOPTS) and Methanol ( $>$  99.9%) were purchased from Fluka (Neu-Ulm, Germany). Alkyne-poly(ethylene glycol)-NH<sub>2</sub> (molecular weight 2 kDa) was purchased from Rapp Polymere (Tübingen, Germany). Ascorbic acid and common chemicals of analytic grade were purchased from Sigma-Aldrich (Deisendorf, Germany). Copper (II) sulfate pentahydrate and common chemicals of analytic grade were purchased from or Merck (Darmstadt, Germany). All chemicals were used without further purification.

ASTM Type I water (TKA GenPure and in-house ELGA LabWater device, named PURELAB® Classic) was used throughout this study (herein referred to as water).

For emulsion preparation and DLS sample preparation an Ultrasonicator Branson 450-D equipped with a 5 mm Tip (G. Heinemann Labortechnik, Germany), for the preparation of particle suspensions for the immobilization a Sonorex Super 10 P ultrasonic bath and a probe sonotrode UW70 with GM70 Sonopulse control unit (both purchased from Bandelin, Germany) were used. The centrifuge used was a Beckmann & Coulter Avanti J-26 XPI with JA-25.50 Rotor.

RfS transducer (1mm D263-glass substrate with a layer of 10 nm Ta<sub>2</sub>O<sub>5</sub> and 330 nm SiO<sub>2</sub> on top) were obtained by Schott AG (Mainz, Germany).

### 7.6.2. Methods

#### Preparation and Modification of MIPs/NIPs

Penicillin G (PenG)-imprinted NAEMA-co-EBA polymer nanoparticles, herein called MIPs, were synthesized via inverse miniemulsion polymerization technique (inverse miniEP) (Fig. 32). A modification of the emulsion formulation described by Niedergall et al. was used (Niedergall, Bach, et al. 2014). Briefly, the functional monomer NAMEA, the crosslinker EBA and the imprinting template PenG were dissolved in phosphate buffer and acted as disperse (aqueous) phase. The surfactant Span 80 and the initiator AIBN were dissolved in cyclohexane and acted as continues (oil) phase. Both solutions were combined and emulsified via probe sonication. This emulsion was heated to 55 °C to initiate polymerization inside the aqueous droplets. The resulting particles were purified by repeated centrifugation. NIPs were prepared identically but in the absence of the template molecule PenG. A detailed description of emulsion formulation and reaction parameters is available in the supporting information (part Si-1). After particle preparation a two-step functionalization was applied in order to obtain azide modified MIPs/NIPs (Fig. 33a). In a first step, remaining crosslinker sites (acrylamides) were reacted with 3-Chloro-1-propanethiole yielding a chloride bearing thioether. The chlorine was then substituted with sodium azide leading to azide functionalized particle. A detailed protocol for this particle modification can be found in the supporting information (part Si-2).

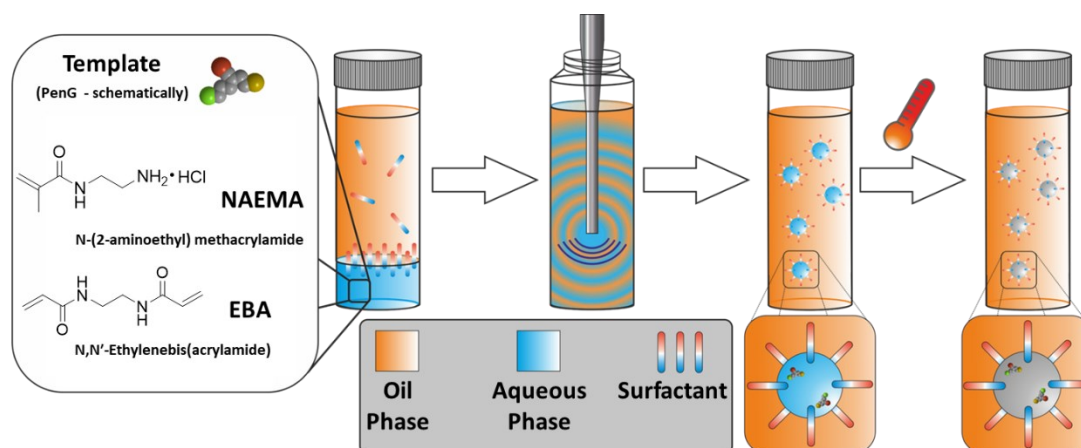


**Fig. 32: Schematical representation of MIP preparation via inverse miniemulsion polymerization technique. (a) Combining of oil phase (containing initiator and surfactant) and water phase (containing monomer, crosslinker and template); (b) Emulsification via probe sonication resulting in stable miniemulsion; (c) thermal initiation of the polymerizing reaction, resulting in imprinted polymer nanoparticles (d).**

### Characterization of MIPs/NIPs

Unmodified and modified MIPs and NIPs were characterized via dynamic light scattering (DLS) to determine their hydrodynamic diameter and zeta potential. Scanning electron microscopy (SEM) was applied to verify the size measured by DLS and for the determination of particle geometry. The azide modification of the particles was verified by infrared spectroscopy. A detailed description of sample preparation and experimental procedure can be found in the supporting information (part Si-3).

### Preparation of the Sensor Surface

The glass transducers were cleaned and activated with KOH (1 min) and freshly prepared piranha solution (15 min), silanized with pure 3-glycidoxypropyltrimethoxysilane (GOPTS) (1 h) and modified with an alkyne bearing PEG (overnight) in accordance to the method described by Mehne and co-workers (Mehne, Markovic, et al. 2008). In a second step, the azide-modified MIPs/NIPs were covalently immobilized (24 h) on the alkyne-modified transducer surface via copper (I) catalyzed 1,3-dipolar cycloaddition. A detailed procedure is described in the Supporting Information (part Si-4).

### 7.6.3. RIfS setup

#### Spectral RIfS

The principle of RIfS (Reflectometric Interference Spectroscopy) is based on multiple reflection on thin layers (Gauglitz 2010). The sensor system is constructed with a halogen lamp (20 W), an optical Y-fiber, a diode array spectrometer Spekol 1100 (Analytik Jena, Jena, Germany) and a Hamilton microfluidic system (Hamilton, Switzerland). White light is guided to the backside of the glass transducer and is partly transmitted and partly reflected at each interface of the sensitive layer and the transducer. The reflected beams superimpose and form a characteristic interference spectrum, which is detected by the diode array spectrometer. If analyte molecules deposit on the sensor surface, a change in optical thickness  $\Delta nd$  (product of the refractive index  $n$  and the physical thickness  $d$ ) can be detected. A more precise description of the RIfS setup can be found in the literature (Schmitt, Brecht, et al. 1997).

#### Calibration and Data Evaluation

The developed sensor has a direct and label-free assay format. A measurement run takes about 20 min. This includes the recording of the baseline (buffer is flushed over the sensor surface), injection of sample (the sample is slowly flushed over the transducer), a dissociation phase (buffer is flushed over the surface), a regeneration phase (the surface is flushed with methanol) and eventually a baseline measurement (buffer is flushed over the surface of the sensor) (see Supporting information Si-5). The sample volume amounts to 1 mL. Each measurement was evaluated at equilibrium binding signal during the sample injection phase. At these conditions the adsorption properties of the system were considered as a Langmuir-Freundlich adsorption isotherm which is a function that describes a relationship between the equilibrium concentration of bound analyte ( $f(x)$ ) and free analyte ( $x$ ) in heterogeneous systems with three fitting parameters ( $a, b, c$ ). Therefore, this isotherm is suitable for fitting the obtained calibration curve (Umpleby, Baxter, et al. 2001).

$$f(x) = \frac{abx^{1-c}}{1+bx^{1-c}}$$

(1)



To obtain this calibration curve randomized triplicate measurements at different concentrations of PenG - including blank measurements - were performed. The mean values and the standard deviations (SD) were calculated and fitted according to eq. 1.

The limit of detection (LOD) is calculated as three times SD of the blank measurements plus the mean value of the blank measurements and the limit of quantification (LOQ) is calculated as ten times SD of the blank measurement plus the mean value of the blank measurements. The recovery rates were determined out of triplicate measurement of different transducers.

## **7.7. Results and Discussion**

### **7.7.1. Preparation and Characterization of the Sensitive Layer**

PenG MIPs/NIPs were prepared via inverse miniemulsion polymerization technique (Fig. 32, Si-1). The oil phase containing cyclohexane, Span 80 and AIBN was prepared prior the preparation of the aqueous phase which consists out of NAEMA, EBA and PenG dissolved in PBS buffer. The buffer solution containing EBA and NAEMA was found to be instable. Within hours, self-polymerization was induced even at low storage temperatures ( $< 7\text{ }^{\circ}\text{C}$ ). Hence, it was not possible to prepare the aqueous phase and store it for later use. Consequently, the aqueous phase was always prepared on demand. As soon as a clear aqueous solution was obtained the two phases were combined (Fig. 32 a) and emulsified by probe sonication (Fig. 32 b). The resulting emulsion (Fig. 32 c) was polymerized by thermal initiation ( $55\text{ }^{\circ}\text{C}$ ) overnight, resulting in crosslinkend MIPs or, if no template was present, NIPs respectively (Fig. 32 d).

## 7 Synthetic Nanoparticles for Sensing

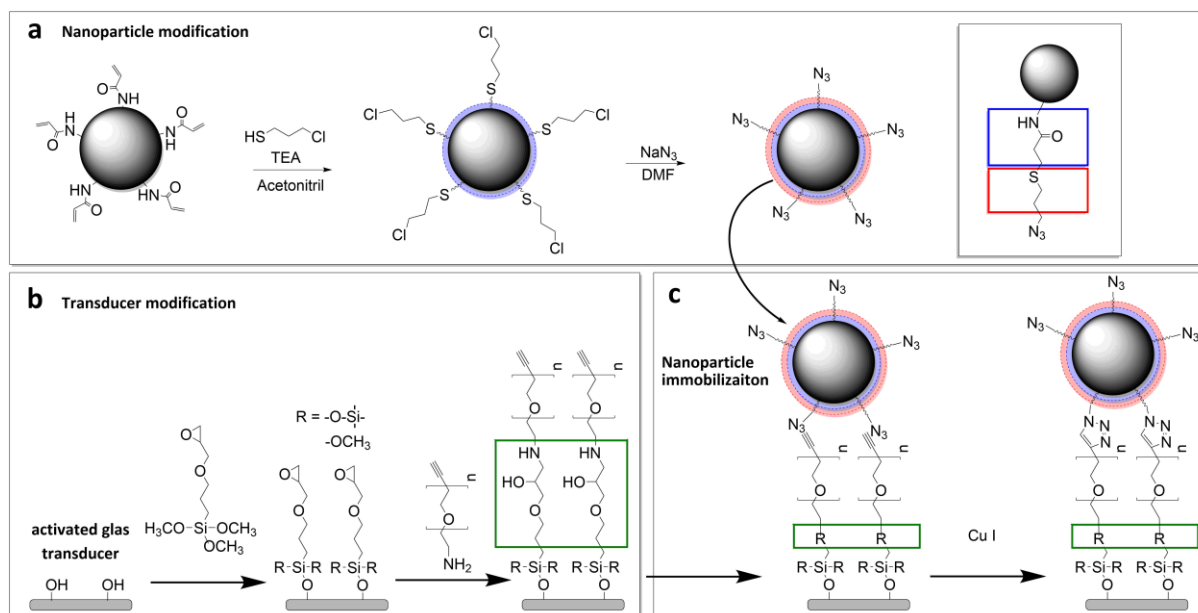


**Fig. 33** Schematically process of particle modification and immobilization of particles on transducer surface. **a)** Modification of MIPs/NIPs resulting in azide-bearing nanoparticles; **b)** modification of transducer surface introducing an alkyne-PEG; **c)** covalent immobilization of MIP-N<sub>3</sub>/NIP-N<sub>3</sub> on the transducer surface via copper (I) catalyzed 1,3-dipolar cycloaddition.

After purification, the pristine MIPs and NIPs were characterized via DLS (Fig. 34 a). Correlation data and intensity distributions can be found in Si-3. The average size (z-average) of unmodified MIPs and NIPs was 206 nm and 212 nm, respectively. The standard deviation for each size measurement (triplicates) was  $\leq 1\%$ . With a PDI (polydispersity index) of 0.022 and 0.046 the DLS-data show a narrow size distribution for the unmodified MIPs as well as for the NIPs. By following the procedure schematically described in Fig. 33a azide modified particles (MIP-N<sub>3</sub>/NIP-N<sub>3</sub>) were obtained. For the modification of particles we chose the remaining acrylamide moieties, originating from not fully reacted crosslinker molecules, to prevent the alteration of NAEMA coordination sites. In a first step the remaining acrylamides were reacted with 3-Chloro-1-propanethiol via trimethylamine catalyzed thiol-Michael addition resulting in a terminally chloride bearing thioether. In a second step, the chlorine was substituted with sodium azide leading to azide functionalized particle (MIP-N<sub>3</sub> / NIP-N<sub>3</sub>).

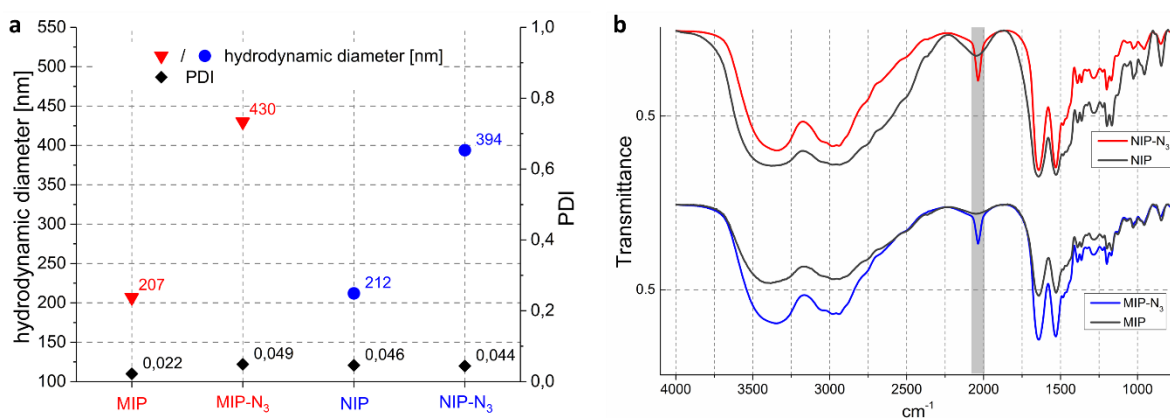


**Fig. 34 a:** Results of DLS measurements (z-average and PDI) of azide-modified and unmodified MIPs/NIPs. Before as well as after azide modification the particles show a high similarity in size and PDI. **b:** FTIR spectra of azide-modified and unmodified MIPs/NIPs. The characteristic azide band at  $2100\text{ nm}^{-1}$  for MIP-N<sub>3</sub>/NIP-N<sub>3</sub> indicates the successful particle modification.

The pristine particles (MIP / NIP) as well as the azide modified ones (MIP-N<sub>3</sub> / NIP-N<sub>3</sub>) were characterized via FTIR-spectroscopy (Fig. 34 b). For the azide-modified particles, the characteristic azide band at  $2100\text{ nm}^{-1}$  indicates the successful particle modification for the MIP-N<sub>3</sub> / NIP-N<sub>3</sub>. Apart from the azide band, the IR spectra show no differences in band pattern neither within the modified/unmodified particles nor between the two particle types, respectively. These results indicate a high similarity of the imprinted and non-imprinted material. As shown in Fig. 34a, the particle modification had a strong impact on the hydrodynamic diameter of the particles. The measured values for modified MIP-N<sub>3</sub> / NIP-N<sub>3</sub> nearly doubled in diameter if compared to the unmodified particles while the PDI stayed in the same range. This finding hints to an altered swelling behavior due to the increase in hydrophilicity induced by the azide modification. Zeta potential measurements confirmed that the presence of primary amine groups was not impaired by the particle functionalization. The zeta potential for both MIPs and NIPs (modified and unmodified) was in the range of  $40\pm 2\text{ mV}$ .

In the herein presented approach we chose a click chemistry (azide/alkyne)-based covalent immobilization of the PenG-imprinted MIPs and NIPs on the surface of the transducer. The immobilization of PenG-MIPs is schematically shown in Fig. 33b,c and followed the procedure described in the material section (part Si-4). An identical procedure was applied to covalently immobilize NIPs. In Fig. 35 SEM micrographs of a covalently immobilized MIPs-N<sub>3</sub> and NIPs-N<sub>3</sub> on a transducer surface are shown.

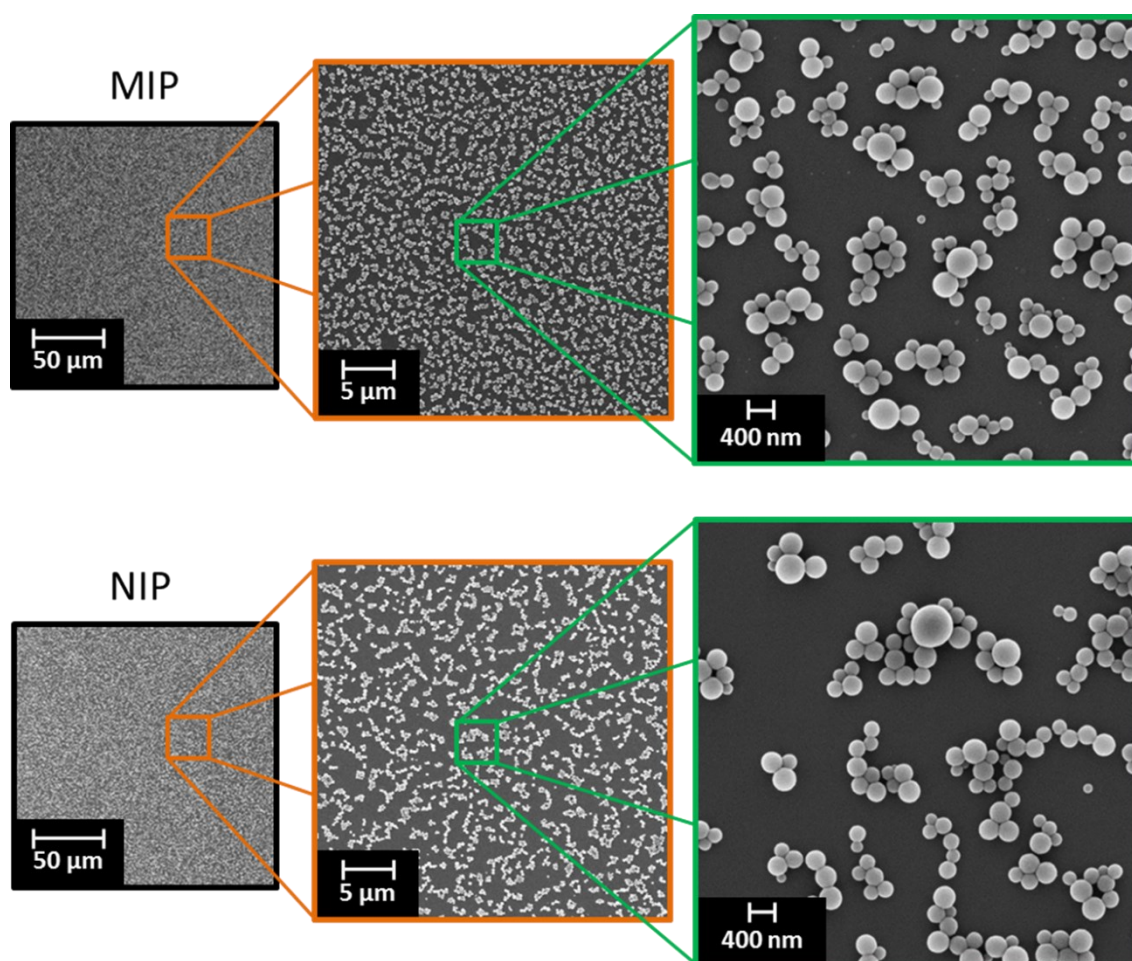


**Fig. 35.** SEM micrographs of a transducer surface with covalently immobilized MIPs-  $N_3$  (top) and NIPs- $N_3$  (bottom) at different magnifications. The surface is covered by the spherical particles in a homogenous statistical way.

The surface is covered by the spherical particles in a homogenous statistical way. For the preparation of SEM samples the particles are in a dry state. For DLS measurements on the other hand, particles are dispersed in water i.e. particles are in a swollen state. The measured size in DLS is the hydrodynamic diameter. It is common that the size determined by DLS is usually slightly higher compared to the size determined by SEM. Hence, the particle size and size distribution shown in the SEM micrographs is in good accordance with the data obtained by DLS measurements.

### 7.7.2. Sensor Stability

The stability of the covalent immobilized nano-MIP layer was analyzed via RfS baseline measurements. We compared two different particle layers - a covalent immobilized particle layer and its non-covalent immobilized counterpart. Covalent immobilized particle layer were prepared by following the protocol mentioned in the experimental section. For the preparation of non-covalent immobilized particle layer the same protocol was used but in the absence of the copper [II] compound. Due to the lack of copper [II], the essential catalytic copper [I] component for the 1,3-dipolar cycloaddition would not form. This would eventually lead to a non-covalent, only physisorbed and therefore instable particle layer. In Fig. 36 the first baseline measurements on the two described transducers are shown pumping buffer over the transducer at a flow rate of  $1 \times 10^{-6}$  L/s. Each baseline was recorded over the course of 30 minutes.

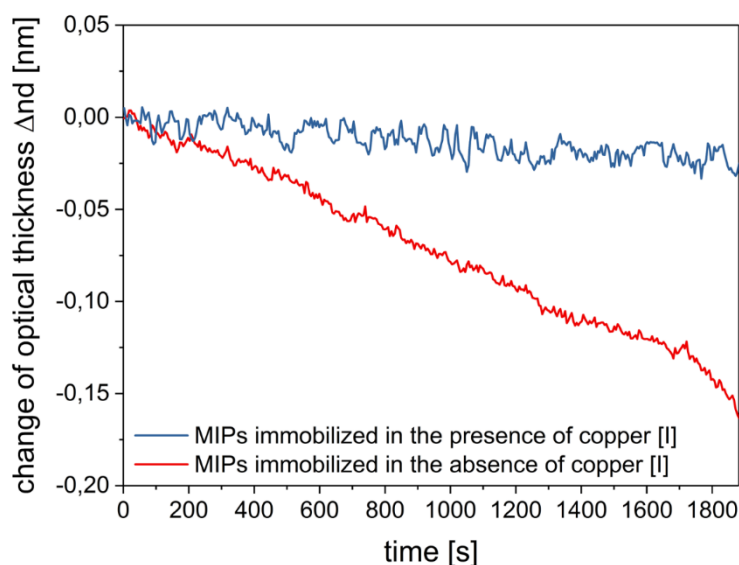


**Fig. 36.** Baseline measurements on a transducer with MIPs immobilized in the presence of catalytically active copper [I] (blue line) and on a transducer with MIPs immobilized in the absence of catalytically active copper [I] (red line).

The blue line is the measurement of a baseline for MIPs (prepared in the presence of the catalytically active copper [I]) and potentially covalent immobilized as described above. The baseline signal shows no significant drift, since no particles were removed from the transducer surface. The baseline measurement of the second transducer (red line) which was functionalized with particles in absence of copper [I] shows a strong,

steady and significant negative drift. Throughout all experiments, essential parameters (temperature, buffer, flowrate) were kept constant, thus a negative change of optical thickness is attributed to particles come off from the transducer surface. These results showed that in the presence of the catalytically active copper compound the covalent immobilization of particles on the transducer surface was successful.

Subsequently, different PenG concentrations (randomized triplicates) were measured to evaluate the sensing layer response behavior and its stability (Si-6). The response time was within the range of  $\approx 1$  minute. Diffusion times are short and the binding sites can be occupied fast, because of the easily available binding sites of the MIPs (Kolarov, Niedergall, et al. 2012). After each measurement, the sensor was easily regenerated by flushing with methanol. We tested the reproducibility of the sensor in 78 measurements during 26 h. The sensor could be regenerated completely after each measurement and the change in optical thickness showed a strong concentration dependency. Further, the sensor showed no instabilities and all measurements were reproducible which indicates a high stability of the covalent immobilized particles.

### 7.7.3. RIIS Measurements – Sensor Calibration

In order to calibrate the sensor, measurements at different PenG concentrations were conducted for a MIP and for a NIP transducer (Fig. 37). For each transducer, thirteen different concentrations in the range of 0.0015 – 0.0195 mol/L were measured in randomized triplicates (including blank measurements). This concentration range resembles the concentrations which occurs in the beginning of a PenG fermentation process. The change of the optical thickness increases with the concentration of PenG. This can not only be observed for the MIP transducer but for the NIP transducer as well. The increase in optical thickness for the NIP transducer is attributed to unspecific interactions of the polymer and the analyte. As expected, even the unspecific interaction lead to a concentration dependency in the change of optical thickness for the NIP transducer. Compared to the NIP transducer, the MIP binding signals were twice as high. The low standard deviation (SD) of measurements on the MIP transducer indicate an excellent selectivity of the imprinted particles.

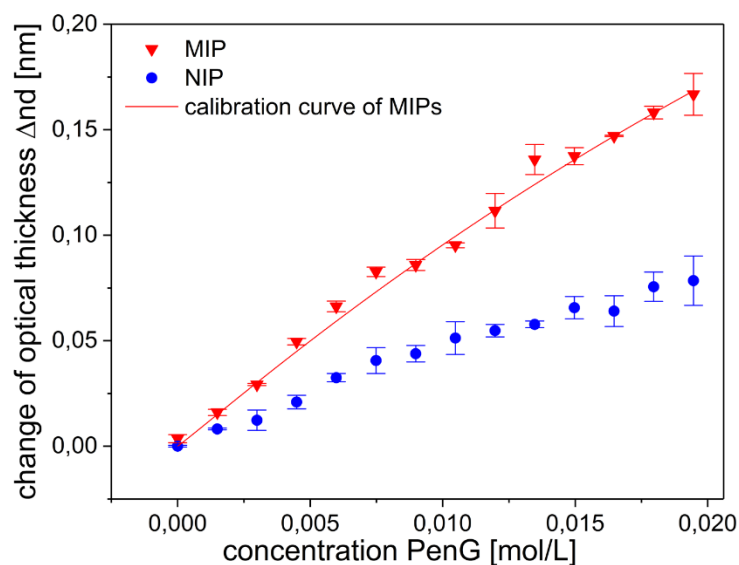


**Fig. 37.** Calibration measurements for a MIP transducer (triangles) and a NIP transducer (dots). The MIP measurements were fitted with Langmuir-Freundlich adsorption isotherms to obtain a calibration curve.

To obtain a calibration curve, the measurements of the MIP transducer were fitted with the Langmuir-Freundlich adsorption isotherms. The received parameters for the fit are shown in Table 6. The coefficient of determination ( $R^2$ ) holds a value of 0.999, which indicates a good correlation of the measurements and the fitted curve. Furthermore, the validation parameters were calculated. For the LOD and LOQ a concentration of 4.32 mmol/L and 6.15 mmol/L were received, respectively. Thus, the sensor is useable for the lower concentration range in a PenG fermentation process. In modern PenG production processes, the concentrations can rise up to 168 mmol/L (Ozcengiz and Demain 2013). As indicated by the calibration curve, the sensor did not reach a saturated state. Hence, it is possible to measure even at higher concentrations of PenG.

To ensure the accuracy and the quality of the measured calibration curve, the determination of recovery rates are unavoidable. Triplicate measurements of three concentrations (0.005 mol/L, 0.010 mol/L and 0.018 mol/L) were performed randomly on three MIP transducers, respectively (Table 7). The binding signals were evaluated by applying the afore-mentioned calibration function to the binding signals. The determined recovery rates were in the range of 70-120 %, which are the recommended range by the AOAC International. The satisfactory results of the recovery rates stand for a good chip-to-chip reproducibility and thus for a reproducible surface modification and a stable sensor.

**Table 6** Parameters of the Langmuir-Freundlich fit plotted in Fig. 6 and validation parameters (LOD, LOQ).

Parameter	Value
a	$0.736 \pm 0.522$
b	$17.537 \pm 22.416$
c	$-0.035 \pm 0.097$
R <sup>2</sup>	0.999
LOD [mol/L]	$4.32 \times 10^{-3}$
LOQ [mol/L]	$6.15 \times 10^{-3}$

**Table 7** Determined recovery rates of MIP transducers. Triplicate measurements with three concentration of PenG on three different MIP chips were measured.

Concentration [mol/L]	Recovery rates [%]	Standard deviation [%]
0.005	118.78	12.91
0.010 0.018	93.36	10.07
0.018	84.41	4.49

#### 7.7.4. Cross Sensitivities with Phenylacetic Acid and 6-APA

For the potential future application of this sensor in a biotechnological fermenter, it is of the utmost importance to know if there are any cross sensitivities between the sensing layer and the educts used in the fermentation process. The building blocks of PenG are phenylacetic acid and 6-aminopenicillanic acid (6-APA). They are structurally very similar to the analyte molecule PenG (Fig. 38).



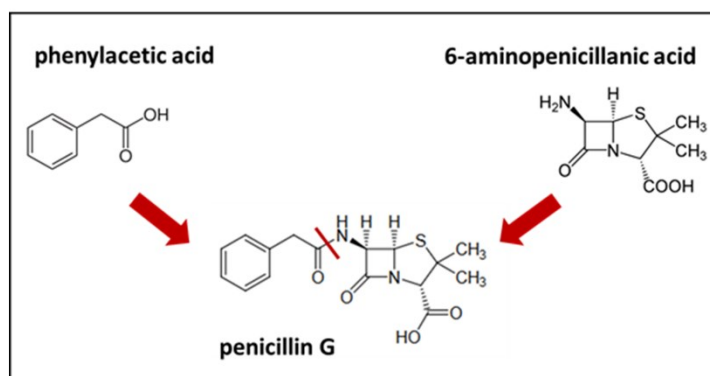


**Fig. 38. Structural formula of the product PenG and its building blocks phenylacetic acid and 6-aminopenicillanic acid (6-APA).**

Therefore, it is essential to investigate the interaction between the polymer particles and the educts. In Fig. 39 these interactions are plotted. Besides the triplicate measurements of PenG on a MIP and NIP transducer, separate triplicate measurements of phenylacetic acid (Fig. 39a) and 6-APA (Fig. 39b) on MIP and NIP transducers are illustrated.

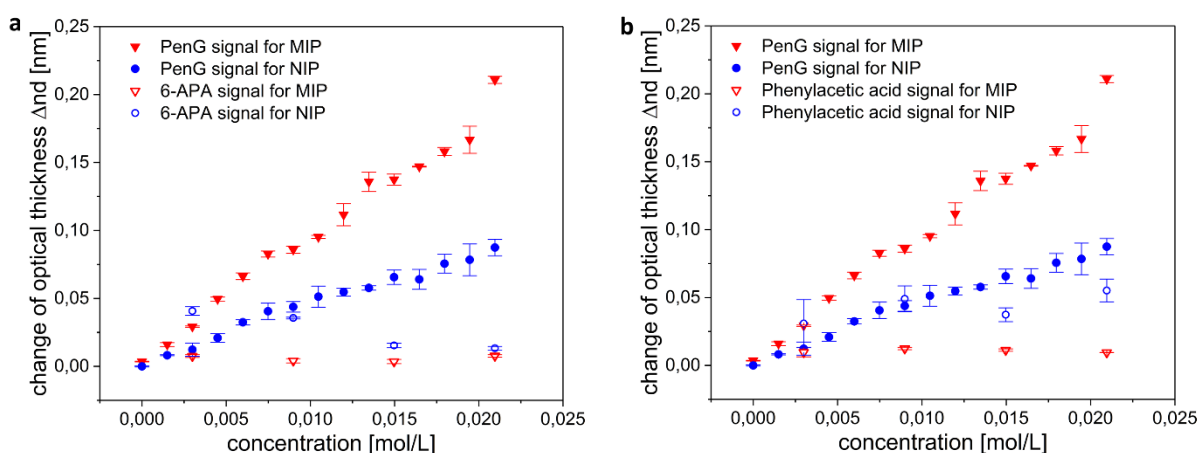


**Fig. 39. In both graphs the concentration dependency triplicate measurements of PenG on MIP transducer (triangles) and NIP transducer (circle) are shown. In graph (a) measurement of 6-APA on a MIP transducer (hollow triangles) and on a NIP transducer (hollow circles). In graph (b) measurements of phenylacetic acid on MIP transducer (hollow triangles) and on a NIP (hollow circles).**

For these experiments concentrations of 0.0030 mol/L, 0.0089 mol/L, 0.0150 mol/L and 0.0210 mol/L were used to compare the interactions between the educts and PenG with the MIPs and NIPs. As shown in Fig. 39, almost no change of the optical thickness on the MIP transducer was detected for both educts. In contrast to these results are the interactions between the educts and the NIP transducer. In this case, a change of the optical thickness is observed in particular for low educt concentrations. For the lowest concentration of educts (0.0030 mol/L), the NIP transducer shows a higher change in

optical thickness than PenG on a MIP transducer. This can only be explained with the LOD (limit of detection) of the calibrated sensor system. A concentration of  $4.32 \times 10^{-3}$  mol/L lies below the LOD thus, the sensor is not reliable in this range. It is not possible to accurately determine concentrations below the LOD. Nevertheless, for the other concentrations the binding signals of both educts on the MIP and NIP transducers are lower than the binding signals of PenG on the MIP transducers.

### 7.7.5. Conclusions

In this study, we developed an optical low cost sensor system for label-free determination of penicillin G (PenG) in aqueous buffer media. The sensing layer is based on PenG-imprinted nano-MIPs combined with RIfS as direct optical sensing method. Nano-MIPs were fully characterized (by SEM, DLS and FTIR-spectroscopy), successfully azide-modified and covalently immobilized on a transducer surface using click chemistry. With this sensing approach, we could show that it is possible to use the combination of nano-MIPs and RIfS for the quick and easy readout of PenG concentration in aqueous buffer media. The data of 78 concentration measurements (26 h) showed that the covalent immobilization of particles resulted in a stable sensing layer. A reproducible calibration of the sensor with PenG was possible. As shown by the calibration function, the sensing layer was not saturated. This allows the detection even of higher PenG concentrations, which for example occur in industrial PenG fermentation processes. Therefore, the future challenge will be the measurement in an entire fermentation stock. Although the presented results indicate, that there are no cross sensitivity with the tested PenG and its precursors, interaction between other components like cells, nutrients and elevated ion concentration cannot be ruled out. In addition, the sensor should be tested at an elevated temperature, which matches the conditions in fermentation processes. Consequently, the sensor for the in-line detection of the PenG titer has to be further tested and optimized to achieve a fully functional sensor for a possible application in a fermentation process.

Due to the straightforward nano-MIP preparation, their simple covalent immobilization and the efficiency of RIfS this approach could be a valuable sensing platform. As a result, the MIP transducers are very cost-efficient. Therefore, they can be applied as a disposable single use item in an industrial process. This will eliminate the need for sensor regeneration. In the future, the unspecific adsorption could be eliminated from the measuring signal by subtracting i.e. referencing the signal of the MIP and NIP transducers. The performance of the sensor array mainly depends on the quality (selectivity) of the

nano-MIPs while the reliability and durability of the sensor relays on the efficiency and stability of the covalent immobilization strategy. Potentially it can be applied to many other hydrophilic target (imprinting) molecules.

### 7.7.6. Acknowledgements

We gratefully acknowledge the help of Monika Riedl (Fraunhofer IGB) for conducting SEM and Tobias Götz (IGVP) for assisting with FT-IR spectroscopy.

This work was supported by a grant from the Ministry of Science, Research and the Arts of Baden-Württemberg, Germany (Az: 7533-7-11.6, program “Ideenwettbewerb Biotechnologie und Medizintechnik Baden-Württemberg”) to G.E.M.T. and G.G.

## 7.8. Supplementary data

### 7.8.1. Si-1: Preparation of MIPs/NIPs

Below, a general experimental procedure for the preparation of penicillin G (PenG) imprinted NAEMA-co-EBA nanoparticles (herein called MIPs) is described. PenG-MIPs were synthesized via inverse miniemulsion polymerization technique (inverse MiniEP). As disperse phase (aqueous phase) 0,168 g EBA (N,N'-Ethylenebisacrylamide, 1,0 mmol), 0,715 g NAEMA (N-(2-aminoethyl) methacrylamide hydrochloride, 4,36 mmol) and 0,036 g PenG (0,1 mmol  $\cong$  2,3 mol % relative to NAEMA) were dissolved in 750  $\mu$ L PBS-buffer (0,001 M phosphate, total ion concentration= 0,013 M) resulting in a slightly yellow colored transparent solution. The required continuous phase (oil phase) was prepared by dissolving 0,650 g Span 80 and 0,075 g AIBN in 12 mL of cyclohexane. These two solutions were combined in a cylindrical glass vial and thoroughly shaken by hand. Subsequently, the desired emulsion was formed by ultrasonication (10 minutes: 10 sec “on” / 5 sec “off”, at 60 % intensity). During sonication an ice bath cooling was applied to prevent emulsion destabilization and premature initiation of polymerization. To prevent freezing of the emulsion (cyclohexane  $T_m \approx 7^\circ\text{C}$ ) the ice cooling was removed immediately after completion of the sonication. The resulting emulsion was placed in a sealable double wall glass reactor containing a magnetic stir bar. The double wall glass was run through by water which was tempered by a heating circulator set to a temperature of 55  $^\circ\text{C}$  to initiate the polymerization. At this temperature, the emulsion was agitated overnight and

## 7 Synthetic Nanoparticles for Sensing

stirred with a speed of 200 rpm. The PenG-MIPs were purified by centrifugation. For this purpose, the emulsion was transferred into two polycarbonate centrifugation tubes (35 mL), broken by adding a sufficient amount of acetone and centrifuged at 75.600 G (25 k rpm) for 10 minutes. The supernatant was discarded; the resulting pellets were redispersed in ethanol (35 mL) via sonication, shaken for 10 minutes and centrifuged. This procedure was repeated three times with ethanol and three times with water. The PenG-MIPs were stored in a small amount of water. For the preparation and purification of NIPs the identical procedure was applied but in the absence of the template molecule PenG.

### 7.8.2. Si-2: Modification of MIPs/NIPs

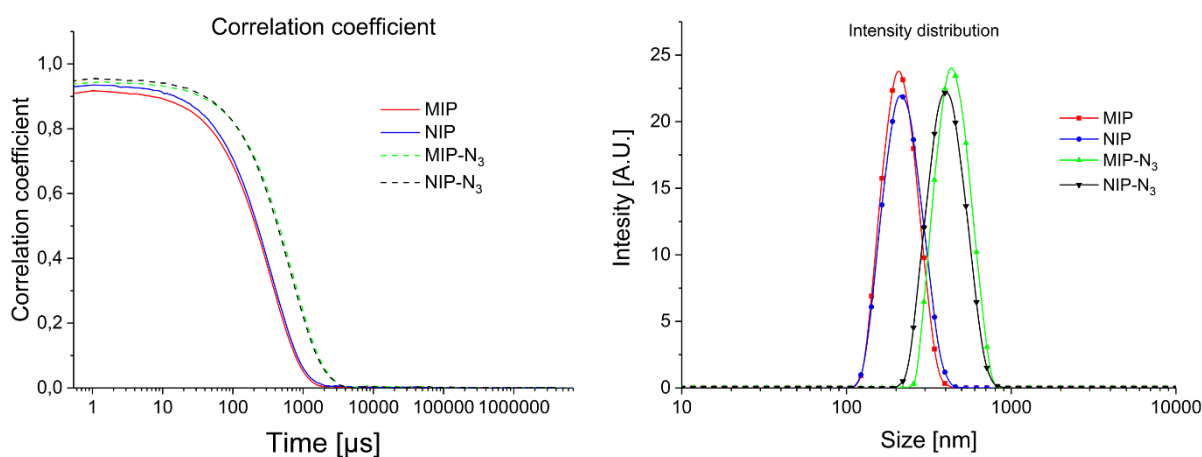
The following two-step reaction was applied in order to obtain azide-modified MIPs. Remaining crosslinker sites (acrylamides) were chosen for particle modification. To obtain a necessary excess of reactants, the particle yield and the amount of available acrylamide moieties was assumed to be 100 %. After the last centrifugation step in water (as described above), nanoparticles of one batch were redispersed via ultrasonication in 80 mL acetonitrile : water (1:1) in a glass vessel. To this suspension 110,6 mg (1,0 mmol) 3-Chloro-1-propanethiol and 30,3 mg TEA (0,3 mmol) were added and stirred at room temperature for 48 h. The suspension was transferred into four polycarbonate centrifugation tubes (35 mL) and centrifuged at 75.600 G (25 k rpm) for 10 minutes to remove excess reactants. The supernatants were discarded; the resulting pellets were redispersed in 35 mL acetonitrile : water (1:1) via sonication, shaken for 10 minutes and centrifuged. This procedure was repeated three times followed by three washing steps with water. The resulting pellets were combined and redispersed via ultrasonication in 80 mL DMF. To this solution, 20 mL of a saturated  $\text{NaN}_3/\text{DMF}$  was added and stirred for 48 h at room temperature. The particles were washed by centrifugation six times with water. Centrifugation parameters were as mentioned above. The resulting azide-modified pellets were redispersed in a small amount of water and stored at 7 °C.

### 7.8.3. Si-3: Characterization of MIPs/NIPs: DLS, FT-IR and SEM

#### Dynamic light scattering (DLS) and Zeta Potential

Measurements of size polydispersity index (PDI) and Zeta potential of synthesized nanoparticles were performed via DLS equipped with a 4 mW He-Ne laser  $\lambda = 632.8 \text{ nm}$  (Zetasizer ZEN 3600 - NanoZS, Malvern Instruments). Scattering photons were collected

in backscattering mode at an angle of  $173^\circ$ . For sample preparation, a sufficient amount of MIPs/NIPs was redispersed in water by applying ultrasonication treatment (5 sec “on” / 5 sec “off”) for 10 seconds. The solvent refractive index of water was applied within the Mavlern Zetasizer software. As material refractive index, the value of polystyrene was used. Measurements were performed in single use polystyrene cuvettes at  $20^\circ\text{C}$ . The reported sizes are the intensity based z-average diameters of three measurements ( $> 10$  runs each). The average zeta potential was determined by microelectrophoresis using the same device.



**Si-3. Number of measurements  $n=3$  for each particles sample. Average values of these triplicate measurements for correlation (left) and intensity distribution (right) are shown.**

### IR-Spectroscopy

Infrared spectra were recorded with a FTIR spectrometer VERTEX 70 from Bruker in a range of  $4000\text{ cm}^{-1}$  to  $400\text{ cm}^{-1}$ . Potassium bromide (KBr) was used as sample matrix. Both, background spectra (200 mg KBr pellet) and sample spectra (200 mg KBr pellet with 2 mg sample) were recorded with 60 scans and  $4\text{ cm}^{-1}$  resolution in transmission using a deuterated triglycine sulfate detector (DTGS).

### Scanning electron microscopy (SEM)

To determine morphology and size of the particles, scanning electron microscopy (SEM) was performed using a Zeiss Leo 1530 VP (Jena, Germany). Diluted dispersions of MIPs/NIPs were placed on silicon wafers and dried at ambient conditions. To minimize electrostatic charging, the samples were sputter-coated with platinum. Instead of using silicon wafers, the same procedure was applied to characterize immobilized nanoparticles on the glass transducers surfaces.

#### **7.8.4. Si-4: Preparation of the sensor surface: Particle immobilization protocol**

The glass transducers were cleaned, silanized and modified with an alkyne-bearing PEG in accordance to the method described by Mehne et al (Mehne, Markovic, et al. 2008)

##### Surface cleaning and activation

Glass transducers were cleaned with 6 M KOH for 1 min and rinsed with water. Afterwards, transducers were activated with a freshly prepared piranha solution (concentrated H<sub>2</sub>SO<sub>4</sub>:H<sub>2</sub>O<sub>2</sub> with the ratio 3:2 v/v) in an ultrasonic bath for 15 min. Finally, the transducers were rinsed with water and dried in a nitrogen stream.

##### Silanization

Activated glass transducers were modified with pure 3-Glycidoxypropyltrimethoxysilane (GOPTS). For this purpose 12 µL of GOPTS were pipetted on the glass surface and covered with another activated glass transducer (sandwich technique). After 1 h, the transducers were rinsed with dry acetone and dried in a nitrogen stream.

##### Immobilization of Polymer

After silanization, 30 µL of a solution of alkyne-PEG-NH<sub>2</sub> in dichloromethane (4 mg/mL) was pipetted onto the transducers. The transducers were kept overnight in an oven at 70°C. Subsequently, the slides were rinsed with water and dried in a nitrogen stream.

##### Immobilization of MIPs/NIPs

Aqueous dispersions of nanoparticles (MIP 0.02974 mg/µL and NIP 0.03474 mg/µL) were prepared in water. A second solution was prepared by dissolving 0.56 mM ascorbid acid and 0.20 mM copper(II) sulfate pentahydrate in 0,056 M DMSO. The two solutions were mixed in the ratio 1:4 (v/v) and were treated 10 min with an ultrasonic bath and 90 s with a probe sonicator resulting in a Huisgen reaction mixture. The transducers were covered by the reaction mixture and gently shaken for 24 h at room temperature. After the incubation, the coated transducers were rinsed with DMSO and

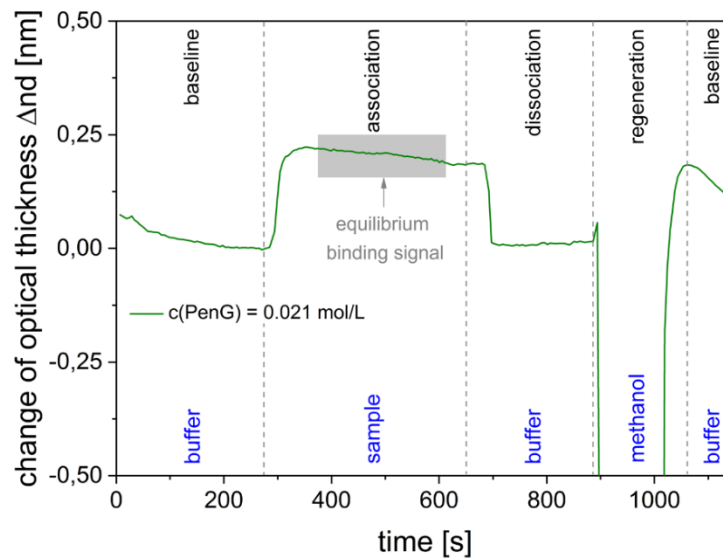
water and dried in a nitrogen stream. The bottom of the transducers was carefully cleaned of non-covalent immobilized polymer particles with ultrapure water and lab wipes.

### 7.8.5. Si-5: Spectral RIfS setup

#### Buffer Solution

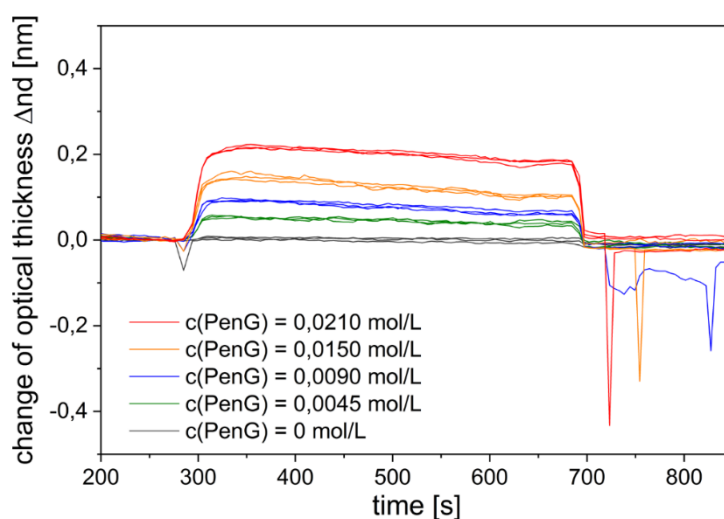
Citrate-buffered saline (pH 7.0, comprising 34.00 mM trisodium citrate dihydrate, 85.5 mM sodium chloride) was used as buffer solution as eluent in all experiments.

#### Calibration and data evaluation



**Si-5. Typical binding signal of PenG on MIPs detected by RIfS. The different steps of the measurement cycle are shown: baseline (buffer is flushed over the sensor surface), association phase (the sample is slowly flushed over the surface), dissociation phase (buffer is flushed over the surface), regeneration (the surface is flushed with methanol) and baseline (buffer is flushed over the sensor). The evaluation of data was determined at the equilibrium binding signal (during the sample injection phase).**

### 7.8.6. Si-6: Evaluation of sensor stability



Si-6. Binding signals of different concentrations of PenG (0 mol/L, 0.0045 mol/L, 0.0090 mol/L, 0.0150 mol/L, 0.0210 mol/L) for a MIP transducer. The measurements of the binding signals are implemented by the measuring procedure described in Si-5. The plotted curves are measured randomized. Triplicate measurements are performed for each concentration.

## 7.9. Further Characterization of the MIPs and NIPs: Surface Area via Nitrogen Sorption and Selectivity via ITC

To investigate the impact of a difference in surface area on the adsorption effects, the surface area of the azide-functionalized NAEME MIPs and NIPs were characterized via nitrogen sorption and analyzed with the BET-theory (Brunauer-Emmett-Teller). The resulting surface areas were  $9.9 \text{ m}^2\text{g}^{-1}$  and  $7.2 \text{ m}^2\text{g}^{-1}$  for MIP and NIP, respectively (Table 8).

These results are comparable with other nonporous, crosslinked polymer nanoparticles in that size range. Macintyre et. al (2006) prepared crosslinked polystyrene nanoparticles with a size of  $\approx 400 \text{ nm}$  and a surface area (BET) of about  $\approx 10 \text{ m}^2 \text{ g}^{-1}$ . The NAEMA MIPs exhibit a surface area roughly 1.4 times larger than the NIPs.



**Table 8** Surface area (BET) of azide functionalized NAEMA MIPs and NIPs

	MIP	NIP	Ratio (MIP/NIP)
Surface area (BET) [m <sup>2</sup> g <sup>-1</sup> ]	9.9	7.2	1,38
V <sub>m</sub> [cm <sup>3</sup> (STP) g <sup>-1</sup> ]	2.3	1.7	1,35

The binding properties of the MIP and NIP were analyzed via ITC (isothermal titration calorimetry). In a first experiment, control experiments were conducted by titrating pure water into MIP and NIP suspensions. The resulting reference signal accounts for dilution heat as well as contributions from the injection process itself. The signal intensities for both measurements were in the desired range and were later for subtracted from the sample signal.

The same experiment was repeated with the PenG titrant solution with concentrations of 151 mM and 203 mM. The dilution heat was recorded and was later also subtracted from the sample signal. The graphs of the control experiments can be found in the appendix (chapter 12.5)

MIP and NIP suspension with a nanoparticle content of 1.8 mg mL<sup>-1</sup> and 1.9 mg mL<sup>-1</sup> were analyzed via ITC. PenG solution (c = 203 mM) was titrated into each particle suspension and the resulting injection heats were recorded (Fig. 40, top left and right).

The measured injection heats were normalized by the amount of titrant injected and fitted (Fig. 40, bottom left and right).

From these graphs the binding heat  $\Delta H$  was calculated. The MIPs and NIPs exhibit a binding heat of -9.74 kcal mol<sup>-1</sup> and -3.18 kcal mol<sup>-1</sup>. The binding of PenG on the MIP is almost three times as effective compared to the NIP.

## 7 Synthetic Nanoparticles for Sensing

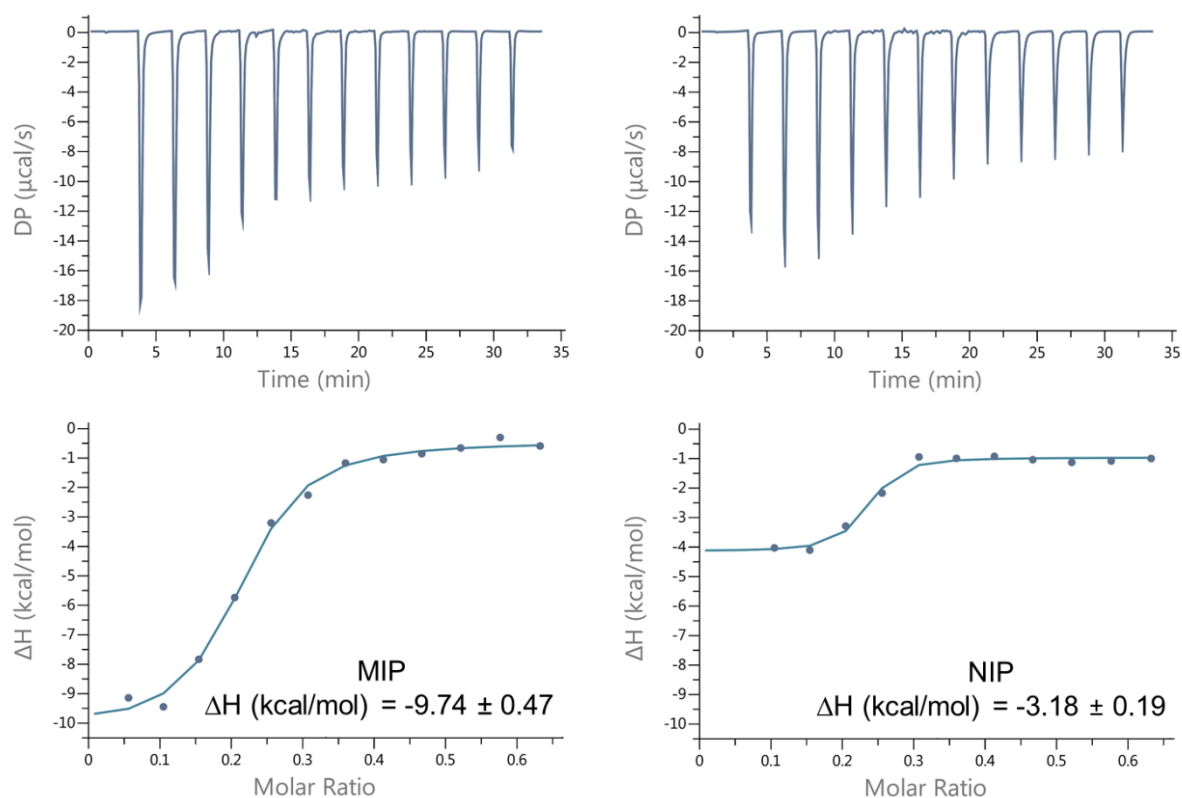


**Fig. 40** Top left and right: Injection heat resulting from the titration of PenG solution ( $c = 203 \text{ mM}$ ) in MIP and NIP suspensions  $1.8 \text{ mg mL}^{-1}$  and  $1.9 \text{ mg mL}^{-1}$ .

Bottom left and right: The measured injection heats were normalized by the amount of titrant injected and fitted. From these graphs the binding heat  $\Delta H$  was calculated.

As shown before, the analytical data from the final RfS sensor application show that the MIPs are about twice as sensitive compared to the corresponding NIPs (Fig. 37), while the ratio of surface area is only 1.38 (Table 8). These results suggest a successful imprinting of PenG and are further supported by the ITC data.

## 8. Novel Ionic Liquid-based miniemulsion

In this chapter, preliminary results for nanoparticle preparation in ionic liquids are shown. Subsequently, the results for the discussion of hypotheses III (8.1) are presented. The dissolution of chitosan in ionic liquids (ILs) and the development of sufficient emulsification strategies can be found in chapter 8.2.1 and 8.2.2. The results of the preparation of chitosan nanoparticles were written in a manuscript style (chapter 8.3), ready for publication as a short communication article in a peer-reviewed journal. The discussion of hypothesis III can be found in the discussion section in chapter 9.3.

### Declaration about my own contribution

*I conceived the study and elaborated the detailed experimental design.*

*This specifically included:*

- *Conceptualization and formulation of the overarching research goals within the study.*
- *Design of the experimental approach for particle synthesis via ultrasonication-assisted miniemulsion crosslinking in ionic liquids.*
- *Investigation and selection of potential ionic liquids suitable for the dissolution of chitosan and emulsification in an oil or water phases.*
- *Investigation and selection of surfactants/surfactant combinations for the preparation of stable ionic liquids emulsions.*
- *Development and validation of the synthesis strategy for the preparation of crosslinked nanoparticles using varying ionic liquids and varying surfactant combination for emulsion preparation.*
- *Determining the range of concentrations and stoichiometric calculation of synthesis educts and components, especially amount of chitosan, amount of ionic liquid, primary amine content, crosslinker, stabilizers and emulsion phase ratios.*
- *Elaboration and implementation of emulsion/particle preparation protocols in terms of selecting emulsification parameters, durations and particle separation/purification.*

## 8 Novel Ionic Liquid-based miniemulsion

- *Elaboration and implementation of sample preparation protocols and the necessary procedures for analytical methods such as scanning electron microscopy (SEM) and dynamic light scattering (DLS) as well as protocols for data evaluation and analysis.*
- *Conceptualization and implementation of the experiments for particle synthesis, particle characterization and reproducibility experiments. The data on synthesis, characterization and reproducibility experiments shown in this study were collected by Bernd Bäurer and Luise Hilfert in the course their master theses under my supervision and by applying my methodology.*
- *Evaluation and discussion of all the particle-related data in an overall context of this study.*
- *Visualization of the acquired data (graphs) and schematic representation.*
- *Writing of the entire original draft of the manuscript and taking the leading role in incorporating changes proposed by co-authors.*

### 8.1. Hypothesis III

*Chitosan dissolved in an ionic liquid (IL) can act as disperse phase in a miniemulsion **formulation** in order to prepare crosslinked Chi-NPs.*

- *It is possible to dissolve chitosan in an oil miscible (water immiscible) ionic liquid. This solution can be emulsified in water resulting in an IL-in-water emulsion.*
- *It is possible to dissolve chitosan in a water miscible (oil immiscible) ionic liquid. This solution can be emulsified in oil resulting in an IL-in-oil emulsion.*

## 8.2. Preliminary Results

Extensive experiments were conducted to find suitable ILs, in which chitosan can be dissolved. After finding a suitable IL, an empirical approach was applied to identify a suitable surfactant (mixture) for the formulation of stable IL in oil emulsions.

### 8.2.1. Dissolving Chitosan in Ionic Liquids (ILs)

The goal of this work was to dissolve chitosan in ionic liquids and to emulsify the resulting solution for the preparation of chitosan nanoparticles via miniemulsion crosslinking technique. Ionic liquids are a relative new class of solvent with unique dissolution properties. One of their main features is that they are liquid at temperatures below 100 °C - although being salts. A sub class of ILs are room temperature ILs (RT-ILs) which, as the names suggests, are in a liquid state at room temperature. In theory it is possible to create up to  $10^{18}$  different ILs by combining different anions and cations (Hayes, Warr, et al. 2015). The actual number of commercially available ILs is much lower being in the range of several hundred.

In preliminary experiments various commercially available ILs were tested for their capability to dissolve up to 3 wt.% of a low molecular weight (low MW) chitosan. We chose two water immiscible (hydrophobic) and four water miscible (hydrophilic) ILs as shown in Fig. 41.

The use of water immiscible ILs as disperse phase is desirable for emulsion-based particle preparation, as they would eliminate the need for a hydrophobic continuous phase. Due to their immiscibility with water, they would allow particle synthesis in IL-in-water emulsions. Instead of hazardous and expensive organic solvents like cyclohexane, water could act as disperse phase. However, the attempts of dissolving any amounts of chitosan in these two *water immiscible* ILs were unsuccessful even at elevated temperature and time. Hence, further experiments were only conducted with the hydrophilic ILs.

## 8 Novel Ionic Liquid-based miniemulsion

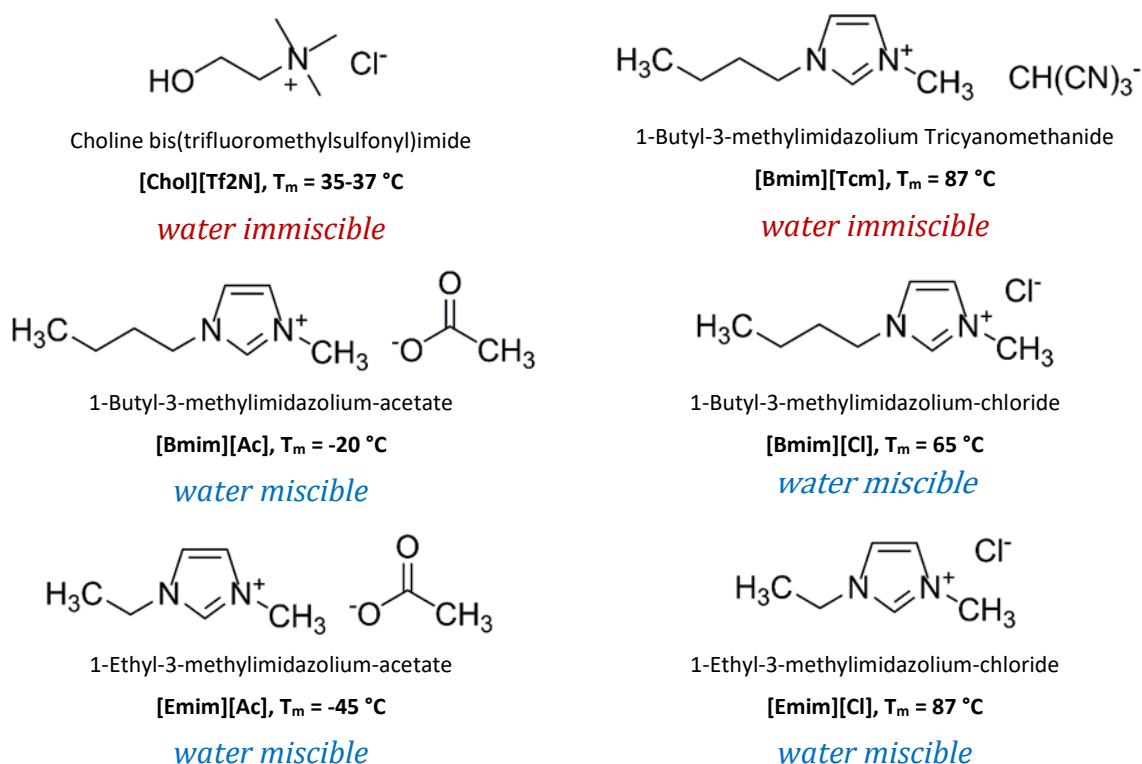


**Fig. 41** Chemical structure, melting point and miscibility of the six ionic liquids (ILs) used in this work. (Melting points taken from the datasheets provided by the manufacturer.)

It is commonly known that hydrophilic ionic liquids (ILs) like [Emim] [Ac] and [Bmim] [Ac] are particularly good solvents for the dissolution of the polysaccharide chitosan (Sun, Tian, et al. 2014; Horinaka, Urabayashi, et al. 2013; Guyomard-Lack, Buchtová, et al. 2015). Also, chloride-based ILs, for example [Emim] [Cl] (Zavrel, Bross, et al. 2009) and [Bmim] [Cl] (Xie, Zhang, et al. 2006), are reported to be able to dissolve polysaccharides like chitosan or cellulose. With the chloride-based imidazolium ILs [Emim][Cl] and [Bmim][Cl], it was not possible to obtain a fully dissolved and optically transparent chitosan solution. However, it was possible to prepare optically transparent solutions with [Bmim] [Ac] and [Emim] [Ac] in accordance with other reports.

Depending on the type of IL and on the amount of dissolved chitosan, these IL/chitosan solutions exhibit a viscosity in the range of several hundred mPa s. For the preparation especially of miniemulsions a low disperse phase viscosity is favorable (Riegger, Bäurer, et al. 2018). Fendt and co-workers (2011) showed that even small amounts of water decrease the viscosity of pristine ILs like [Bmim] [Ac] and [Emim] [Ac]. In a more recent work, Sun et al. (2014) investigated the effect of water content in [Bmim] [Ac]/water systems on their ability to dissolve chitosan. At a water content of 5 % or more, chitosan did no longer dissolve in [Bmim] [Ac]. Le, et.al, (2012) investigated the

impact of water on the viscosity of [Emim] [Ac]-cellulose solutions. They showed, that an increasing water content decreases the viscosity of the [Emim] [Ac]-cellulose solutions. To the best of our knowledge, similar experiments for [Emim] [Ac] and chitosan have not yet been described in the literature.

As stated above, a low disperse phase viscosity is favorable in miniemulsion processes. Hence, it was tried to harness the good solubility properties of pristine ILs in combination with the viscosity decreasing effect of subsequent addition of water. We successfully dissolved 3 wt % chitosan in both ILs at 100 °C for 72 h resulting in optical transparent solutions. When 5 % water was added, the solutions stayed optically transparent. To verify the dissolution of chitosan characterization via polarization/DIC (differential interference contrast) microscopy was conducted (Fig. 42).

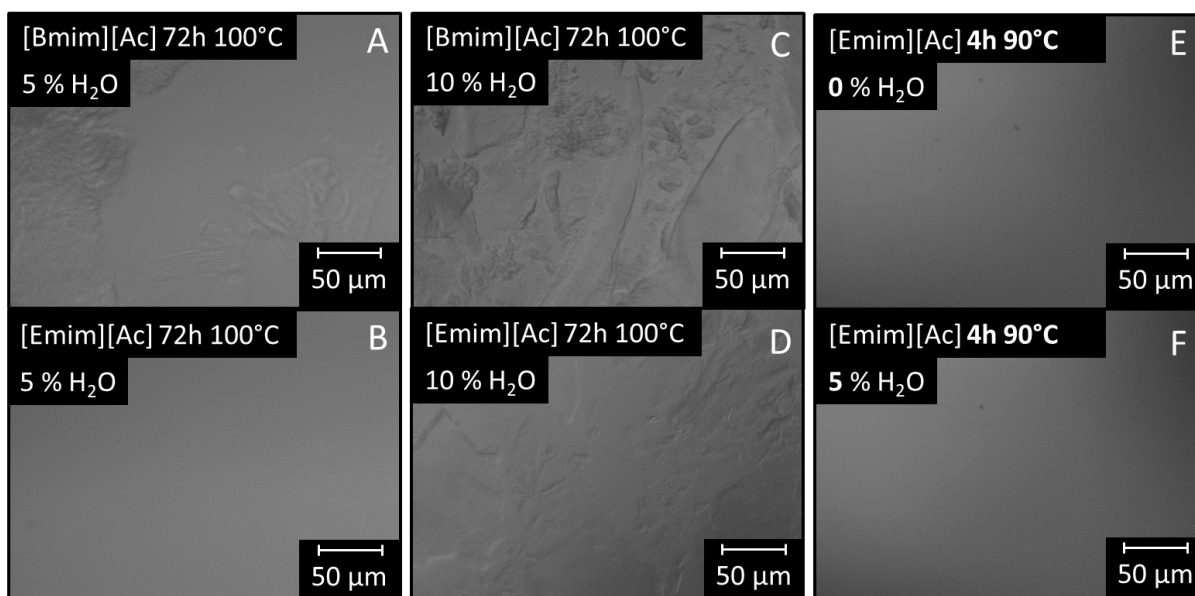


**Fig. 42.** Polarization/DIC microscopy images of 3 % chitosan dissolved in [Bmim] [Ac] and [Emim] [Ac] at different temperatures and dissolution times. Water content was varied between 0 %, 5 % and 10 %.

The crystalline parts, which can be seen in the polarization microscopy image (Fig. 42 A), indicate that for [Bmim] [Ac] the addition of 5 % water after dissolving the chitosan leads to precipitation. In the case of [Emim] [Ac] containing 5 % water (Fig. 42 B) no such crystalline parts, hence no precipitation was observed. The chitosan stayed in solution although 5 % water were present in the IL. A further increase of water content to 10 % (Fig. 42 C and D) lead to considerable precipitation of chitosan for both ILs. Hence, the dissolution process was optimized in terms of duration and temperature at 5 % water

content. As Fig. 42 E indicates chitosan can be completely dissolved in neat [Emim] [Ac] at 90 °C for 4 h. Even after the addition of 5 % water (Fig. 42 F) no precipitation of the polymer occurred. These results indicate that the dissolution of chitosan in [Emim] [Ac] with a water content of 5 % at 90 °C over the course of 4 h is the preferred choice.

To quantify the influence of water on the IL/chitosan viscosity, we conducted rheological experiments with both solutions containing no and 5 % water.

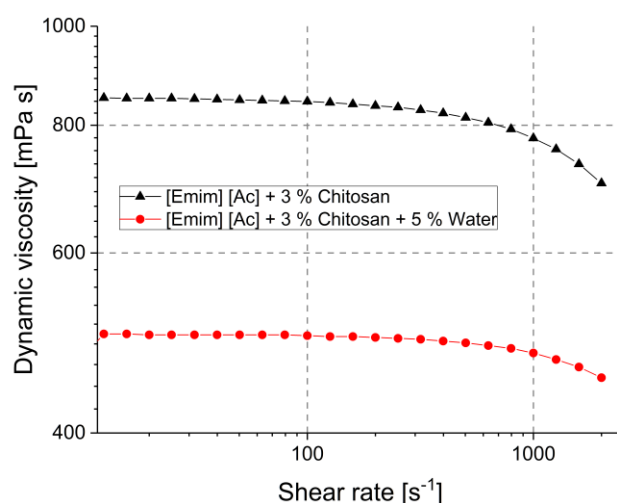


Fig. 43. Dynamic viscosity of [Emim] [Ac] solutions with 3% chitosan.

A shear rate sweeps from 0 s<sup>-1</sup> up to 1000 s<sup>-1</sup> (Fig. 43) was performed. At shear rates higher than  $\approx 300$  s<sup>-1</sup>, a shear-thinning behavior was observed for [Emim] [Ac] solutions with and without water. In contrast, pristine [Emim] [Ac] showed a viscosity of  $\approx 100$  mPa s and exhibited a Newtonian behavior (Gonsior, Hetzer, et al. 2010). A comparable solution containing 3 wt. % low MW chitosan in acetic acid also showed Newtonian behavior and a viscosity in the range of 20 mPa s (Riegger, Bäurer, et al. 2018). It is assumed, that the increased viscosity and the shear-thinning properties of the Chitosan/IL solutions may be attributed to interactions between the IL and the polysaccharide, which results in the formation of a physical gel-like network. At a constant shear rate of 100 s<sup>-1</sup> the [Emim] [Ac]/chitosan solution containing 0 % and 5 % water showed a viscosity of 838.5 mPa s and 498.3 mPa s respectively. These data suggest that a water content of 5 % reduces the viscosity of an [Emim] [Ac]/chitosan solution by about 50 %. Hence, the clear brown [Emim] [Ac]/chitosan solution containing 5 % water was used for the formulation of IL-in-oil miniemulsions.



### 8.2.2. IL Emulsions

The challenge was to prepare stable IL-in-oil miniemulsions with chitosan dissolved in [Emim] [Ac] acting as disperse (polar i.e. aqueous) phase and cyclohexane as continuous (nonpolar i.e. oil) phase. In the literature there are a few publications on IL-based microemulsions in general (Yuan, Guo, et al. 2015) and about IL microemulsions for the preparation of starch nanoparticles (G. Zhou, Luo, et al. 2014a, 2014b; Ji, Luo, et al. 2016). But thus far, published research in the field of emulsifying ionic liquids, particularly in the form of miniemulsions (also called nanoemulsions) for the preparation of nanoparticles, is sparse (Mahamat Nor, Woi, et al. 2017)(J. Li, Zhang, Han, Zhao, et al. 2012). Frank et al. (2009) reported the synthesis of polyimide nanoparticles in miniemulsion using an IL as continuous phase (oil in IL emulsion), replacing water, which is usually used in this synthesis.

The necessary HLB value for the preparation of a miniemulsion with these particular disperse and continuous phases (*[Emim] [Ac]/chitosan - in - cyclohexane*) was unknown. There is no data available of a systematic investigation for the preparation of IL-in-oil miniemulsion for particle preparation. Hence, an empirical approach was chosen to find a suitable surfactant or surfactant mixture for the preparation of IL-in-oil miniemulsion. As it was assumed that ionic surfactants would exhibit enhanced - and therefore more unpredictable - interactions with the ILs, solely nonionic surfactants were chosen.

The different surfactants and corresponding surfactant mixtures including their HLB-values are listed in Table 9. The HLB system allows to predict, which type of emulsion (W/O or O/W) is favored depending on the chemical composition of the surfactant (Davis 1994). The HLB values of the surfactant mixtures were calculated using the formula shown below (ICI Americas Inc 1980).

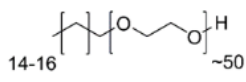
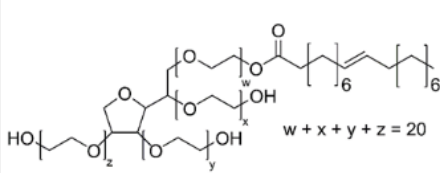
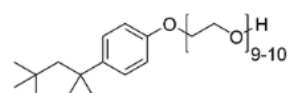
$$HLB_{Blend (AB)} = \frac{(X_A * HLB_A) + (X_B * HLB_B)}{X_{AB}}$$

Several surfactant and surfactant mixtures with varying HLB value were tested in order to create an IL-in-oil emulsion. We attempted to prepare stable emulsions with a phase ratio of 1/20 (IL/oil) with these surfactants and their corresponding mixtures. The amount of surfactant, in relation to the oil phase, was 4 % (w/w) in all experiments. We deliberately

## 8 Novel Ionic Liquid-based miniemulsion

added no osmotic agent as we assumed that due to its hydrophilicity the IL itself acts as such.

**Table 9 Overview of the surfactants and surfactant mixtures used in the empirical approach to prepare [Emim] [Ac]/chitosan - in - cyclohexane miniemulsions. For each pristine surfactant the HLB and the chemical structure is shown (also see Table 1). The HLB for the surfactant mixtures was calculated.**

Surfactant	HLB	Structure
100 % Lutensol AT 50	18.0	
75 % AT 50   25 % Span 80	14.6	⋮
50 % AT 50   50 % Span 80	11.2	
25 % AT 50   75 % Span 80	7.7	
100 % Span 80	4.3	
25 % Tween 80   75 % Span 80	7.0	⋮
50 % Tween 80   50 % Span 80	9.6	
75 % Tween 80   25 % Span 80	12.3	
100 % Tween 80	15.0	
Triton X-100	13.4	

All four of the tested surfactants (Triton™ X-100 – an ethoxylated octyl phenol, Lutensol® AT 50 – ethoxylated cetostearyl alcohol, Span® 80 – an ester of sorbitan and oleic acid and Tween® 80 a polyethoxylated sorbitan esterified with oleic acid) are nonionic, polymeric surfactants. The experiments showed that it was neither possible to produce stable emulsions with unblended Triton and Tween nor with mixtures of Tween and Span. Solely, the use of a combination of 75 % Lutensol AT 50 and 25 % Span 80 lead

to stable miniemulsions. The optimization and results of particle preparation with this emulsion formulation are discussed in the next chapter.

Benjamin R. Riegger, Bernd Bäurer, Luise Hilfert, Günter E.M. Tovar, Monika Bach. **“8.3. Miniemulsification of the ionic liquid *EMIM Ac* in cyclohexane for the preparation of glutaraldehyde-crosslinked chitosan nanoparticles.”**

*Manuscript in preparation/submission*

### **8.3. Miniemulsification of the ionic liquid *EMIM Ac* in cyclohexane for the preparation of glutaraldehyde-crosslinked chitosan nanoparticles**

Benjamin R. Riegger<sup>a</sup>, Bernd Bäurer<sup>a</sup>, Luise Hilfert<sup>a</sup>, Günter E.M. Tovar<sup>\*a,b</sup>, Monika Bach<sup>\*a,‡</sup>

\*Corresponding Authors: E-mail: monika.bach@uni-hohenheim.de and guenter.tovar@igvp.uni-stuttgart.de

<sup>a</sup>Institute for Interfacial Process Engineering and Plasma Technology IGVP, University of Stuttgart, Nobelstr. 12, 70569 Stuttgart, Germany. Tel: +49 711 685 68162;

<sup>b</sup>Fraunhofer Institute for Interfacial Engineering and Biotechnology IGB, Nobelstr. 12, 70569 Stuttgart, Germany.

<sup>‡</sup>Present address: Core Facility, University of Hohenheim, Emil-Wolff-Straße 12, 70599 Stuttgart, Germany. Tel: +49 711 45922735

#### **Unpublished Manuscript for Short communication**

Ionic liquids (ILs) attracted considerable attention in various scientific fields. This is mainly due to the sheer number of possible combinations of anions and cations resulting in a broad variety of ILs with adjustable properties. Ionic liquids are of special interest in the field of heterophases i.e. emulsion. Being so variable in their solution properties, ionic liquids pose as a completely new class of either “oil-” or “water-phase” which need to be explored. There already is literature about IL-based microemulsions in general (Yuan, Guo, et al. 2015; Kuchlyan, Kundu, et al. 2016), about IL microemulsions for the preparation of starch nanoparticles (G. Zhou, Luo, et al. 2014a, 2014b; Ji, Luo, et al. 2016) as well as research in the field of ionic liquid miniemulsions (also called nanoemulsions) (Mahamat Nor, Woi, et al. 2017; J. Li, Zhang, Han, Peng, et al. 2012; Damarla, Rachuri, et al. 2018). Ionic liquids were used as continuous phase for the preparation of nanoparticles via miniemulsion- and dispersion polymerization, respectively (Frank, Ziener, et al. 2009; Minami, Yoshida, et al. 2008; Minami, Kimura, et al. 2010). The use of ILs as disperse phase

was described for the preparation of gel particles via microsuspension polymerization (Minami, Fukami, et al. 2013; Suzuki, Ichikawa, et al. 2013). However, to the best of our knowledge, no work has yet been published on a method using ionic liquid as disperse phase in miniemulsions for the preparation of polymer nanoparticles.

It is commonly known that water miscible (hydrophilic) ionic liquids (ILs) such as [Emim] [Ac] (1-Ethyl-3-methylimidazolium-acetate) and [Bmim] [Ac] (1-Butyl-3-methylimidazolium acetate) are particularly good solvents for the dissolution of the polysaccharide chitosan (Sun, Tian, et al. 2014; Horinaka, Urabayashi, et al. 2013; Guyomard-Lack, Buchtová, et al. 2015). Depending on the type of IL and on the amount of dissolved chitosan, these IL/chitosan solutions exhibit a viscosity in the range of several hundred mPa s. However, a high disperse phase viscosity is undesirable, as it can lead to ineffective emulsification, especially in probe sonication-based processes. Therefore, a low disperse phase viscosity is beneficial for the preparation of chitosan nanoparticles via probe sonication-assisted miniemulsion (Riegger, Bäurer, et al. 2018). Hence, the process of dissolving chitosan in [Emim] [Ac] was optimized in preliminary experiments, in order to decrease the viscosity of the resulting solution. A complete dissolution of chitosan was verified via DIC (differential interference contrast) microscopy. Fendt and co-workers (2011) showed that even small amounts of water decrease the viscosity of pristine ILs such as [Bmim] [Ac] and [Emim] [Ac]. In a more recent work, Sun et al. (2014) investigated the effect of water content in [Bmim] [Ac]/water systems on their ability to dissolve chitosan. At a water content of 5 % and higher, chitosan did not dissolve in [Bmim] [Ac] anymore. Le, et al. (2012) investigated the impact of water on the viscosity of cellulose in [Emim] [Ac] solutions. They showed, that an increasing water content decreases the viscosity of the cellulose in [Emim] [Ac] solutions.

Based on the literature data shown above, we dissolved chitosan (3 wt %) in [Emim] [Ac] at 90 °C under constant stirring over the course of 4 h. The chitosan used in this work was a low molecular weight (MW) chitosan with a degree of deacetylation (DD) of  $\approx$  94 %. Data on characterization of MW (via SEC), DD (via  $^1\text{H-NMR}$ ) and rheology of this low MW chitosan can be found in a previous work (Riegger, Kowalski, et al. 2018). The viscosity of the resulting chitosan in IL solution was 838.5 mPa s. When 5 % (v/w) water was added (under stirring, 1 h, at 90 °C) after complete dissolution of the chitosan, the viscosity of the resulting solution was 498.3 mPa s.

Pure [Emim] [Ac] is hygroscopic, and adsorbed water can alter its properties significantly, especially regarding its ability to dissolve chitosan or other polysaccharides. Therefore,

the deliberate addition of water eases the handling of the hygroscopic IL, and on top decreases the viscosity.

The resulting chitosan solution (3 wt % chitosan, in [Emim] [Ac], 5 %water (v/w)) was used as disperse phase, in order to prepare IL in oil ([Emim] [Ac]/chitosan in cyclohexane) miniemulsions. Based on previous works, cyclohexane was used as oil phase (continuous phase) (Riegger, Bäurer, et al. 2018; Riegger, Kowalski, et al. 2018). The phase ratio of IL : oil was 1 : 20, while the amount of surfactant was 4 % (w/w) in relation to cyclohexane. The pulse sequence for emulsification via probe sonication was 5 s on, 5 s off (net sonication time: 10 min). The use of different ratios of Lutensol® AT 50 (ethoxylated cetostearyl alcohol) and Span® 80 (ester of sorbitan and oleic acid) for the preparation of [Emim] [Ac]/chitosan - in - cyclohexane miniemulsions were investigated.

The photograph (Fig. 44) of the resulting emulsions shows, that in all cases emulsions were created to some extent, except with unblended Span 80. Nevertheless, all the emulsions showed substantial creaming, except for the combination of 75 % Lutensol AT 50 and 25 % Span 80. Solely this combination resulted in an orange/brownish emulsion which was optically stable over the course of 24 h. For conventional inverse (water in oil) emulsions, surfactants with a low HLB of 4-6, for example pure Span 80, are usually necessary for successful emulsification i.e. emulsion stability (Kobitskaya, Ekinici, et al. 2010). However, we assume that due to the characteristic properties of the IL, a HLB value of 14.6 (75 % Lutensol / 25 % Span) was necessary for a successful emulsification. These results are in accordance with the work of Mahamat Nor et al. (2017). They investigated the preparation of IL in oil miniemulsions using two oil-insoluble ILs, namely 1-hexyl-3-methylimidazolium chloride [Hmim][Cl] and 1-butyl-3-methylimidazolium hexafluorophosphate [Bmim][PF<sub>6</sub>] emulsified in Labrafac LipophileWL 1349 (oil) as drug delivery system. They used different mixtures of Tween 80 and Span 20 resulting in a HLB of  $\approx 12$ .

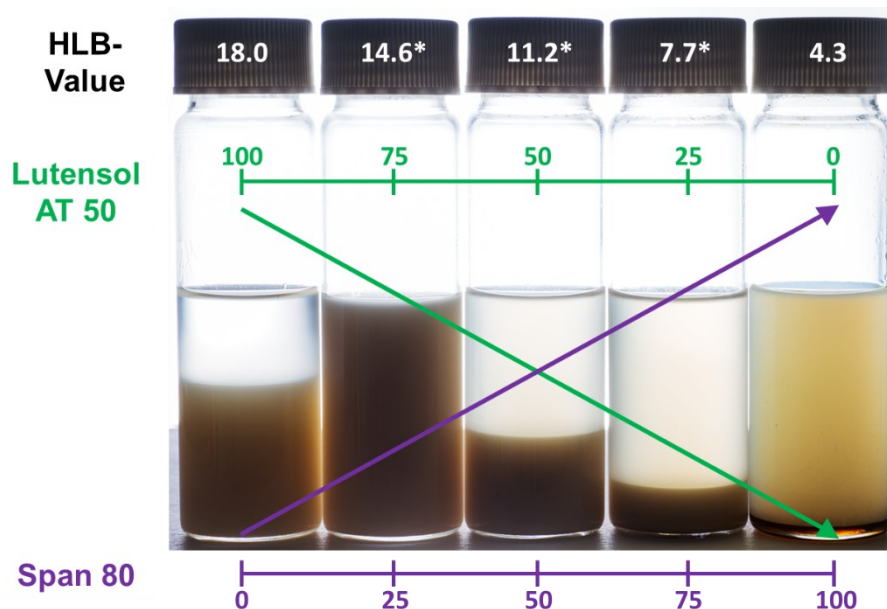


**Fig. 44** Photographic picture of different [Emim] [Ac]/chitosan in cyclohexane miniemulsions using different ratios of Span 80 and Lutansol AT 50. The amount of surfactant was 4 % (w/v) in all experiments. \*HLB values of these surfactant blends were calculated.

We tested other surfactants and surfactant mixtures for the emulsification of [Emim] [Ac]/chitosan in cyclohexane. It is notable, that the comparable HLB values of Triton (HLB = 13.4) or a Tween 80/Span 80 mixture (75 / 25, HLB = 12.3) did not lead to a stable emulsions. Interestingly, the use of Triton for the emulsification of water in a water-immiscible ILs (water in IL) has been reported before (J. Li, Zhang, Han, Zhao, et al. 2012). As the authors explained correctly, such an emulsion prepared with a high HLB surfactant should result in an IL in water emulsion. Yet, due to the solubility of Triton in the IL, a water in IL emulsion is formed. Apparently, however not surprisingly, regular considerations concerning surfactant solubility and HLB values as used for the preparation of conventional W/O or O/W emulsions may not fully apply when working with ILs as continuous and/or disperse phase.

To increase nanoparticle yield, the [Emim] [Ac]/chitosan in cyclohexane emulsion, using 75 % Lutensol AT 50 and 25 % Span 80 was further optimized regarding the disperse- and continuous phase ratio. The IL : oil phase ratio was increased from 1 : 20 to 4 : 20 resulting in an emulsion viscosity of 70,2 mPa s at a shear rate of 100 s<sup>-1</sup>. These emulsions were optically stable over the course of 72 h. Higher phase ratios such as 6 : 20 led to highly viscous emulsions, which may be undesirable for a subsequent addition of a crosslinking reagent as the increased viscosity can impair mixing and diffusion.

## 8 Novel Ionic Liquid-based miniemulsion

Glutaraldehyde was used as crosslinker for the preparation of crosslinked chitosan nanoparticles. While the crosslinking reaction of chitosan with glutaraldehyde has been known for a long time (Monteiro and Airoidi 1999), Guyomard-Lack et al. (2015) were the first to report crosslinking of chitosan with glutaraldehyde in a [Emim] [Ac]. In our work, we used a stoichiometric ratio of 1 mole glutaraldehyde per mole primary amine (originating from chitosan). The glutaraldehyde (25 % in aqueous solution) was added to the [Emim] [Ac]/chitosan in cyclohexane emulsion under stirring and reacted overnight und constant agitation. These experiments were repeated five times. The DLS-data of the resulting particles is shown in Fig. 45. While the particle size varies, ranging from  $\approx 200 - 400$  nm, the low PDI indicates particles with a very low size distribution for all five samples. The SEM micrograph reveals chitosan nanoparticles. Due to their swelling behavior and the SEM sample preparation, which involves drying, they lost some of their structural integrity and are strongly agglomerated.

This research has shown that chitosan dissolved in [Emim] [Ac] can be emulsified under the right circumstances, such as surfactant composition (unconventionally high HLB) and disperse/continuous phase ratio. The resulting emulsions can be used for the preparation of narrow distributed chitosan nanoparticles. The variation in size reveals that the emulsion formulation needs to be further optimized. The presented IL-miniemulsion crosslinking technique could also be viable for the preparation of nanoparticles from usually insoluble polysaccharides such as chitin or starch.

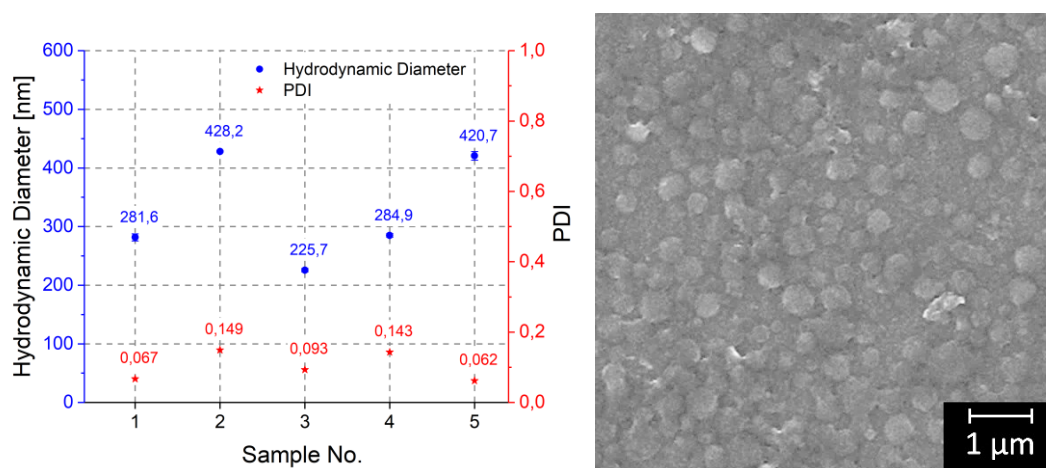


**Fig. 45** DLS-data (Polydispersity index (PDI) and hydrodynamic diameter) of chitosan nanoparticles prepared in five different emulsion batches (left). SEM-micrograph of resulting chitosan nanoparticles.



## 9. Discussion

In the course of this thesis titled *“Synthesis of bio- and synthetic-based functional nanoparticles via inverse miniemulsion for the adsorption and detection of pharmaceuticals in aqueous media”*, several different nanomaterials in the form of crosslinked nanoparticles were prepared via *inverse miniemulsion technique*. In order to do so, different emulsion formulations were developed and optimized. The synthesized nanomaterials were used for adsorption applications in general. On the one hand, as absorbent material in membrane-based water purification processes (hypothesis I) and on the other hand as sensitive layer in an optical sensor application (hypothesis II).

The bio-based nanoparticles used for water remediation were synthesized by processing an already existing biopolymer, namely chitosan, via *inverse miniemulsion crosslinking*. These results arising from the investigation of hypothesis I were published in two peer-reviewed papers with the titles *“Systematic approach for preparation of chitosan nanoparticles via emulsion crosslinking as potential adsorbent in wastewater treatment”* (chapter 5) and *“Chitosan nanoparticles via high-pressure homogenization-assisted miniemulsion crosslinking for mixed-matrix membrane adsorber”* (chapter 6).

Secondly, the synthetic nanoparticles used for sensing were prepared by polymerization of several different hydrophilic monomers in *inverse miniemulsion polymerization*. These results from the examination of hypothesis II were published in a peer-reviewed paper with the title *“Nano-MIP based sensor for penicillin G: Sensitive layer and analytical validation”* (chapter 7).

In a third research project, the third hypothesis was investigated by the emulsification of novel ionic liquids (ILs) for the preparation of chitosan nanoparticles in novel IL-in-oil (inverse) miniemulsions. These results are presented in chapter 8 and were partly written in a manuscript style for publication as short communication.

## 9.1. Hypothesis I

### Preface

The initial work on chitosan nanoparticles (Chi-NPs) in this thesis covered the efforts on finding the critical parameters for a reproducible synthesis of narrowly distributed Chi-NPs employing inverse miniemulsion crosslinking. The hypothesis for this part reads as follows:

#### 9.1.1. Hypothesis I.I

*It is possible to prepare crosslinked chitosan nanoparticles (Chi-NPs) reproducibly via inverse miniemulsion crosslinking technique using highly deacetylated chitosans with different molecular weight.*

- *The molecular weight (MW) has an impact on particle size.*
- *Compared to pristine chitosan, the crosslinked Chi-NPs show a superior adsorption behavior for a relevant active pharmaceutical ingredient (API).*

For this purpose, the impact of several parameters on the formation of inverse miniemulsion and chitosan nanoparticle preparation were investigated. As the power input of conventional stirring or agitating is not sufficient to produce droplets in the necessary range of 50 – 500 nm, high shear homogenization devices (probe sonication, high-pressure homogenization) need to be applied. When the emulsion droplets reach a size below  $\approx$  500 nm, they can be effectively stabilized against coalescing with a surfactant (see chapter: 4.1.3 Colloidal Stability: EDL and (X)DLVO-Theory). Compared to other emulsion-based particle preparation techniques, miniemulsions do not need a continuous and precisely controlled agitation to keep the emulsion stable after preparation.

The impact of glutaraldehyde (glut) concentration and molecular weight (MW) of six commercially available, highly deacetylated chitosans on Chi-NP formation via inverse miniemulsion crosslinking was investigated. Glut, being a water soluble homo-bifunctional aldehyde, was chosen in this work, as it is the most commonly used crosslinker for chitosan (Crini and Badot 2008). Opposed to ionic gelation crosslinking induced by tripolyphosphate (TPP) (Agnihotri, Mallikarjuna, et al. 2004), the crosslinking via glut happens in a covalent manner including imine formation (Fig. 15). Covalent

crosslinking is desired, in particular if the material is used in adsorption applications, which can include regeneration processes (adsorption/desorption) with strong pH or electrolyte concentration shifts.

Different glut concentrations were used for particle preparation. The successful formation of particles was confirmed via DLS and SEM. The density of the resulting nanomaterials was determined by helium pycnometry (Fig. 16). As expected, the density decreased with increasing degree of crosslinking, as the glut acts as spacer between the chitosan chains resulting in a less dense polymer network. These results are in accordance with the work of Uragami et al. (1994). An increase of the glut concentration higher than a molar glut : primary amine ratio of 1 : 1 did not lead to further decrease in density. The ratio of 1 : 1 was found to be optimal for the preparation of narrowly distributed, spherical Chi-NPs over a broad range of chitosan MW with a high yield. The use of NaCl as osmotic agent for improving emulsion stability was examined. The presence of an osmotic agent hinders Oswald ripening of a miniemulsion, and therefore increases its stability as described in chapter 4.1.5 “Emulsion Stability: Droplet Loss Mechanism” and chapter 4.1.6 “Different Types of Emulsion-based Polymerization Techniques: Suspension-, Macro-, Micro- and Miniemulsion Polymerization”. The results showed that a concentration of 0.1 M NaCl in the disperse phase leads to emulsions, which are stable over the course of 18 h. As shown via DLS and SEM (Fig. 18 A and B) it was possible to reproducibly prepare glut-crosslinked Chi-NPs with six different MWs ranging from  $M_n \approx 12.7 \text{ kg mol}^{-1}$  up to  $M_n \approx 121.4 \text{ kg mol}^{-1}$  (Fig. 17) via ultrasonication-assisted miniemulsion crosslinking (Fig. 14). These findings confirm the main statement of hypothesis I.I. An increasing Chi MW resulted in larger particle sizes ranging from 109.9 nm, for the lowest MW, up to 200.3 nm for the highest MW. These findings confirm the first sub hypothesis of I.I.

For further understanding of the used emulsion processes, the viscosity of the chitosan solutions was determined. The results showed, that the viscosity increased with the MW of chitosan (ranging from 19.3 mPa s to 2149.5 mPa s from low to high MW) (Fig. 18 C). As emulsification via probe sonication is less effective with increasing viscosities, it is assumed that the size of the resulting particles increases with increasing viscosity i.e. increasing MW. With increasing viscosity the droplet disruption, i.e. the emulsification efficiency decreases and therefore, droplet size increases as shown in Fig. 18 A and B. Presumably, this is the reason for an increased Chi-NP size with increasing Chi-MW.

Accordingly, to the second sub hypothesis of I.I the static adsorption behavior of the Chi-NPs and untreated chitosan for two APIs (active pharmaceutical ingredient) was evaluated. The drugs carbamazepine (CBZ) and diclofenac (DCL) were used in single point adsorption experiments (Fig. 19) as these are the most common drugs found in drinking water bodies (Yongjun Zhang, Geissen, et al. 2008). Fixed amounts of Chi-NPs were brought in contact with aqueous solutions with known concentrations of DCL and CBZ overnight. Afterwards, the remaining concentration was analyzed via HPLC. An adsorption capacity of up to  $351.8 \text{ mg g}^{-1}$  DCL for low MW Chi-NPs was observed and all Chi-NPs showed superior adsorption capacity, when compared to untreated chitosan. The highest adsorption capacity was measured for the smallest Chi-NPs. This is most likely due to their favorable surface-to-volume ratio. These results are in accordance with the literature (Poon, Wilson, et al. 2014). They also found an increased adsorption capacity, in their case for *p*-nitrophenol, onto glut-crosslinked chitosan when compared to pristine chitosan. The adsorption of the uncharged CBZ was low on Chi-NPs as well as on pristine chitosan. In both cases, the pristine chitosan showed low adsorption capacities ranging from  $\approx 1 \text{ mg g}^{-1}$  for CBZ and up to  $\approx 70 \text{ mg g}^{-1}$  for DCL. The use of Chi-NPs did not lead to any improvement in the adsorption of carbamazepine. These results confirm the second sub hypothesis of I.I for the adsorption of DCL, however not for CBZ.

### 9.1.2. Hypothesis I.II

The objective of the next step was to characterize the Chi-NPs even further and evaluate their use as filler in mixed-matrix membrane adsorbers for dynamic adsorption processes. To reach this goal, it was necessary to prepare larger amounts of Chi-NPs. As the throughput of sonication-based emulsification is quite limited in terms of volume, a different emulsification technique was applied. The emulsion formulation used in the sonication process was transferred to a high-pressure homogenization-assisted (HPH) emulsification process for the preparation of larger quantities of Chi-NPs. The hypothesis for this part reads as follows:

*It is possible to transfer an emulsion formulation, which was optimized for a discontinuous ultrasonication emulsification to a continuous high-pressure homogenization (HPH)-based process.*

- *Similar to the ultrasonication emulsification it is possible to process chitosan of different MW via high-pressure homogenization to reproducibly prepare Chi-NPs.*

As shown in Fig. 21, the results from DLS results and SEM analytics show that it was possible to prepare chitosan nanoparticles (Chi-NPs) via high-pressure homogenization-assisted miniemulsion crosslinking (homogenizing pressure 40 MPa). The emulsion formulation used was identical to the emulsion formulation optimized for ultrasonication from chapter 5 (water phase: chitosan dissolved in acetic acid; oil phase: cyclohexane with Span 80). For the homogenization i.e. emulsification of this mixture, seven homogenization cycles were run. These findings confirm the main statement of hypothesis I.II.

In order to evaluate the impact of disperse phase viscosity (Fig. 20), three highly deacetylated (> 90 %) chitosans of different MWs (low, medium and high MW) were used. Three different chitosans (low, medium and high MW) ranging from  $M_n \approx 24.0 \text{ kg mol}^{-1}$  up to  $M_n \approx 121.4 \text{ kg mol}^{-1}$  were tested. While emulsification, i.e. particle preparation, was possible with the low and medium MW chitosan, it was not possible to sufficiently emulsify the high MW chitosan at the chosen homogenization parameters due to the increased viscosity (Fig. 20). The homogenizing product for high MW chitosan did not result in stable emulsion i.e. did not result in nanoparticles. For a successful emulsification of low and medium MW chitosan solution via HPH a minimum of four, respectively five homogenization cycles were necessary.

The size of the resulting low and medium Chi-NPs was analyzed via DLS and was in the range of  $\approx 180 \text{ nm}$  and  $\approx 260 \text{ nm}$ , respectively (Fig. 21). The particles prepared with the medium MW chitosan were larger compared to the particles prepared with the low MW chitosan. This behavior is similar to the findings from the sonication-based particle preparation and it is presumed to be attributed to the increased disperse phase viscosity for medium MW chitosan. These results concur with the findings of Stang et al. (2001) who demonstrated that the droplet size, which correlates with particle size, in HPH emulsification processes increased with increasing disperse phase viscosity. These findings are further supported by the work of Shi and co-workers (2011). They investigated the HPH-assisted miniemulsion crosslinking formulation for the preparation of starch nanoparticles. They found that the aqueous phase with the lowest starch concentration (i.e. lowest viscosity) results in the smallest starch nanoparticles.

As it was possible to prepare particles with varying MW (low and medium MW) chitosan, the sub statement of hypothesis I.II was confirmed.

Additionally, the static adsorption behavior as well as adsorption kinetics for diclofenac (DCL) were tested in batch experiments for low and medium MW Chi-NPs (Fig. 24). In HPLC-assisted, static adsorption experiments, the DCL adsorption capacity of the low and medium MW Chi-NPs was tested in aqueous buffer media (pH = 7) for nine different concentrations ( $0.3 \text{ mg L}^{-1}$  -  $2500 \text{ mg L}^{-1}$ ) at 15 points in time ranging from 125 seconds to 62 minutes (Fig. 24 A and B). All particles showed a rapid sorption rate ( $< 2 \text{ min}$ ) with an adsorption capacity of up to  $256.2 \text{ mg g}^{-1}$  DCL. The adsorption capacities are comparable with the results from the sonication-based Chi-NPs (chapter 5). Zhang and co-workers (2014) found a similar rapid adsorption rate ( $< 0.5 \text{ min}$ ) for DCL on glut-crosslinked magnetic chitosan nanoparticles. Since the adsorption was so fast, no kinetic could be determined. Especially, for dynamic, i.e. membrane-based adsorption processes, the fast kinetics are favorable, as the contact time in such processes is rather short.

Subsequently, adsorption isotherms were modeled and fitted by Langmuir, Freundlich and Sips isotherms using the adsorption capacities obtained by the kinetic experiments (Fig. 25). The models show similar behavior for both particle types (isotherm parameters Table 5). The Freundlich model, accounting for multilayer adsorption, shows a poor fit for the experimental data and is therefore not suited as a model to describe the adsorption of DCL on Chi-NPs. The Sips and the Langmuir model show coefficients of determination ( $R^2$ ) of  $> 0.99$  for both particle types. The high similarity in correlation and parameters for both fits can be explained by  $n_s$  (Sips heterogeneity factor) being  $\approx 1$ . For  $n_s = 1$  the Sips model is reduced to a model with Langmuir behavior (Repo, Warchol, et al. 2010; Poon, Wilson, et al. 2014). A value of  $n_s \approx 1$  also indicates heterogenic sorption sites. The maximum adsorption capacity ( $q_{\max}$ ) for the low MW Chi-NPs is  $358.3 \text{ mg g}^{-1}$  for the Langmuir model and  $502.5 \text{ mg g}^{-1}$  for the Sips model. Thus, the Sips model predicts a substantially higher  $q_{\max}$  for DCL on low MW Chi-NPs. The values calculated for the medium MW Chi-NPs are similar for both models ( $305.3 \text{ mg g}^{-1}$  and  $317.3 \text{ mg g}^{-1}$  for Langmuir and Sips models, respectively). Nevertheless, the isotherm results (Langmuir and Sips model) as well as the experimental data (Fig. 24) show a higher adsorption capacity for the low MW Chi-NPs compared to medium MW Chi-NPs.

In a final step, particles were incorporated in mixed-matrix membranes to enhance the adsorption capacity in dynamic adsorption processes. Further, the membranes were

characterized in terms of pore size, flux and dynamic adsorption capacity. The hypothesis for this part reads as follows:

### 9.1.3. Hypothesis I.III

*It is possible to disperse the Chi-NPs from I.II in a membrane polymer solution in order to prepare Chi-NP-loaded mixed-matrix membranes.*

- *The Chi-NP mixed-matrix membranes can be applied for the adsorption of pharmaceutical compounds in aqueous media.*

Mixed-matrix membrane adsorbers were prepared by processing low and medium MW Chi-NPs into porous polyether sulfone (PES) microfiltration membranes via a casting and phase inversion process. The solvent used for the preparation of membrane polymer solutions was N-Ethylpyrrolidone (NEP), while the non-solvent in the membrane formation process (precipitation) was water. For membrane preparation, the polymer solution is casted via a doctor blade. Subsequently, this polymer solution film is submerged in a bath of non-solvent (water). As the NEP is soluble in water, it will be extracted from the polymer film. As PES is only soluble in NEP but not in water, this process results in the precipitation of PES due to the removal (dilution) of NEP. In this process, the polymer forms a porous flat sheet membrane.

As the Chi-NPs come in aqueous dispersion after their preparation, a solvent exchange protocol was developed to replace the water by NEP. The low and medium MW Chi-NPs could then be successfully dispersed in polyether sulfone polymer/NEP solution. Subsequently, mixed-matrix membranes were prepared via casting of the particle containing polymer solution (Fig. 26 A, B, C), followed by a phase inversion (precipitation) process in water. The membranes contained 6.4 w.t. % and 7.4 w.t. % low and medium MW Chi-NPs, respectively. Hence, the statement of the main hypothesis I.III was confirmed.

The pore size and the flux of these membranes, as well as of blank (reference) membranes were characterized (Fig. 26 D). Membrane preparation and membrane characterization was done in triplicates. The reference membrane and low MW Chi-NP membrane had comparable pore sizes with 0.3  $\mu\text{m}$  and 0.43  $\mu\text{m}$ , respectively. The low MW Chi-NP

## 9 Discussion

membrane shows a flux performance of  $5355 \text{ L m}^{-2} \text{ h}^{-1} \text{ bar}^{-1}$  which is similar to the reference membrane ( $5119 \text{ L m}^{-2} \text{ h}^{-1} \text{ bar}^{-1}$ ). These values are common for microfiltration membranes (Niedergall, Kopp, et al. 2016; Niedergall, Bach, et al. 2014). However, the presence of medium MW Chi-NPs in the membrane solution, supposedly lead to unwanted defects in the membrane. These defects are responsible for the flux and a pore size of the medium Mw Chi-NP-filled membrane being roughly being twice as high as that of the reference membrane.

Subsequently, all three membranes were tested in HPLC-assisted dynamic adsorption experiments with diclofenac solutions (Fig. 27 A). The membrane, which contained medium MW Chi-NPs, had an adsorption capacity slightly higher than the reference membrane. The larger pores resulting in higher flux are presumably responsible for unsatisfying adsorption performance. The membrane containing low MW Chi-NPs on the other hand exhibited an adsorption capacity of  $3.6 \text{ mg m}^{-2}$  while the corresponding reference membrane had a capacity of  $1.6 \text{ mg m}^{-2}$ . These results confirm the statement of sub hypothesis I.III when using low MW Chi-NPs in mixed-matrix membranes.



## 9.2. Hypothesis II

### Preface

In the second part of the thesis, the polymerization of several different hydrophilic monomers in inverse miniemulsion polymerization was conducted (chapter 7). The goal was to find sufficient polymer nanoparticle platforms, which could be used for the preparation of molecularly imprinted nanoparticles (nano-MIPs) in general. MIPs are widely investigated as selective adsorbents for water purification and as sensitive layer in various sensing platforms (Wackerlig and Lieberzeit 2015; Shen, Xu, et al. 2013). In this work, the nano-MIPs should be applied as sensitive layer in an optical sensor for the quantitative detection of pharmaceutical compounds in aqueous (process) media. Due to the molecular imprint, the resulting material should exhibit an increased selectivity for the adsorption of the template, i.e. the imprinted molecule. Compared to other suitable materials, which can form a sensitive layer, (e.g. antibodies), the requirements for those nanoparticles was a low size distribution, a reproducible spherical architecture and a certain mechanical stability, which allow them to keep their spherical shape even after centrifugation and drying. These requirements are mandatory for the reproducible preparation of homogeneous sensing layers.

Especially due to their polymeric matrix, MIPs exhibit a high thermal, chemical and temporal stability (Pichon 2007). In contrast to a bio-based recognition layer (i.e. antibodies, peptides), MIPs can be sterilized by autoclaving (Ramström, Ye, et al. 1996; Molinelli, Janotta, et al. 2008).

The preparation of crosslinked polymer nanoparticles, which fulfill the above-mentioned requirements, was successfully conducted using EBA as crosslinker and four monomers (namely 3-(Methacryloylamino)propyl] trimethylammonium chloride - MAPTAC, 3-Sulfopropyl methacrylate potassium salt - SPM, 2-Acrylamido-2-methyl-1-propanesulfonic acid sodium salt - AMPS, N-(2-aminoethyl) methacrylamide hydrochloride - NAEMA)) as shown in Fig. 28 and Fig. 30. Crucial parameters for the choice of the monomers was their water solubility, accessibility and the presence of moieties suitable for radical polymerization. All four monomers are radically polymerizable methacrylates or methacrylamides, which have their high water solubility and their possession of a charged functionality (primary amines, quaternary amines or sulfonates) in common. In order to prepare stable emulsions with these monomers, different

surfactants were evaluated. The impact on disperse phase monomer content on the particle formation was investigated using different concentrations of AMPS (Fig. 31). The particles were characterized via DLS and SEM. As long as the total monomer/crosslinker content stayed above  $\approx 40\%$ , the synthesis resulted in spherical particles, which hold their shape after centrifugation and/or drying. With decreasing monomer content, the particles formed showed less spherical structure and unfavorable high polydispersity index (PDIs). The goal was to prepare nano-MIPs and covalently immobilize them so that they could serve as sensing layer in an optical sensor (Reflectometric Interference Spectroscopy – RIfS). RIfS is based on multiple reflection on thin layers (Gauglitz 2010). If analyte molecules deposit on the sensor surface, a change in optical thickness  $\Delta nd$  (product of the refractive index  $n$  and the physical thickness  $d$ ) can be detected (chapter 7.6.3). The target molecule in the sensing application was penicillin G (Benzylpenicillin, PenG). The hypothesis for this part reads as follows:

### 9.2.1. Hypothesis II.I

*By using appropriate functional monomers, it is possible to prepare imprinted polymer nanoparticles via miniemulsion polymerization, which exhibit a selective adsorption behavior towards penicillin G.*

This promising technique of molecular imprinting has strongly risen scientifically interest in recent years (Uzun and Turner 2016). Molecularly imprinted polymers (MIPs) are tailor-made crosslinked polymer materials, which exhibit binding sites with a high affinity and selectivity towards a specified template molecule. The selectivity/affinity arises from “imprinted” binding sites, which match the template molecule in shape, size and complementary spatial (steric) configuration of functional groups. Template coordination in those nanocavities depends on the chosen monomer(s) and crosslinker(s) and thus, is based on non-covalent forces such as ionic, electrostatic, hydrophobic/hydrophilic, Van der Waals, hydrogen bond or  $\pi$ - $\pi$  interactions (Vaihinger, Landfester, et al. 2002; Gryshchenko and Bottaro 2014). As PenG is an anion (sodium salt), the cationic NAEMA was chosen as monomer from the four monomers discussed above. Narrowly distributed MIPs were prepared via inverse miniemulsion polymerization in the presence of PenG as

template (Fig. 32). Non-imprinted NAEMA/EBA nanoparticles (NIPs) were prepared identically but in the absence of PenG and were used as reference material. Characterization via DLS showed that the MIPS and NIPs exhibited a very low size distribution ( $PDI < 0.05$ ) and a size in the range of  $\approx 200$  nm (Fig. 34 a).

In the RIfS setup, MIP binding signals were about twice as high as the NIP binding signals (which will be further discussed in hypothesis II.II). Additionally, to evaluate the specificity of MIPS and NIPs they were characterized via nitrogen sorption (specific surface area, SSA) and isothermal titration calorimetry (ITC). These results showed that the MIPS exhibit a surface area roughly 1.4 times larger than that of the NIPs (Table 8). The binding heat  $\Delta H$  for the MIPS measured by ITC was roughly three times higher than that of the NIPs (Fig. 40). The ratio of surface area of MIPS/NIPs can be set in context to the specificity ratios of MIPS/NIPs from the RIfS (Fig. 37) and ITC results. While the surface area for the MIP is only 1.4 times larger, the RIfS/ITC results show that the MIP is roughly twice/three times as sensitive compared to the NIPs. As the increased specificity cannot only be attributed to a larger surface area for the MIPS, these results further support the presence of molecularly imprinted binding sites. These results confirm the statement of hypothesis II.I

### 9.2.2. Hypothesis II.II

*Through suitable functionalization of the nanoparticles they can be covalently immobilized on the sensor surface.*

- *This covalently immobilized sensitive layer is impervious against overflow in the measuring chamber and despite the functionalization still bears its ability to selectively bind penicillin G in aqueous solution.*
- *The covalent immobilization benefits the sensors lifespan.*

Although a nano-MIP sensing layer provides many advantages, one drawback would be the stability of such a nanoscaled recognition layer. If nano-MIPs are immobilized in a non-covalent manner (i.e. via electrostatic interactions), there is a high chance of particles being detached when in contact with the aqueous reagent flow during the sensing process. In order to allow for covalent immobilization of these particles on the sensor surface, they

were functionalized with azide moieties in a two-step reaction (Fig. 33). In a first step, the remaining acrylamides originating from not fully reacted crosslinker were functionalized via thiol-Michael addition resulting in a terminally, chloride-bearing thioether. In a second step, the chlorine was substituted with sodium azide leading to azide-functionalized particles. The successful reaction was confirmed via FT-IR spectroscopy (Fig. 34 b).

While the MIPs and NIPs exhibited a hydrodynamic radius of about 200 nm before the modification, the radius increase to  $\approx 400$  nm after the modification (Fig. 34 a). This is mainly attributed to an altered swelling behavior of the particles due to the chemical modification with azide functionalities (Fig. 33 a). The corresponding sensor surface, a glass transducer, was alkyne-modified via silane chemistry (Fig. 33 b). Subsequently, the particles were covalently immobilized on alkyne-modified glass transducers by copper(I)-catalyzed 1,3-dipolar cycloaddition (Fig. 33 c). Baseline measurements were performed with these transducers. The baseline signal was constant, showing that the particle layer was stable and no particle detaching occurred. As reference, transducers were prepared with particles in the absence of the catalytic active copper(I), i.e. the cycloaddition could not occur. When these transducers were used in baseline measurements, the signal showed a constant decrease, indicating particles detaching from the transducer surface. This confirms the stability of the covalently immobilized particle layer on the transducer and therefore, the main statement of hypothesis II.II.

For sensor calibration 14 randomized triplicate concentration dependency measurements were conducted for covalent immobilized MIP and NIP transducers with different PenG concentrations ranging from 0.0015 - 0.0195 mol/L. Recovery rates of three different transducers were determined in the range of 70 - 120 %, which indicates a good chip-to-chip reproducibility. Sensor cross-sensitivities between PenG and its structural building blocks phenylacetic acid and 6-aminopenicillanic acid were evaluated indicating a high selectivity for the presented sensor system. These findings confirm the statement of the first sub hypothesis of II.II.

The longevity of the sensitive layer was further proven by performing 78 reproducible PenG measurements over the course of 26 h. The covalent immobilized sensitive layer allowed for reproducible concentration measurements over this extended period of time. These findings confirm the statements of the second sub hypotheses of II.II.

### 9.3. Hypothesis III

#### Preface

The third part of the thesis explores the use of a relatively new class of solvents – ionic liquids (ILs) – as disperse phase in miniemulsions (Chapter 8). Most commonly ionic liquids are defined as salts (cation and anion) with a melting point of below 100 °C (Plechova and Seddon 2008). Due to the non-volatility and their adjustable dissolution properties, the application of these solvents is of high interest. The goal was to use these emulsions for the preparation of chitosan nanoparticles (Chi-NPs). The hypothesis for this part reads as follows:

#### **Hypothesis III**

*Chitosan dissolved in an ionic liquid (IL) can act as disperse phase in a miniemulsion formulation in order to prepare crosslinked Chi-NPs.*

- *It is possible to dissolve chitosan in an oil miscible (water immiscible) ionic liquid. This solution can be emulsified in water resulting in an IL-in-water emulsion.*
- *It is possible to dissolve chitosan in a water miscible (oil immiscible) ionic liquid. This solution can be emulsified in oil resulting in an IL-in-oil emulsion.*

Data on several ionic liquids which dissolve chitosan have been published (Sun, Tian, et al. 2014; Horinaka, Urabayashi, et al. 2013; Guyomard-Lack, Buchtová, et al. 2015). All these ILs have in common that they are *water miscible*. However, the use of *water immiscible* ILs (Fig. 41) is highly desirable for the dissolution of chitosan because they eliminate the need to use organic solvents for the preparation of emulsion. Instead, these chitosan-in-IL solutions could be emulsified in water. However, it was not possible to dissolve chitosan in the two chosen water immiscible ILs, namely [Chol][Tf2N] and [Bmim][Tcm]. So far scientific literature does not show any record of chitosan being dissolved in a water immiscible IL. Hence, it was not possible to confirm the first sub hypotheses of III.

On the other hand, the dissolution of chitosan in *water miscible* ILs is described in the scientific literature as mentioned above. It is commonly known that *water miscible* ionic liquids (ILs) such as [Emim] [Ac] (1-Ethyl-3-methylimidazolium-acetate) and [Bmim] [Ac]

(1-Butyl-3-methylimidazolium acetate) are particularly good solvents for the dissolution of the polysaccharide chitosan. In this work, this dissolution process was optimized in order to achieve a preferably low viscosity of the resulting chitosan-in-IL solution. A low disperse phase viscosity is beneficial for the preparation of chitosan nanoparticles via probe sonication-assisted miniemulsion (Riegger, Bäurer, et al. 2018). Fendt and co-workers (2011) showed that even small amounts of water decreases the viscosity of pristine ILs such as [Bmim] [Ac] and [Emim] [Ac]. In a more recent work Sun et al. (2014) investigated the effect of water content in [Bmim] [Ac]/water systems on their ability to dissolve chitosan. At a water content of 5 % and higher, chitosan did not dissolve in [Bmim] [Ac] anymore. Le, et.al, (2012) investigated the impact of water on the viscosity of cellulose in [Emim] [Ac] solutions. They showed that an increasing water content decreases the viscosity of the cellulose – in – [Emim] [Ac] solutions.

Decreasing the viscosity of the chitosan in IL solutions used in this work was achieved through the addition of small amounts of water (5 %) to the IL after dissolving the chitosan. To verify the dissolution of chitosan, characterization via polarization/DIC (differential interference contrast) microscopy was conducted (Fig. 42).

For [Bmim] [Ac] the addition of 5 % water after dissolving the chitosan leads to precipitation. As Fig. 42 E indicates, chitosan can be completely dissolved in neat [Emim] [Ac] at 90 °C for 4 h. Even after the addition of 5 % water (Fig. 42 F) no precipitation of the polymer occurred. These results indicate that the dissolution of chitosan in [Emim] [Ac] with a water content of 5 % at 90 °C over the course of 4 h is the preferred choice. These findings confirm the second sub-hypothesis of III.

To quantify the influence of water on the IL/chitosan viscosity, rheological experiments with both solutions containing no and 5 % water were conducted. It transpired that the addition of 5 % decreases the viscosity of the IL/chitosan solution by about 40 % (Fig. 43).

The resulting chitosan-in-[Emim] [Ac] solution subsequently was emulsified in cyclohexane via probe sonication. In the literature, the use of ILs as continuous phase is described for the preparation of nanoparticles via miniemulsion- and dispersion polymerization, respectively (Frank, Ziener, et al. 2009; Minami, Yoshida, et al. 2008; Minami, Kimura, et al. 2010). However, only few works have been published on the topic of using ILs as disperse phase in emulsions. The use of ILs as disperse phase was described for the preparation of gel particles via microsuspension polymerization (Minami, Fukuami, et al. 2013; Suzuki, Ichikawa, et al. 2013). Even after an extensive search, so far,

no publication on a method using ionic liquid as disperse phase in miniemulsions for the preparation of polymer nanoparticles was found.

Hence, an empirical approach was applied, testing several known surfactants frequently used in water in oil emulsions, in order to find a suitable surfactant for the emulsification of [Emim] [Ac]/chitosan solutions in cyclohexane (Table 9). The surfactants in question were nonionic, polymeric surfactants namely: Triton™ X-100 – an ethoxylated octyl phenol, Lutensol® AT 50 – ethoxylated cetostearyl alcohol, Span® 80 – an ester of sorbitan and oleic acid and Tween® 80 a polyethoxylated sorbitan esterified with oleic acid. The pristine surfactants as well as different surfactant mixtures were tested. Solely a mixture of 75 % Lutensol AT 50 and 25 % Span 80 (calculated HLB = 14.6) resulted in optically stable [Emim] [Ac]/chitosan/5 % water in cyclohexane miniemulsions over the course of at least 24 h (Fig. 44).

It is notable, that the surfactants Triton (HLB = 13.4) or a Tween 80/Span 80 mixture (75 / 25, HLB = 12.3), which possess comparable HLB values to the 75 % Lutensol AT 50 and 25 % Span 80 mixture did not lead to a stable emulsion. Interestingly the use of Triton™ X-100 for the emulsification of water in a water-immiscible ILs (water in IL) has been reported before (J. Li, Zhang, Han, Zhao, et al. 2012). According to classic HLB theory, such an emulsion, prepared with a high HLB surfactant, should result in an IL in water emulsion. Nevertheless, a water-in-IL emulsion is formed due to the solubility of Triton™ X-100 in the IL as explained correctly by the authors. Apparently, however not surprisingly, regular considerations concerning surfactant solubility and HLB values as used for the preparation of conventional water in oil or oil in water emulsions may not fully apply when working with ILs as continuous and/or disperse phase.

With the formulation, using 75 % Lutensol AT 50 and 25 % Span 80 mixture as surfactant, it was possible to prepared stable [Emim] [Ac]/chitosan/5 % water-in-cyclohexane miniemulsions for the synthesis of glut-crosslinked chitosan nanoparticles. A stoichiometric ratio of 1 mole glut per mole primary amine (originating from chitosan) was used. The glut (25 % in aqueous solution) was added to the [Emim] [Ac]/chitosan-in-cyclohexane emulsion under stirring and reacted overnight und constant agitation. These experiments were reproduced five times, producing particles in the range of about 200 nm - 400 nm confirmed by DLS and SEM (Fig. 45). This particle size variation indicates the need to further optimize this preparation method via IL-based miniemulsion crosslinking.

## 9 Discussion

In conclusion, this thesis covered the preparation of different polymer nanoparticles via inverse miniemulsion technique. Particles were prepared in inverse miniemulsion by crosslinking of an already existing biopolymer (chitosan) or the polymerization of synthetic monomers. In order to do so, several different emulsion formulations were developed and optimized.

The resulting particles were characterized and successfully used as adsorbent materials in water purification and as sensitive layer in a RfS sensor application. Further, novel miniemulsion formulations were developed using ionic liquids as disperse phase. With these IL in oil miniemulsions, crosslinked chitosan nanoparticles were prepared.



## 10. Conclusion & Outlook

**Chitosan nanoparticles:** The objective of the first section of this thesis (hypothesis I, chapter 5 and 6) was to contribute to the knowledge about the preparation of chitosan nanoparticles via miniemulsion crosslinking and their use as adsorbent in water treatment. Relevant process parameters such as the use of an osmotic agent for emulsion stabilization and the impact of chitosan molecular weight on particle formation were investigated. Further, the amount of glutaraldehyde was optimized in order to prepare crosslinked chitosan nanoparticles. Next to emulsion preparation of miniemulsion via probe sonication, larger amounts of emulsions i.e. particles were successfully prepared via high-pressure homogenization.

The adsorption of diclofenac onto chitosan nanoparticles was extensively investigated in static adsorption experiments. It was shown that the particle size decreases with decreasing molecular weight of chitosan. The smallest chitosan nanoparticles exhibited the highest adsorption capacity. Further, the adsorption experiments showed, that the adsorption kinetics of diclofenac on chitosan nanoparticles are rather fast (< 2 min). The fast kinetic is especially favorable as the particles were subsequently used in membrane based dynamic adsorptions processes with very short contact times. Chitosan nanoparticle filled mixed-matrix membranes were prepared via casting and a phase inversion process. The effectiveness of Chi-NP-filled mixed-matrix membrane adsorbers was successfully shown in a proof-of-concept manner.

For further investigations, the Chi-NP mixed-matrix membranes should be evaluated on their ability to adsorb other organic compounds e.g. sulfamethoxazole or penicillin G as well as metal ions like platinum, copper or cadmium (and combinations of these).

For future works, it would also be interesting to find a method of processing any kind of highly deacetylated chitosan into Chi-NPs independent of their molecular weight. A promising approach could be to optimize the parameters of the emulsification via high-pressure homogenization to depolymerize the chitosan in a first step and emulsify it in a second step. In consequence, there would be no limitation in terms of chitosan MW, i.e. viscosity, which would be highly desirable for an industrial process. Further, the use of high concentrations of oligomeric (very low viscosity) chitosan in the aqueous phase should be investigated. For the mixed-matrix membranes the evaluation of adsorptions cycles should be tested in adsorption/desorption experiments.

**Synthetic nanoparticles:** The second part (hypothesis II, chapter 7) of this thesis was dedicated to the development of molecular imprinted polymer nanoparticles as sensitive layer in a sensing application.

In a first step, crosslinked polymer nanoparticles were successfully prepared with four different functional monomers via inverse miniemulsion polymerization (namely MAPTAC, NAEMA, SPM and AMPS). Different surfactants were investigated for the successful preparation of stable miniemulsions. Further, the impact of the amount of monomer dissolved in the disperse phase on particle formation was investigated.

For the preparation of penicillin G-sodium salt (PenG) imprinted nanoparticles (PenG MIPs), NAEMA was chosen as monomer due to its charge (primary amine). In order to covalently immobilize the PenG-MIPs on to the sensor surface, they were chemically functionalized with azide moieties. The sensors surface was functionalized with alkyne moieties. This combination allowed the immobilization of particles via copper (I)-catalyzed azide-alkyne Huisgen cycloaddition. The project partners at the University of Tübingen (group of Prof. Gaugulitz) successfully showed the stability of the sensitive MIP layer in sensor experiments. Further, they were able to calibrate the sensor to allow a reproducibly determination of PenG concentration in aqueous buffer media. Reference measurements using non-imprinted NAEMA particles (NIPs) showed that the MIPs have an increased affinity towards PenG. These results were successfully validated via ITC measurements of MIPs and NIPs. Further concentration measurements with structural PenG building blocks showed that the MIPs selectively adsorbed PenG while the unspecific adsorption of the building blocks was low.

In future, the unspecific adsorption of building blocks or other compounds could be eliminated from the measurements by using MIP- and NIP-functionalized transducers in parallel. This would allow subtracting i.e. referencing the signal of the MIP and NIP transducers. Potentially, this sensor concept can be applied to many other hydrophilic target (imprinting) molecules. To achieve this, other MIPs need to be developed for each specific target molecule. This could be achieved by imprinting NAEMA particles, or one of the other polymer nanoparticles shown in this thesis, with the desired templates. Finally, the sensor array should be tested in a real sample medium e.g. a fermentation broth used in biotechnological PenG production to investigate the use of this sensor for production monitoring.

**Ionic liquid-based miniemulsion:** The third chapter was dedicated to the development of novel miniemulsion formulations containing an ionic liquid (IL) as disperse phase for the preparation of chitosan nanoparticles (hypothesis III, chapter 8). Different ILs were investigated for their dissolution capacity of chitosan. [Emim] [Ac] (1-Ethyl-3-methylimidazolium-acetate) showed the best dissolution properties. With this IL it was possible to dissolve chitosan even after the addition of up to 5 % water. The addition of water led to a decrease in viscosity. A preferable low viscosity is desired as it increases the emulsification efficiency i.e. the droplet formation. Different surfactants and surfactant mixtures were tested for the emulsification of the IL in cyclohexane. Solely a mixture of 75 % Lutensol AT 50 and 25 % Span 80 (HLB = 14.6) lead to stable emulsions. The HLB value of this surfactant mixture was unconventional high when compared to common water in oil emulsions. However, as the IL differs significantly from water in its chemical and physical properties, regular considerations concerning surfactant solubility and HLB values in emulsion preparation do not fully apply. By the addition of glutaraldehyde to the emulsions which contain chitosan in the disperse (IL) phase, crosslinked chitosan nanoparticles were successfully prepared.

The particle size varied between batches, which indicates that the emulsion formulation i.e. the process of particle synthesis via IL miniemulsions needs further optimization. Other surfactants and surfactant mixtures should be tested for their use to create even more stable and reliable emulsions. In future, such an IL-based emulsion could be used for the preparation of nanoparticles with mostly insoluble polymers such as chitin or starch. In addition, combinations of polymers which are not insoluble in common solvents or at different pH values could potentially be combined in IL solution. Further, this emulsion system should be tested on its use in miniemulsion polymerization. As ILs used as reaction media can promote certain chemical reactions, this formulation could open new possibilities for the preparation of polymeric or inorganic nanomaterials. As miniemulsions possess good heat-removal capabilities, this formulation could be a tool for very precisely temperature-controlled synthesis of small molecule in ILs.

## 11. Publications

**B.R. Riegger**, B. Bäurer, L. Hilfert G.E.M. Tovar, M. Bach, **Miniemulsification of the ionic liquid *EMIM Ac* in cyclohexane for the preparation of glutaraldehyde crosslinked chitosan nanoparticles**, (in preparation)

**B.R. Riegger**, R. Kowalski, L. Hilfert, G.E.M. Tovar, M. Bach, **Chitosan nanoparticles via high-pressure homogenization-assisted miniemulsion crosslinking for mixed-matrix membrane adsorbers**, *Carbohydr. Polym.* 201 (2018) 172–181.

doi: 10.1016/j.carbpol.2018.07.059

P. Weber §, **B.R. Riegger** §, K. Niedergall, G.E.M. Tovar, M. Bach, G. Gauglitz, **Nano-MIP based sensor for penicillin G: Sensitive layer and analytical validation**, *Sensors Actuators B Chem.* 267 (2018) 26–33. doi: 10.1016/j.snb.2018.03.142

§ joint first authors

**B.R. Riegger**, B. Bäurer, A. Mirzayeva, G.E.M. Tovar, M. Bach, **A systematic approach of chitosan nanoparticle preparation via emulsion crosslinking as potential adsorbent in wastewater treatment**, *Carbohydr. Polym.* 180 (2018) 46–54.

doi: 10.1016/j.carbpol.2017.10.002

N. Hoppe, P. Scheck, R. Sweidan, P. Diersing, L. Rathgeber, W. Vogel, **B. Riegger**, A. Southan, M. Berroth, **Silicon Integrated Dual-Mode Interferometer with Differential Outputs**, *Biosensors.* 7 (2017) 37. doi: 10.3390/bios7030037

## 12. Appendix

The procedure for the preparation of the synthetic nanoparticles (AMPS, SPM, MAPTAC, NAEMA) presented in chapter 7.2 is shown in the following chapters (12.1 to 12.4).

### 12.1. Preparation of AMPS Nanoparticles

Experimental results can be found in chapter 7.2 *Polymer Nanoparticles via Inverse Miniemulsion Polymerization: Preliminary Results*.

The following amounts of cyclohexane, the nonionic surfactant Addconate H (PIBSA) and AIBN were mixed together. Subsequently, the monomer (AMPS; 2-Acrylamido-2-methyl-1-propanesulfonic acid sodium salt) in the form of a 50 wt. % solution as provided by the manufacturer, crosslinker (EBA; N,N'-Ethylenbisacrylamid) and hydrophile (NaCl) were mixed and dissolved (in the aqueous AMPS solution). As the AMPS comes in 50 % aqueous solution, no further addition of water or buffer was necessary. When the compounds in the aqueous phase were fully dissolved, it was instantly combined with the oil phase and emulsified via probe sonication. The net sonication time was 10 minutes with a pulse sequence of 10 sec "on" / 5 sec "off", at 60 % intensity. During sonication, an ice bath cooling was applied to prevent emulsion destabilization and premature initiation of polymerization.

To prevent freezing of the emulsion (cyclohexane  $T_m \approx 7^\circ\text{C}$ ) the ice cooling was removed immediately after completion of the sonication. After polymerization over night at  $55^\circ\text{C}$ , the resulting emulsion/suspension was broken by adding a sufficient amount of ethanol (~25 vol % regarding total emulsion volume). Afterwards, the particles were purified via repeated centrifugation and washing with cyclohexane (three times, to remove PIBSA), ethanol as phase mediator and finally with water (three times).

Type	Name	Molar mass in g/mol	Amount in g	Amount in mL
<b>Aqueous phase (disperse phase)</b>				
Monomer	<b>AMPS</b>	229.23	<b>3.861</b>	<b>3.203</b>
Crosslinker	<b>EBA</b>	168.09	<b>0.906</b>	-
Hydrophil	<b>NaCl</b>	58.44	<b>0.138</b>	-
<b>Oil phase (continuous phase)</b>				
Organic solvent	<b>Cyclohexane</b>	84.16	<b>40.56</b>	<b>52.00</b>
Initiator	<b>AIBN</b>	164.21	<b>0.324</b>	-
Tensid	<b>PIBSA</b>	-	<b>0.702</b>	-

The particles may be freeze-dried. However, the impact of “if and how” freeze-drying impacts AMPS-nanoparticle stability and redispersibility was not investigated in this work, as the particles were needed in suspension anyway. If one wants to make sure that the drying process does not impair the particle architecture, the particles should be stored in aqueous suspension.

## 12.2. Preparation of SPM Nanoparticles

Experimental results can be found in chapter 7.2 *Polymer Nanoparticles via Inverse Miniemulsion Polymerization: Preliminary Results*.

The following amounts of cyclohexane, the nonionic surfactant Addconate H (PIBSA) and AIBN were mixed together. Subsequently, the monomer (SPM; 3-Sulfopropyl methacrylate potassium salt), crosslinker (EBA; N,N'-Ethylenbisacrylamid), water as solvent and hydrophile (NaCl) were mixed and dissolved. As the SPM is a solid, the water was used for the preparation of an aqueous solution. When the compounds in the aqueous phase were fully dissolved, it was instantly combined with the oil phase and emulsified via probe

sonication. The net sonication time was 10 minutes with a pulse sequence of 10 sec “on” / 5 sec “off”, at 60 % intensity. During sonication, an ice bath cooling was applied to prevent emulsion destabilization and premature initiation of polymerization.

To prevent freezing of the emulsion (cyclohexane  $T_m \approx 7^\circ\text{C}$ ) the ice cooling was removed immediately after completion of the sonication. After polymerization over night at  $55^\circ\text{C}$  the resulting emulsion/suspension was broken by adding a sufficient amount of ethanol (~25 vol % regarding total emulsion volume). Afterwards the particles were purified via repeated centrifugation and washing with cyclohexane (three times, to remove PIBSA), ethanol as phase mediator and finally with water (three times).

The particles may be freeze-dried. However, the impact of “if and how” freeze-drying impacts SPM-nanoparticle stability and redispersibility was not investigated in this work, as the particles were needed in suspension anyway. If one wants to make sure that the drying process does not impair the particle architecture, the particles should be stored in aqueous suspension.

Type	Name	Molar mass in g/mol	Amount in g	Amount in mL
<b>Aqueous phase (disperse phase)</b>				
Monomer	<b>SPM</b>	246.32	<b>0.925</b>	-
Crosslinker	<b>EBA</b>	168.09	<b>0.435</b>	-
Solvent	<b>Water</b>	18.02	<b>0.97</b>	-
Hydrophil	<b>NaCl</b>	58.44	<b>0.028</b>	-
<b>Oil phase (continuous phase)</b>				
Organic solvent	<b>Cyclohexane</b>	84.16	<b>12.88</b>	<b>16.58</b>
Initiator	<b>AIBN</b>	164.21	<b>0.103</b>	-
Tensid	<b>PIBSA</b>	-	<b>0.224</b>	-

### 12.3. Preparation of MAPTAC Nanoparticles

Experimental results can be found in chapter 7.2 *Polymer Nanoparticles via Inverse Miniemulsion Polymerization: Preliminary Results*.

The following amounts of cyclohexane, the nonionic surfactant Span 80 and AIBN were mixed together. Subsequently, the monomer (MAPTAC; [3-(Methacryloylamino)propyl]trimethylammonium chloride) in the form of a 50 wt. % solution as provided by the manufacturer, crosslinker (EBA; N,N'-Ethylenbisacrylamid) and hydrophilic (NaCl) were mixed and dissolved (in the aqueous AMPS solution). As the MAPTAC comes in 50 % aqueous solution, no further addition of water or buffer was necessary. When the compounds in the aqueous phase were fully dissolved, it was instantly combined with the oil phase and emulsified via probe sonication. The net sonication time was 10 minutes with a pulse sequence of 10 sec "on" / 5 sec "off", at 60 % intensity. During sonication, an ice bath cooling was applied to prevent emulsion destabilization and premature initiation of polymerization.

Type	Name	Molar mass in g/mol	Amount in g	Amount in mL
<b>Aqueous phase (disperse phase)</b>				
Monomer	<b>MAPTAC</b>	220.74	-	<b>3</b>
Crosslinker	<b>EBA</b>	168.09	<b>0.4</b>	-
Hydrophilic	<b>NaCl</b>	58.44	<b>16.65</b>	-
<b>Oil phase (continuous phase)</b>				
Organic solvent	<b>Cyclohexane</b>	84.16	<b>11.232</b>	<b>14.4</b>
Initiator	<b>AIBN</b>	164.21	<b>0.324</b>	-
Tensid	<b>Span 80</b>	-	<b>0.702</b>	-

To prevent freezing of the emulsion (cyclohexane  $T_m \approx 7^\circ\text{C}$ ) the ice cooling was removed immediately after completion of the sonication. After polymerization over night at  $55^\circ\text{C}$  the resulting emulsion/suspension was broken by adding a sufficient amount of ethanol



(~25 vol % regarding total emulsion volume). Afterwards the particles were purified via repeated centrifugation and washing with ethanol (three times, to remove Span 80) and finally with water (three times).

The particles may be freeze-dried. However, the impact of “if and how” freeze-drying impacts MAPTAC-nanoparticle stability and redispersibility was not investigated in this work, as the particles were needed in suspension anyway. If one wants to make sure that the drying process does not impair the particle architecture, the particles should be stored in aqueous suspension.

## 12.4. Preparation of NAEMA Nanoparticles

Experimental results can be found in chapter 7.2 *Polymer Nanoparticles via Inverse Miniemulsion Polymerization: Preliminary Results* and 7.8.1 *Si-1: Preparation of MIPs/NIPs*.

The following amounts of cyclohexane, the nonionic surfactant Span 80 and AIBN were mixed together. Subsequently, the monomer (NAEMA; N-(2-aminoethyl) methacrylamide hydrochloride), crosslinker (EBA; N,N'-Ethylenbisacrylamid), PBS-buffer (0.1 M, acting as solvent and hydrophile at the same time) were mixed and dissolved. As NAEMA is a solid, the buffer was used for the preparation of an aqueous solution. When the compounds in the aqueous phase were fully dissolved, it was instantly combined with the oil phase and emulsified via probe sonication. The net sonication time was 10 minutes with a pulse sequence of 10 sec “on” / 5 sec “off”, at 60 % intensity. During sonication, an ice bath cooling was applied to prevent emulsion destabilization and premature initiation of polymerization.

To prevent freezing of the emulsion (cyclohexane  $T_m \approx 7^\circ\text{C}$ ) the ice cooling was removed immediately after completion of the sonication. After polymerization over night at  $55^\circ\text{C}$  the resulting emulsion/suspension was broken by adding a sufficient amount of ethanol (~25 vol % regarding total emulsion volume). Afterwards the particles were purified via repeated centrifugation and washing with ethanol (three times, to remove Span 80) and finally with water (three times).

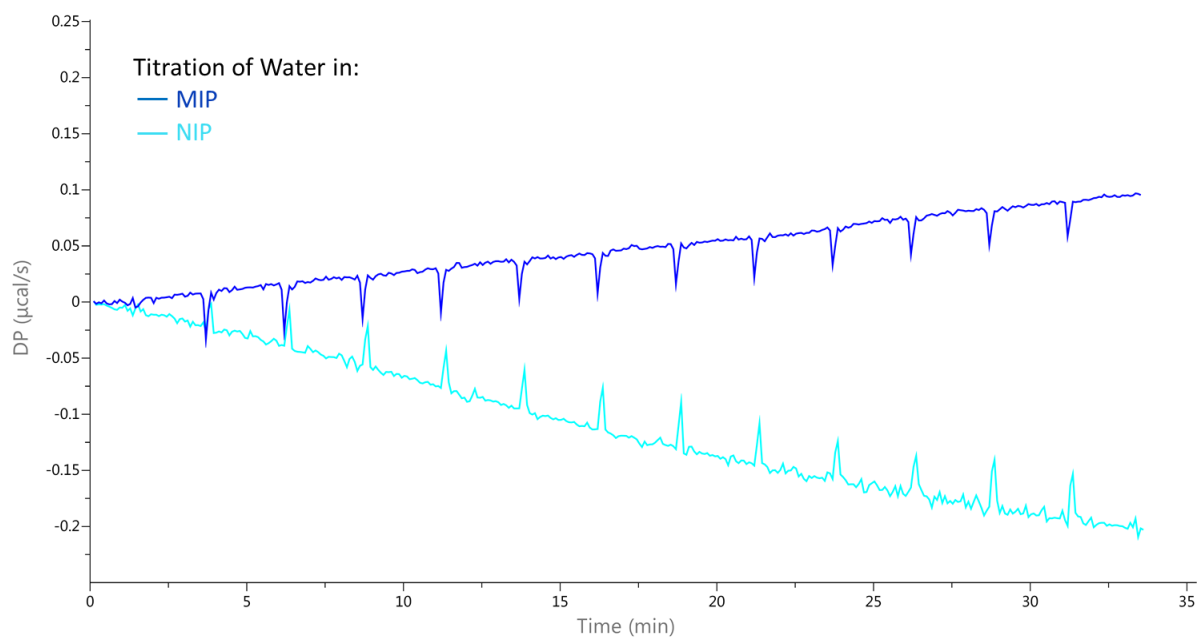
The particles may be freeze-dried. However, the impact of “if and how” freeze-drying impacts NAEMA-nanoparticle stability and redispersibility was not investigated in this work, as the particles were needed in suspension anyway. If one wants to make sure that the drying process does not impair the particle architecture, the particles should be stored in aqueous suspension.

## 12 Appendix

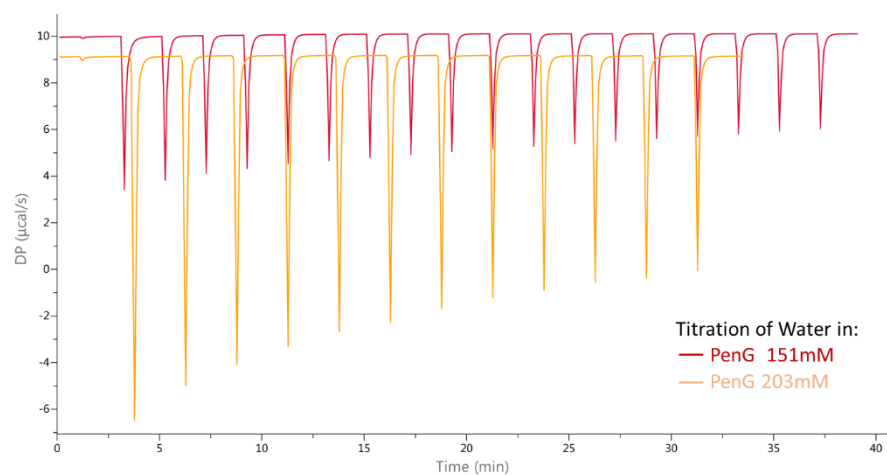
A detailed procedure for the preparation of NEAME-MIPs (penicillin G imprinted) and particle modification with azide-moieties is presented in chapter 7.6 and the corresponding *Supplementary data* in 7.8.1 and 7.8.2

Type	Name	Molar mass in g/mol	Amount in g	Amount in mL
<b>Aqueous phase (disperse phase)</b>				
Monomer	<b>NAEMA</b>	164.07	<b>2.574</b>	-
Crosslinker	<b>EBA</b>	168.09	<b>0.606</b>	-
Hydrophil	<b>PBS buffer 0.1 M</b>		<b>2.70</b>	-
<b>Oil phase (continuous phase)</b>				
Organic solvent	<b>Cyclohexane</b>	84.16	<b>43.200</b>	-
Initiator	<b>AIBN</b>	164.21	<b>0.270</b>	-
Tensid	<b>SPAN 80</b>	-	<b>2.340</b>	-

## 12.5. ITC control experiments



**ITC reference experiment to determine the dissolution heat of water into MIP and NIP suspension.**



**ITC reference experiment the titration heat of PenG solution in pure water.**

## 13. Image Index

For permissions for the re-use of graphic contents which are included in the peer-reviewed publications please contact the publisher/journal of the respective publication. For permissions for the re-use of graphic contents which are *not* included in peer-reviewed publications please contact the *Institute of Interfacial Process Engineering and Plasma Technology, University of Stuttgart*.

**Note:** All figures (schematical representations, graphics, graphs and structural formulas) have been designed and generated by me with the help of computer software such as Origin by OriginLab, CorelDRAW Graphics Suite by Corel, ChemDraw by PerkinElmer and PowerPoint by Microsoft. Credit is given, if the representation/graphic was based on an already published template.

Fig. 1 Structure of this thesis and schematic representation of the three main topics a) “Biobased Chitosan Nanoparticles”, b) “Synthetic Nanoparticles” and c) “Chitosan Nanoparticles – Synthesis with Ionic Liquids” which were investigated. All three topics are based on the use of inverse miniemulsion technique for nanoparticle preparation. ....	9
Fig. 2 Schematic representation of demixing (A) and stabilization (B) process with and without surfactant in an oil in water (O/W) emulsion. ....	15
Fig. 3 Schematical representation of a surfactant. ....	15
Fig. 4 Schematical representation of the electrical double layer (EDL). Own representation based on (M. A. Alsharif, Taha, et al. 2017) .....	20
Fig. 5 Schematical representation of DLVO and XDLVO. ....	22
Fig. 6 The three homogenization devices used in this work. (A) rotor-stator, (B) probe sonication and (C) high-pressure homogenizer (HPH). Schematical representation of the preparation of oil-in-water emulsions. Schematic representation of the high-pressure homogenizer (C) is an own representation based on <a href="https://commons.wikimedia.org/wiki/File:Homogenizing_valve.svg">https://commons.wikimedia.org/wiki/File:Homogenizing_valve.svg</a> (accessed in September 2020) .....	26

Fig. 7. Schematical representation of the four main droplet loss mechanisms on the example of an oil in water emulsion.....	28
Fig. 8 Schematical representation of suspension-, emulsion-, microemulsion- and miniemulsion polymerization.....	31
Fig. 9 Schematical representation for the preparation of a miniemulsion containing monomer and the subsequent process of conducting a miniemulsion polymerization. ...	35
Fig. 10 Schematical representation for the preparation of a miniemulsion containing polymer and the subsequent process of crosslinking. ....	37
Fig. 11 Schematical representation of fully acetylated chitin (top left) and completely deacetylated chitosan (top right). If the degree of deacetylation of chitin is > 50 % it is called chitosan. Usually chitosan is not deacetylated completely. Thus, the degree of deacetylation (DD) describes the percentage of free primary amines while the 100-DD (also called degree of <i>acetylation</i> - DA) describes the reaming acetylated amines (bottom). The deacetylation does usually not appear locally as implied by the bottom figure – chitosan is no block-copolymer. Deacetylation is randomly distributed all over the polymer.....	38
Fig. 12 Schematical representation of nano-MIP preparation via inverse miniemulsion technique.....	41
Fig. 13: Photographs of chitosan emulsions after 18 h stirring without glut (Fig. 13 A) with backlight (left) and with glut (Fig. 13 B) at ambient light (right). No phase separation was observed with 0.1 M NaCl in contrast to phase separation with no NaCl or 0.01 M NaCl with or without glutaraldehyde present. ....	54
Fig. 14: Schematic representation of emulsion crosslinking technique.....	55
Fig. 15: Simplified chitosan/glut crosslinking mechanism.....	56
Fig. 16: SEM-micrographs (a-c) and pycnometry (d) of Chi-NPs synthesized with different glut concentrations (the line is drawn to guide the eye) . ....	57

Fig. 17: SEC measurements of the six used chitosans showing  $M_n$ ,  $M_w$  and PDI..... 59

Fig. 18: A: SEM-micrographs of synthesized Chi-NPs with six different chitosan types. . 60

Fig. 19: Adsorption behavior of Chi-NPs for A) Carbamazepine at a concentration of  $100 \mu\text{g mL}^{-1}$ , B) Diclofenac at  $100 \mu\text{g mL}^{-1}$  and C) Diclofenac at  $5000 \mu\text{g mL}^{-1}$ . All measurements were done in triplicates and the error bars indicate the standard deviation among them. The numbers above the bars indicate the adsorption capacity (mg drug adsorbed per g adsorbent at a certain drug concentration)..... 64

Fig. 20: The shear-dependent dynamic viscosity of the low, medium and high MW chitosans solutions (3 % chitosan solutions in 1 % acetic acid, containing 0.1 M NaCl).81

Fig. 21: DLS measurements of low MW Chi-NPs (A) and medium MW Chi-NPs (B) after varied HPH cycles. Particles were prepared and measured in triplicates. .... 82

Fig. 22: SEM micrographs of the low and medium Mw Chi-NPs show spherically shaped, narrowly distributed particles. .... 83

Fig. 23 SEC MW distribution of low (A) and medium (B) MW chitosan after 0, 1 and 7 cycles of HPH. .... 85

Fig. 24: Adsorption kinetics of low MW (A) and medium MW Chi-NPs (B) at different DCL concentrations..... 86

Fig. 25: Adsorption isotherms for DCL in low MW Chi-NPs and medium Chi-NPs fitted with Freundlich, Sips and Langmuir at ambient conditions. .... 87

Fig. 26: SEM micrographs (cross section) of the reference membrane (A), low MW Chi-NP membrane (B) and medium MW Chi-NP membrane (C) with magnification of the porous membrane structure. (D) Mean pore size (capillary flow porometry) and flux (at 1 bar) for all three membranes. In both cases, the error bars indicate the standard deviation of nine different measurements for each sample type. .... 91

Fig. 27: Mean dynamic adsorption plot of DCL for the adsorption chamber, the reference membrane and low and medium MW Chi-NP membrane including standard deviation of

triplicate measurements (A). The dashed line in (A) indicates the breakthrough point (10 %) of the membranes. The resulting adsorption capacity of DCL for the respective membranes in  $\text{mg m}^{-2}$  (B) at the breakthrough point. For each membrane type, the adsorption experiment was performed with three different membrane samples. .... 92

Fig. 28 Chemical structures of water-soluble radically polymerizable monomers and crosslinkers HYMOPTA (3-methacryloyloxypropyltrimethyl-ammonium chloride), vinylphosphonic acid (also called vinylphosphonate, VPS) *N,N'*-Ethylenbisacrylamid (EBA) and *N,N'*-Methylenbisacrylamid (MBA) used in the beginning of this work for the preparation of nanoparticles via inverse miniemulsion. .... 98

Fig. 29 SEM-micrographs of HYMOPTA nanoparticles (left) and VPS nanoparticles (right) crosslinked with EBA. Both prepared via inverse MiniEP. .... 98

Fig. 30 Summary of nanoparticles prepared with water-soluble monomers via inverse MiniEP. All particles are crosslinked with EBA (see Fig. 28). SEM micrographs, the hydrodynamic diameter ( $d_H$  via DLS) and Polydispersity index (PDI) are shown. .... 100

Fig. 31 AMPS nanoparticles were prepared with different monomer/crosslinker content in the disperse phase (decreasing monomer content from top to bottom). EBA was used as crosslinker. The oil phase used was identical for all five particle syntheses. SEM micrographs and DLS measurements (intensity based particle diameter) including correlation curves are shown. With decreasing monomer content, the ability of the resulting particles to keep their shape decreases. .... 102

Fig. 32: Schematical representation of MIP preparation via inverse miniemulsion polymerization technique. (a) Combining of oil phase (containing initiator and surfactant) and water phase (containing monomer, crosslinker and template); (b) Emulsification via probe sonication resulting in stable miniemulsion; (c) thermal initiation of the polymerizing reaction, resulting in imprinted polymer nanoparticles (d). .... 111

Fig. 33 Schematically process of particle modification and immobilization of particles on transducer surface. a) Modification of MIPs/NIPs resulting in azide-bearing nanoparticles; b) modification of transducer surface introducing an alkyne-PEG; c) covalent

immobilization of MIP-N3/NIP-N3 on the transducer surface via copper (I) catalyzed 1,3-dipolar cycloaddition. ....	114
Fig. 34 a: Results of DLS measurements (z-average and PDI) of azide-modified and unmodified MIPs/NIPs. Before as well as after azide modification the particles show a high similarity in size and PDI. b: FTIR spectra of azide-modified and unmodified MIPs/NIPs. The characteristic azide band at $2100\text{ nm}^{-1}$ for MIP-N3/NIP-N3 indicates the successful particle modification. ....	115
Fig. 35. SEM micrographs of a transducer surface with covalently immobilized MIPs- N <sub>3</sub> (top) and NIPs-N <sub>3</sub> (bottom) at different magnifications. The surface is covered by the spherical particles in a homogenous statistical way. ....	116
Fig. 36. Baseline measurements on a transducer with MIPs immobilized in the presence of catalytically active copper [I] (blue line) and on a transducer with MIPs immobilized in the absence of catalytically active copper [I] (red line). ....	117
Fig. 37. Calibration measurements for a MIP transducer (triangles) and a NIP transducer (dots). The MIP measurements were fitted with Langmuir-Freundlich adsorption isotherms to obtain a calibration curve. ....	119
Fig. 38. Structural formula of the product PenG and its building blocks phenylacetic acid and 6-aminopenicillanic acid (6-APA). ....	121
Fig. 39. In both graphs the concentration dependency triplicate measurements of PenG on MIP transducer (triangles) and NIP transducer (circle) are shown. In graph (a) measurement of 6-APA on a MIP transducer (hollow triangles) and on a NIP transducer (hollow circles). In graph (b) measurements of phenylacetic acid on MIP transducer (hollow triangles) and on a NIP (hollow circles). ....	121
Fig. 40 Top left and right: Injection heat resulting from the titration of PenG solution ( $c = 203\text{ mM}$ ) in MIP and NIP suspensions $1.8\text{ mg mL}^{-1}$ and $1.9\text{ mg mL}^{-1}$ . ....	130
Fig. 41 Chemical structure, melting point and miscibility of the six ionic liquids (ILs) used in this work. (Melting points taken from the datasheets provided by the manufacturer.) .....	134



- Fig. 42. Polarization/DIC microscopy images of 3 % chitosan dissolved in [Bmim] [Ac] and [Emim] [Ac] at different temperatures and dissolution times. Water content was varied between 0 %, 5 % and 10 %..... 135
- Fig. 43. Dynamic viscosity of [Emim] [Ac] solutions with 3% chitosan. .... 136
- Fig. 44 Photographic picture of different [Emim] [Ac]/chitosan in cyclohexane miniemulsions using different ratios of Span 80 and Lutanensol AT 50The amount of surfactant was 4 % (w/v) in all experiments. \*HLB values of these surfactant blends were calculated. .... 143
- Fig. 45 DLS-data (Polydispersity index (PDI) and hydrodynamic diameter) of chitosan nanoparticles prepared in five different emulsion batches (left). SEM-micrograph of resulting chitosan nanoparticles. .... 144

## 14. References

Abbott, Prof Steven. (2015). **Surfactant Science: Principles and Practice**. DEStech Publications, Inc. <https://www.stevenabbott.co.uk/practical-surfactants/the-book.php>

Agnihotri, Sunil a; Mallikarjuna, Nadagouda N; and Aminabhavi, Tejraj M. (2004). “**Recent Advances on Chitosan-Based Micro- and Nanoparticles in Drug Delivery.**” *Journal of Controlled Release: Official Journal of the Controlled Release Society* 100 (1): 5–28. <https://doi.org/10.1016/j.jconrel.2004.08.010>

Alexander, Cameron; Andersson, Håkan S.; Andersson, Lars I.; Ansell, Richard J.; Kirsch, Nicole; Nicholls, Ian A.; O'Mahony, John; and Whitcombe, Michael J. (2006). “**Molecular Imprinting Science and Technology: A Survey of the Literature for the Years up to and Including 2003.**” *Journal of Molecular Recognition* 19 (2): 106–80. <https://doi.org/10.1002/jmr.760>

Alves, N.M.; and Mano, J.F. (2008). “**Chitosan Derivatives Obtained by Chemical Modifications for Biomedical and Environmental Applications.**” *International Journal of Biological Macromolecules* 43 (5): 401–14. <https://doi.org/10.1016/j.ijbiomac.2008.09.007>

Ash, Michael.; and Ash, Irene. (2004). **Handbook of Green Chemicals**. 2nd ed. Endicott, USA: Synapse Information Resources Inc

Asua, José M. (2007). **Polymer Reaction Engineering**. Edited by José M. Asua. Oxford, UK: Blackwell Publishing Ltd. <https://doi.org/10.1002/9780470692134>

Azlan, Kamari; Wan Saime, Wan Ngah; and Lai Ken, Liew. (2009). “**Chitosan and Chemically Modified Chitosan Beads for Acid Dyes Sorption.**” *Journal of Environmental Sciences* 21 (3): 296–302. [https://doi.org/10.1016/S1001-0742\(08\)62267-6](https://doi.org/10.1016/S1001-0742(08)62267-6)

Banerjee, Tanima; Mitra, Susmita; Kumar Singh, Ajay; Kumar Sharma, Rakesh; and Maitra, Amarnath. (2002). “**Preparation, Characterization and Biodistribution of Ultrafine Chitosan Nanoparticles.**” *International Journal of Pharmaceutics* 243 (1–2): 93–105. [https://doi.org/10.1016/S0378-5173\(02\)00267-3](https://doi.org/10.1016/S0378-5173(02)00267-3)

Bang, Jin Ho; and Suslick, Kenneth S. (2010). “**Applications of Ultrasound to the Synthesis of Nanostructured Materials.**” *Advanced Materials* 22 (10): 1039–59. <https://doi.org/10.1002/adma.200904093>

Barbosa, Marta O.; Moreira, Nuno F.F.; Ribeiro, Ana R.; Pereira, Manuel F.R.; and Silva, Adrián M.T. (2016). “**Occurrence and Removal of Organic Micropollutants: An Overview of the Watch List of EU Decision 2015/495.**” *Water Research* 94 (May): 257–79. <https://doi.org/10.1016/j.watres.2016.02.047>

Bard, Allen J.; and Faulkner, Larry R. (2001). **Electrochemical Methods: Fundamentals and Applications**. 2nd ed. John Wiley & Sons, Inc

- Becher, Paul. (1957). **Emulsion: Theory and Practice**. New York: Reinhold Publishing Corporation
- Becher, Paul. (1983). **Encyclopedia of Emulsion Technology, Vol. 1: Basic Theory**. Marcel Dekker
- Belmont, Anne Sophie; Jaeger, Stefanie; Knopp, Dietmar; Niessner, Reinhard; Gauglitz, Guenter; and Haupt, Karsten. (2007). "**Molecularly Imprinted Polymer Films for Reflectometric Interference Spectroscopic Sensors.**" *Biosensors and Bioelectronics* 22 (12): 3267–72. <https://doi.org/10.1016/j.bios.2007.01.023>
- Beppu, M. M.; Arruda, E. J.; Vieira, R. S.; and Santos, N. N. (2004). "**Adsorption of Cu(II) on Porous Chitosan Membranes Functionalized with Histidine.**" *Journal of Membrane Science* 240 (1–2): 227–35. <https://doi.org/10.1016/j.memsci.2004.04.025>
- Brandenburg, Albrecht; Hinkov, Vladimir; and Konz, Werner. (2008). "**Integrated Optic Sensors.**" In *Sensors*, 399–420. Weinheim, Germany: Wiley-VCH Verlag GmbH. <https://doi.org/10.1002/9783527620173.ch16>
- Brunel, Fabrice; Véron, Laurent; Ladavière, Catherine; David, Laurent; Domard, Alain; and Delair, Thierry. (2009). "**Synthesis and Structural Characterization of Chitosan Nanogels.**" *Langmuir* 25 (16): 8935–43. <https://doi.org/10.1021/la9002753>
- Cacciatore, Giuseppe; Petz, Michael; Rachid, Shwan; Hakenbeck, Regine; and Bergwerff, Aldert A. (2004). "**Development of an Optical Biosensor Assay for Detection of  $\beta$ -Lactam Antibiotics in Milk Using the Penicillin-Binding Protein 2x\*.**" *Analytica Chimica Acta* 520 (1–2): 105–15. <https://doi.org/10.1016/j.aca.2004.06.060>
- Capek, Ignác. (2010). "**On Inverse Miniemulsion Polymerization of Conventional Water-Soluble Monomers.**" *Advances in Colloid and Interface Science* 156 (1–2): 35–61. <https://doi.org/10.1016/j.cis.2010.02.006>
- Chang, E.-E.; Wan, Jan-Chi; Kim, Hyunook; Liang, Chung-Huei; Dai, Yung-Dun; and Chiang, Pen-Chi. (2015). "**Adsorption of Selected Pharmaceutical Compounds onto Activated Carbon in Dilute Aqueous Solutions Exemplified by Acetaminophen, Diclofenac, and Sulfamethoxazole.**" *The Scientific World Journal* 2015: 1–11. <https://doi.org/10.1155/2015/186501>
- Chappat, M. (1994). "**Some Applications of Emulsions.**" *Colloids and Surfaces A: Physicochemical and Engineering Aspects* 91 (C): 57–77. [https://doi.org/10.1016/0927-7757\(94\)02976-8](https://doi.org/10.1016/0927-7757(94)02976-8)
- Chauhan, Divya; Dwivedi, Jaya; and Sankararamakrishnan, Nalini. (2014). "**Novel Chitosan/PVA/Zerivalent Iron Biopolymeric Nanofibers with Enhanced Arsenic Removal Applications.**" *Environmental Science and Pollution Research* 21 (15): 9430–42. <https://doi.org/10.1007/s11356-014-2864-1>
- Chen, Arh-Hwang; and Chen, Shin-Ming. (2009). "**Biosorption of Azo Dyes from Aqueous Solution by Glutaraldehyde-Crosslinked Chitosans.**" *Journal of Hazardous Materials* 172 (2–3): 1111–21. <https://doi.org/10.1016/j.jhazmat.2009.07.104>

Chiou, M S; and Li, H Y. (2003). **“Adsorption Behavior of Reactive Dye in Aqueous Solution on Chemical Cross-Linked Chitosan Beads.”** *Chemosphere* 50 (8): 1095–1105. <http://www.ncbi.nlm.nih.gov/pubmed/12531717>

Choi, Y. T.; El-Aasser, M. S.; Sudol, E. D.; and Vanderhoff, J. W. (1985). **“Polymerization of Styrene Miniemulsions.”** *Journal of Polymer Science: Polymer Chemistry Edition* 23 (12): 2973–87. <https://doi.org/10.1002/pol.1985.170231206>

Colthup, Norman B.; Daly, Lawrence H.; and Wiberley, Stephen E. (1990). **“VIBRATIONAL AND ROTATIONAL SPECTRA.”** In *Introduction to Infrared and Raman Spectroscopy*, 1–73. Elsevier. <https://doi.org/10.1016/B978-0-08-091740-5.50004-1>

Crini, Grégorio. (2005). **“Recent Developments in Polysaccharide-Based Materials Used as Adsorbents in Wastewater Treatment.”** *Progress in Polymer Science* 30 (1): 38–70. <https://doi.org/10.1016/j.progpolymsci.2004.11.002>

Crini, Grégorio; and Badot, Pierre-Marie. (2008). **“Application of Chitosan, a Natural Aminopolysaccharide, for Dye Removal from Aqueous Solutions by Adsorption Processes Using Batch Studies: A Review of Recent Literature.”** *Progress in Polymer Science* 33 (4): 399–447. <https://doi.org/10.1016/j.progpolymsci.2007.11.001>

Damarla, Krishnaiah; Rachuri, Yadagiri; Suresh, Eringathodi; and Kumar, Arvind. (2018). **“Nanoemulsions with All Ionic Liquid Components as Recyclable Nanoreactors.”** Research-article. *Langmuir* 34 (34): 10081–91. <https://doi.org/10.1021/acs.langmuir.8b01909>

Davis, H.T. (1994). **“Factors Determining Emulsion Type: Hydrophile—Lipophile Balance and Beyond.”** *Colloids and Surfaces A: Physicochemical and Engineering Aspects* 91 (C): 9–24. [https://doi.org/10.1016/0927-7757\(94\)02929-6](https://doi.org/10.1016/0927-7757(94)02929-6)

Debnath, Biplab K; Saha, Ujjwal K; and Sahoo, Niranjana. (2015). **“A Comprehensive Review on the Application of Emulsions as an Alternative Fuel for Diesel Engines.”** *Renewable and Sustainable Energy Reviews* 42 (February): 196–211. <https://doi.org/10.1016/j.rser.2014.10.023>

Dey, Rebecca E; Wimpenny, Ian; Gough, Julie E; Watts, David C; and Budd, Peter M. (2018). **“Supporting: Poly(Vinylphosphonic Acid- Co -Acrylic Acid) Hydrogels: The Effect of Copolymer Composition on Osteoblast Adhesion and Proliferation.”** *Journal of Biomedical Materials Research Part A* 106 (1): 255–64. <https://doi.org/10.1002/jbm.a.36234>

Divya, K.; and Jisha, M. S. (2018). **“Chitosan Nanoparticles Preparation and Applications.”** *Environmental Chemistry Letters* 16 (1): 101–12. <https://doi.org/10.1007/s10311-017-0670-y>

Doolaanea, Abd Almonem; Haran Ismail, Ahmed Fahmi; Mansor, Nur’Izzati; Mohd Nor, Nurul Hafziah; and Mohamed, Farahidah. (2015). **“Effect of Surfactants on Plasmid DNA Stability and Release from Poly (D,L-Lactide-Co-Glycolide) Microspheres.”** *Tropical Journal of Pharmaceutical Research* 14 (10): 1769. <https://doi.org/10.4314/tjpr.v14i10.6>

- Fendt, Sebastian; Padmanabhan, Sasisanker; Blanch, Harvey W.; and Prausnitz, John M. (2011). "Viscosities of Acetate or Chloride-Based Ionic Liquids and Some of Their Mixtures with Water or Other Common Solvents." *Journal of Chemical & Engineering Data* 56 (1): 31–34. <https://doi.org/10.1021/je1007235>
- Fonseca, Gabriela E.; McKenna, Timothy F.; and Dubé, Marc A. (2010). "Miniemulsion vs. Conventional Emulsion Polymerization for Pressure-Sensitive Adhesives Production." *Chemical Engineering Science* 65 (9): 2797–2810. <https://doi.org/10.1016/j.ces.2010.01.017>
- Fontenot, K; and Schork, F J. (1993). "Batch Polymerization of Methyl Methacrylate in Mini/Macroemulsions." *Journal of Applied Polymer Science* 49 (4): 633–55. <https://doi.org/10.1002/app.1993.070490410>
- Frank, Hendrik; Ziener, Ulrich; and Landfester, Katharina. (2009). "Formation of Polyimide Nanoparticles in Heterophase with an Ionic Liquid as Continuous Phase." *Macromolecules* 42 (20): 7846–53. <https://doi.org/10.1021/ma901392h>
- Gauglitz, Günter. (2010). "Direct Optical Detection in Bioanalysis: An Update." *Analytical and Bioanalytical Chemistry* 398 (6): 2363–72. <https://doi.org/10.1007/s00216-010-3904-4>
- Gerente, C.; Lee, V. K. C.; Cloirec, P. Le; and McKay, G. (2007). "Application of Chitosan for the Removal of Metals From Wastewaters by Adsorption—Mechanisms and Models Review." *Critical Reviews in Environmental Science and Technology* 37 (1): 41–127. <https://doi.org/10.1080/10643380600729089>
- Ghaee, A.; Shariaty-Niassar, M.; Barzin, J.; and Matsuura, T. (2010). "Effects of Chitosan Membrane Morphology on Copper Ion Adsorption." *Chemical Engineering Journal* 165 (1): 46–55. <https://doi.org/10.1016/j.cej.2010.08.051>
- Giesecking, Björn; Jäck, Berthold; Preis, Eduard; Jung, Stefan; Forster, Michael; Scherf, Ullrich; Deibel, Carsten; and Dyakonov, Vladimir. (2012). "Excitation Dynamics in Low Band Gap Donor-Acceptor Copolymers and Blends." *Journal of Applied Polymer Science* 124 (4): 2682–90. <https://doi.org/10.1002/aenm.201200304>
- Gonsior, Nina; Hetzer, Martin; Kulicke, Werner-Michael; and Ritter, Helmut. (2010). "First Studies on the Influence of Methylated  $\beta$ -Cyclodextrin on the Rheological Behavior of 1-Ethyl-3-Methyl Imidazolium Acetate." *The Journal of Physical Chemistry B* 114 (39): 12468–72. <https://doi.org/10.1021/jp1036684>
- Goycoolea, Francisco M.; Brunel, Fabrice; Gueddari, Nour E El; Coggiola, Anna; Lollo, Giovanna; Moerschbacher, Bruno M.; Remuñán-López, Carmen; Delair, Thierry; Domard, Alain; and Alonso, María J. (2016). "Physical Properties and Stability of Soft Gelled Chitosan-Based Nanoparticles." *Macromolecular Bioscience* 16 (12): 1873–82. <https://doi.org/10.1002/mabi.201600298>
- Gryshchenko, Andriy O.; and Bottaro, Christina S. (2014). "Development of Molecularly Imprinted Polymer in Porous Film Format for Binding of Phenol and Alkylphenols from Water." *International Journal of Molecular Sciences* 15 (1): 1338–57. <https://doi.org/10.3390/ijms15011338>

- Gupta, V K; and Suhas. (2009). **“Application of Low-Cost Adsorbents for Dye Removal-a Review.”** *Journal of Environmental Management* 90 (8): 2313–42. <https://doi.org/10.1016/j.jenvman.2008.11.017>
- Guyomard-Lack, a.; Buchtová, N.; Humbert, B.; and Bideau, J. Le. (2015). **“Ion Segregation in an Ionic Liquid Confined within Chitosan Based Chemical Ionogels.”** *Physical Chemistry Chemical Physics* 17 (37): 23947–51. <https://doi.org/10.1039/C5CP04198H>
- HARTE, FEDERICO; and VENEGAS, ROCÍO. (2010). **“A MODEL FOR VISCOSITY REDUCTION IN POLYSACCHARIDES SUBJECTED TO HIGH-PRESSURE HOMOGENIZATION.”** *Journal of Texture Studies* 41 (1): 49–61. <https://doi.org/10.1111/j.1745-4603.2009.00212.x>
- Haupt, Karsten; and Mosbach, Klaus. (2000). **“Molecularly Imprinted Polymers and Their Use in Biomimetic Sensors.”** *Chemical Reviews* 100 (7): 2495–2504. <https://doi.org/10.1021/cr990099w>
- Hayes, Robert; Warr, Gregory G; and Atkin, Rob. (2015). **“Structure and Nanostructure in Ionic Liquids.”** *Chemical Reviews* 115 (13): 6357–6426. <https://doi.org/10.1021/cr500411q>
- Hiemenz, Paul C. (1977). **Principles of Colloid and Surface Chemistry. Third Edition, Revised and Expanded.** 3rd ed. New York: Marcel Dekker
- Hirai, Asako; Odani, Hisashi; and Nakajima, Akio. (1991). **“Determination of Degree of Deacetylation of Chitosan by <sup>1</sup>H NMR Spectroscopy.”** *Polymer Bulletin* 26 (1): 87–94. <https://doi.org/10.1007/BF00299352>
- Holmberg, Krister; Jönsson, Bo; Kronberg, Bengt; and Lindman, Björn. (2002). **Surfactants and Polymers in Aqueous Solution.** *Archives of General Psychiatry*. Vol. 32. Chichester, UK: John Wiley & Sons, Ltd. <https://doi.org/10.1002/0470856424>
- Horinaka, Jun-ichi; Urabayashi, Yuhei; Takigawa, Toshikazu; and Ohmae, Masashi. (2013). **“Entanglement Network of Chitin and Chitosan in Ionic Liquid Solutions.”** *Journal of Applied Polymer Science* 130 (4): 2439–43. <https://doi.org/10.1002/app.39459>
- Hoshino, Yu; Kodama, Takashi; Okahata, Yoshio; and Shea, Kenneth J. (2008). **“Peptide Imprinted Polymer Nanoparticles: A Plastic Antibody.”** *Journal of the American Chemical Society* 130 (46): 15242–43. <https://doi.org/10.1021/ja8062875>
- Hotze, Ernest M.; Phenrat, Tanapon; and Lowry, Gregory V. (2010). **“Nanoparticle Aggregation: Challenges to Understanding Transport and Reactivity in the Environment.”** *Journal of Environment Quality* 39 (6): 1909. <https://doi.org/10.2134/jeq2009.0462>
- Hristovski, Kiril; Baumgardner, Andrew; and Westerhoff, Paul. (2007). **“Selecting Metal Oxide Nanomaterials for Arsenic Removal in Fixed Bed Columns: From Nanopowders to Aggregated Nanoparticle Media.”** *Journal of Hazardous Materials* 147 (1–2): 265–74. <https://doi.org/10.1016/j.jhazmat.2007.01.017>
- Hu, Z.G.; Zhang, J.; Chan, W.L.; and Szeto, Y.S. (2006). **“The Sorption of Acid Dye onto Chitosan Nanoparticles.”** *Polymer* 47 (16): 5838–42. <https://doi.org/10.1016/j.polymer.2006.05.071>

- Huang, Yan; Cai, Yuhang; and Lapitsky, Yakov. (2015). "Factors Affecting the Stability of Chitosan/Tripolyphosphate Micro- and Nanogels: Resolving the Opposing Findings." *J. Mater. Chem. B* 3 (29): 5957–70. <https://doi.org/10.1039/C5TB00431D>
- Hussain, M.; Iqbal, N.; and Lieberzeit, P. A. (2013). "Acidic and Basic Polymers for Molecularly Imprinted Folic Acid Sensors - QCM Studies with Thin Films and Nanoparticles." *Sensors and Actuators, B: Chemical* 176: 1090–95. <https://doi.org/10.1016/j.snb.2012.09.082>
- ICI Americas Inc. (1980). **The HLB SYSTEM a Time-Saving Guide to Emulsifier Selection.** ICI Americas Inc. [http://www.firp.ula.ve/archivos/historicos/76\\_Book\\_HLB\\_ICI.pdf](http://www.firp.ula.ve/archivos/historicos/76_Book_HLB_ICI.pdf)
- Iqbal, Javed; Wattoo, Feroza Hamid; Wattoo, Muhammad Hamid Sarwar; Malik, Rukhsana; Tirmizi, Syed Ahmad; Imran, Muhammad; and Ghangro, Allah Bux. (2011). "Adsorption of Acid Yellow Dye on Flakes of Chitosan Prepared from Fishery Wastes." *Arabian Journal of Chemistry* 4 (4): 389–95. <https://doi.org/10.1016/j.arabjc.2010.07.007>
- Israelachvili, Jacob N. (2011). **Intermolecular and Surface Forces.** 3rd ed. Elsevier. <https://doi.org/10.1016/C2009-0-21560-1>
- Janata, Jiri. (2009). **Principles of Chemical Sensors.** Boston, MA: Springer US. <https://doi.org/10.1007/b136378>
- Ji, Guangyin; Luo, Zhigang; Xiao, Zhigang; and Peng, Xichun. (2016). "Synthesis of Starch Nanoparticles in a Novel Microemulsion with Two ILs Substituting Two Phases." *Journal of Materials Science* 51 (15): 7085–92. <https://doi.org/10.1007/s10853-016-9952-1>
- Julinová, Markéta; and Slavík, Roman. (2012). "Removal of Phthalates from Aqueous Solution by Different Adsorbents: A Short Review." *Journal of Environmental Management* 94 (1): 13–24. <https://doi.org/10.1016/j.jenvman.2011.09.006>
- Jury, W. A.; and Vaux, H. (2005). "The Role of Science in Solving the World's Emerging Water Problems." *Proceedings of the National Academy of Sciences* 102 (44): 15715–20. <https://doi.org/10.1073/pnas.0506467102>
- Kamra, Tripta; Chaudhary, Shilpi; Xu, Changgang; Johansson, Niclas; Montelius, Lars; Schnadt, Joachim; and Ye, Lei. (2015). "Covalent Immobilization of Molecularly Imprinted Polymer Nanoparticles Using an Epoxy Silane." *Journal of Colloid and Interface Science* 445 (May): 277–84. <https://doi.org/10.1016/j.jcis.2014.12.086>
- Kamra, Tripta; Chaudhary, Shilpi; Xu, Changgang; Montelius, Lars; Schnadt, Joachim; and Ye, Lei. (2016). "Covalent Immobilization of Molecularly Imprinted Polymer Nanoparticles on a Gold Surface Using Carbodiimide Coupling for Chemical Sensing." *Journal of Colloid and Interface Science* 461 (January): 1–8. <https://doi.org/10.1016/j.jcis.2015.09.009>
- Kildeeva, N. R.; Perminov, P. a.; Vladimirov, L. V.; Novikov, V. V.; and Mikhailov, S. N. (2009). "About Mechanism of Chitosan Cross-Linking with Glutaraldehyde." *Russian Journal of Bioorganic Chemistry* 35 (3): 360–69. <https://doi.org/10.1134/S106816200903011X>

- Kinge, Sachin; Gang, Tian; Naber, Wouter J M; Wiel, Wilfred G. van der; and Reinhoudt, David N. (2011). **"Magnetic Nanoparticle Assembly on Surfaces Using Click Chemistry."** *Langmuir* 27 (2): 570–74. <https://doi.org/10.1021/la103715y>
- Kobitskaya, Elena; Ekinci, Duygu; Manzke, Achim; Plettl, Alfred; Wiedwald, Ulf; Ziemann, Paul; Biskupek, Johannes; Kaiser, Ute; Ziener, Ulrich; and Landfester, Katharina. (2010). **"Narrowly Size Distributed Zinc-Containing Poly(Acrylamide) Latexes via Inverse Miniemulsion Polymerization."** *Macromolecules* 43 (7): 3294–3305. <https://doi.org/10.1021/ma902553a>
- Kolarov, Felix; Niedergall, Klaus; Bach, Monika; Tovar, Günter E M; and Gauglitz, Günter. (2012). **"Optical Sensors with Molecularly Imprinted Nanospheres: A Promising Approach for Robust and Label-Free Detection of Small Molecules."** *Analytical and Bioanalytical Chemistry* 402 (10): 3245–52. <https://doi.org/10.1007/s00216-011-5592-0>
- Kong, Ming; Chen, Xi Guang; Xing, Ke; and Park, Hyun Jin. (2010). **"Antimicrobial Properties of Chitosan and Mode of Action: A State of the Art Review."** *International Journal of Food Microbiology* 144 (1): 51–63. <https://doi.org/10.1016/j.ijfoodmicro.2010.09.012>
- Kong, Yiyang; Hu, Binjie; Choy, Kwang-Leong; Li, Xiaoyu; and Chen, Guangdi. (2015). **"Study of Miniemulsion Formulation Containing 1-Octyl-3-Methylimidazolium Hexafluorophosphate for Its Application in Low-Emitting Coating Products."** *Soft Matter* 11 (7): 1293–1302. <https://doi.org/10.1039/C4SM02215G>
- Koryta, Jiri; Dvorak, Jiri; and Kavan, Ladislav. (1993). **Principles of Electrochemistry.** John Wiley & Sons Ltd
- Kretschmann, E.; and Raether, H. (1968). **"Notizen: Radiative Decay of Non Radiative Surface Plasmons Excited by Light."** *Zeitschrift Für Naturforschung A* 23 (12): 2135–36. <https://doi.org/10.1515/zna-1968-1247>
- Kreyling, Wolfgang G.; Semmler-Behnke, Manuela; and Chaudhry, Qasim. (2010). **"A Complementary Definition of Nanomaterial."** *Nano Today* 5 (3): 165–68. <https://doi.org/10.1016/j.nantod.2010.03.004>
- Kuchlyan, Jagannath; Kundu, Niloy; and Sarkar, Nilmoni. (2016). **"Ionic Liquids in Microemulsions: Formulation and Characterization."** *Current Opinion in Colloid & Interface Science* 25 (October): 27–38. <https://doi.org/10.1016/j.cocis.2016.05.011>
- Kulisiewicz, Leszek; Wierschem, Andreas; Rauh, Cornelia; and Delgado, Antonio. (2012). **Industrial High Pressure Applications.** Edited by Rudolf Eggers. *Industrial High Pressure Applications: Processes, Equipment and Safety.* Weinheim, Germany: Wiley-VCH Verlag GmbH & Co. KGaA. <https://doi.org/10.1002/9783527652655>
- Kurita, Keisuke. (2006). **"Chitin and Chitosan: Functional Biopolymers from Marine Crustaceans."** *Marine Biotechnology* 8 (3): 203–26. <https://doi.org/10.1007/s10126-005-0097-5>



- Kyzas, George Z.; Bikiaris, Dimitrios N.; Seredych, Mykola; Bandosz, Teresa J.; and Deliyanni, Eleni A. (2014). "Removal of Dorzolamide from Biomedical Wastewaters with Adsorption onto Graphite Oxide/Poly(Acrylic Acid) Grafted Chitosan Nanocomposite." *Bioresource Technology* 152 (January): 399–406. <https://doi.org/10.1016/j.biortech.2013.11.046>
- Kyzas, George Z.; Fu, Jie; Lazaridis, Nikolaos K.; Bikiaris, Dimitrios N.; and Matis, Kostas A. (2015). "New Approaches on the Removal of Pharmaceuticals from Wastewaters with Adsorbent Materials." *Journal of Molecular Liquids* 209: 87–93. <https://doi.org/10.1016/j.molliq.2015.05.025>
- Kyzas, George Z.; Kostoglou, Margaritis; Lazaridis, Nikolaos K.; Lambropoulou, Dimitra A.; and Bikiaris, Dimitrios N. (2013). "Environmental Friendly Technology for the Removal of Pharmaceutical Contaminants from Wastewaters Using Modified Chitosan Adsorbents." *Chemical Engineering Journal* 222 (April): 248–58. <https://doi.org/10.1016/j.cej.2013.02.048>
- Landfester, Katharina. (2001). "Polyreactions in Miniemulsions." *Macromolecular Rapid Communications* 22 (12): 896–936. [https://doi.org/10.1002/1521-3927\(20010801\)22:12<896::AID-MARC896>3.0.CO;2-R](https://doi.org/10.1002/1521-3927(20010801)22:12<896::AID-MARC896>3.0.CO;2-R)
- Landfester, Katharina; and Musyanovych, Anna. (2010). "Hydrogels in Miniemulsions." In *Romanian Reports of Physics*, 54:39–63. [https://doi.org/10.1007/12\\_2010\\_68](https://doi.org/10.1007/12_2010_68)
- Landfester, Katharina; Willert, Mirjam; and Antonietti, Markus. (2000). "Preparation of Polymer Particles in Nonaqueous Direct and Inverse Miniemulsions." *Macromolecules* 33 (7): 2370–76. <https://doi.org/10.1021/ma991782n>
- Le, Kim Anh; Sescousse, Romain; and Budtova, Tatiana. (2012). "Influence of Water on Cellulose-EMIMAc Solution Properties: A Viscometric Study." *Cellulose* 19 (1): 45–54. <https://doi.org/10.1007/s10570-011-9610-3>
- Lechner, M. D.; Gehrke, Klaus; and Nordmeier, Eckhard H. (2014). *Makromolekulare Chemie*. Berlin, Heidelberg: Springer Berlin Heidelberg. <https://doi.org/10.1007/978-3-642-41769-6>
- Lehr, Claus-Michael; Bouwstra, Joke A.; Schacht, Etienne H.; and Junginger, Hans E. (1992). "In Vitro Evaluation of Mucoadhesive Properties of Chitosan and Some Other Natural Polymers." *International Journal of Pharmaceutics* 78 (1–3): 43–48. [https://doi.org/10.1016/0378-5173\(92\)90353-4](https://doi.org/10.1016/0378-5173(92)90353-4)
- Li, Jianshen; Zhang, Jianling; Han, Buxing; Peng, Li; and Yang, Guanying. (2012). "Ionic Liquid-in-Ionic Liquid Nanoemulsions." *Chemical Communications* 48 (85): 10562. <https://doi.org/10.1039/c2cc36089f>
- Li, Jianshen; Zhang, Jianling; Han, Buxing; Zhao, Yueju; and Yang, Guanying. (2012). "Formation of Multiple Water-in-Ionic Liquid-in-Water Emulsions." *Journal of Colloid and Interface Science* 368 (1): 395–99. <https://doi.org/10.1016/j.jcis.2011.10.083>
- Li, Songjun; Cao, Shunsheng; Whitcombe, Michael J.; and Piletsky, Sergey A. (2014). "Size Matters: Challenges in Imprinting Macromolecules." *Progress in Polymer Science* 39 (1): 145–63. <https://doi.org/10.1016/j.progpolymsci.2013.10.002>

- Liu, Chunxiu; and Bai, Renbi. (2006). "Adsorptive Removal of Copper Ions with Highly Porous Chitosan/Cellulose Acetate Blend Hollow Fiber Membranes." *Journal of Membrane Science* 284 (1–2): 313–22. <https://doi.org/10.1016/j.memsci.2006.07.045>
- Liu, Zonghua; Jiao, Yanpeng; Wang, Yifei; Zhou, Changren; and Zhang, Ziyong. (2008). "Polysaccharides-Based Nanoparticles as Drug Delivery Systems." *Advanced Drug Delivery Reviews* 60 (15): 1650–62. <https://doi.org/10.1016/j.addr.2008.09.001>
- Lovell, Peter A; and Wiley, John. (1997). **Emulsion Polymerization and Emulsion Polymers**. Edited by Peter A. Lovell and Mohamed S. El-Aasser. New York: Wiley
- Lucklum, Ralf; and Hauptmann, Peter. (2006). "Acoustic Microsensors—the Challenge behind Microgravimetry." *Analytical and Bioanalytical Chemistry* 384 (3): 667–82. <https://doi.org/10.1007/s00216-005-0236-x>
- Lyons, Deidra Shannon. (2011). "Depolymerization of Chitosan by High-Pressure Homogenization and the Effect on Antimicrobial Properties." *Master's Thesis, University of Tennessee*
- M. A. Alsharef, Jamal; Taha, Mohd Raihan; and Ahmed Khan, Tanveer. (2017). "PHYSICAL DISPERSION OF NANOCARBONS IN COMPOSITES—A REVIEW." *Jurnal Teknologi* 79 (5): 69–81. <https://doi.org/10.11113/jt.v79.7646>
- Ma, Jie; Zhuang, Yuan; and Yu, Fei. (2015). "Facile Method for the Synthesis of a Magnetic CNTs-C@Fe-Chitosan Composite and Its Application in Tetracycline Removal from Aqueous Solutions." *Phys. Chem. Chem. Phys.* 17 (24): 15936–44. <https://doi.org/10.1039/C5CP02542G>
- Macintyre, Fiona S.; Sherrington, David C.; and Tetley, Laurence. (2006). "Synthesis of Ultrahigh Surface Area Monodisperse Porous Polymer Nanospheres." *Macromolecules* 39 (16): 5381–84. <https://doi.org/10.1021/ma0610010>
- Mahamat Nor, Siti Balkis; Woi, Pei Meng; and Ng, Sook Han. (2017). "Characterisation of Ionic Liquids Nanoemulsion Loaded with Piroxicam for Drug Delivery System." *Journal of Molecular Liquids* 234 (May): 30–39. <https://doi.org/10.1016/j.molliq.2017.03.042>
- Mamedov, Emil. (2015). "Manufacture and Stabilisation of Highly Concentrated Emulsions Using Polyhedral Oligomeric Silsesquioxane Nanomolecules." Cape Peninsula University of Technology
- Martin, Bret A.; and Hager, Harold E. (1989). "Flow Profile above a Quartz Crystal Vibrating in Liquid." *Journal of Applied Physics* 65 (7): 2627–29. <https://doi.org/10.1063/1.342771>
- Mathur, Nawal K.; and Narang, Chander K. (1990). "Chitin and Chitosan, Versatile Polysaccharides from Marine Animals." *Journal of Chemical Education* 67 (11): 938. <https://doi.org/10.1021/ed067p938>
- Matthews, B.A.; and Rhodes, C.T. (1970). "Use of the Derjaguin, Landau, Verwey, and Overbeek Theory to Interpret Pharmaceutical Suspension Stability." *Journal of Pharmaceutical Sciences* 59 (4): 521–25. <https://doi.org/10.1002/jps.2600590417>

Mazzotta, Elisabetta; Turco, Antonio; Chianella, Iva; Guerreiro, Antonio; Piletsky, Sergey A.; and Malitesta, Cosimino. (2016). **“Solid-Phase Synthesis of Electroactive Nanoparticles of Molecularly Imprinted Polymers. A Novel Platform for Indirect Electrochemical Sensing Applications.”** *Sensors and Actuators, B: Chemical* 229: 174–80. <https://doi.org/10.1016/j.snb.2016.01.126>

Mehne, Jochen; Markovic, Goran; Pröll, Florian; Schweizer, Nina; Zorn, Stefan; Schreiber, Frank; and Gauglitz, Günter. (2008). **“Characterisation of Morphology of Self-Assembled PEG Monolayers: A Comparison of Mixed and Pure Coatings Optimised for Biosensor Applications.”** *Analytical and Bioanalytical Chemistry* 391 (5): 1783–91. <https://doi.org/10.1007/s00216-008-2066-0>

Migneault, Isabelle; Dartiguenave, Catherine; Bertrand, Michel J.; and Waldron, Karen C. (2004). **“Glutaraldehyde: Behavior in Aqueous Solution, Reaction with Proteins, and Application to Enzyme Crosslinking.”** *BioTechniques* 37 (5): 790–96, 798–802. <https://doi.org/10.2144/3705A0790>

Minami, Hideto; Fukuami, Hiroki; Okubo, Masayoshi; and Suzuki, Toyoko. (2013). **“Preparation of Ionic Liquid-Encapsulated Polymer Particles.”** *Colloid and Polymer Science* 291 (1): 45–51. <https://doi.org/10.1007/s00396-012-2691-1>

Minami, Hideto; Kimura, Akira; Kinoshita, Keigo; and Okubo, Masayoshi. (2010). **“Preparation of Poly(Acrylic Acid) Particles by Dispersion Polymerization in an Ionic Liquid.”** *Langmuir: The ACS Journal of Surfaces and Colloids* 26 (9): 6303–7. <https://doi.org/10.1021/la904115s>

Minami, Hideto; Yoshida, Kazuhiro; and Okubo, Masayoshi. (2008). **“Preparation of Polystyrene Particles by Dispersion Polymerization in an Ionic Liquid.”** *Macromolecular Rapid Communications* 29 (7): 567–72. <https://doi.org/10.1002/marc.200700810>

Molinelli, Alexandra; Janotta, Markus; and Mizaikoff, Boris. (2008). **“Molecularly Imprinted Polymers for Biomolecular Recognition.”** In *Protein Nanotechnology*, 300:243–54. New Jersey: Humana Press. <https://doi.org/10.1385/1-59259-858-7:243>

Monteiro, O a; and Airoidi, C. (1999). **“Some Studies of Crosslinking Chitosan-Glutaraldehyde Interaction in a Homogeneous System.”** *International Journal of Biological Macromolecules* 26 (2–3): 119–28. <http://www.ncbi.nlm.nih.gov/pubmed/10517518>

Mosbach, Klaus; and Ramström, Olof. (1996). **“The Emerging Technique of Molecular Imprinting and Its Future Impact on Biotechnology.”** *Nature Biotechnology* 14 (2): 163–70. <https://doi.org/10.1038/nbt0296-163>

Myers, Drew. (2005). **Surfactant Science and Technology**. 3rd ed. Vol. 44. Hoboken, NJ, USA: John Wiley & Sons, Inc. <https://doi.org/10.1002/047174607X>

Nam, Seung-Woo; Choi, Dae-Jin; Kim, Seung-Kyu; Her, Namguk; and Zoh, Kyung-Duk. (2014). **“Adsorption Characteristics of Selected Hydrophilic and Hydrophobic Micropollutants in Water Using Activated Carbon.”** *Journal of Hazardous Materials* 270 (April): 144–52. <https://doi.org/10.1016/j.jhazmat.2014.01.037>

- Nazarzadeh, Elijah; and Sajjadi, Shahriar. (2010). **“Viscosity Effects in Miniemulsification via Ultrasound.”** *AIChE Journal* 56 (10): 2751–55. <https://doi.org/10.1002/aic.12133>
- Nguyen, Sophie; Hisiger, Steve; Jolicoeur, Mario; Winnik, Françoise M.; and Buschmann, Michael D. (2009). **“Fractionation and Characterization of Chitosan by Analytical SEC and 1H NMR after Semi-Preparative SEC.”** *Carbohydrate Polymers* 75 (4): 636–45. <https://doi.org/10.1016/j.carbpol.2008.09.002>
- Niedergall, Klaus; Bach, Monika; Hirth, Thomas; Tovar, Günter E.M.; and Schiestel, Thomas. (2014). **“Removal of Micropollutants from Water by Nanocomposite Membrane Adsorbers.”** *Separation and Purification Technology* 131 (June): 60–68. <https://doi.org/10.1016/j.seppur.2014.04.032>
- Niedergall, Klaus; Bach, Monika; Schiestel, Thomas; and Tovar, Günter E.M. (2013). **“Nanostructured Composite Adsorber Membranes for the Reduction of Trace Substances in Water: The Example of Bisphenol A.”** *Industrial & Engineering Chemistry Research* 52 (39): 14011–18. <https://doi.org/10.1021/ie303264r>
- Niedergall, Klaus; Kopp, Denis; Besch, Sandra; and Schiestel, Thomas. (2016). **“Mixed-Matrix Membrane Adsorbers for the Selective Binding of Metal Ions from Diluted Solutions.”** *Chemie Ingenieur Technik* 88 (4): 437–46. <https://doi.org/10.1002/cite.201400144>
- Nopper, Dirk; Lammershop, Olaf; Wulff, Günter; and Gauglitz, Günter. (2003). **“Amidine-Based Molecularly Imprinted Polymers-New Sensitive Elements for Chiral Chemosensors.”** *Analytical and Bioanalytical Chemistry* 377 (4): 608–13. <https://doi.org/10.1007/s00216-003-2145-1>
- Ohya, Yuichi; Shiratani, Masahiro; Kobayashi, Hironao; and Ouchi, Tatsuro. (1994). **“Release Behavior of 5-Fluorouracil from Chitosan-Gel Nanospheres Immobilizing 5-Fluorouracil Coated with Polysaccharides and Their Cell Specific Cytotoxicity.”** *Journal of Macromolecular Science, Part A* 31 (5): 629–42. <https://doi.org/10.1080/10601329409349743>
- Oladoja, N a; Adelagun, R O a; Ahmad, a L; Unuabonah, E I; and Bello, H a. (2014). **“Preparation of Magnetic, Macro-Reticulated Cross-Linked Chitosan for Tetracycline Removal from Aquatic Systems.”** *Colloids and Surfaces. B, Biointerfaces* 117 (May): 51–59. <https://doi.org/10.1016/j.colsurfb.2014.02.006>
- Oldham, Keith B. (2008). **“A Gouy–Chapman–Stern Model of the Double Layer at a (Metal)/(Ionic Liquid) Interface.”** *Journal of Electroanalytical Chemistry* 613 (2): 131–38. <https://doi.org/10.1016/j.jelechem.2007.10.017>
- Olivera, Sharon; Muralidhara, Handanahally Basavarajaiah; Venkatesh, Krishna; Guna, Vijay Kumar; Gopalakrishna, Keshavanarayana; and Kumar K., Yogesh. (2016). **“Potential Applications of Cellulose and Chitosan Nanoparticles/Composites in Wastewater Treatment: A Review.”** *Carbohydrate Polymers* 153: 600–618. <https://doi.org/10.1016/j.carbpol.2016.08.017>
- Ozcengiz, Gulay; and Demain, Arnold L. (2013). **“Recent Advances in the Biosynthesis of Penicillins, Cephalosporins and Clavams and Its Regulation.”** *Biotechnology Advances* 31 (2): 287–311. <https://doi.org/10.1016/j.biotechadv.2012.12.001>

- Panzarasa, Guido; Osypova, Alina; Sicher, Alba; Bruinink, Arie; and Dufresne, Eric. (2018). **“Controlled Formation of Chitosan Particles by a Clock Reaction.”** *Soft Matter* 14: 6415–18. <https://doi.org/10.1039/C8SM01060A>
- Particle Sciences. (2011). **“Emulsion Stability and Testing.”** *Particle Sciences - Technical Brief* 2
- Paul, Edward L; Atiemo-obeng, Victor A; and Kresta, Suzanne M. (2003). **Handbook of Industrial Mixing.** Edited by Edward L. Paul, Victor A. Atiemo-Obeng, and Suzanne M. Kresta. Hoboken, NJ, USA: John Wiley & Sons, Inc. <https://doi.org/10.1002/0471451452>
- Pennacchio, Anna; Varriale, Antonio; Esposito, Maria Grazia; Scala, Andrea; Marzullo, Vincenzo Manuel; Staiano, Maria; and D’Auria, Sabato. (2015). **“A Rapid and Sensitive Assay for the Detection of Benzylpenicillin (PenG) in Milk.”** Edited by Serge Muyldermans. *PLOS ONE* 10 (7): e0132396. <https://doi.org/10.1371/journal.pone.0132396>
- Pichon, Valérie. (2007). **“Selective Sample Treatment Using Molecularly Imprinted Polymers.”** *Journal of Chromatography A*. <https://doi.org/10.1016/j.chroma.2007.02.109>
- Plechkova, Natalia V; and Seddon, Kenneth R. (2008). **“Applications of Ionic Liquids in the Chemical Industry.”** *Chemical Society Reviews* 37 (1): 123–50. <https://doi.org/10.1039/b006677j>
- Polte, Jörg. (2015). **“Fundamental Growth Principles of Colloidal Metal Nanoparticles - a New Perspective.”** *CrystEngComm* 17 (36): 6809–30. <https://doi.org/10.1039/c5ce01014d>
- Poma, Alessandro; Guerreiro, Antonio; Whitcombe, Michael J; Piletska, Elena V; Turner, Anthony P F; and Piletsky, Sergey A. (2013). **“Solid-Phase Synthesis of Molecularly Imprinted Polymer Nanoparticles with a Reusable Template-‘Plastic Antibodies.’”** *Advanced Functional Materials* 23 (22): 2821–27. <https://doi.org/10.1002/adfm.201202397>
- Poma, Alessandro; Turner, Anthony P.F.; and Piletsky, Sergey A. (2010). **“Advances in the Manufacture of MIP Nanoparticles.”** *Trends in Biotechnology* 28 (12): 629–37. <https://doi.org/10.1016/j.tibtech.2010.08.006>
- Poon, Louis; Wilson, Lee D; and Headley, John V. (2014). **“Chitosan-Glutaraldehyde Copolymers and Their Sorption Properties.”** *Carbohydrate Polymers* 109 (August): 92–101. <https://doi.org/10.1016/j.carbpol.2014.02.086>
- Poon, Louis; Younus, Shaguftah; and Wilson, Lee D. (2014). **“Adsorption Study of an Organo-Arsenical with Chitosan-Based Sorbents.”** *Journal of Colloid and Interface Science* 420 (April): 136–44. <https://doi.org/10.1016/j.jcis.2014.01.003>
- Ramström, Olof; Ye, Lei; and Mosbach, Klaus. (1996). **“Artificial Antibodies to Corticosteroids Prepared by Molecular Imprinting.”** *Chemistry & Biology* 3 (6): 471–77. [https://doi.org/10.1016/S1074-5521\(96\)90095-2](https://doi.org/10.1016/S1074-5521(96)90095-2)
- Ravi Kumar, Majeti N.V. (2000). **“A Review of Chitin and Chitosan Applications.”** *Reactive and Functional Polymers* 46 (1): 1–27. [https://doi.org/10.1016/S1381-5148\(00\)00038-9](https://doi.org/10.1016/S1381-5148(00)00038-9)

Raz, S Rebe; Bremer, MEGE; and Haasnoot, W. (2009). "Label-Free and Multiplex Detection of Antibiotic Residues in Milk Using Imaging Surface Plasmon Resonance-Based Immunosensor." *Chemistry* 81 (18): 7743–49. <http://pubs.acs.org/doi/abs/10.1021/ac901230v>

Reddy, S.R; and Fogler, H.S. (1981). "Emulsion Stability: Delineation of Different Particle Loss Mechanisms." *Journal of Colloid and Interface Science* 79 (1): 105–13. [https://doi.org/10.1016/0021-9797\(81\)90053-9](https://doi.org/10.1016/0021-9797(81)90053-9)

Repo, Eveliina; Warchol, Jolanta K.; Kurniawan, Tonni Agustiono; and Sillanpää, Mika E.T. (2010). "Adsorption of Co(II) and Ni(II) by EDTA- and/or DTPA-Modified Chitosan: Kinetic and Equilibrium Modeling." *Chemical Engineering Journal* 161 (1–2): 73–82. <https://doi.org/10.1016/j.cej.2010.04.030>

Riegger, Benjamin R.; Kowalski, Regina; Hilfert, Luise; Tovar, Günter E.M.; and Bach, Monika. (2018). "Chitosan Nanoparticles via High-Pressure Homogenization-Assisted Miniemulsion Crosslinking for Mixed-Matrix Membrane Adsorbers." *Carbohydrate Polymers* 201 (December): 172–81. <https://doi.org/10.1016/j.carbpol.2018.07.059>

Riegger, Benjamin R.; Bäurer, Bernd; Mirzayeva, Aziza; Tovar, Günter E.M.; and Bach, Monika. (2018). "A Systematic Approach of Chitosan Nanoparticle Preparation via Emulsion Crosslinking as Potential Adsorbent in Wastewater Treatment." *Carbohydrate Polymers* 180 (January): 46–54. <https://doi.org/10.1016/j.carbpol.2017.10.002>

Rinaudo, Marguerite. (2006). "Chitin and Chitosan: Properties and Applications." *Progress in Polymer Science* 31 (7): 603–32. <https://doi.org/10.1016/j.progpolymsci.2006.06.001>

Rouget, Charles Marie Benjamin. (1859). "Des Substances Amylacées Dans Les Tissus Des Animaux, Spécialement Des Articulés (Chitine)." *Compt Rend* 48: 792–795

Santhosh, Chella; Velmurugan, Venugopal; Jacob, George; Jeong, Soon Kwan; Grace, Andrews Nirmala; and Bhatnagar, Amit. (2016). "Role of Nanomaterials in Water Treatment Applications: A Review." *Chemical Engineering Journal* 306: 1116–37. <https://doi.org/10.1016/j.cej.2016.08.053>

Santos, Hugo Miguel; Lodeiro, Carlos; and Capelo-Martnez, Jos-Luis. (2008). "The Power of Ultrasound." In *Ultrasound in Chemistry*, edited by Jos-Luis Capelo-Martnez, 1–16. Weinheim, Germany: Wiley-VCH Verlag GmbH & Co. KGaA. <https://doi.org/10.1002/9783527623501.ch1>

Sawai, H; and Orgel, L E. (2009). *IUPAC Compendium of Chemical Terminology*. Edited by Miloslav Nič, Jiří Jiráť, Bedřich Košata, Aubrey Jenkins, and Alan McNaught. *Journal of the American Chemical Society*. Vol. 97. Research Triangle Park, NC: IUPAC. <https://doi.org/10.1351/goldbook>

Saylan, Yeşeren; Yilmaz, Fatma; Özgür, Erdoğan; Derazshamshir, Ali; Yavuz, Handan; and Denizli, Adil. (2017). "Molecular Imprinting of Macromolecules for Sensor Applications." *Sensors (Switzerland)* 17 (4). <https://doi.org/10.3390/s17040898>

- Schmitt, Hans-Martin; Brecht, Andreas; Piehler, Jacob; and Gauglitz, Günter. (1997). "**An Integrated System for Optical Biomolecular Interaction Analysis.**" *Biosensors and Bioelectronics* 12 (8): 809–16. [https://doi.org/10.1016/S0956-5663\(97\)00046-8](https://doi.org/10.1016/S0956-5663(97)00046-8)
- Schork, F. Joseph; Luo, Yingwu; Smulders, Wilfred; Russum, James P.; Butté, Alessandro; and Fontenot, Kevin. (2005). "**Miniemulsion Polymerization.**" *Advances in Polymer Science* 175: 129–255. <https://doi.org/10.1007/b100115>
- Schuchmann, Heike P.; Karbstein, Née; Hecht, Lena L.; Gedrat, Marion; and Köhler, Karsten. (2012). "**High-Pressure Homogenization for the Production of Emulsions.**" In *Industrial High Pressure Applications*, 97–122. Weinheim, Germany: Wiley-VCH Verlag GmbH & Co. KGaA. <https://doi.org/10.1002/9783527652655.ch5>
- Schuchmann, Heike P.; and Schuchmann, Harald. (2005). **Lebensmittelverfahrenstechnik**. Weinheim, Germany: Wiley-VCH Verlag GmbH & Co. KGaA. <https://doi.org/10.1002/9783527623549>
- Schultz, Stefan; Wagner, Gerhard; Urban, Kai; and Ulrich, Joachim. (2004). "**High-Pressure Homogenization as a Process for Emulsion Formation.**" *Chemical Engineering & Technology* 27 (4): 361–68. <https://doi.org/10.1002/ceat.200406111>
- Sener, Gulsu; Uzun, Lokman; Say, Rıdvan; and Denizli, Adil. (2011). "**Use of Molecular Imprinted Nanoparticles as Biorecognition Element on Surface Plasmon Resonance Sensor.**" *Sensors and Actuators B: Chemical* 160 (1): 791–99. <https://doi.org/10.1016/j.snb.2011.08.064>
- SEPPIC. (2016). "**Performance Materials Product Portfolio - SIMALINE IE 501.**" 2016. [https://www.seppic.com/sites/seppic/files/2016/12/14/seppic\\_-\\_index\\_performance\\_materials.pdf](https://www.seppic.com/sites/seppic/files/2016/12/14/seppic_-_index_performance_materials.pdf)
- Shen, Xiantao; Xu, Changgang; and Ye, Lei. (2013). "**Molecularly Imprinted Polymers for Clean Water: Analysis and Purification.**" *Industrial & Engineering Chemistry Research* 52 (39): 13890–99. <https://doi.org/10.1021/ie302623s>
- Shi, Ai-min; Li, Dong; Wang, Li-jun; Li, Bing-zheng; and Adhikari, Benu. (2011). "**Preparation of Starch-Based Nanoparticles through High-Pressure Homogenization and Miniemulsion Cross-Linking: Influence of Various Process Parameters on Particle Size and Stability.**" *Carbohydrate Polymers* 83 (4): 1604–10. <https://doi.org/10.1016/j.carbpol.2010.10.011>
- Singer, Heinz P.; Wössner, Annika E.; McArdell, Christa S.; and Fenner, Kathrin. (2016). "**Rapid Screening for Exposure to 'Non-Target' Pharmaceuticals from Wastewater Effluents by Combining HRMS-Based Suspect Screening and Exposure Modeling.**" *Environmental Science & Technology* 50 (13): 6698–6707. <https://doi.org/10.1021/acs.est.5b03332>
- Slomkowski, Stanislaw; Alemán, José V.; Gilbert, Robert G.; Hess, Michael; Horie, Kazuyuki; Jones, Richard G.; Kubisa, Przemyslaw; Meisel, Ingrid; Mormann, Werner; Penczek, Stanislaw; and Stepto, Robert F. T. (2011). "**Terminology of Polymers and Polymerization Processes in Dispersed Systems (IUPAC Recommendations 2011).**" *Pure and Applied Chemistry* 83 (12): 2229–59. <https://doi.org/10.1351/PAC-REC-10-06-03>

- Stang, M.; Schuchmann, H.; and Schubert, H. (2001). "Emulsification in High-Pressure Homogenizers." *Engineering in Life Sciences* 1 (4): 151. [https://doi.org/10.1002/1618-2863\(200110\)1:4<151::AID-ELSC151>3.0.CO;2-D](https://doi.org/10.1002/1618-2863(200110)1:4<151::AID-ELSC151>3.0.CO;2-D)
- Stepito, Robert F. T. (2009). "Dispersity in Polymer Science (IUPAC Recommendations 2009)." *Pure and Applied Chemistry* 81 (2): 351–53. <https://doi.org/10.1351/PAC-REC-08-05-02>
- Suc, Nguyen Van; and Ly, Ho Thi Yeu. (2013). "Lead (II) Removal from Aqueous Solution by Chitosan Flake Modified with Citric Acid via Crosslinking with Glutaraldehyde." *Journal of Chemical Technology and Biotechnology* 88 (9): 1641–49. <https://doi.org/10.1002/jctb.4013>
- Suen, Shing-Yi; Caracotsios, Mike; and Etzel, Mark R. (1993). "Sorption Kinetics and Axial Diffusion in Binary-Solute Affinity-Membrane Bioseparations." *Chemical Engineering Science* 48 (10): 1801–12. [https://doi.org/10.1016/0009-2509\(93\)80350-Y](https://doi.org/10.1016/0009-2509(93)80350-Y)
- Sun, Xiaofu; Tian, Qingqing; Xue, Zhimin; Zhang, Yuwei; and Mu, Tiancheng. (2014). "The Dissolution Behaviour of Chitosan in Acetate-Based Ionic Liquids and Their Interactions: From Experimental Evidence to Density Functional Theory Analysis." *RSC Adv.* 4 (57): 30282–91. <https://doi.org/10.1039/C4RA02594F>
- Suzuki, Toyoko; Ichikawa, Hiroko; Nakai, Masaya; and Minami, Hideto. (2013). "Preparation of Free-Standing Thermosensitive Composite Gel Particles Incorporating Ionic Liquids." *Soft Matter* 9 (6): 1761–65. <https://doi.org/10.1039/C2SM27393D>
- Svenson, Johan; and Nicholls, Ian A. (2001). "On the Thermal and Chemical Stability of Molecularly Imprinted Polymers." *Analytica Chimica Acta* 435 (1): 19–24. [https://doi.org/10.1016/S0003-2670\(00\)01396-9](https://doi.org/10.1016/S0003-2670(00)01396-9)
- Thinh, Nguyen Ngoc; Hanh, Pham Thi Bich; Ha, Le Thi Thanh; Anh, Le Ngoc; Hoang, Tran Vinh; Hoang, Vu Dinh; Dang, Le Hai; Khoi, Nguyen Van; and Lam, Tran Dai. (2013). "Magnetic Chitosan Nanoparticles for Removal of Cr(VI) from Aqueous Solution." *Materials Science and Engineering C* 33 (3): 1214–18. <https://doi.org/10.1016/j.msec.2012.12.013>
- Umpleby, Robert J; Baxter, Sarah C; Chen, Yizhao; Shah, Ripal N; and Shimizu, Ken D. (2001). "Characterization of Molecularly Imprinted Polymers with the Langmuir–Freundlich Isotherm." *Analytical Chemistry* 73 (19): 4584–91. <https://doi.org/10.1021/ac0105686>
- Uragami, Tadashi; Matsuda, Toshiko; Okuno, Hiroshi; and Miyata, Takashi. (1994). "Structure of Chemically Modified Chitosan Membranes and Their Characteristics of Permeation and Separation of Aqueous Ethanol Solutions." *Journal of Membrane Science* 88 (2–3): 243–51. [https://doi.org/10.1016/0376-7388\(94\)87010-1](https://doi.org/10.1016/0376-7388(94)87010-1)
- Uzun, Lokman; and Turner, Anthony P.F. (2016). "Molecularly-Imprinted Polymer Sensors: Realising Their Potential." *Biosensors and Bioelectronics* 76 (February): 131–44. <https://doi.org/10.1016/j.bios.2015.07.013>



- Vaihinger, Dorothea; Landfester, Katharina; Kräuter, Iris; Brunner, Herwig; and Tovar, Günter E. M. (2002). **"Molecularly Imprinted Polymer Nanospheres as Synthetic Affinity Receptors Obtained by Miniemulsion Polymerisation."** *Macromolecular Chemistry and Physics* 203 (13): 1965–73. [https://doi.org/10.1002/1521-3935\(200209\)203:13<1965::AID-MACP1965>3.0.CO;2-C](https://doi.org/10.1002/1521-3935(200209)203:13<1965::AID-MACP1965>3.0.CO;2-C)
- Vakili, Mohammadtaghi; Rafatullah, Mohd; Salamatinia, Babak; Abdullah, Ahmad Zuhairi; Ibrahim, Mahamad Hakimi; Tan, Kok Bing; Gholami, Zahra; and Amouzgar, Parisa. (2014). **"Application of Chitosan and Its Derivatives as Adsorbents for Dye Removal from Water and Wastewater: A Review."** *Carbohydrate Polymers* 113 (November): 115–30. <https://doi.org/10.1016/j.carbpol.2014.07.007>
- Vanderhoff, J.W.; El-Aasser, M.S.; Micale, F.J.; Sudol, E.D.; Tseng, CM.; Silwanowicz, A.; Kornfeld, D.M.; and Vicente, F.A. (1984). **"PREPARATION OF LARGE-PARTICLE-SIZE MONODISPERSE LATEXES IN SPACE: POLYMERIZATION KINETICS AND PROCESS DEVELOPMENT."** *Journal of Dispersion Science and Technology* 5 (3–4): 231–46. <https://doi.org/10.1080/01932698408943220>
- Varma, J; Deshpande, S; and Kennedy, J. (2004). **"Metal Complexation by Chitosan and Its Derivatives: A Review."** *Carbohydrate Polymers* 55 (1): 77–93. <https://doi.org/10.1016/j.carbpol.2003.08.005>
- Vedenyapina, M. D.; Stopp, P.; Weichgrebe, D.; and Vedenyapin, A. A. (2016). **"Adsorption of Diclofenac Sodium from Aqueous Solutions on Activated Carbon."** *Solid Fuel Chemistry* 50 (1): 46–50. <https://doi.org/10.3103/S0361521916010109>
- Vert, Michel; Doi, Yoshiharu; Hellwich, Karl-heinz; Hess, Michael; Hodge, Philip; Kubisa, Przemyslaw; Rinaudo, Marguerite; and Schué, François. (2012). **"Terminology for Biorelated Polymers and Applications (IUPAC Recommendations 2012)."** *Pure and Applied Chemistry* 84 (2): 377–410. <https://doi.org/10.1351/PAC-REC-10-12-04>
- Wackerlig, Judith; and Lieberzeit, Peter A. (2015). **"Molecularly Imprinted Polymer Nanoparticles in Chemical Sensing – Synthesis, Characterisation and Application."** *Sensors and Actuators B: Chemical* 207 (February): 144–57. <https://doi.org/10.1016/j.snb.2014.09.094>
- Wan Ngah, W.S.; Teong, L.C.; and Hanafiah, M.a.K.M. (2011). **"Adsorption of Dyes and Heavy Metal Ions by Chitosan Composites: A Review."** *Carbohydrate Polymers* 83 (4): 1446–56. <https://doi.org/10.1016/j.carbpol.2010.11.004>
- Wang, Ke; Yuan, Xun; Guo, Zhenpeng; Xu, Jiying; and Chen, Yi. (2014). **"Red Emissive Cross-Linked Chitosan and Their Nanoparticles for Imaging the Nucleoli of Living Cells."** *Carbohydrate Polymers* 102 (February): 699–707. <https://doi.org/10.1016/j.carbpol.2013.10.100>
- Weber, Patricia; Riegger, Benjamin R.; Niedergall, Klaus; Tovar, Günter E.M.; Bach, Monika; and Gauglitz, Günter. (2018). **"Nano-MIP Based Sensor for Penicillin G: Sensitive Layer and Analytical Validation."** *Sensors and Actuators B: Chemical* 267 (August): 26–33. <https://doi.org/10.1016/j.snb.2018.03.142>

- Westerhoff, Paul; Yoon, Yeomin; Snyder, Shane; and Wert, Eric. (2005). **"Fate of Endocrine-Disruptor, Pharmaceutical, and Personal Care Product Chemicals during Simulated Drinking Water Treatment Processes."** *Environmental Science & Technology* 39 (17): 6649–63. <https://doi.org/10.1021/es0484799>
- Wiechers, Susann; and Schmidt-Naake, Gudrun. (2008). **"Copolymerization of 2-Acrylamido-2-Methyl-1-Propanesulfonic Acid and 1-Vinylimidazole in Inverse Miniemulsion."** *Macromolecular Reaction Engineering* 2 (2): 126–34. <https://doi.org/10.1002/mren.200700036>
- Wiechers, Susann; and Schmidt-Naake, Gudrun. (2009). **"The Influence of Reaction Conditions on the Copolymer Composition in Inverse Miniemulsion."** *Macromolecular Symposia* 281 (1): 47–53. <https://doi.org/10.1002/masy.200950706>
- Wu, Liping; and Zhang, Zhengpu. (2013). **"Preparation of Polyamidoamine Dendrons Supported on Chitosan Microspheres and the Adsorption of Bilirubin."** *Journal of Applied Polymer Science* 130 (1): 563–71. <https://doi.org/10.1002/app.39193>
- Wu, Ta Yeong; Guo, Ningqun; Teh, Chee Yang; and Hay, Jacqueline Xiao Wen. (2013). **Advances in Ultrasound Technology for Environmental Remediation.** SpringerBriefs in Molecular Science. Dordrecht: Springer Netherlands. <https://doi.org/10.1007/978-94-007-5533-8>
- Wu, Tao; Zivanovic, Svetlana; Hayes, Douglas G.; and Weiss, Jochen. (2008). **"Efficient Reduction of Chitosan Molecular Weight by High-Intensity Ultrasound: Underlying Mechanism and Effect of Process Parameters."** *Journal of Agricultural and Food Chemistry* 56 (13): 5112–19. <https://doi.org/10.1021/jf073136q>
- Wulff, G; and Sarhan, A. (1972). **"Über Die Anwendung von Enzymalog Gebauten Polymeren Zur Racemattrennung."** *Angewandte Chemie* 293 (669): 1972. <https://doi.org/10.1002/ange.19720840838>
- Wulff, Günter. (1995). **"Molecular Imprinting in Cross-Linked Materials with the Aid of Molecular Templates— A Way towards Artificial Antibodies."** *Angewandte Chemie International Edition in English* 34 (17): 1812–32. <https://doi.org/10.1002/anie.199518121>
- Xie, Haibo; Zhang, Suobo; and Li, Shenghai. (2006). **"Chitin and Chitosan Dissolved in Ionic Liquids as Reversible Sorbents of CO<sub>2</sub>."** *Green Chemistry* 8 (7): 630. <https://doi.org/10.1039/b517297g>
- Yang Thompson, M., Duncan-Hewitt, W. C., M. (1993). **"Interfacial Properties and the Response of the Thickness Shear-Mode Acoustic Wave Sensor in Liquids."** *Langmuir* 9 (12): 802–11
- Yuan, Chao; Guo, Jiangna; Si, Zhihong; and Yan, Feng. (2015). **"Polymerization in Ionic Liquid-Based Microemulsions."** *Polymer Chemistry* 6 (22): 4059–66. <https://doi.org/10.1039/C5PY00423C>
- Yuwei, Chen; and Jianlong, Wang. (2011). **"Preparation and Characterization of Magnetic Chitosan Nanoparticles and Its Application for Cu(II) Removal."** *Chemical Engineering Journal* 168 (1): 286–92. <https://doi.org/10.1016/j.cej.2011.01.006>

- Zavrel, Michael; Bross, Daniela; Funke, Matthias; Büchs, Jochen; and Spiess, Antje C. (2009). "High-Throughput Screening for Ionic Liquids Dissolving (Ligno-)Cellulose." *Bioresource Technology* 100 (9): 2580–87. <https://doi.org/10.1016/j.biortech.2008.11.052>
- Zhang, Lei; Zeng, Yuexian; and Cheng, Zhengjun. (2016). "Removal of Heavy Metal Ions Using Chitosan and Modified Chitosan: A Review." *Journal of Molecular Liquids* 214 (February): 175–91. <https://doi.org/10.1016/j.molliq.2015.12.013>
- Zhang, Yalei; Shen, Zhe; Dai, Chaomeng; and Zhou, Xuefei. (2014). "Removal of Selected Pharmaceuticals from Aqueous Solution Using Magnetic Chitosan: Sorption Behavior and Mechanism." *Environmental Science and Pollution Research* 21 (22): 12780–89. <https://doi.org/10.1007/s11356-014-3212-1>
- Zhang, Yongjun; Geissen, Sven-Uwe; and Gal, Carmen. (2008). "Carbamazepine and Diclofenac: Removal in Wastewater Treatment Plants and Occurrence in Water Bodies." *Chemosphere* 73 (8): 1151–61. <https://doi.org/10.1016/j.chemosphere.2008.07.086>
- Zhi, Jia; Wang, Yujun; and Luo, Guangsheng. (2005). "Adsorption of Diuretic Furosemide onto Chitosan Nanoparticles Prepared with a Water-in-Oil Nanoemulsion System." *Reactive and Functional Polymers* 65 (3): 249–57. <https://doi.org/10.1016/j.reactfunctpolym.2005.06.009>
- Zhou, Gang; Luo, Zhigang; and Fu, Xiong. (2014a). "Preparation and Characterization of Starch Nanoparticles in Ionic Liquid-in-Oil Microemulsions System." *Industrial Crops and Products* 52 (January): 105–10. <https://doi.org/10.1016/j.indcrop.2013.10.019>
- Zhou, Gang; Luo, Zhigang; and Fu, Xiong. (2014b). "Preparation of Starch Nanoparticles in a Water-in-Ionic Liquid Microemulsion System and Their Drug Loading and Releasing Properties." *Journal of Agricultural and Food Chemistry* 62 (32): 8214–20. <https://doi.org/10.1021/jf5018725>
- Zhou, Limin; Xu, Jianping; Liang, Xizhen; and Liu, Zhirong. (2010). "Adsorption of Platinum(IV) and Palladium(II) from Aqueous Solution by Magnetic Cross-Linking Chitosan Nanoparticles Modified with Ethylenediamine." *Journal of Hazardous Materials* 182 (1–3): 518–24. <https://doi.org/10.1016/j.jhazmat.2010.06.062>
- Zimmerman, Steven C; and Lemcoff, N Gabriel. (2004). "Synthetic Hosts via Molecular Imprinting—Are Universal Synthetic Antibodies Realistically Possible?" *Chem. Commun.*, no. 1: 5–14. <https://doi.org/10.1039/B304720B>
- Zinadini, S.; Zinatizadeh, A.A.; Rahimi, M.; Vatanpour, V.; Zangeneh, H.; and Beygzadeh, M. (2014). "Novel High Flux Antifouling Nanofiltration Membranes for Dye Removal Containing Carboxymethyl Chitosan Coated Fe<sub>3</sub>O<sub>4</sub> Nanoparticles." *Desalination* 349 (September): 145–54. <https://doi.org/10.1016/j.desal.2014.07.007>

